Synthesis and Modification of Polymer Membranes for Pervaporation and Gas Separation

by

Shude Xiao

A thesis
presented to the University of Waterloo
in fulfillment of the
thesis requirement for the degree of
Doctor of Philosophy
in
Chemical Engineering

Waterloo, Ontario, Canada, 2007

AUTHOR'S DECLARATION

I hereby declare that I am the sole author of this thesis. This is a true copy of the thesis, including any required final revisions, as accepted by my examiners.

I understand that my thesis may be made electronically available to the public.

Abstract

Trimesoyl chloride (TMC) crosslinked poly(vinyl alcohol) (PVA) / chitosan (CS) membranes and synthetic polyimide membranes were prepared for pervaporation dehydration of isopropanol and gas separation.

PVA membranes were interfacially crosslinked with different amounts of TMC/hexane, and the degree of crosslinking was characterized by Fourier Transform Infrared Spectroscopy - Attenuated Total Reflectance Spectroscopy (FTIR-ATR) and water uptake. The asymmetric structure of the PVA-TMC membranes was revealed by FTIR-ATR. Thermal analysis was performed to understand the pyrolysis mechanism, which was supposed to be a combination of elimination of water and/or trimesic acid followed by breakage of the main chain. Water permeation and pervaporation dehydration of isopropanol were conducted, and the results showed that PVA-3TMC had the best overall pervaporation properties among the four PVA-TMC membranes studied.

Sorption properties and pervaporation behavior of the PVA-3TMC membrane were investigated. The effects of water/isopropanol on the polymer matrix and the possible change of the degree of crystallinity induced by the sorbed water were believed to account for the sorption properties. For water permeation and pervaporation dehydration of isopropanol in a heating-cooling cycle, the permeation flux did not change significantly, and the selectivity was improved by the formation of crystallites during the heating run. For pervaporation in the diluting and concentrating runs at 60 °C, there was no change in the membrane permeability.

Chitosan membranes were interfacially crosslinked in TMC/hexane with different crosslinking time. The membrane with a higher degree of crosslinking showed a higher degree of swelling in water at room temperature. A two-stage thermal decomposition mechanism was proposed based on thermal analyses. Pure gas permeation was performed with CO_2 and N_2 at room temperature, and CS-TMC-2 showed the best performance, with a CO_2 permeability of ~163 Barrer and a CO_2/N_2 permeability ratio of ~42. Pervaporation was carried out for dehydration of isopropanol with the unconditioned and conditioned membranes, and the CS-TMC-3 membrane showed the best pervaporation performance. Pervaporation and gas separation properties were affected by the crosslinking-induced relaxation and the mobility/packing properties of the CS-TMC matrices.

4,4'-(Hexafluoroisopropylidene) diphthalic anhydride (6FDA)-based and 2,2-bis[4-(3,4-dicarboxyphenoxy) phenyl]propane dianhydride (BPADA)-based copolyimides were synthesized from one-step high-temperature polymerization in *m*-cresol. Polymers were characterized with Gel

Permeation Chromatography (GPC), FTIR, Nuclear Magnetic Resonance Spectroscopy (NMR), Differential Scanning Calorimetry (DSC) and Thermogravimetric Analysis (TGA). Surface free energies and interfacial free energies were calculated from contact angles to characterize hydrophilicity of the polyimide membranes. Gas permeation properties of 6FDA-based copolyimide membranes were studied with N_2, O_2, H_2, He and CO_2, and pervaporation dehydration of isopropanol was performed with 6FDA-based and BPADA-based membranes. An empirical linear moiety contribution approach was proposed, and the moiety contribution factors were used to illustrate the effects of dianhydrides and diamines on permselectivities of the copolyimide membranes. Bulky side groups, flexibility of polymer main chains, structures of monomer moieties, and interactions between gas molecules and polymer chains were shown to affect gas permselectivities, while in pervaporation, both sorption and diffusion properties were affected by the interactions between penetrants and polymer matrices as well as the steric effects of monomer moieties.

Keywords: Poly(vinyl alcohol), Chitosan, Polyimides, Membranes, Pervaporation, Gas permeation, Trimesoyl chloride, Crosslinking, Sorption, Thermal analysis, Polycondensation, Contact angles.

Acknowledgements

I wish to express my gratitude to those who helped me in the past four years during my study in Waterloo, and to those who contributed to the completion of this thesis.

First of all, I would like to express my sincere appreciation to my supervisors, Dr. Robert Y.M. Huang and Dr. Xianshe Feng, for their constant encouragement and beneficial guidance.

I appreciate the assistance from my colleagues, and I am thankful to Dr. Kun Liu, Dr. Yufeng Zhang, Dr. Yingshu Liu, Dr. You-In Park, Dr. Marcelino L. Gimenes, Dr. Zhijun Zhou, and Dr. Yong Zhou for the helpful discussions that widened my academic horizons. I am very grateful to my colleague Runhong Du for the valuable discussions, suggestions and comments on lab work and thesis writing, and I also appreciate the suggestions from my colleague Elaine Y.H. Lin.

I would like to thank Dr. Neil McManus and Dr. Jialong Wu for GPC tests, and to thank Dr. Leonardo Simon and Dr. Dongyu Fang for FTIR measurements. I am grateful to Janet Venne, Ralph Dickhout, Dennis Herman, Bert Habicher, Ron Neill, Rick Hecktus and Ravindra Singh for their technical supports, and I appreciate the services from Patricia Anderson, Liz Bevan, and other departmental secretaries.

I would like to thank the examination committee for the comments on my thesis.

Special thanks go to Dr. Robert Huang and Mrs. Ritsuko Huang for their kindness and affection that made me feel at home. Additionally, I would like to thank all my friends with whom I enjoyed friendship in the past four years.

Finally, from deep within my heart, I am greatly indebted to my parents for their endless love and support, and I am sincerely grateful to my brothers for their constant encouragement and help.

This thesis was financially supported by the Natural Sciences and Engineering Research Council (NSERC) of Canada. University of Waterloo, Department of Chemical Engineering and Faculty of Engineering provided financial aids for my Ph.D. studies.

To My Parents and Brothers

Table of Contents

List of Figures xii
List of Tables xvi
Chapter 1 Introduction 1
1.1 Background 1
1.2 Purpose of the Study 3
1.2.1 Dehydration of Isopropanol 3
1.2.2 Conventional Hydrophilic Membranes for Pervaporation 3
1.2.3 High-Performance Polyimides in Membrane Separation 4
1.2.4 Structure of the Research 5
1.3 Research Objectives 5
1.4 Outline of the Thesis 6
Chapter 2 Literature Review 8
2.1 Separation Principles 8
2.2 Mass Transport in Pervaporation Membranes 8
2.2.1 Solution-Diffusion Model 9
2.2.2 Pore-Flow Model 11
2.2.3 Carrier Transport Mechanism 13
2.3 Polymer Materials for Pervaporation 14
2.3.1 Conventional Pervaporation Membranes 15
2.3.2 Polyimide Pervaporation Membranes 19
2.4 Polyimides for Pervaporation 19
2.4.1 Synthesis of Polyimides 19
2.4.2 Polyimide Membranes for Dehydration 22
2.4.3 Polyimide Membranes for Separation of Organics 25
2.4.4 Polyimide Membranes for Extraction of Organics from Water 27
2.5 Non-porous Membranes for Gas Separation 27
2.5.1 Gas Transport in Dense Membranes 28
2.5.2 Polyimide Membranes for Gas Separation 31
Part I Trimesoyl Chloride Crosslinked Poly(vinyl alcohol) and Chitosan Membranes for Pervaporation and Gas Separation 34

Chapter 3 Trimesoyl Chloride Crosslinked Poly(vinyl alcohol) Membranes for Pervaporation Dehydration of Isopropanol. I. Preparation and Characterization 35
3.1 Introduction 35
3.2 Experimental 37
3.2.1 Chemicals and Materials 37
3.2.2 Membrane Preparation 37
3.2.3 Fourier Transform Infrared Spectroscopy (FTIR) 38
3.2.4 Swelling in Water 38
3.2.5 Thermal Characterization 38
3.2.6 Pervaporation Experiments 39
3.3 Results and Discussion 41
3.3.1 Membrane Preparation and Crosslinking 41
3.3.2 FTIR-ATR Analysis 41
3.3.3 Swelling Behavior 46
3.3.4 DSC Thermograms 47
3.3.5 Thermal Stability and Degradation 47
3.3.6 Pervaporation Properties of PVA-TMC Membranes 52
3.4 Conclusions 59
Chapter 4 Trimesoyl Chloride Crosslinked Poly(vinyl alcohol) Membranes for Pervaporation Dehydration of Isopropanol. II. Sorption Properties and Pervaporation Behaviors under Different Operating Conditions 60
4.1 Introduction 60
4.2 Experimental 62
4.2.1 Materials and Membrane Preparation 62
4.2.2 Pervaporation Experiments 62
4.2.3 Swelling and Sorption Experiments 64
4.3 Results and Discussion 64
4.3.1 Effect of Temperature on Sorption Properties 64
4.3.2 Effect of Feed Concentration on Sorption Properties 66
4.3.3 Pervaporation Behavior in a Thermal Cycle 69
4.3.4 Pervaporation in a Concentration Cycle 72
4.3.5 Dynamic Pervaporation Process 76
4.4 Conclusions 78

Chapter 5 Trimesoyl Chloride Crosslinked Chitosan Membranes: Gas Separation and Pervaporation Properties 79
5.1 Introduction 79
5.2 Experimental 81
5.2.1 Preparation of CS-TMC Membranes 81
5.2.2 DSC and TGA Measurements 82
5.2.3 Water Uptake 82
5.2.4 Pure N_2/CO_2 Permeation 82
5.2.5 Pervaporation Dehydration of Isopropanol 83
5.3 Results and Discussion 84
5.3.1 Crosslinking in a Non-solvent 84
5.3.2 Effect of Crosslinking on Thermal Properties 85
5.3.3 Membrane Swelling in Water 90
5.3.4 Gas Permeation Properties 91
5.3.5 Pervaporation Properties 94
5.3.6 Comparison of Separation Properties with Other Membranes 101
5.4 Conclusions 103
Part II Synthetic Polyimide Membranes for Pervaporation and Gas Separation 105
Chapter 6 4,4'-(Hexafluoroisopropylidene) Diphthalic Anhydride (6FDA) - 4-Aminophenyl Ether (ODA) - Based Polyimide Membranes for Gas Separation and Pervaporation. I. Polyimides Containing Side Groups or Functional Groups 106
6.1 Introduction 106
6.2 Experimental 108
6.2.1 Materials 108
6.2.2 One-Step Polymerization 108
6.2.3 Characterization 109
6.2.4 Polyimide Membranes 110
6.2.5 Pure Gas Permeation 110
6.2.6 Pervaporation Tests 113
6.3 Results and Discussion 113
6.3.1 Synthesis of Polyimides 113
6.3.2 Properties of Polyimides 116
6.3.3 Gas Permeation Properties 122

6.3.4 Pervaporation Properties 128
6.4 Conclusions 135
Chapter 7 4,4'-(Hexafluoroisopropylidene) Diphthalic Anhydride (6FDA) - 4-Aminophenyl Ether (ODA) - Based Polyimide Membranes for Gas Separation and Pervaporation. II. Polyimides Containing Moieties with Different Chain Structures 136
7.1 Introduction 136
7.2 Experimental 137
7.2.1 Synthesis of Monomers 138
7.2.2 Polymers and Membranes 138
7.3 Results and Discussion 140
7.3.1 Preparation of Monomers and Polymers 140
7.3.2 Properties of Polyimides 144
7.3.3 Gas Permeation Properties 148
7.3.4 Pervaporation Properties 152
7.4 Conclusions 156
Chapter 8 4,4'-(Hexafluoroisopropylidene) Diphthalic Anhydride (6FDA) - 4,4'-Methylenedianiline (MDA) - Based Polyimide Membranes for Gas Separation and Pervaporation 157
8.1 Introduction 157
8.2 Experimental 157
8.3 Results and Discussion 160
8.3.1 Polymerization and Polymers 160
8.3.2 Properties of Polyimides 162
8.3.3 Gas Permeation Properties 165
8.3.4 Pervaporation Properties 166
8.4 Conclusions 174
Chapter 9 2,2-Bis[4-(3,4-dicarboxyphenoxy) phenyl]propane dianhydride (BPADA) - Based Polyimide Membranes for Pervaporation Dehydration of Isopropanol: Characterization and Comparison with 4,4'-(Hexafluoroisopropylidene) Diphthalic Anhydride (6FDA) - Based Polyimide Membranes 175
9.1 Introduction 175
9.2 Experimental 175
9.3 Results and Discussion 177
9.3.1 BPADA-Based Polyimides 177

9.3.2 Properties of Polyimides 179
9.3.3 Pervaporation Properties 185
9.4 Conclusions 190
Chapter 10 Conclusions and Recommendations 191
10.1 General Contributions 191
10.1.1 Trimesoyl Chloride Crosslinked PVA Membranes 191
10.1.2 Trimesoyl Chloride Crosslinked Chitosan Membranes 192
10.1.3 Synthetic Polyimide Membranes 193
10.2 Recommendations for Future Work 194
Nomenclature 196
Abbreviations 199
Appendix A Solubility Parameters 200
Appendix B Calculation of the Apparent Activation Energy from the Arrhenius Equation 203
Appendix C FTIR and NMR Data of Polyimides and Monomers 204
Appendix D Linear Moiety Contribution Method for Gas Selectivity 210
Appendix E Linear Moiety Contribution Method for Total Flux in Pervaporation 213
Appendix F Linear Moiety Contribution Method for Water Flux in Pervaporation 216
Bibliography 219
Publications and Presentations 238

List of Figures

Figure 1.1 Schematic membrane separation process 2
Figure 1.2 Vapor-liquid equilibrium of isopropanol-water at 60 °C 4
Figure 1.3 The structure of the research 6
Figure 2.1 Solution diffusion model for mass transport in membranes 10
Figure 2.2 Schematic description of pore-flow model 12
Figure 2.3 Schematic description of mass transport by the carrier transport mechanism 13
Figure 2.4 Chemical structure of chitosan 17
Figure 2.5 The two-step method for polyimide synthesis 20
Figure 2.6 Formation of poly(amic acid) 20
Figure 2.7 Thermal imidization of poly(amic acid) 21
Figure 2.8 Chemical imidization of poly(amic acid) 21
Figure 2.9 Possible reaction mechanism for solution imidization 22
Figure 2.10 H-bonding between the imide ring and water molecules 23
Figure 2.11 Chemical structures of some commercial polyimides 23
Figure 2.12 A dianhydride with hydroxyl groups and diamines with bulky pendant groups 25
Figure 2.13 Gas transport mechanism in membranes 28
Figure 2.14 Relationship between temperature and specific volume of a polymer 30
Figure 2.15 Illustration of "extreme" cases for gas transport in polymers of different states 31
Figure 3.1 Pervaporation setup 39
Figure 3.2 Schematic permeation cell 40
Figure 3.3 ATR spectra of PVA-TMC top and bottom layers 43
Figure 3.4 Integration of peak areas for ATR spectra 44
Figure 3.5 Degrees of swelling of PVA-TMC membranes in water at room temperature 46
Figure 3.6 Schematic crosslinking of PVA with TMC 47
Figure 3.7 DSC curves of the uncrosslinked PVA and PVA-TMC membranes 48
Figure 3.8 TGA and DTG curves of the PVA and PVA-TMC membranes 50
Figure 3.9 Pyrolysis reactions of PVA and PVA-TMC 51
Figure 3.10 Pure water permeation at different temperatures 52
Figure 3.11 Total permeation flux at different temperatures (20 wt. % water in the feed) 54
Figure 3.12 Permeate water contents and separation factors of water/isopropanol at different temperatures (20 wt. % water in the feed) 55

Figure 3.13 Effects of feed water contents on permeation flux at 60 °C 56
Figure 3.14 Effects of feed water contents on permeate water contents and separation factors of water/isopropanol at 60 °C 57
Figure 4.1 Schematic pervaporation cell 63
Figure 4.2 Schematic permeate collection system 63
Figure 4.3 Sorption selectivities and sorbed water contents for membranes in water/isopropanol sorption mixtures at 19.5 ± 0.3 wt. % water 67
Figure 4.4 Degree of swelling for the membrane in water/isopropanol mixtures at 60 °C 68
Figure 4.5 Weight ratios of the sorbed water and isopropanol to the membrane material in swollen membranes at 60 °C 68
Figure 4.6 Sorption selectivity and sorbed water content for the membrane in water/ isopropanol at 60 °C 70
Figure 4.7 Pure water permeation in a thermal cycle 71
Figure 4.8 Pervaporation dehydration of isopropanol in a thermal cycle (a) Permeation flux and separation factor (b) Permeate water content 73
Figure 4.9 Diffusion selectivity for pervaporation in a thermal cycle 74
Figure 4.10 Pervaporation dehydration of isopropanol in a concentration cycle (a) Permeation flux and separation factor (b) Permeate water content 75
Figure 4.11 Diffusion selectivity for pervaporation in a concentration cycle at 60 °C 76
Figure 4.12 Batch operation of pervaporation dehydration of isopropanol (a) Water contents in the feed and permeate (b) Permeation flux and separation factor 77
Figure 5.1 Gas permeation setup 83
Figure 5.2 Schematic diagram of the crosslinked structure of CS-TMC membranes 85
Figure 5.3 DSC plots of CS-TMC membranes 86
Figure 5.4 TGA and DTG plots of CS-TMC membranes 87
Figure 5.5 The degree swelling of CS-TMC membranes in water at room temperature 90
Figure 5.6 Gas permeabilities to CO_2 and N_2 and CO_2/N_2 permeability ratios 92
Figure 5.7 Effect of temperature on the normalized flux of CS-TMC membranes for pervaporation of water/isopropanol mixtures 95
Figure 5.8 Effect of temperature on separation factor of CS-TMC membranes for water/isopropanol separation by pervaporation 97
Figure 5.9 Effect of the feed water content on the normalized flux of the water/isopropanol through CS-TMC membranes 99

Figure 5.10 Effect of feed water content on separation factor of water/isopropanol through CS-TMC membranes 100
Figure 5.11 The CO_2/N_2 gas separation and water/isopropanol pervaporation performance of chitosan membranes as compared with other membranes reported in the literature 102
Figure 6.1 Monomers of polyimides 109
Figure 6.2 One-step polymerization of 6FDA-8ODA-2DAPy 112
Figure 6.3 Gas permeation setup 112
Figure 6.4 ^{1}H NMR spectra of polyimides 114
Figure 6.5 FTIR spectra of polyimides (film on NaCl) 115
Figure 6.6 TGA and DTG curves of polyimides 119
Figure 6.7 Determination of the contact angle from a sessile drop on a horizontal surface 120
Figure 6.8 Permeance ratios of gas pairs for membranes at different pressures 124
Figure 6.9 Comparison of experimental data with the predicted permeance ratios for polyimide membranes 128
Figure 6.10 Permeate water contents of polyimide membranes in pervaporation dehydration of isopropanol (a) operating temperature 60 °C (b) feed water content ~20 wt. % 130
Figure 6.11 Comparison of the concentration coefficients and permeation activation energies from predictions using linear moiety contributions with those from experimental data 134
Figure 7.1 Synthesis of DABN 138
Figure 7.2 Monomers of polyimides 140
Figure 7.3 ^{1}H NMR spectra (a) BABP and DABN, and (b) 6FDA-ODA-based copolyimides 143
Figure 7.4 FTIR spectra of 6FDA-ODA-based copolyimides 144
Figure 7.5 TGA and DTG curves of polyimides 146
Figure 7.6 Permeance ratios of gas pairs for membranes at different pressures 149
Figure 7.7 Comparison of experimental permeance ratios with the predicted values for polyimide membranes 151
Figure 7.8 Permeate water contents of polyimide membranes in pervaporation dehydration of isopropanol 152
Figure 7.9 Comparison of concentration coefficients and permeation activation energies from predictions with those from experimental data 155
Figure 8.1 Monomers of 6FDA-MDA-based polyimides 158
Figure 8.2 FTIR spectra of polyimides 161
Figure 8.3 ^{1}H NMR spectra of polyimides 162

Figure 8.4 TGA and DTG curves of polyimides 163
Figure 8.5 Permeance ratios of gas pairs for membranes at different pressures 168
Figure 8.6 Permeate water contents in pervaporation dehydration of isopropanol with different feed water contents at 60 °C 169
Figure 8.7 Permeate water contents in pervaporation dehydration of isopropanol with the water content of ~20 wt. % 171
Figure 9.1 Chemical structures of monomers 177
Figure 9.2 FTIR spectra of polyimides 179
Figure 9.3 ^{1}H NMR of BPADA-MDA 180
Figure 9.4 ^{1}H NMR spectra of BPADA-based polyimides 181
Figure 9.5 TGA (a) and DTG (b) curves of BPADA-based polyimides 183
Figure 9.6 Permeation flux and permeate water contents for pervaporation dehydration of isopropanol at 60 °C 186
Figure 9.7 Total flux and permeate water contents for pervaporation with feed water contents of ~20 wt. % 189

List of Tables

Table 2.1 Comparison of various membrane separation processes 9
Table 2.2 PVA membranes for pervaporation dehydration of organics 16
Table 2.3 PVA membranes for pervaporation separation of organic mixtures 17
Table 2.4 Chitosan membranes for pervaporation dehydration of organics 18
Table 2.5 Chitosan membranes for pervaporation separation of organic mixtures 19
Table 2.6 Polyimide membranes for pervaporation separation of organic mixtures 26
Table 2.7 Polyimide membranes for pervaporation extraction of phenol and VOCs 27
Table 2.8 Properties of common gas molecules 29
Table 2.9 Modifications of polyimides for gas separation membranes 32
Table 3.1 Membrane formation and crosslinking conditions 37
Table 3.2 Relative integration of absorption peaks and estimated degrees of crosslinking 45
Table 3.3 T_m onset temperature from DSC and weight changes of materials from TGA 49
Table 3.4 Peak values of DTG 51
Table 3.5 Activation energies of pure water permeation and water/isopropanol permeation 53
Table 3.6 Comparison of pervaporation performance of PVA-3TMC with those of other PVA crosslinked membranes for water/isopropanol mixtures at 60 °C 58
Table 4.1 Parameters calculated for sorption in water and sorption in water/isopropanol at different temperatures 65
Table 4.2 Permeation activation energies in the heating/cooling runs, for water permeation and for total flux and water/isopropanol individual flux 72
Table 5.1 Crosslinking time and dry thicknesses of membranes 82
Table 5.2 Thermal analysis data 88
Table 5.3 Apparent activation energies for thermal decomposition and pervaporation 89
Table 6.1 6FDA-ODA copolyimides and their molecular weights 111
Table 6.2 Characteristic temperatures from DSC, TGA and DTG 118
Table 6.3 Contact angles of liquids on polyimide membranes at room temperature 120
Table 6.4 Surface free energy components (in mJ/m^2) of liquids used in measurement of contact angles at room temperature 121
Table 6.5 Surface free energy components (mJ/m^2) and membrane-water interfacial free energies (mJ/m^2) of polyimides at room temperature 122
Table 6.6 Gas separation properties of polyimide membranes at room temperature 123

Table 6.7 Contribution of monomer moieties to the membrane selectivity 127
Table 6.8 Concentration coefficients and permeation activation energies for pervaporation 132
Table 6.9 Moiety contributions to concentration coefficients and permeation activation energies ... 133
Table 7.1 6FDA-ODA copolyimides and molecular weights 139
Table 7.2 Characteristic temperatures from DSC, TGA and DTG..... 145
Table 7.3 Contact angles of liquids on polyimide membranes at room temperature 147
Table 7.4 Surface free energy components (mJ/m^2) and membrane-water interfacial free energies (mJ/m^2) of polyimides at room temperature..... 147
Table 7.5 Gas separation properties of polyimide membranes at room temperature 150
Table 7.6 Contributions of monomer moieties to permeance ratios..... 151
Table 7.7 Concentration coefficients and permeation activation energies for pervaporation 154
Table 7.8 Moiety contributions to concentration coefficients and permeation activation energies ... 154
Table 8.1 Polyimides and molecular weights..... 159
Table 8.2 Characteristic temperatures from DSC, TGA and DTG..... 164
Table 8.3 Contact angles of liquids on polyimide membranes at room temperature 165
Table 8.4 Surface free energy components (in mJ/m^2) of liquids used in measurement of contact angles at room temperature 165
Table 8.5 Gas separation properties of polyimide membranes at room temperature 167
Table 8.6 Contributions of monomer moieties to permeance ratios..... 168
Table 8.7 Concentration coefficients and permeation activation energies for pervaporation 172
Table 8.8 Moiety contributions to concentration coefficients and permeation activation energies ... 172
Table 9.1 Synthesis of BPADA copolyimides and molecular weights 176
Table 9.2 Characteristic temperatures from DSC, TGA and DTG and estimated apparent activation energies for thermal decomposition 182
Table 9.3 Contact angles of liquids on polyimide membranes at room temperature 184
Table 9.4 Surface free energy components (mJ/m^2) and membrane-water interfacial free energies (mJ/m^2) of polyimides at room temperature..... 184
Table 9.5 Comparison of concentration coefficients and permeation activation energies for BPADA-based membranes and 6FDA-based membranes..... 187
Table 9.6 Moiety contributions to concentration coefficients and permeation activation energies for total flux and water flux 188

Chapter 1
Introduction

1.1 Background

Compared with traditional separation processes, such as distillation, extraction and filtration, membrane technology is a relatively new method that has been developed in the past few decades, but it has been widely adopted in many industries. The membrane processes have the following distinguishing characteristics [Mulder 1991]:

1) Continuity and simplicity of the processes,
2) Adjustability of the separation properties,
3) Feasibility of incorporation into hybrid processes,
4) Low energy consumption and moderate operating conditions.

Developments in membrane formation techniques and materials science accelerate the research and applications of membrane technology. Now commercial membrane applications have successfully displaced some conventional processes, and membrane technology has become an indispensable component in many industrial fields and our daily life.

Figure 1.1 shows a schematic membrane process [Mulder 1991; Baker 2004]. Separation membranes are located between the feed side and the permeate side. In most membrane processes, such as gas separation, reverse osmosis and ultrafiltration, both the feed and the permeate sides are in the same phases, gas or liquid, while in pervaporation, the liquid feed is separated into vaporous permeates with the aid of vacuum or a purge gas in the downstream side.

Pervaporation has become a very important technique to separate azeotropes, close-boiling mixtures, and recover volatile organic chemicals from liquid mixtures, and now it has emerged as a good choice for separating heat sensitive products. The phenomenon of pervaporation was first discovered in 1917 by Kober [1995], but no extensive research was carried out until in the 1950s by Binning *et al.* [1961]. In 1982, the first industrial application of the pervaporation process was launched by Gesellschaft für Trenntechnik (GFT) mbH of Germany (now acquired by Sulzer Chemtech) for dehydration of ethanol using PVA/PAN composite membranes [Huang 1990]. Currently, pervaporation membranes and processes are being studied in many laboratories and companies, such as Sulzer Chemtech, MTR, Exxon and Texaco [Moon 2000; Baker 2004].

In pervaporation processes with functional polymer membranes, the non-porous dense membranes are essential. By choosing proper membranes, pervaporation has great advantages as an alternative separation method in the following separation tasks:

1) Dehydration of organic solvents,
2) Removal of organics from water,
3) Separation of organic liquids.

Non-porous dense membranes can also be applied in other separation processes such as gas separation. Furthermore, both gas separation and pervaporation can be interpreted with the solution-diffusion mechanism for mass transport in membranes.

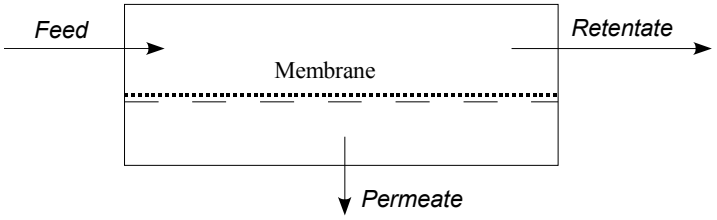

Figure 1.1 Schematic membrane separation process

Gas permeation was first studied by Graham in 1860s, but it was not until the 1940s that Knudsen diffusion exploited in large scale use to separate $U^{235}F_6$ from $U^{238}F_6$ with finely microporous metal membranes [Hwang and Kammermeyer 1984; Baker 2004]. Nevertheless, commercial gas separation membranes are based on the development of polymer membranes. In 1980, Permea (now Air Products and Chemicals) launched its hydrogen-separating Prism® membrane, after which cellulose acetate membranes for CO_2/CH_4 were developed by Cynara (now Natco), Separex (now UOP) and GMS (now Kvaerner). Later, Generon (now MG) introduced a membrane system to separate nitrogen from air, followed by the competitive membranes from Dow, Ube and Du Pont [Baker 2002]. Applications of membrane gas separation technology keep expanding, and further growth is likely to continue for the next decade [Baker 2004]. On the basis of the growing industrial demand and new developments in polymer materials and membrane technologies, the next generation of membrane processes should maintain attractive economics associated with the current polymer-based membranes, while greatly extending performance properties [Koros 2002].

Studies on the relationship between polymer materials and gas separation properties were carried out to understand membrane permeability and selectivity in order to maximize the membrane

efficiency and to provide directions for new membranes or new processes [Stern *et al.* 1989; Robeson 1994; Hirayama 1996a; 1996b; Li *et al.* 1996; Maier 1998; Powell and Qiao 2006]. Based on the experimental structure-property results, some mathematical methods were developed to predict the permeability of polymers to gases [Salame 1986; Jia and Xu 1991; Park and Paul 1997; Robeson *et al.* 1997; Yampolskii *et al.* 2006].

As mentioned before, pervaporation and gas separation, where non-porous membranes are used, follow the same mass transport mechanism. Therefore, it is possible to develop a theoretical or empirical method from the structure-property relationship, to interpret these results or predict membrane properties for both pervaporation and gas separation processes.

1.2 Purpose of the Study

1.2.1 Dehydration of Isopropanol

Isopropanol is widely used as a disinfectant. A large amount of high purity isopropanol is always in demand for cleansing in industries, especially in the electronics industry. However, isopropanol and water form an azeotrope (water ~12.6 wt. % at 80.3 °C, 101325 Pa) in common distillation. The liquid-vapor equilibrium data are shown in Figure 1.2 [Wikipedia 2007, Sada and Morisue 1975]. Separation/purification of isopropanol from water by traditional distillation is difficult, and alternative methods are needed.

Because of its outstanding characteristics, pervaporation has become one of the promising techniques that can be used for dehydration of isopropanol. This thesis, therefore, is aimed at developing new pervaporation membranes and also trying to understand the relationship between membrane materials and separation performance.

1.2.2 Conventional Hydrophilic Membranes for Pervaporation

Hydrophilic membranes are required for pervaporation dehydration of isopropanol. Poly(vinyl alcohol) and chitosan have been selected because of their hydrophilicity and good film forming properties. However, these materials must be crosslinked to prevent membrane from excessive swelling, so as to attain long-term stability.

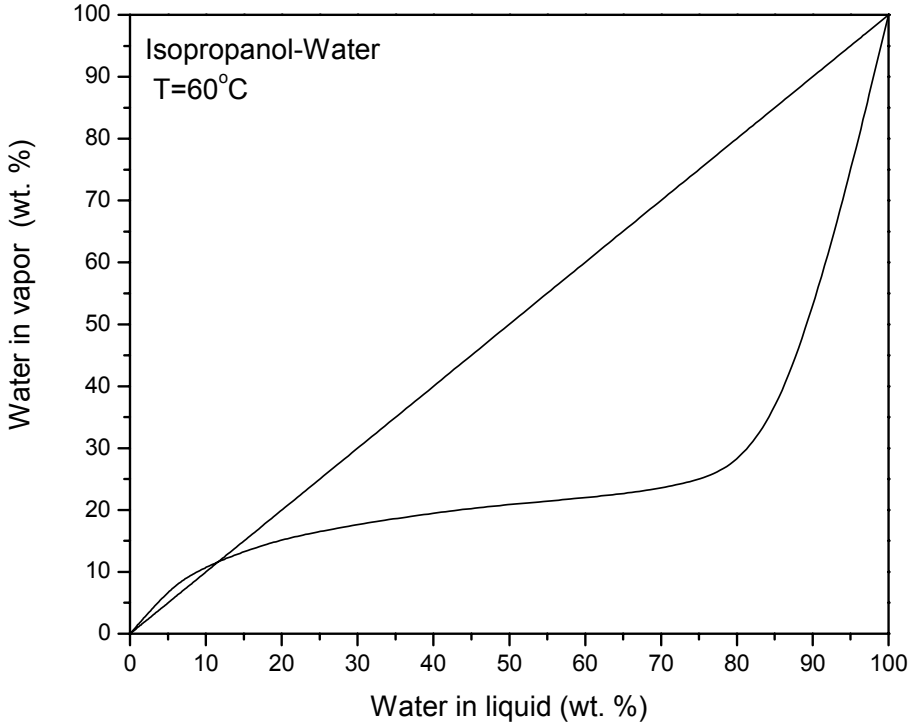

Figure 1.2 Vapor-liquid equilibrium of isopropanol-water at 60 °C

Therefore, in this thesis, interfacial crosslinking with trimesoyl chloride was carried out, and the membranes were investigated for pervaporation dehydration of isopropanol. The gas permeation properties of the crosslinked chitosan membranes were also studied.

1.2.3 High-Performance Polyimides in Membrane Separation

On the other hand, polyimides, a category of high performance polymers, have attracted interest because of their excellent chemical resistance and outstanding thermal stabilities. They can be used under harsh conditions where the conventional polymer membranes cannot work well. Since polyimides are hydrophilic materials because of the imide structures, they are expected to work for pervaporation dehydration of organic solvents.

However, there comes a problem: polyimides are glassy polymers, and the permeability is low. Therefore, polyimides must be prepared with tailored chemical structures to obtain a high permselectivity. But only a little work has been carried out for their gas permeation applications. To

find out a relationship between the chemical structure and pervaporation properties, a study on the gas separation properties was done first in this thesis. Since membrane gas separation is a promising technique for removal of greenhouse gases and purification of hydrogen and oxygen in the chemical and fuel industries, it was thus decided to study the gas separation properties in this thesis as well.

Based on the structure-property relationship derived from gas separation properties, pervaporation properties of the polyimide membranes were studied further. An attempt was made to correlate the chemical structure of polyimides and the permeability of the membranes.

1.2.4 Structure of the Research

In this thesis, various membrane materials were investigated for applications in pervaporation and gas separation. Figure 1.3 illustrates the structure of the research. As a result, the thesis work consists of two parts: one focuses on trimesoyl chloride crosslinked poly(vinyl alcohol) and chitosan membranes and their applications in pervaporation and gas separation, and the other on synthesis of polyimides and investigation of their gas separation and pervaporation properties.

1.3 Research Objectives

Chemical crosslinking of the existing polymers (i.e. poly(vinyl alcohol) and chitosan) and synthesis of new polymers (polyimides) as well as their applications in pervaporation and gas separation are the main concerns of this thesis, as shown in Figure 1.3. The selection of pervaporation membrane materials, preparation/modification of the membranes, and the applications of dense membranes in gas separations are all covered in this thesis.

To systematically study the relationship between polymer materials and their separation performances, modified conventional polymer materials, poly(vinyl alcohol) and chitosan, and synthetic high-performance copolyimides were developed and explored. Accordingly the research objectives are:

1) Modified poly(vinyl alcohol) membranes: Preparation, characterization and investigation of sorption properties of trimesoyl chloride crosslinked poly(vinyl alcohol) membranes for pervaporation dehydration of isopropanol

2) Modified chitosan membranes: Preparation and characterization of trimesoyl chloride crosslinked chitosan membranes for CO_2/N_2 separation and pervaporation dehydration of isopropanol.

3) Synthetic polyimide membranes: Synthesis and characterization of polyimides from 6FDA and BPADA; Investigation of gas separation and pervaporation properties of the polyimide membranes; Development of empirical methods to interpret separation behaviors based on the chemical structures of the polyimides.

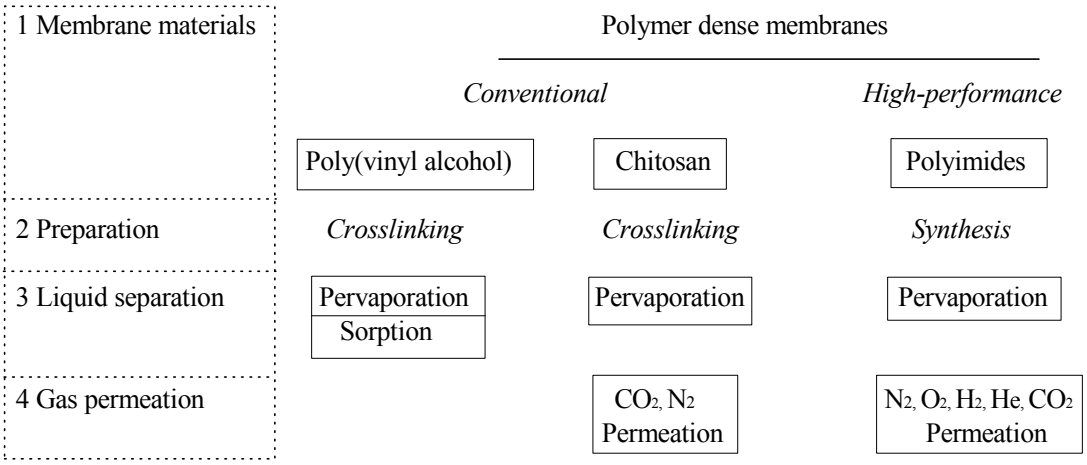

Figure 1.3 The structure of the research

1.4 Outline of the Thesis

Chapter 1 presents an overview of pervaporation and gas separation technologies and describes the objectives of the research.

Chapter 2 reviews the literature on pervaporation membranes and processes as well as the applications of dense membranes in gas separation processes. Both the conventional poly(vinyl alcohol) and chitosan membranes and the high-performance polyimide membranes are surveyed in pervaporation applications, and a brief study on the applications of polyimide dense membranes in gas separations is also made in the review.

Part I deals with trimesoyl chloride crosslinked poly(vinyl alcohol) and chitosan membranes for pervaporation and gas separation. The preparation, characterization and pervaporation properties of trimesoyl chloride crosslinked poly(vinyl alcohol) membranes for dehydration of isopropanol are described in Chapter 3. The sorption properties and pervaporation behavior of the trimesoyl chloride

crosslinked poly(vinyl alcohol) membranes under different operating conditions for dehydration of isopropanol are presented in Chapter 4. Chapter 5 demonstrates the preparation of interfacially crosslinked chitosan membranes using trimesoyl chloride, and studies are conducted on their CO_2/N_2 separation properties and pervaporation performances in dehydration of isopropanol.

Part II is concerned with synthetic polyimide membranes for pervaporation and gas separation. 4,4'-(hexafluoroisopropylidene) diphthalic anhydride (6FDA) - 4-aminophenyl ether (ODA)-based copolyimides are synthesized and characterized in Chapters 6 and 7, and their gas separation and pervaporation properties are investigated. Chapter 6 focuses on the effects of the functional groups of polyimides on the separation performances, whereas Chapter 7 places an emphasis on the relationship between monomer structures and separation properties. In Chapter 8, synthetic 6FDA - 4,4'-methylenedianiline (MDA)-based copolyimide membranes are prepared for pervaporation dehydration of isopropanol and for gas separations, and introduction of diamine/dianhydride third monomers in the polyimide main chains is supposed to account for the differences of the permeation properties. In Chapter 9, pervaporation membranes derived from 2,2-bis[4-(3,4-dicarboxyphenoxy) phenyl]propane dianhydride (BPADA)-based copolyimides are developed for dehydration of isopropanol. Comparison is made between the pervaporation performances of BPADA-based membranes and 6FDA-based membranes. A linear moiety contribution method is developed from the experimental data of pervaporation and gas separations in Chapters 6-8, and the results are utilized to interpret the separation properties of 6FDA-based copolyimide membranes (in Chapters 6-8), as well as the pervaporation performance of BPADA-based copolyimide membranes (in Chapter 9).

Chapter 10 summarizes the original contributions of the thesis and presents recommendations for future work.

Chapter 2
Literature Review

2.1 Separation Principles

In separation technologies, membranes are defined as the semi-permeable inter-phase media between two bulk phases [Paul and Yampol'skii 2000]. A membrane process allows selective and controlled transfer of species from one bulk phase to the other. The permeability and selectivity define the characteristics of separation membranes. Generally speaking, components in a mixture are separated by membranes based on the principles as follows [Huang 1990]:

1) Separation occurs because of size/steric effects that are related with macroscopic pores in porous membranes or molecular level interspace between macromolecules in non-porous membranes. The size difference of the two components results in the difference in flow rates, components with large sizes diffusing with more resistance than those with smaller steric factors. A good selectivity can be achieved for mixtures of components with dissimilar steric factors.

2) Separation properties are related with the interactions between the membrane materials and the components to be separated. In non-porous membranes, these factors are often dominant in controlling the separation performances.

Mass transport in a membrane occurs when there exists a driving force or a potential difference across the membrane [Timashev and Kemp 1991]. Table 2.1 shows the driving forces and separation mechanisms for different membrane processes [Moon 2000; Matsuura 1994; Mulder 1991]. Mass transport in non-porous membranes is complicated, but gas separation and pervaporation share many characteristics.

2.2 Mass Transport in Pervaporation Membranes

Different from other membrane processes, pervaporation occurs between two different phases in the feed and permeate sides. Some mass transport models have been developed to describe pervaporation processes [Feng and Huang 1997; Shao 2003]. There is not a fully accepted theory for pervaporation, but the following models give some explanation of specific properties.

Table 2.1 Comparison of various membrane separation processes

Membrane processes	Phases of feed / permeate	Driving forces	Separation mechanism
Microfiltration	Liquid / Liquid	Hydrostatic pressure	Sieving
Ultrafiltration	Liquid / Liquid	Hydrostatic pressure	Sieving
Hyperfiltration	Liquid / Liquid	Effective pressure	Preferential sorption and capillary flow
Dialysis	Liquid / Liquid	Concentration gradient	Sieving and hindered diffusion
Electrodialysis	Liquid / Liquid	Electrical potential gradient	Counter-ion transport
Reverse osmosis	Liquid / Liquid	Hydrostatic pressure	Preferential sorption and capillary flow
Pervaporation	Liquid / Vapor	Chemical potential gradient	Solution-diffusion
Vapor permeation	Vapor / Vapor	Chemical potential gradient	Solution-diffusion
Gas separation	Gas / Gas	Partial pressure difference	Solution-diffusion and sieving

2.2.1 Solution-Diffusion Model

The solution-diffusion model is the most widely accepted transport mechanism for many membrane processes, such as reverse osmosis, gas separation and pervaporation [Wijmans and Baker 1995; Baker 2004]. The earliest application of the solution-diffusion model in pervaporation was proposed by Binning *et al.* [1961], and he suggested that the selectivity took place in a boundary layer between the liquid zone and the gas zone in the membrane. Later, many researchers tried to interpret pervaporation processes based on the solution-diffusion model, and this model is now widely accepted. According to this model, the mass transport can be divided into three steps, as shown in Figure 2.1:

1) Sorption of liquids into the membrane at the feed side,
2) Diffusion of the sorbed components through the membrane,
3) Desorption/evaporation of the sorbed components at the permeate side.

Vaporization at the permeate side of the membrane is generally considered to be a fast and non-selective step if the partial pressure is kept low, *i.e.* far less than the saturated vapor pressure of the permeates [Ho and Sirkar 1992]. The selectivity and permeability of a pervaporation membrane

mainly depend on the first two steps, that is, the solubility and diffusivity of the components in the membrane.

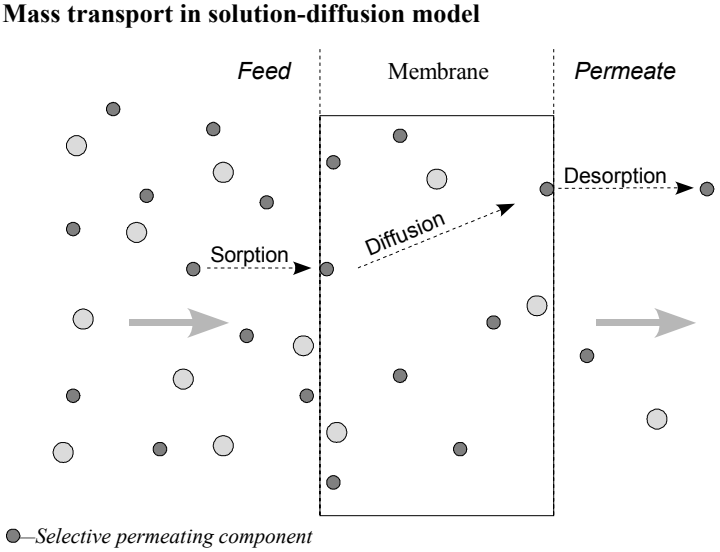

Figure 2.1 Solution diffusion model for mass transport in membranes

For a component i in a pervaporation system, the permeability can be expressed as follows:

$$P_i = S_i \cdot D_i \tag{2.1}$$

where P_i is the permeability coefficient, S_i is the solubility coefficient, and D_i is the diffusivity coefficient.

The transport equation for pervaporation can be formulated on the basis of Fick's law (Equation 2.2) using different expressions of concentration dependencies of solubility and diffusivity [Baker 2004].

$$J_i = -D_i \frac{dc_i}{dx} \tag{2.2}$$

where J_i is the flux of component i, dc_i / dx is the concentration gradient of component i, and D_i is the diffusion coefficient.

Lee [1975] attempted to compare the mass transport in pervaporation with those of reverse osmosis and gas separation based on the solution-diffusion model under isothermal conditions. In his approach, the gradient of the chemical potential across the membrane is considered to be the driving force for the mass transfer.

$$d\mu_i = RTd\ln(\gamma_i n_i) + \upsilon_i dp \tag{2.3}$$

where μ_i is the chemical potential of component i, γ_i is the activity coefficient, n_i is the mole fraction, and υ_i is the molar volume of component i. The pressure p across the membrane is considered to be constant, and the pressure falls discontinuously at the surface of the membrane at the permeate side. With this assumption, $\upsilon_i dp$ can be ignored, and integration yields the flux equation, which is in the same form as in reverse osmosis.

$$J_i = -D_i \frac{c_i^o - c_i^l}{l} \tag{2.4}$$

where l is the thickness of the membrane, and $(c_i^o - c_i^l)$ is the concentration difference of component i across the membrane.

Blume *et al.* [1990] considered the separation performance of a pervaporation process as a combination of an evaporation step and a diffusion step. Pervaporation is assumed to be a diffusion-controlled process, in which the fluids on either side of the membrane are in equilibrium with their respective surfaces. To facilitate the mathematical treatment and to understand the difference between pervaporation and evaporation, the overall separation is considered to be the overall contribution of an evaporation step and a membrane separation step.

$$\beta_{pv} = \beta_{evap}\beta_{mem} \tag{2.5}$$

where β_{pv}, β_{evap} and β_{mem} are the separation factors of pervaporation, evaporation and the membrane, respectively.

When the permeate pressure is zero (e.g. a high vacuum is maintained on the permeate side, or the permeate is continuously condensed at a very low temperature), the equation becomes:

$$\beta_{pv} = \beta_{evap}\alpha_{mem} \tag{2.6}$$

where α_{mem} is the intrinsic selectivity of the membrane materials.

2.2.2 Pore-Flow Model

The pore-flow model for pervaporation was first proposed by Sourirajan *et al.* [Matsuura 1994], and Okada *et al.* [1991] used this model to interpret experimental observations in pervaporation.

In the pore-flow model, it is assumed that there are a bundle of straight cylindrical pores of specific lengths penetrating across the active surface layer of the membrane, and all pores are in an isothermal condition [Matsuura 1994]. The mass transport involves

1) Liquid transport from the pore inlet to the liquid-vapor phase boundary,

2) Evaporation at the phase boundary,

3) Vapor transport from the phase boundary to the pore outlet.

The main difference between the solution-diffusion model and the pore-flow model is the phase change location in the membrane. In the pore-flow model, as shown in Figure 2.2, the phase change occurs at a certain distance from the membrane surface contacting with the liquid feed, and accordingly the transport mechanism changes from liquid permeation to vapor permeation at the liquid-vapor boundary [Matsuura 1994].

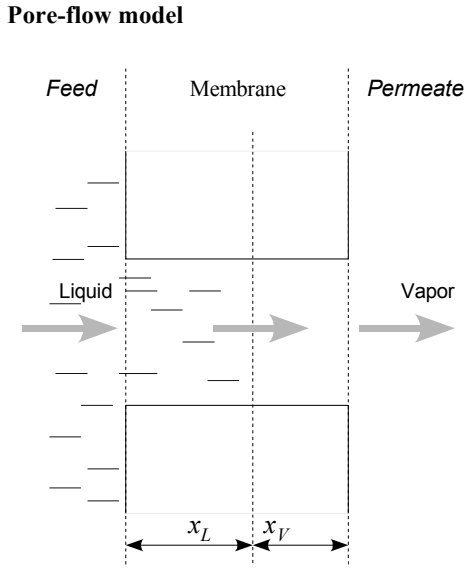

Figure 2.2 Schematic description of pore-flow model

The pore-flow model is on the basis of the presence of pores in the membranes, so whether the pores really exist or how small the pore size is remains hard to answer. Nonetheless, the theoretical calculations based on the pore flow model have been shown to be able to reproduce semi-empirical features of the experimental results [Matsuura 1994].

2.2.3 Carrier Transport Mechanism

The basic idea of the carrier transport mechanism for pervaporation comes from biological membranes consisting of polypeptides, and is based on the similarity of the molecular interactions between the peptides and the functional groups in synthetic polymers [Moon 2000]. Membranes with carriers are classified into two categories [Shimidzu and Yoshikawa 1991]: Non-fixed carrier membrane (Liquid membrane) and fixed carrier membrane.

Figure 2.3 shows the mass transport in non-fixed carrier membranes and fixed carrier membranes. The transport energy in the fixed carrier membranes is much higher than that in the non-fixed carrier membranes, since adsorption and desorption are repeated continuously when a permeating component forms a complex with a carrier in the membrane. On the other hand, once a component forms a complex with a carrier in a non-fixed carrier membrane, the other component can move only after one carrier is released from the former complex formed previously, for which high selectivity is achieved.

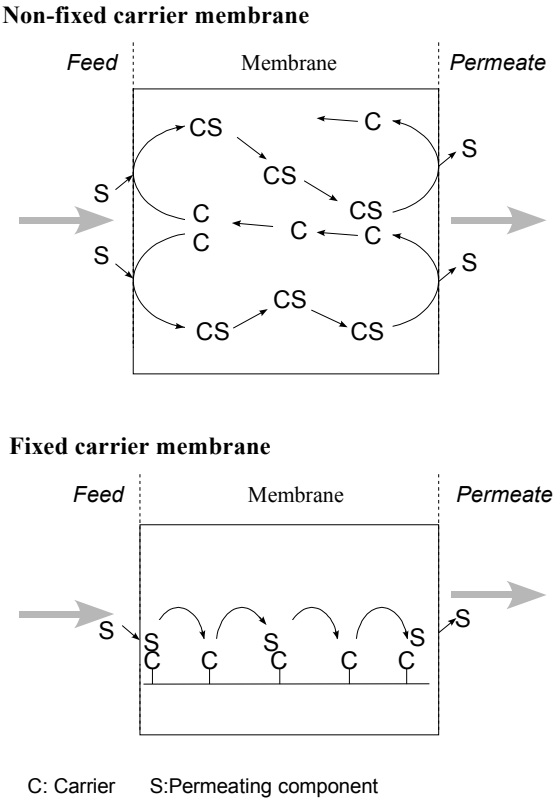

Figure 2.3 Schematic description of mass transport by the carrier transport mechanism

2.3 Polymer Materials for Pervaporation

Potentially plastics and rubbers, including homopolymers, copolymers and polymer blends, can be used as membrane materials in pervaporation processes [Huang 1990]. Besides the mechanical properties, chemical and thermal stabilities, high permeability and high selectivity are the important factors that should be considered when choosing polymer materials for membranes. Among these factors, the selectivity should be emphasized over the others, because low separation factors cannot be compensated by other properties [Huang 1990]. A high permeation flux and a high separation factor are always desired for industrial applications.

The properties of a pervaporation membrane are determined by the chemical structure and physical properties of the membrane, and the interactions between the membrane material and the permeant. Several methods have been developed for the selection of pervaporation membrane materials [Feng and Huang 1997]:

1) Solubility parameter approach [Matsuura 1994; Mulder 1991],
2) Surface thermodynamics approach [Van Oss *et al.* 1983; Lee *et al.* 1989],
3) Polarity approach [Shimidzu and Yoshikawa 1991],
4) Chromatographic approach [Matsuura 1994; Pawlish *et al.* 1987, 1988],
5) Contact angle approach [Lukas *et al.* 1997; Nabe *et al.* 1997].

From a material point of view, there are three strategies for developing new membranes:

1) Blends of polymers or other materials [Huang and Shieh 1998; Svang-Ariyaskul *et al.* 2006],

2) Chemical or physical modification of polymer materials or membranes [Wang *et al.* 1998; Rhim *et al.* 2002; Pithan *et al.* 2002b],

3) Synthesis of new polymers based on structure-property relationships and molecular design principles [Schauer *et al.* 1996; Okamoto *et al.* 1999; Fang *et al.* 2000].

For pervaporation dehydration of organic liquids, hydrophilic polymers are the most suitable membrane materials. The hydrophilicity of a polymer is caused by the functional groups that are able to interact with water molecules by H-bonding or dipole-dipole interactions. Water normally permeates through hydrophilic membranes preferentially. Poly(vinyl alcohol), poly(acrylic acid), poly(vinyl pyrrolidone), chitosan and polyelectrolytes are the hydrophilic polymers commonly used.

For the removal of organics from water, rubbery polymers are favorable. Organic components can preferentially penetrate rubbery polymers, and the membranes show relatively high permeation flux.

However, for separation of organic liquids, the criteria for selecting proper polymer materials are not very clear yet. Both rubbery polymers and glassy polymers have been used in research.

2.3.1 Conventional Pervaporation Membranes

2.3.1.1 Poly(vinyl alcohol) Pervaporation Membranes

Poly(vinyl alcohol) (PVA) is one of the most important water-soluble vinyl polymers, prepared by partial or complete hydrolysis of poly(vinyl acetate) [Chiellini 2003]. The hydroxyl groups in PVA can form strong hydrogen bonds between intra- and intermolecular hydroxyl groups, which causes PVA to show a high affinity to water [Finch 1973]. The solubility parameters of PVA and the affinity to solvents are shown in Appendix A. Therefore, in pervaporation, PVA is mainly used for dehydration of organic solvents. To be used as membranes, PVA is usually modified before use to attain long-term stability [Finch 1973].

The first commercial composite membrane, crosslinked poly(vinyl alcohol) on a microporous polyacrylonitrile (PAN) support, was developed by GFT in 1982 to dehydrate ethanol/water mixtures [Huang 1990; Volkov 1994]. Though continuous efforts are made to develop new membranes and to explore new separation applications, PVA is still attracting significant interest from researchers because of its excellent film forming property and hydrophilicity.

Lee and Hong [1997] investigated the relationship between the degree of hydrolysis of PVA membranes and the pervaporation performance for separation of isopropanol/water mixtures. Upadhyay and Bhat [2005] modified PVA membranes with lithium chloride to investigate the effect of addition of alkali salt on dehydration of isopropanol, and it was shown that the PVA membrane became amorphous by addition of lithium chloride, and the separation performance was also affected.

Rhim *et al.* [1998] crosslinked PVA membranes with sulfosuccinic acid (containing $–SO_3H$), and investigated the effect of the crosslinking density on the pervaporation properties in dehydration of water-alcohol mixtures. The performance for water/methanol separation is not good due to the existence of sulfonic acid groups, but the membranes containing 7 wt. % sulf-succinic acid showed good selectivity for water-ethanol mixtures. Extensive research was conducted on the pervaporation properties of the metal-ion-exchanged PVA/sulfosuccinic acid membranes [Rhim *et al.* 2002]. Peters *et al.* [2006] dip-coated PVA on ceramic hollow fiber supports, and crosslinked the ultra-thin layer of PVA with maleic anhydride for dehydration of alcohols.

Nam *et al.* [1999] prepared carboxymethylated PVA composite membranes for dehydration of

isopropanol: PVA was treated with NaOH, followed by adding monochloroacetic acid, and the dense PVA layer of the composite membranes was crosslinked with glutaraldehyde.

In addition to dehydration of alcohols, PVA membranes were also used for dehydration of other organic compounds, as listed in Table 2.2. Hybrid separation processes for the dehydration of organics using PVA membranes have also been reported [Sommer and Melin 2004; Liu *et al.* 2001]. Table 2.3 summarizes the organic mixtures that can be separated by pervaporation using PVA membranes.

Table 2.2 PVA membranes for pervaporation dehydration of organics

Organics	PVA Membranes	References
Acetic acid	PERVAP® 2201 (Sulzer Chemtech)	Van Baelen *et al.* [2005]
	PVA membranes crosslinked with glutaraldehyde (GA)	Yeom and Lee [1996]
	PVA membranes crosslinked with GA and formaldehyde	Durmaz-Hilmioglu *et al.* [2001]
	PVA membranes crosslinked with malic acid	Isiklan and Sanli [2005]
Benzene	PVA/PAN composite membranes crosslinked with formaldehyde, GA and maleic acid	Li *et al.* [2002]
Butanone, butyric acid, dioxane,	PVA/PAN composite membranes (Mitsui Shipping and building, Japan)	Shaban [1996]
ε-Caprolactam	Thermally crosslinked PVA dense membranes	Zhang *et al.* [2006]
	PVA/PAN and PVA/PES composite membranes crosslinked with GA	Zhang *et al.* [2007a]
	PVA/PAN and PVA/CA composite membranes	Cai [2006]
Methacrylic acid, 2,2,2-trifluoroethyl methacrylate	PVA/PES composite membranes crosslinked with GA	Ahn *et al.* [2005]

2.3.1.2 Chitosan Pervaporation Membranes

Chitosan, poly[β(1→4)-2-amino-2-deoxy-D-glucopyranose], is a linear polysaccharide obtained by deacetylation of chitin, poly[β(1→4)-2-acetamido-2-deoxy-D-glucopyranose]. Chitin exists naturally in many creatures such as crustaceans and insects, and is industrially produced from the shells of marine crustaceans. The poor solubility and low reactivity limit the direct use of chitin. However

chitosan, with a better solubility due to the protonation of amino groups, has found more applications and usages.

Table 2.3 PVA membranes for pervaporation separation of organic mixtures

Organic Mixtures	PVA Membranes	References
Benzene / Cyclohexane	PERVAP® 2200 (Sulzer Chemtech)	Sarkhel *et al.* [2003]
	Homogeneous and asymmetric PVA membranes	Yamasaki *et al.* [1997]
Benzene / Isopropanol	Homogeneous PVA membranes	Mandal and Pangarkar [2003]
Benzene / *n*-Hexane	Homogeneous and asymmetric PVA membranes	Yamasaki *et al.* [1997]
MTBE / Methanol	PVA/CA and PVA/PAN composite membranes	Cai *et al.* [2001]
Toluene / Isopropanol	Homogeneous PVA membranes	Mandal and Pangarkar [2003]

Chitosan has a structure (Figure 2.4) similar to that of cellulose, and the difference lies in the substitution of 2-hydroxy group (in cellulose) by the 2-amino group (in chitosan). The solubility of chitosan guarantees the processability. In addition to the anti-bacterial property, chitosan is widely used as a functional chemical in biological and biomedical areas, as well as a food additive [Krajewska 2005]. On the other hand, chitosan has good biocompatibility and biodegradability [Krajewska 2005], and has also been used as a functional polymer material in membrane technologies.

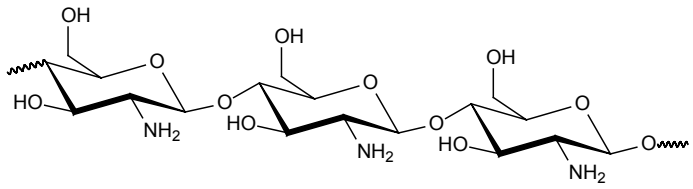

Figure 2.4 Chemical structure of chitosan

Chitosan bears two types of functional groups, –OH groups and $–NH_2$ groups, from which hydrophilicity and the potential grafting/crosslinking sites are formed. The solubility parameters of chitosan and the affinity to solvents are shown in Appendix A. Therefore, in pervaporation, chitosan membranes are mainly used as hydrophilic membranes for dehydration of organic solvents.

As shown in Table 2.4, chitosan membranes can be crosslinked with various crosslinking agents for the improved chemical stability. The $-NH_2$ groups in chitosan can be further modified by reacting with propylene oxide [Wang *et al.* 1998], glyoxylate acid monohydrate [Shen *et al.* 2007], and maleic anhydride [Zhang *et al.* 2007b]. These modifications influence the permeation flux and selectivity.

Table 2.4 Chitosan membranes for pervaporation dehydration of organics

Organics	Chitosan Membranes	References
Ethanol	CS/hydroxyethylcellulose composite membranes	Jiraratananon *et al.* [2002a, 2002b]
	CS membranes crosslinked with sulfuric acid	Guo *et al.* [1995], Ge *et al.* [2000]
	CS membranes crosslinked with copper ions	Wang and Shen [2000]
	CS membranes crosslinked with 3-aminopropyl triethoxysilane	Chen *et al.* [2007]
	CS crosslinked with glutaraldehyde (GA) and surface-modified with maleic anhydride	Zhang *et al.* [2007b]
Ethanol and isopropanol	Ionically surface crosslinked CS composite membranes	Lee *et al.* [1997]
Isopropanol	CS/PSF composite membranes crosslinked with GA	Huang *et al.* [1999]
	CS/PSF composite membranes crosslinked with 1,6-hexamethylene diisocyanate	Nawawi and Huang [1997]
	CS/PTFE composite membranes crosslinked with γ-(glycidyloxypropyl)trimethoxysilane	Liu *et al.* [2007]
	CS crosslinked with toluene-2,4-diisocyanate	Devi *et al.* [2005]
	CS/hydrolyzed PAN composite membranes	Wang *et al.* [1996]
	CS/CA composite hollow fiber membranes	Tsai *et al.* [2004]
	Carboxymethyl Chitosan/PSF composite hollow fiber membrane crosslinked with GA	Shen *et al.* [2007]
Isopropanol and *n*-propanol	Hydroxypropylated CS membranes crosslinked with GA and copper ions	Wang *et al.* [1998]
Ethylene glycol	CS/PSF composite membranes	Feng and Huang [1996b]
	CS/PSF composite membranes crosslinked with sulfuric acid	Nam and Lee [1999a]
tert-Butanol	CS membranes crosslinked with toluene-2,4-diisocyanate	Biduru *et al.* [2005]
Dimethylhydrazine	CS membranes crosslinked with GA	Sridhar *et al.* [2001]

Chitosan membranes were also used for the separation of organic mixtures. As shown in Table 2.5, Dimethyl carbonate (DMC)/methanol/water and methyl tertiary-butyl ether (MTBE)/methanol azeotropic mixtures can be broken by pervaporation. Huang *et al.* [2000] made efforts to partially *N*-acetylate chitosan membranes with acetic anhydride, and the membranes could be used to separate toluene from ethanol.

Table 2.5 Chitosan membranes for pervaporation separation of organic mixtures

Organic Mixtures	Chitosan Membranes	References
DMC / Methanol / Water	Crosslinked/non-crosslinked CS membranes	Won *et al.* [2002, 2003]
MTBE / Methanol	CS/anionic surfactant complex membranes	Huang *et al.* [2001a]
	Crosslinked CS/PSF membranes modified with surfactants	Nam and Lee [1999b]
Toluene / Ethanol	*N*-acetylated CS membranes	Huang *et al.* [2000]

2.3.2 Polyimide Pervaporation Membranes

Aromatic polyimides are heterocyclic polymers having conjugated rigid structures, and they are well-known for their excellent thermal stability, mechanical properties, and chemical resistance [Adrova *et al.* 1970; Bessonov *et al.* 1987; Carraher and Swift 2002; Feger *et al.* 1989]. They are widely used in aerospace and automotive industries as high-temperature resins [Sillion *et al.* 2003].

Polyimide membranes, due to their superior physiochemical and mechanical properties, received attention from industry and academia. It is estimated that about 47 % of polyimide membranes are used in gas separation, and around 5 % in pervaporation processes [Ohya *et al.* 1996]. Some polyimide materials are commercially available in the market [Huang and Feng 1992; Zhou and Koros 2006; Qiao *et al.* 2005]. However, tailored polyimide membranes are needed to meet the requirements for specific applications, such as pervaporation and gas separation [Koros and Fleming 1993].

2.4 Polyimides for Pervaporation

2.4.1 Synthesis of Polyimides

Polyimides can be synthesized by many routes, such as aromatic nucleophilic displacement polymerization, polycondensation of tetracarboxylic acids and diamines, but commonly they are

synthesized from dianhydrides and diamines [Sokolov 1968; Mittal 1984]. In this section, only the synthesis based on polycondensation of dianhydrides and diamines is discussed. From dianhydrides and diamines, there are two ways to synthesize polyimides, namely, the two-step polymerization and the one-step polymerization.

2.4.1.1 Two-Step Synthesis of Polyimides

In the two-step method of polyimide synthesis (shown in Figure 2.5), a tetracarboxylic acid dianhydride is added to a solution of diamine in a polar and aprotic solvent (such as *N*, *N*-dimethylformamide (DMF), *N*, *N*-dimethylacetamide (DMAc), and *N*-methylpyrrolidone (NMP)) at 15–75 °C. The poly(amic acid) generated is then cyclodehydrated to form polyimide by heating at elevated temperatures or by treatment with chemical dehydrating agents. A mechanism that describes the formation of the precursor poly(amic acid) is shown in Figure 2.6 [Wilson *et al.* 1990].

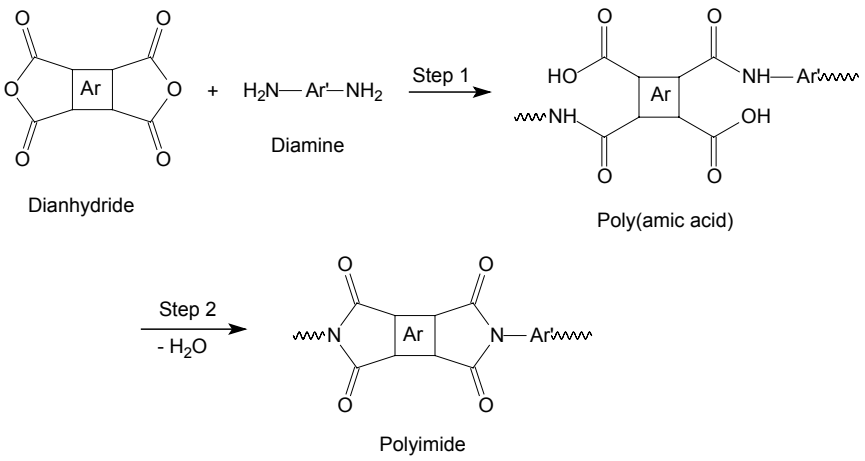

Figure 2.5 The two-step method for polyimide synthesis

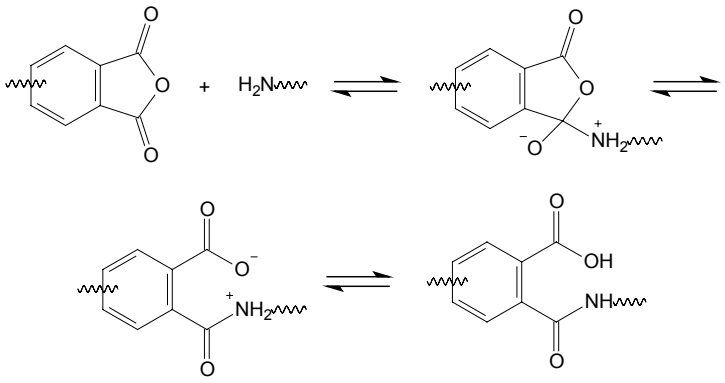

Figure 2.6 Formation of poly(amic acid)

Since polyimide is often insoluble and infusible, the polymer is usually processed in the form of poly(amic acid), which can be thermally imidized [Sroog *et al.* 1965].

1) Thermal imidization of poly(amic acid)s: This involves heating the poly(amic acid) in the solid state to 250–400 °C. A poly(amic acid) solution may be used to cast a film, form a coating layer or form a fiber. Two possible reaction pathways for this imidization process are shown in Figure 2.7 [Wilson *et al.* 1990].

2) Chemical imidization of poly(amic acid)s: Poly(amic acid)s are converted to the corresponding polyimides at ambient temperature by treatment with mixtures of aliphatic carboxylic acid dianhydrides with tertiary amines as catalysts. Acetic anhydride and pyridine or triethyl amine are normally used. The mechanism of chemical imidization is shown in Figure 2.8 [Wilson *et al.* 1990].

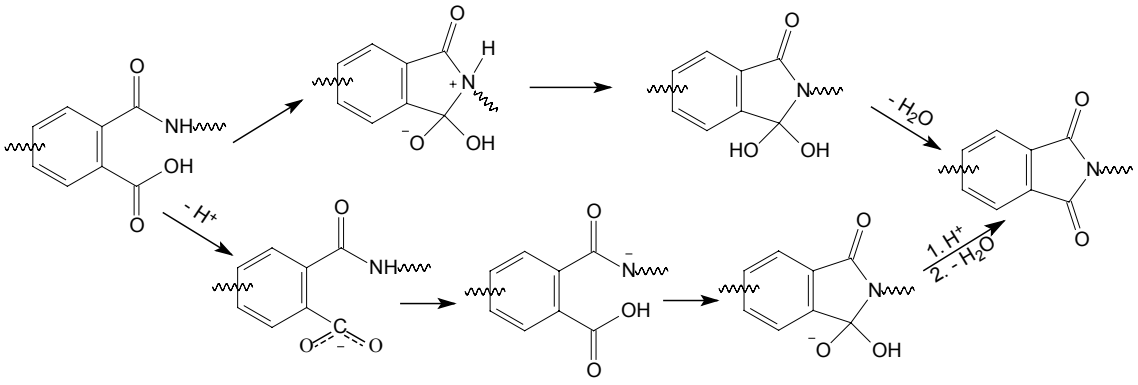

Figure 2.7 Thermal imidization of poly(amic acid)

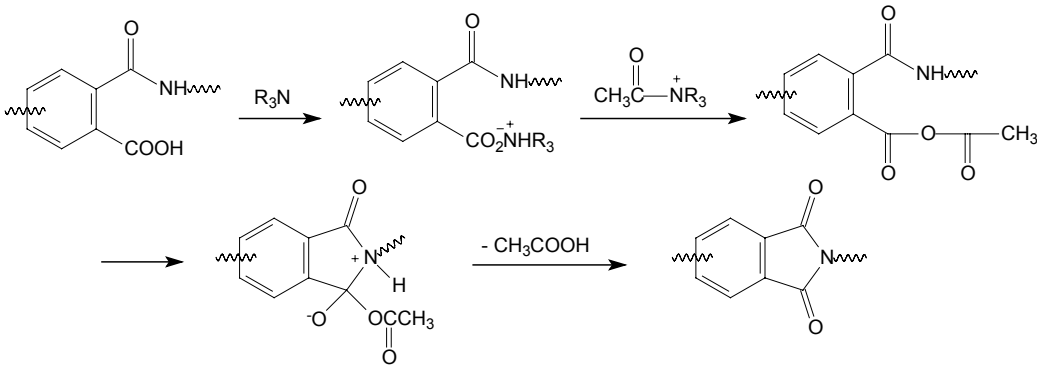

Figure 2.8 Chemical imidization of poly(amic acid)

2.4.1.2 One-Step Synthesis of Polyimides

Polyimides having flexible bonds in the main chains or having pendant side groups, which are likely to be soluble in strong polar and aprotic solvents, are often prepared by the one-step or single-stage method. In this method, the dianhydride and diamine are stirred in a high-boiling organic solvent at 180–220 °C. Under these conditions, chain growth and imidization occur spontaneously. The water generated by imidization is usually distilled off from the reaction mixture. Nitrobenzene, α-chloronaphthalene and *m*-cresol containing isoquinoline are solvents most widely used [Wilson *et al.* 1990; Sroog 1991].

A reaction mechanism for the solution imidization process was proposed by Kim *et al.* [1993b] as shown in Figure 2.9. The nucleophilicity of the amide nitrogen influences the reaction rate; electron-donating bridge units, incorporated from relatively basic diamines such as 4-aminophenyl ether (ODA), tend to lead to a higher reaction rate [Kim *et al.* 1993b; Dunson 2000].

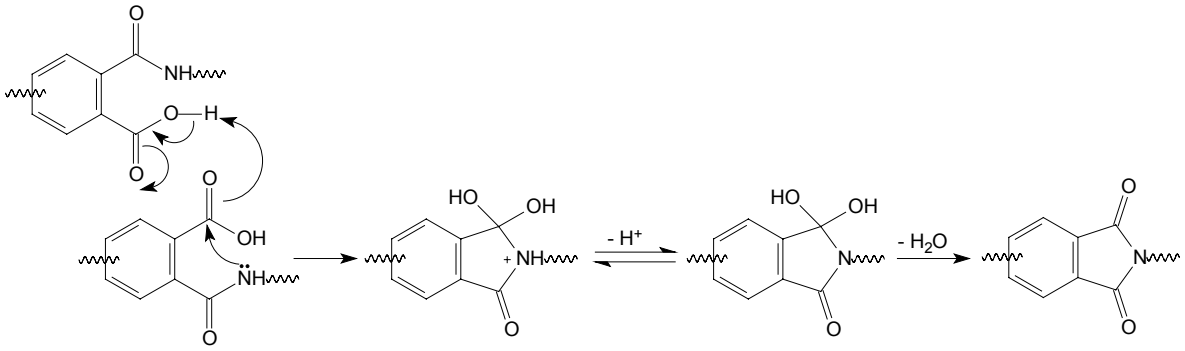

Figure 2.9 Possible reaction mechanism for solution imidization

2.4.2 Polyimide Membranes for Dehydration

Polyimide has a high permeability to water because of the specific interactions (mainly H-bonding, as shown in Figure 2.10) between water molecules and the acyl groups in the imide rings [Ohya *et al.* 1996]. The solubility parameters of some polyimides and their affinity to solvents are shown in Appendix A. Polyimides have good chemical resistance, and the rigid structure restricts swelling in solvents. Therefore, polyimide membranes can be used in pervaporation dehydration of organic solvents.

2.4.2.1 Commercial Polyimides

Some commercial polyimide materials (Figure 2.11) have been used in pervaporation dehydration processes. Huang and Feng [1992, 1993a, 1993b] investigated the pervaporation properties of Ultem® 1000 (G.E. Plastics) for dehydration of ethanol and isopropanol [Feng and Huang 1996a]. Yanagishita *et al.* [1994] prepared asymmetric membranes for water/ethanol separation using PI-2080 (Dow Chemical). Various P84™ polyimide (BTDA-TDI/MDI, HP Polymer GmbH) membranes were used in dehydration of alcohols [Liu *et al.* 2005; Qiao *et al.* 2005; Qiao and Chung 2005]. Guo and Chung [2005] studied the thermal hysteresis behavior in pervaporation dehydration with Matrimid® 5218 polyimide (Ciba Polymers) membranes, and Zhou and Koros [2006] used Matrimid® hollow fibers to dehydrate acetic acid. In addition, some research focused on modifications of the commercial polyimides to optimize their dehydration properties [Kaba *et al.* 2005; Qariouh *et al.* 1999; Qiao and Chung 2006].

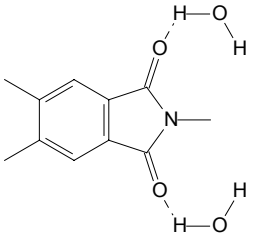

Figure 2.10 H-bonding between the imide ring and water molecules

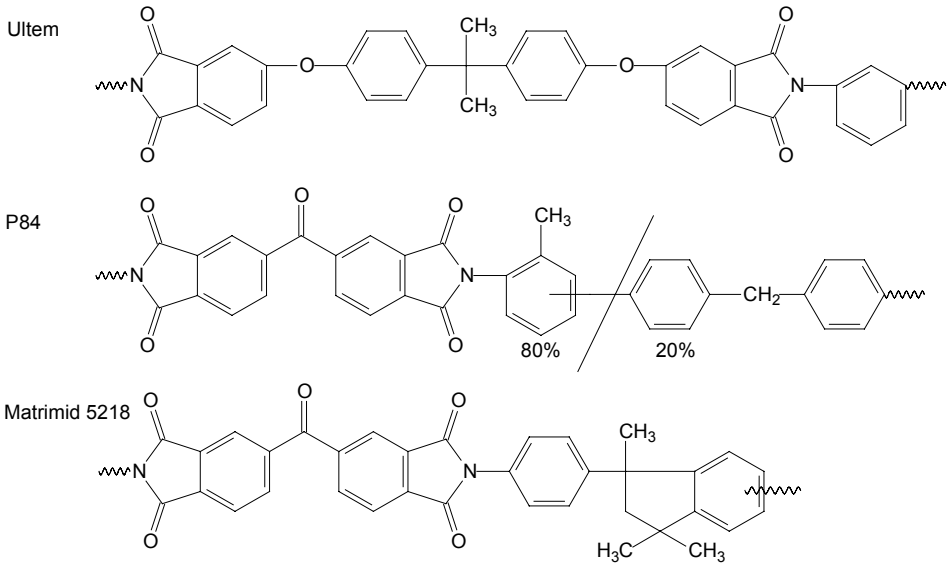

Figure 2.11 Chemical structures of some commercial polyimides

2.4.2.2 Polyimides from Interfacial Polymerization

Kim *et al.* [2000b] prepared polyimide composite membranes by interfacial polymerization / thermal imidization method. Poly(amic methyl ester) precursor layers were formed on the top of a porous polysulfone (PSF) support by interfacial polymerization of water-soluble diamines with 2,5-bis(methoxycarbonyl) terephthaloyl chloride in toluene, followed by thermal conversion to polyimide under vacuum at 180 °C. Pervaporation dehydration of ethanol was shown to be affected by the properties of the skin layer, the support layer and curing conditions.

Yanagishita *et al.* [2001] synthesized poly(amic acid)triethylamine salt and dip-coated it on PI-2080 asymmetric membranes, and a polyimide skin layer was obtained by annealing at 200 °C *in vacuo*. The membranes were tested for dehydration of ethanol.

2.4.2.3 Polyimides with Side Groups

Polyimide membranes with side groups were prepared from 3,5-diaminobenzoic acid (DABA), dimethyl-3,7-diamino-dibenzothiophene-5,5-dioxide (DDBT) and 4,4'-diamino-3,3'-dimethyldiphenyl methane (DMMDA), and their pervaporation dehydration properties were investigated with aqueous ethanol solutions [Kang *et al.* 1993; Okamoto *et al.* 1992; Wang *et al.* [2006a]. The changes in the pervaporation properties were believed to be caused by the monomers with side groups [Kang *et al.* 1993; Okamoto *et al.* 1992].

A series of soluble polyimides was prepared from one-step polymerization of BHTDA and diamines with bulky side groups (shown in Figure 2.12), and the pervaporation dehydration properties were investigated by Li and Lee [2006] and Teng *et al.* [2006]. The packing densities of the BHTDA-BADTB membranes were lower than those of BHTDA-BATB and BHTDA-DBAPB membranes, and the increase in the molecular volume for the substituent group in the polymer backbone increased the permeation rate.

Wang *et al.* [2005] synthesized soluble polyimides from two-step polycondensation based on a diamine of 3,3-bis[4-(4-aminophenoxy)phenyl] phthalide (BAPP) and various dianhydrides. The BAPP-based membranes had a high affinity to alcohols because of the addition of hydrophobic groups to the polymer backbones. 6FDA-BAPP showed higher permeation flux in dehydration of ethanol, which was explained by the interactions between the membrane and the permeant: 6FDA-BAPP had a high solubility to ethanol, and the bulky hexafluoropropane groups resulted in an amorphous structure, and accordingly, a decreased packing density of the polymer chains.

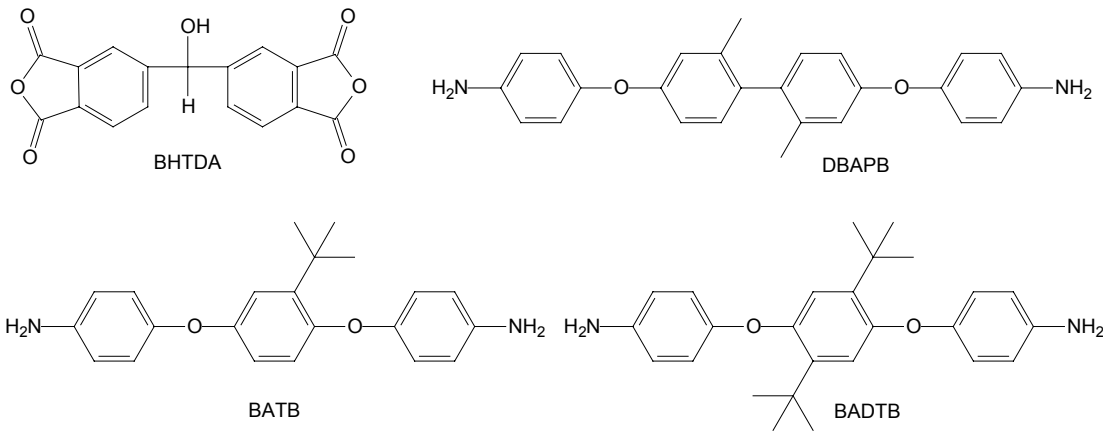

Figure 2.12 A dianhydride with hydroxyl groups and diamines with bulky pendant groups

Xu *et al.* [2006] studied the pervaporation properties of polyimides from four diamines: benzidine (BZD), bis(4-aminophenyl)phenyl phosphate (BAPP), 4,4'-methylenedianiline (MDA), and 4-aminophenyl ether (ODA). The permeation flux through the membranes with the same dianhydrides appeared in such an order: BZD < ODA < MDA < BAPP, which was in agreement with their *d*-spacing and free volume. High rigidity and low mobility of the polymer chains were supposed to help increase selectivity, but loose packing of the segmental chains led to a high flux [Xu *et al.* 2006]. Xu *et al.* [2007] attempted to correlate pervaporation performance with the physical properties of polymers, and it was shown that $\ln flux \propto d$-spacing.

2.4.3 Polyimide Membranes for Separation of Organics

Separation of the close-boiling-point or azeotropic organic mixture is one of the most challenging issues in the petrochemical industry, and the currently used separation processes, such as extractive distillation, are both capital and energy intensive [Xu *et al.* 2003]. Pervaporation is a promising alternative to current commercial processes due to its simplicity and potential for energy savings. Unlike distillation, pervaporation separation is not limited by the relative volatility of the components but relies mainly on the difference in sorption and diffusion properties of the feed components in the membrane [Hao *et al.* 1997].

Since many polyimides are extremely resistant to solvent dissolution, these polymers are of particular interest for preparing membranes used for organic-organic separations where the membrane stability is often a primary consideration due to the relatively harsh conditions. Table 2.6 lists polyimide membranes and their applications in pervaporation separation of organic liquid mixtures.

Some polyimide membranes in Table 2.6 were also used in separation of other organic systems, such as acetone/cyclohexane [Tanihara *et al.* 1994; Tanihara *et al.* 1995] and benzene/*n*-hexane [Wang *et al.* 2000a; Fang *et al.* 2000; Okamoto *et al.* 1999; Tanihara *et al.* 1995].

Table 2.6 Polyimide membranes for pervaporation separation of organic mixtures

Organics	Polyimide Materials and Membranes	References
Benzene / Cyclohexane	6FDA-based polyimide from diamines of 4MPD and 6FpDA, DABA as a crosslinking site.	Pithan *et al.* [2002b], Ren *et al.* [2001], Katarzynski and Staudt-Bickel [2006]
	Copolyimides containing crown ether	Yang *et al.* [2005]
	Poly(ethylene oxide imide) segmented copolymer membranes crosslinked by ethylene glycol diglycidyl ether	Wang *et al.* [2000b]
	Polyimides containing methyl side groups and DABA moieties	Tanihara *et al.* [1994]
	Polyimides with pendant phosphonate ester groups	Okamoto *et al.* [1999]
	Polyimide containing sulfonyl groups	Wang *et al.* [2000a]
	polyimides containing thianthrene-5,5,10,10-tetraoxide	Fang *et al.* [2000]
	PEO/PE/PTHF segmented poly(ether imide)	Tanihara *et al.* [1995]
	Copolyimides containing ethynyl groups	Fang *et al.* [1999]
	Polyimide containing sulfonyl groups	Hao *et al.* [1997]
Ethanol / ETBE	Poly(urethane-amide-imide) block copolymers	Jonquieres *et al.* [1995, 1996a, 1996b, 1996c, 2005]
	Poly(amide imide) membranes derived from TMACl	Jonquieres *et al.* [2000]
Ethanol / Toluene	Polyimide/polydimethylsiloxane block copolymers	Schauer *et al.* [1996]
Toluene / iso-Octane	Polyimide containing sulfonyl groups	Hao *et al.* [1997]
	copolyimides containing ethynyl groups	Fang *et al.* [1999]
	6FDA-DMA/DABA membranes	Xu *et al.* [2003]
Thiophene / *n*-Heptane	6FDA-MDA membranes	Wang *et al.* [2006b]
o-Xylene / *p*-Xylene	6FDA-based polyimide containing DABA as a crosslinking site.	Schleiffelder and Staudt-Bickel [2001]

2.4.4 Polyimide Membranes for Extraction of Organics from Water

There are some processes requiring the removal of organic compounds from aqueous solutions, such as recycling process water and recovering a small amount of organic compounds from water. Traditional separation techniques, such as steam/air stripping, distillation, aeration and adsorption have been suggested, but in pervaporation processes pollutants can be selectively removed from contaminated water without further treatments [Kim *et al.* 2000a]. Table 2.7 lists synthetic polyimide membranes used to remove high-boiling organics and volatile organic compounds (VOCs).

Table 2.7 Polyimide membranes for pervaporation extraction of phenol and VOCs

Organics	Polyimide Materials and Membranes	References
Phenol	BTDA-ODA membranes	Pradhan *et al.* [2002]
	Copolyimides from 6FDA, DABA and fluorinated diamines (6FpDA and 8FBA), modified with TDFO	Pithan *et al.* [2002a]
	Crosslinked copolyimides from 6FDA, DABA and fluorinated diamines (6FpDA and 6FpODA), 4MPD	Pithan and Staudt-Bickel [2003]
	Polyimides from dianhydrides (PMDA and 6FDA) and α,ω-(bisaminopropyl) dimethylsiloxane oligomers	Krea *et al.* [2004]
VOCs	BTDA-ODA/PDMS segmented copolymers	Lai *et al.* [1994]
	Silicalite-filled BTDA-based poly(siloxane imide) membranes	Liu and Xiao [2004]
	Poly(siloxane imide)s from dianhydrides of 6FDA, BTDA and PMDA	Chang *et al.* [2000]
	Polyimides from 6FDA, bis(3-aminopropyl) terminated poly(dimethylsiloxane), and 2-(perfluorohexyl) ethyl -3,5-diaminobenzoate	Chang *et al.* [2005]
	6FDA-PFDAB,ODPA-PFDAB with fluorinated alkyl side groups	Kim *et al.* [2000a]

2.5 Non-porous Membranes for Gas Separation

Depending on the pore size, pores in membranes are classified as macropores (> 50 nm), mesopores (50–2 nm) and micropores (< 2 nm) [Javaid 2005]. Gas transport in porous membranes may occur via different mechanisms that are largely dependent on the pore size and the size of the diffusing molecules. As shown in Figure 2.13 [Koros and Fleming 1993; Perry *et al.* 2006], Knudsen diffusion, surface diffusion, capillary condensation, and molecular sieving are the main transport mechanisms for microporous membranes. However, high selectivity cannot be achieved using porous polymer

membranes [Pandey and Chauhan 2001], and the difficulty in fabricating membranes with uniform pores also restricts the applications of porous membranes in gas separation processes.

As shown in Figure 2.13, no apparent continuous passages exist in non-porous dense membranes, and gas transport follows the solution-diffusion mechanism [Koros and Fleming 1993; Perry *et al.* 2006]. Glassy polymer membranes are usually used as size-selective membranes for non-condensable gases, while rubbery polymer membranes are solubility-selective, and selectively permeable to large-size VOCs or hydrocarbons [Freeman and Pinnau 1997].

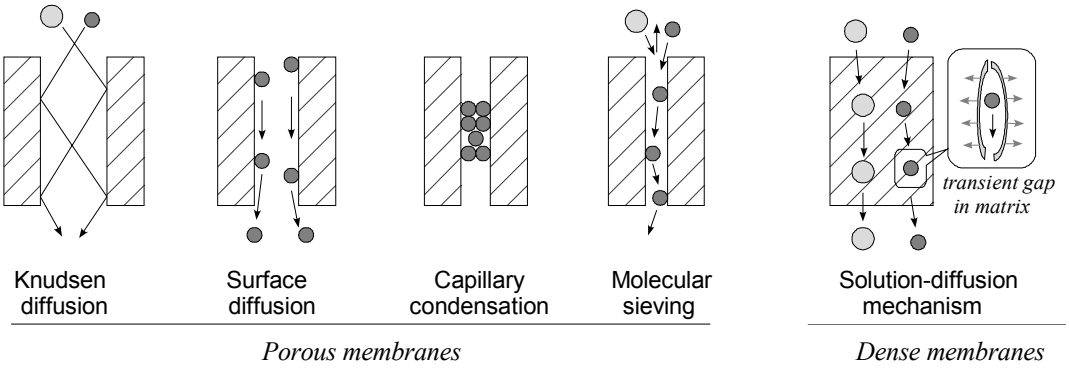

Figure 2.13 Gas transport mechanism in membranes

2.5.1 Gas Transport in Dense Membranes

The solution-diffusion model in pervaporation discussed in 2.2.1 can also be used to describe mass transport of gases in dense polymer membranes. Gas molecules dissolve into the polymer membrane, and then diffuse through the membrane under the chemical potential (partial pressure) gradient, followed by desorption at the downstream side of the membrane.

Studies on membrane permeabilities show that there is an inverse relationship between permeability and selectivity: the membrane selectivity generally decreases as the gas permeability increases for different gas pairs [Stern 1994]. Robeson [1991] suggested that an upper bound exists in the selectivity vs. permeability plot for binary gas mixtures of He, H_2, O_2, N_2, CH_4 and CO_2. For various gas pairs, rubbery polymers exhibit a high permeability and a low selectivity, while glassy polymers show a low permeability and a high selectivity [Stern 1994].

Permeability is an intrinsic property of the gas-polymer system, and is determined by solubility and diffusivity. Because gases are much simpler molecules than polymers, correlations between

diffusion and solubility coefficients for different gases in a given polymer are available [Yampolskii *et al.* 2006]. There are also some studies on correlation of polymer properties with diffusivity, solubility and permeability values for a given gas permeant, which leads to the group contribution method proposed to predict the permeability of polymers to gases [Salame 1986; Jia and Xu 1991; Robeson *et al.* 1997; Park and Paul 1997; Yampolskii *et al.* 2006].

2.5.1.1 Effects of Gas Properties on Gas Permeation

The thermal motion of polymer chain segments generates penetrant-scale transient gaps in the polymer matrix, which selectively allows gas molecules to permeate from the upstream side to the downstream side of the membrane. Generally, the physical properties (as shown in Table 2.8) of a gas influence its permeability in non-porous polymer membranes [Koros and Fleming 1993; Yampolskii *et al.* 2006]. Small molecular size and high critical temperature tend to produce high permeability, because small molecular size yields a high diffusion coefficient and a high critical temperature promotes solubility in the membrane [Koros and Fleming 1993].

Table 2.8 Properties of common gas molecules

Gas	Kinetic diameter d_k (nm)	Collision diameter [a] d_{LJ} (nm)	Critical temperature T_C (K)
He	0.26	0.26	5.2
H_2O	0.27	0.26	647.3
H_2	0.29	0.28	33.2
CO_2	0.33	0.39	304.1
O_2	0.35	0.35	154.6
N_2	0.36	0.38	126.2
CH_4	0.38	0.38	190.4
C_3H_8	0.43	0.51	369.8

[a] Lennard-Jones collision diameter

The solubility of a gas is directly related to the condensability that can be measured by its critical temperature. O_2 has a higher critical temperature than N_2, and thus O_2 is more soluble than N_2 in most media including polymers. The typical solubility selectivity towards O_2/N_2 varies in the range of 1.35–1.89, which is not sufficient to produce a desirable separation factor, without a favorable

contribution from the mobility selectivity [Koros and Fleming 1993]. The interactions between gas molecules and polymers are another factor that can affect the solubility of a gas in polymer materials.

The mobility selectivity arises from the difference in gas molecules. The molecular size determines the relative abilities of the penetrants to execute diffusive jumps through the transient gaps in the polymer matrix [Koros and Fleming 1993]. A linear correlation between $\log D$ and d^2 is shown to be fairly good for spherical molecules [Yampolskii *et al.* 2006].

2.5.1.2 Effects of Polymer Properties on Gas Permeation

Gas permeability is sensitive to the parameters that are related to the chain packing properties, such as polymer density, mean interchain distance (*d*-spacing from wide-angle X-ray diffraction), or free volume [Yampolskii *et al*. 2006]. Figure 2.14 shows the typical specific volumes of polymers at different temperatures [Toshima 1992; Sperling 2001].

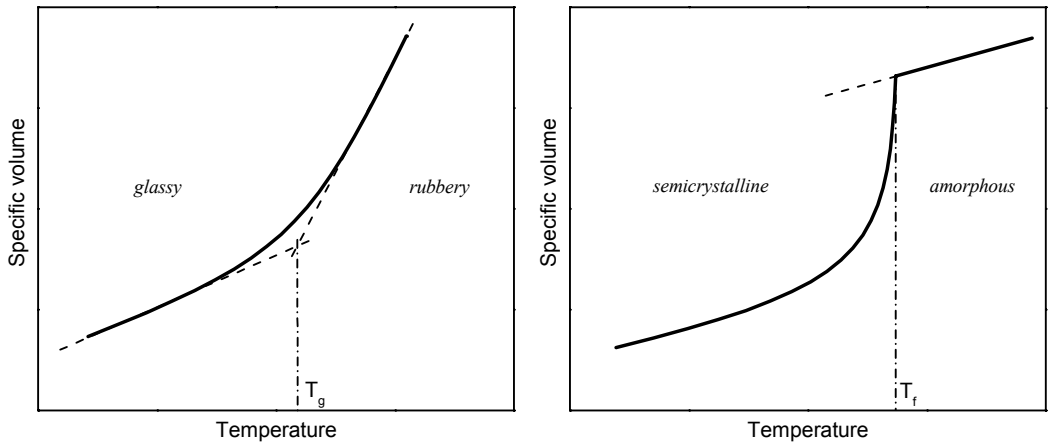

Figure 2.14 Relationship between temperature and specific volume of a polymer

For amorphous polymers, the glass transition occurs when the specific volume changes sharply, where glass transition temperature (T_g) is defined. The free volume theory offers an alternative way to describe the glass transition temperature. It is postulated that the glassy expansion is much weaker than rubbery expansion, and a further proposition reads that the glass transition occurs at a constant value of the difference between the glassy expansion and the rubbery expansion times the temperature [Sperling 2001]. Therefore, for a specific polymer, the free volume in the rubbery state is much larger

than that in the glassy state. As illustrated in Figure 2.15 [Paul and Yampol'skii 2000], polymer chains are frozen in the matrix in the glassy state, and the polymer matrix acts like a "molecular sieve", allowing gas molecules to permeate selectively. The polymer turns into rubbery state when the temperature is higher than T_g. The free volume in such media, like in liquids, undergoes rapid fluctuations [Yampolskii *et al.* 2006]. Thus, larger transient gaps are produced, and gas molecules with a larger size can also pass through. However, separation may still occur based on the solubility difference in rubbery membranes [Freeman and Pinnau 1997; Javaid2005].

Figure 2.14 also shows the specific volume change of semicrystalline polymers. The polymer chains in the crystalline region are packed regularly and densely, and thus the permeability is greatly restricted, as illustrated in Figure 2.15.

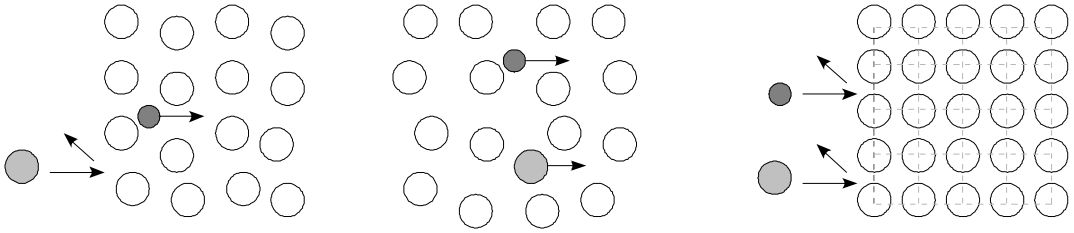

Figure 2.15 Illustration of "extreme" cases for gas transport in polymers of different states

The glass transition and crystallinity of a polymer are derived from its chemical structure. Side chains/groups [Muruganandam *et al.* 1987; McHattie *et al.* 1991], polar bondings [Allen *et al.* 1977], cis/trans configuration [Morisato *et al.* 1993], para vs. meta linkages [Aitken *et al.* 1992] and connector groups [Coleman and Koros 1990] are all found to influence gas permeability [Yampolskii *et al.* 2006]. Therefore, the group contribution methods have been proposed to predict the permeability of polymers [Salame 1986; Jia and Xu 1991; Robeson *et al.* 1997; Park and Paul 1997; Alentiev *et al.* 2000; Yampolskii *et al.* 2006].

2.5.2 Polyimide Membranes for Gas Separation

Because of the excellent thermal, chemical, mechanical and film-forming properties, polyimides become a popular material for gas separation. Polyimide membranes normally exhibit better gas separation performance than the commonly used glassy polymers such as poly(aryl ether)s and poly(aryl ester)s. Furthermore, the structure-property relationship can be established based on

molecular design by varying the dianhydride and diamine monomers in the polymerization [Yampolskii *et al.* 2006].

It is suggested that the polyimides used for gas separation should have the following characteristics [Hoehn 1974]:

1) The repeating unit of the main chain has at least one rigid divalent subunit.

2) The main chain is sterically unable to rotate 360° around at least one of the bonds noted in 1).

3) The polymer has 50 % or more aromatic rings in the repeating unit.

To enhance the selectivity and permeability of polyimides toward light gases, structure modifications are suggested from the structure-property relationship [Stern 1994]:

1) The backbone chains must be stiffened by inhibiting their intrasegmental (rotational) mobility.

2) Intersegmental packing of the polymer chains must be simultaneously prevented.

3) Interchain interactions must be weakened and if possible, eliminated.

Table 2.9 Modifications of polyimides for gas separation membranes

Side groups	Polyimide Membranes	References
$-SO_3H$	Sulfonated NTDA-based membranes	Piroux *et al.* [2002a, 2002b, 2004], Tanaka [2006],
	Pyrolytic sulfonated NTDA-based membranes	Islam *et al.* [2005]
	Metal-containing sulfonated BTDA-based membranes	Kim *et al.* [2002]
–COOH	6FDA-based membranes and DABA as a crosslinking site	Staudt-Bickel and Koros [1999], Wind *et al.* [2004]
$-CF_3$, $-OCH_3$	ODPA-based membranes	Pinel *et al.* [2002]
$-CH_3$	Polyimides from 4,4'-(1,4-phenylenedioxy) diphthalic anhydride and 2,2'-dimethyl-4,4'-methylenedianiline	Li *et al.* [1997]
	Polyimides from substituted terphenylenes and 6FDA	Al-Masri *et al.* [1999]
	6FDA-based polyimides	Singh-Ghosal and Koros [1999], Heuchel and Hofmann [2002], Niwa *et al.* [2006]
	Polyimides from $-CH_3$ and $-OCH_3$substituted catechol bis(etherphthalic anhydride)s	Al-Masri *et al.* [2000]
	6FDA-based polyimides with $-CH_3$, –Cl, –OH	[Shimazu *et al.* 1999, 2000]
t-butyl and phenyl groups	Polyimides from substituted 1,3-bis(3,4-dicarboxybenzoyl) benzene dianhydrides	Ayala *et al.* [2003]

The relationship between gas permeation properties and the polyimide main chains has been studied [Stern *et al.* 1989; Robeson 1994; Hirayama 1996a, 1996b; Li *et al.* 1996; Maier 1998; Powell and Qiao 2006]. Introduction of side groups in polyimide main chains will change gas permeation properties. Table 2.9 summarizes the modification of polyimides by side groups. On one hand, the free volume may be changed, and the diffusivity of gas molecules in the polymer matrix will be influenced. On the other hand, the side groups may interact with gas molecules, thus resulting in a change in the solubility/diffusivity of gases.

Part I

Trimesoyl Chloride Crosslinked Poly(vinyl alcohol) and Chitosan Membranes for Pervaporation and Gas Separation

Poly(vinyl alcohol) and chitosan are hydrophilic polymers (their affinities to solvents are shown in Appendix A in terms of solubility parameters), and are widely used in dehydration of solvents by pervaporation due to their good film-forming properties. However, in pervaporation, uncrosslinked poly(vinyl alcohol) and chitosan membranes usually undergo severe swelling. Therefore, crosslinking of the membranes is required to attain long-term stability.

Although there are several crosslinking agents for poly(vinyl alcohol) and chitosan, some of them have the problems associated with too slow or too fast crosslinking reactions. Better crosslinking agents are needed that will not only provide more options to solve these problems, but also expand the application of the membranes.

To this end, trimesoyl chloride/hexane was studied as a new crosslinking system to interfacially crosslink poly(vinyl alcohol) and chitosan membranes. Emphasis was put on the effect of crosslinking on pervaporation performance of the membranes in dehydration of isopropanol. The changes in swelling behavior, sorption properties and thermal stabilities were also investigated. Gas permeation experiments were conducted with the crosslinked chitosan membranes for potential application in CO_2/N_2 separation.

Chapter 3

Trimesoyl Chloride Crosslinked Poly(vinyl alcohol) Membranes for Pervaporation Dehydration of Isopropanol. I. Preparation and Characterization*

Trimesoyl chloride (TMC) crosslinked PVA membranes (PVA-TMC) with different degrees of crosslinking were prepared by applying TMC/hexane to the surface of the dried PVA membranes. The asymmetric structure of PVA-TMC membranes was revealed by FTIR-ATR, and the degree of crosslinking was estimated by the loss of hydroxyl groups from FTIR-ATR spectra. DSC and TGA curves showed that PVA-TMC membranes had better thermal stabilities than the uncrosslinked PVA. TGA/DTG thermograms were investigated and a pyrolysis mechanism was proposed, which was a combination of elimination of water and/or trimesic acid followed by the breakage of the main chain. Pervaporation properties were studied through water permeation and dehydration of isopropanol/water mixtures at different temperatures and feed concentrations. PVA-3TMC had the best overall pervaporation properties among the four PVA-TMC membranes.

3.1 Introduction

Poly(vinyl alcohol) (PVA) is soluble in hot water, and its solubility depends on the degrees of polymerization and hydrolysis [Finch 1973]. PVA is a hydrophilic material, and in membrane technology, it is mainly used for dehydration of solvents in pervaporation. However, to be used as membranes, PVA is often chemically modified to attain long-term stability [Finch 1973]. There are several ways to crosslink PVA:

1) Chemical modification of PVA [Chiang and Chen 1998, Chiang and Lin 2002; Gholap *et al.* 2004; Gimenez *et al.* 1997, 1999; Ruiz *et al.* 2001],

2) Radiation-induced crosslinking [Hegazy *et al.* 2004; Miranda *et al.* 2001; Zhai *et al.* 2002],

* Portions of this work have been published in *Journal of Membrane Science*, vol. 286 (2006), pp. 245–254.

3) Treatments with a multi-functional additive for chemical crosslinking.

In 3), when the additive has a very low reactivity with PVA under ambient conditions, blends of PVA and the additive can get crosslinked by thermal treatments [Arndt *et al.* 1999; Gohil *et al.* 2006; Huang and Shieh 1998; Kumeta and Nagashima 2003; Oikawa *et al.* 2001; Rhim *et al.* 1998]. If the additive is able to react with PVA quickly, crosslinking can be formed directly by blending [Ahn *et al.* 2005; Hirai *et al.* 1996; Kariduraganavar *et al.* 2005; Krumova *et al.* 2000; Rhim *et al.* 1998; Touil *et al.* 2005; Wang *et al.* 1999]. PVA membranes can also be crosslinked when soaked into a crosslinking medium, gases [Metayer and M'Bareck 1997; Silva *et al.* 2002] or liquid solutions [Durmaz-Hilmioglu *et al.* 2001; Yu *et al.* 2002]. Aqueous glutaraldehyde solutions containing suitable catalysts are one of the most commonly used crosslinking systems for PVA crosslinking [Rhim *et al.* 1998; Durmaz-Hilmioglu *et al.* 2001; Yu *et al.* 2002]: glutaraldehyde diffuses into the PVA membrane and reacts in the interior to form acetal groups between polymer chains. Usually inorganic salts are used to prevent PVA from dissolving, which results in a lower degree of crosslinking and a higher degree of swelling [Yeom and Lee 1996]. Therefore, Yeom and Lee [1996] used acetone, a non-solvent for PVA, instead of aqueous salt solutions, as the reaction medium for PVA crosslinking with glutaraldehyde, and successfully prepared crosslinked PVA pervaporation membranes with different degrees of crosslinking.

PVA is the hydrolysis product of PVAc. The reverse reaction, acetylation of PVA, was studied by McDowell and Kenyon [1940]. Acid chlorides with a high reactivity can react with PVA to produce poly(vinyl ester)s, but they can only be kept in aprotic solvents because of their moisture sensitivity. Dimethyl sulfoxide (DMSO) and *N*-methylpyrrolidone (NMP) were used as solvents to form homogenous solutions of PVA and acid chlorides [Gimenez *et al.* 1996]. Tsuda [1964] prepared poly(vinyl cinnamate) by Schotten-Baumann esterification of PVA and cinnamoyl chloride in a basic medium. [Gimenez *et al.* [1996] modified PVA with water-stable acid chlorides. Some applications were reported for interfacial reactions of poly(vinyl alcohol)-containing solutions with trimesoyl chloride (TMC) to form a thin layer coating on porous substrates [Kim *et al.* 2003], but crosslinking of PVA membranes using TMC has not been studied.

Therefore, this work focused on developing a crosslinking method for homogeneous PVA membranes using TMC/hexane, and on characterizing these crosslinked membranes with FTIR-ATR and thermal analysis techniques, as well as their applications in pervaporation dehydration.

3.2 Experimental

3.2.1 Chemicals and Materials

Poly(vinyl alcohol) (99 mol % hydrolyzed, MW ~133,000) was provided by Polysciences Inc. Hexane (ACS reagent, ≥ 98.5 %), trimesoyl chloride (TMC) (98 %) and isopropanol (IPA) (anhydrous, 99.5 %) were obtained from Sigma-Aldrich. Trimesoyl chloride was kept in a sealed glass container with Drierite™ adsorbent (from Fisher Scientific). Water was deionized with the conductivity ≤ 2 μS/cm.

3.2.2 Membrane Preparation

3.2.2.1 Membrane Formation

PVA was dissolved in water by stirring in a water bath above 85 °C to form a 5 w/w % viscous and transparent solution. The PVA aqueous solution was degassed *in vacuo* over a period of 2 h. Glass rings (Ø75 mm) were used to hold 10 mL PVA solutions on the surface of a polyethylene film. The membranes were dried by evaporation of water in ambient air at 25 °C for at least 3 days.

3.2.2.2 Membrane Crosslinking

The crosslinking solution was prepared by dissolving 1 g of trimesoyl chloride in 40 mL of hexane to get a 2.5 w/v % TMC/hexane solution. Different volumes of TMC/hexane solution were poured onto the dried membranes in the glass rings. Crosslinking reaction started immediately, and the glass rings with membranes were kept in dry air at 25 °C overnight. The membrane preparation conditions were listed in Table 3.1.

Table 3.1 Membrane formation and crosslinking conditions

Membranes	PVA/Water (5 w/w %) (mL) [a]	TMC/Hexane (2.5 w/v %) (mL) [a]
PVA-1TMC	10	2.5
PVA-3TMC	10	7.5
PVA-5TMC	10	12.5
PVA-7TMC	10	17.5

[a] Glass rings (Ø75 mm × 75 mm) were used to hold the solutions.

The crosslinked membranes were peeled off from the polyethylene films. These membranes were thoroughly rinsed with large amounts of isopropanol and water to remove the residual chemicals in the membrane. They were then kept in isopropanol for 2 days, and then in water for 3 days. The thicknesses of membranes were measured with a micrometer to be in the range of 50–60 μm.

3.2.3 Fourier Transform Infrared Spectroscopy (FTIR)

Attenuated total reflectance spectra (ATR) were recorded with Bruker TENSOR™ 27 FTIR Spectrometer and MVP2™ Single reflection ATR accessory with a Si Crystal (MVP2-ATR-E, from Harrick Scientific Products Inc.). Samples of the membranes were dried *in vacuo* at 85 °C overnight. The ATR spectra were measured for both surfaces of each membrane, and were labeled as –B (the bottom surface) and –T (the top surface). Measurements were repeated for different membranes to ensure reproducibility.

3.2.4 Swelling in Water

The degrees of swelling in water were determined for the uncrosslinked PVA membrane and the PVA-TMC membranes at room temperature. The tests were repeated with different membranes to guarantee reproducibility. After weighing, dry membrane samples were immersed in water for 3 days at ambient temperature. The swollen membranes were then taken out and the surface water was quickly removed with Kimwipes® Delicate Task Wipers, and the weights of the water swollen membranes were recorded. The degree of swelling (*SD*) was determined using the following equation:

$$SD = \frac{W_s - W_o}{W_o} \tag{3.1}$$

where W_s is the weight of the swollen membrane at sorption equilibrium, and W_o is the initial weight of the dry membrane.

3.2.5 Thermal Characterization

All membrane samples for thermal studies were dried *in vacuo* at 85 °C for at least 10 h. Differential scanning calorimetry (DSC) was measured with TA Instruments (Model DSC 2920) Differential Scanning Calorimeter, from 0 to 275 °C at a heating rate of 10 °C/min. Liquid nitrogen was used to

decrease the temperature from 30 to –30 °C before every run. DSC was run for an empty aluminum DSC sample cell, and the obtained DSC curve was used as the baseline for DSC measurements of all samples. TA Instruments (Model SDT 2960) Simultaneous DSC-TGA was used for thermogravimetric analysis (TGA). The temperature range for TGA was 50–650 °C with a heating rate of 10 °C/min. DSC and TGA were both conducted in a helium atmosphere.

3.2.6 Pervaporation Experiments

Pervaporation experiments were carried out for separation of isopropanol/water with different PVA-TMC membranes. The temperature range in the feed tank (1.5 L) can be controlled within ±1 °C with a heating mantle, Dyna-Sense® Thermoregulator Control System, a thermometer and a circulation pump (March MFG. Inc., Model BC-2CP-MD), as shown in Figure 3.1.

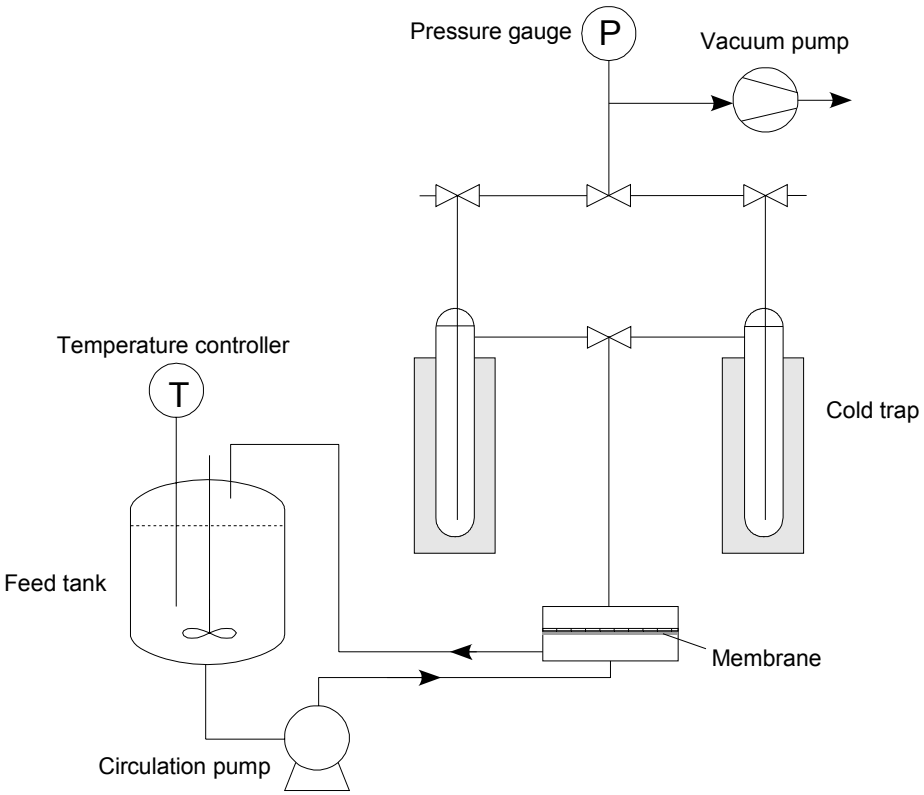

Figure 3.1 Pervaporation setup

The membranes were preconditioned in water before the pervaporation experiment. They were placed on a porous stainless steel plate and tightly sealed in the pervaporation cell (shown in Figure 3.2) with a rubber O-ring (Ø55 mm). The effective membrane area was 2.38×10^{-3} m^2. The

circulation pump fed the liquid solutions to the membrane cell at a high flow rate to decrease the possible boundary layer effect. The side labeled as T-surface of each membrane was in contact with the feed solutions, and the other side (B-surface) contacting the porous plate was under vacuum below 300 Pa (absolute pressure). Permeate samples were collected in cold traps by liquid nitrogen. A Hewlett-Packard (5890 Series II) Gas Chromatograph with a thermal conductivity detector (TCD) and a HP 3396 Series II Integrator was used to determine the feed and permeate concentrations.

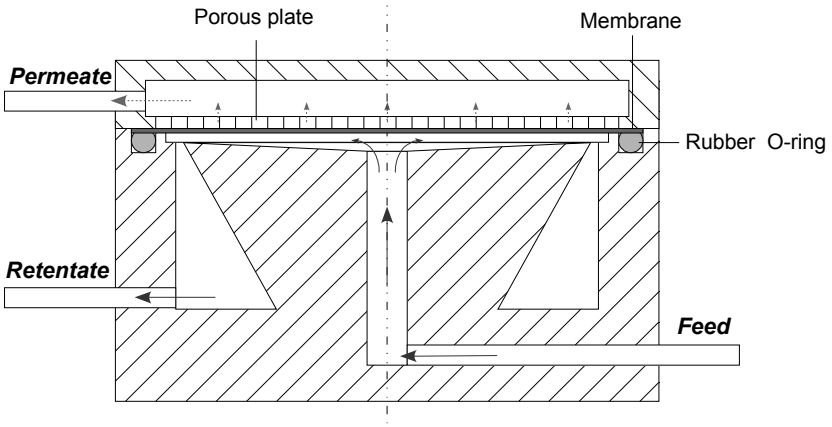

Figure 3.2 Schematic permeation cell

The membrane performance is characterized by permeability and selectivity, in terms of permeation flux and separation factor, respectively. The permeation flux, *F*, is determined from

$$F = \frac{Q}{S \cdot t} \tag{3.2}$$

where *Q*, *S* and *t* are the amount of permeate, membrane area and operating time, respectively.

The membrane selectivity for a binary system is expressed in terms of the separation factor, α, defined as

$$\alpha = \frac{y_w / y_a}{x_w / x_a} \tag{3.3}$$

where y_w and y_a are water and isopropanol concentrations in the permeate, respectively, and x_w, x_a are water and isopropanol concentrations in the feed, respectively.

Pervaporation of pure water through PVA-TMC membranes was studied at 30, 40, 50, 60 °C, respectively. Pervaporation dehydration of isopropanol was conducted in the following procedures.

First, to study the temperature dependence of pervaporation, the feed temperature was controlled to vary from 30 to 60 °C for a given isopropanol/water feed concentration (approximately 20 wt.% water). Second, to study the concentration dependence of pervaporation, the feed temperature was kept at 60 °C, and the feed water content was varied from 10 to 50 wt.%. All pervaporation experiments were repeated with different membranes to verify the reproducibility. Before samples were collected for analysis, pervaporation was operated for at least 1 h to attain steady states.

3.3 Results and Discussion

3.3.1 Membrane Preparation and Crosslinking

Homogeneous PVA membranes were prepared by evaporation of water from an aqueous PVA solution. In the step of crosslinking, TMC reacted with the hydroxyl groups in PVA to form poly(vinyl ester)s. Since acid chlorides are very sensitive to water, an appropriate solvent must be found for the crosslinking of PVA with TMC. Hexane is a non-solvent for PVA. When PVA was soaked in hexane, the solvent molecules could not penetrate into PVA, and PVA did not show significant changes in appearance. However, when the TMC/hexane solution was applied to the surface of a PVA membrane, swelling occurred. Apparently, TMC/hexane diffused from the top surface to the bottom of the membrane. This phenomenon can be interpreted by the polarity difference between hexane and TMC/hexane. Hexane acted as a solvent for TMC and it facilitated the diffusion of TMC in PVA. Meanwhile, it prevented PVA from further swelling by TMC, and could possibly control the degree of crosslinking to some extent if TMC/hexane was used as a crosslinking agent.

The reaction time of PVA crosslinking with TMC/hexane was determined by the evaporation rate of hexane. As hexane evaporated, the concentration of TMC increased though there was a consumption of TMC by PVA. As a result, the diffusion rate of TMC increased, which was also affected by the resistance from the crosslinked top layer. Consequently, the top and bottom surfaces of the membrane were anticipated to be different, and this method of crosslinking should lead to crosslinked membranes with an asymmetric structure at molecular level.

3.3.2 FTIR-ATR Analysis

Attenuated total reflection infrared spectroscopy (ATR-IR), also known as Internal Reflection Spectroscopy, is a technique for analyzing the surfaces of materials. ATR-FTIR spectra can be

obtained by pressing a small piece of membrane against the internal reflection element (IRE), *i.e.* the Si crystal in this work. IR light enters the IRE and penetrates a short distance from the surface of the IRE into the membrane [Almeida *et al.* 2002; Hind *et al.* 2001]. FTIR-ATR has found various applications in coating and membrane industries as well as some other research areas.

In this work, FTIR-ATR spectra were measured for both top and bottom surfaces of the crosslinked membranes, to determine the degrees of crosslinking from the difference in absorbance. The absorbance values of the peaks around 2930 cm^{-1} were set to 1 in all ATR-IR spectra, and therefore the relative ATR absorbance can be compared. The ATR spectra of PVA and the top/bottom layers of PVA-TMC membranes are presented in Figure 3.3.

In the ATR spectrum of the uncrosslinked PVA film, the broad peak at around 3300 cm^{-1} is for the intermolecular hydrogen bonding and the O–H stretch vibration. Absorptions for asymmetrical stretching vibration and symmetrical stretching vibration of $–CH_2$ occur at 2935 cm^{-1} and 2898 cm^{-1}, respectively [Miranda *et al.* 2001; Silverstein *et al.* 1997; Smirnov *et al.* 1967]. The two peaks at 1426 cm^{-1} and 1324 cm^{-1} are attributed to the coupling of the secondary O–H in-plane bending and the C–H wagging vibrations. Absorption in the region of 1260–1000 cm^{-1} is due to C–O stretching vibration [Smirnov *et al.* 1967]. From Acros FTIR database, partially hydrolyzed PVA and PVAc have strong absorptions at 1730 cm^{-1} and 1734 cm^{-1}, respectively, where the diagnostic absorption bands of C=O are located. In the ATR spectrum of the uncrosslinked PVA, there exists a very week peak in the region around 1730 cm^{-1}, which is believed to be the absorption band of C=O in the unhydrolyzed acetate groups.

The ATR absorbance of the uncrosslinked PVA and PVA-7TMC-T differs at 3300 cm^{-1}, and also in the regions of 1800–1500 cm^{-1} and 1500–1200 cm^{-1}. The C=O absorption band of benzoate esters appears in the region of 1730–1715 cm^{-1}. From Acros FTIR database, methylbenzoate and ethylbenzoate show strong absorption of C=O at 1727 cm^{-1} and 1723 cm^{-1}, respectively; while for PVA-7TMC-T, there is a peak at 1719 cm^{-1}, which can be identified to be C=O in trimesoyl ester groups. The peak of O–H vibration at 3300 cm^{-1} is too broad and overlays all unsaturated C–H peaks possibly occurring above 3000 cm^{-1}. The skeletal vibrations of carbon-carbon stretching within the benzene ring absorb at 1603 cm^{-1} and 1607 cm^{-1} for methylbenzoate and ethylbenzoate, respectively, from Acros FTIR database; while in the ATR spectrum of PVA-7TMC-T, two peaks can be found at 1635 cm^{-1} and 1590 cm^{-1}.

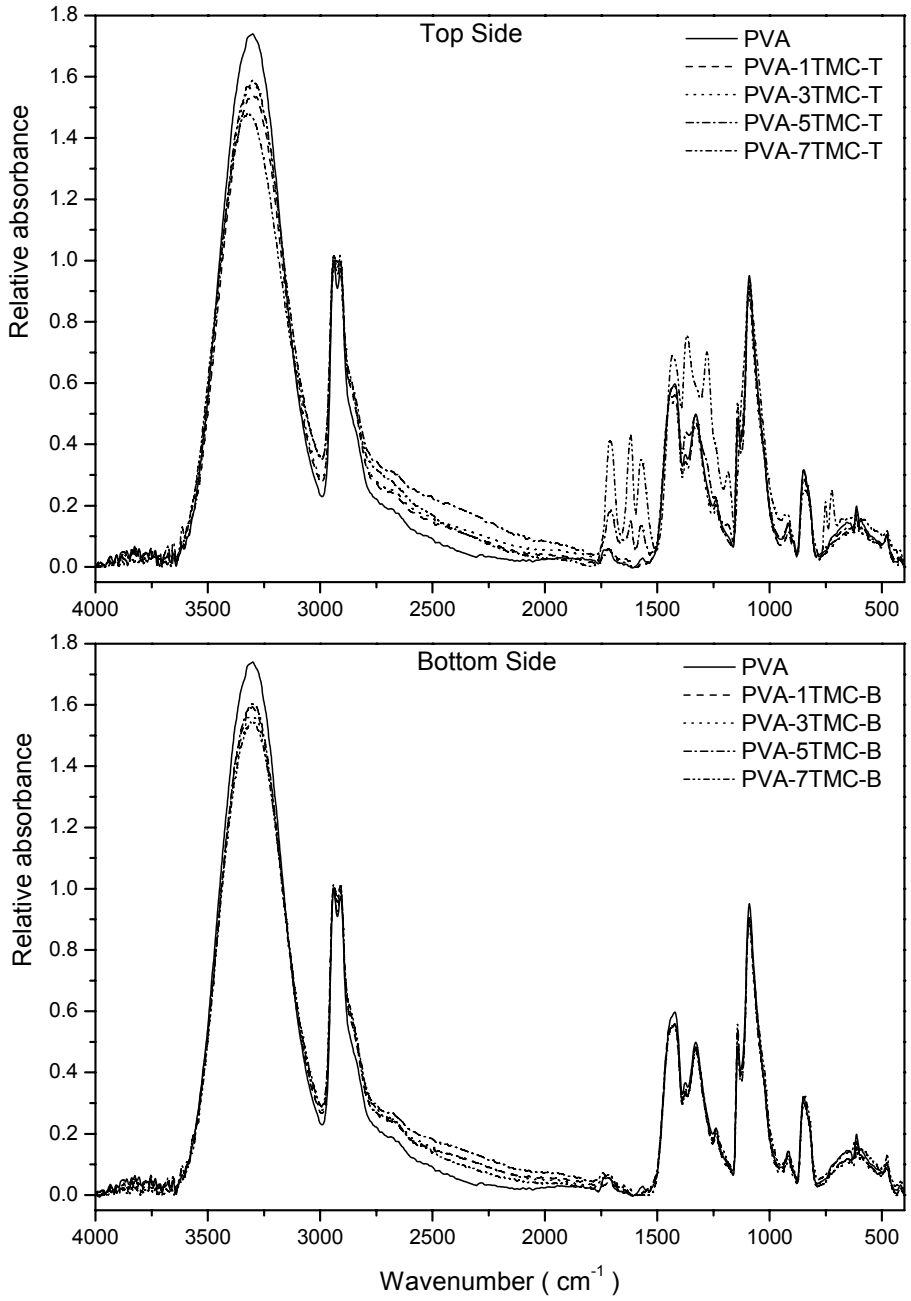

Figure 3.3 ATR spectra of PVA-TMC top and bottom layers

Integrations were made using the method of baseline integration [Alexy *et al.* 2002] (shown in Figure 3.4) for each ATR spectrum in the regions of 3630–3000 cm^{-1}, 3000–2750 cm^{-1} and 1790–1660 cm^{-1}. As shown in Table 3.2, the peak areas of 3000–2750 cm^{-1} were set to be 1, and all data

obtained from the integration were used on a relative scale. Because of the absorption overlay of O–H and C–H in 3630–3000 cm^{-1}, the contents of O–H could not be determined. However, the effects of C–H could be ignored due to the low levels of crosslinking and low contents of benzene rings introduced. By using TMC to induce crosslinking, the contents of hydroxyl groups decreased and the contents of ester groups increased. The uncrosslinked PVA had 1 % unhydrolyzed esters, which was used as a standard for the crosslinked PVA, *i.e.* loss of O–H to be 1 %, TMC moiety to be 0 %, and C=O content to be 1 %. The results are listed in Table 3.2.

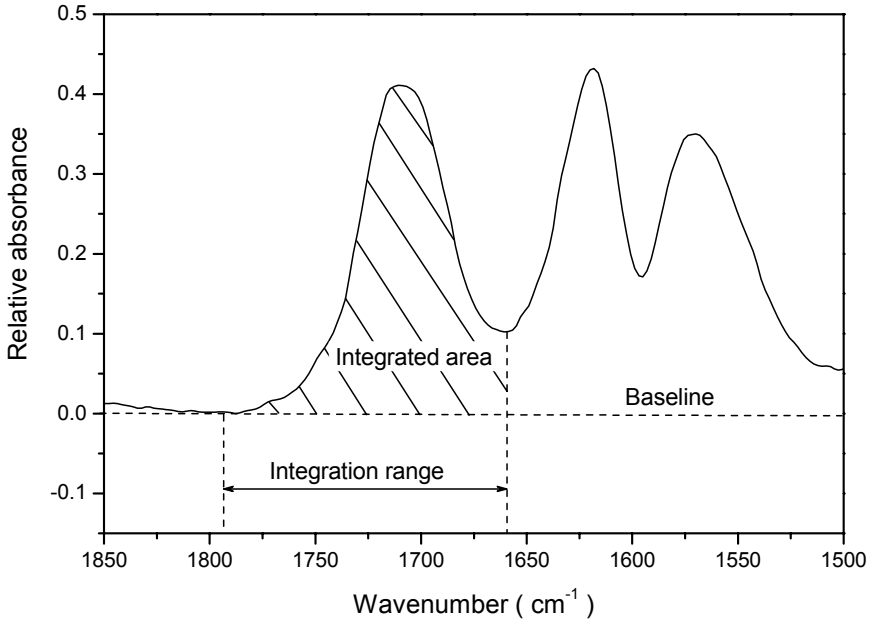

Figure 3.4 Integration of peak areas for ATR spectra

Losses of O–H are three times as much as TMC moieties if one TMC molecule reacts with three hydroxyl groups. A difference can be observed between the uncrosslinked PVA and the crosslinked PVA, and between the top layers and bottom layers of the TMC crosslinked PVA membranes. The top layer had a higher degree of crosslinking than the bottom layer for a given PVA-TMC membrane. Obviously, there is a significant difference between the results from losses of O–H and those from C=O contents. This can be explained by the measurement errors of the results from C=O contents, based on the fact that the peak areas of 1790–1660 cm^{-1} are much smaller than those of 3630–3000 cm^{-1} as shown in Table 3.2. Therefore, the losses of O–H should be used to estimate the degrees of crosslinking.

Table 3.2 Relative integration of absorption peaks and estimated degrees of crosslinking

Membranes	3630–3000 cm^{-1} O–H (=C-H)	3000–2750 cm^{-1} –C–H [a]	1790–1660 cm^{-1} C=O	Loss of O–H	TMC moiety [b]	C=O contents
PVA	4.54	1	0.030	~1 %	0	~1 %
PVA-1TMC-B	3.98	1	0.027	13.3 %	4.4 %	~1 %
PVA-1TMC-T	3.80	1	0.029	17.1 %	5.7 %	~1 %
PVA-3TMC-B	3.88	1	0.038	15.4 %	5.1 %	~1 %
PVA-3TMC-T	3.83	1	0.028	16.6 %	5.6 %	~1 %
PVA-5TMC-B	3.83	1	0.045	16.4 %	5.5 %	1.5 %
PVA-5TMC-T	3.74	1	0.084	18.4 %	6.1 %	2.8 %
PVA-7TMC-B	3.76	1	0.033	18.0 %	6.0 %	~1 %
PVA-7TMC-T	3.67	1	0.155	19.9 %	6.6 %	5.2 %

[a] Set to be 1 as a standard.

[b] Calculated from loss of O–H.

3.3.3 Swelling Behavior

Figure 3.5 shows the degrees of swelling of PVA and PVA-TMC membranes in water at room temperature. It is observed that the PVA-TMC membranes with a lower degree of crosslinking *i.e.* PVA-1TMC and PVA-2TMC, have lower degrees of swelling than the uncrosslinked PVA, while the membranes with higher degrees of crosslinking *i.e.* PVA-5TMC and PVA-7TMC, show much higher degrees of swelling than the uncrosslinked PVA.

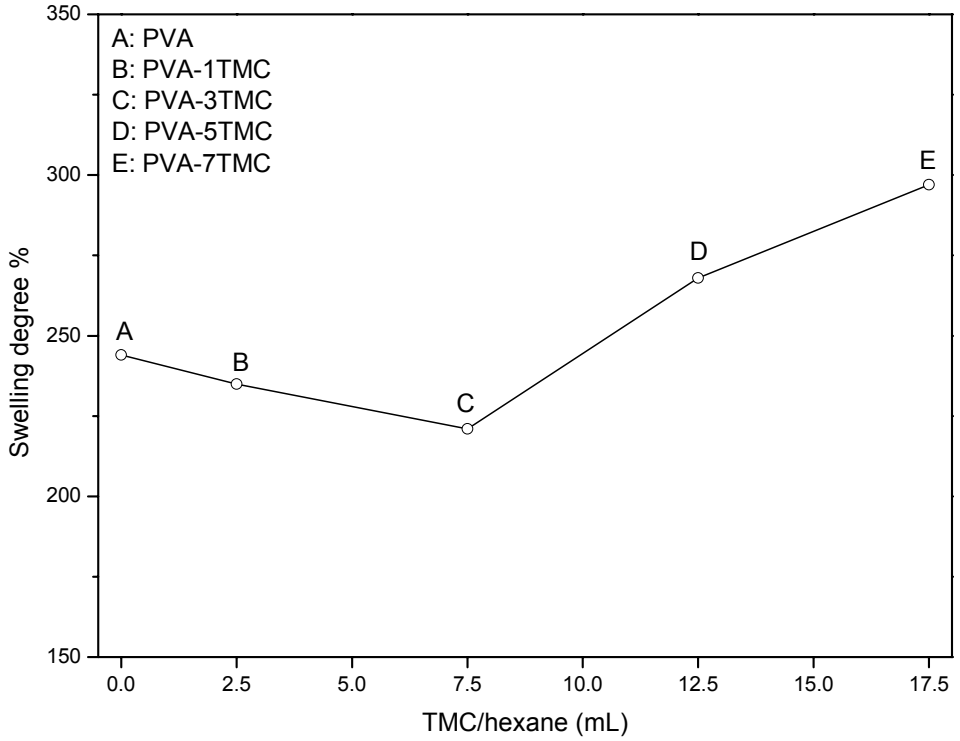

Figure 3.5 Degrees of swelling of PVA-TMC membranes in water at room temperature

It is known that crosslinking of the polymer chains restricts their mobility and reduces the swelling of the polymer matrix, which agrees with the swelling behavior of PVA-1TMC and PVA-2TMC membranes. However, as shown in Figure 3.6, The TMC moiety is much larger than the repeating unit of PVA, and introduction of the TMC moieties increases the interchain space within the PVA matrix. Therefore, more space is produced for the sorbed water molecules. When the crosslinked PVA membranes are soaked in water, there exist two opposite effects: the crosslinking effect and the steric effect. In addition, the unreacted acid chloride groups of TMC will form –COOH,

which will have strong interactions with water, will also help increase the membrane swelling. All these factors eventually lead to a decrease (crosslinking effect is controlling) and then an increase (steric effect is controlling) in the degree of swelling.

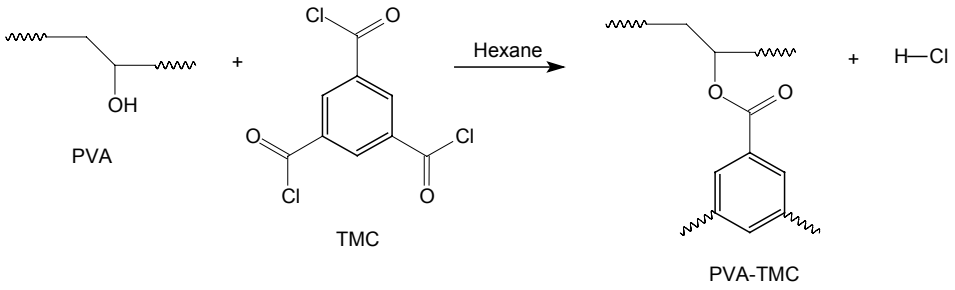

Figure 3.6 Schematic crosslinking of PVA with TMC

3.3.4 DSC Thermograms

Differential scanning calorimetry (DSC) was measured on a corrected baseline obtained from heating an empty aluminum pan under the measurement conditions. The corrected DSC curves are presented in Figure 3.7, with all crosslinked PVA curves plotted through the same points at 50 and 250 °C, and the PVA curve through 50 °C only.

No distinguishing transitions can be found below 150 °C for all the curves. The uncrosslinked PVA showed a typical DSC thermogram [Gohil *et al.* 2006; Mallapragada and Peppas 1996]. Table 3.3 presents the melting temperature (T_m onset) data. The T_m did not change much with the degree of crosslinking. However, PVA-1TMC showed the highest T_m. At a higher degree of crosslinking, the T_m decreased to almost the same as that of the uncrosslinked PVA. This interesting phenomenon is believed to result from the change in the crystalline morphology induced by TMC moieties or between the mechanisms of crystallinity [Park *et al.* 2001]. Furthermore, the more TMC moieties in the PVA matrices, the lower their T_ms.

When heated above T_m, the uncrosslinked PVA showed to be unstably endothermic from 237 °C, while the DSC curves of the crosslinked PVA appeared to be fairly flat. This result indicates that PVA-TMC membranes are more stable at high temperatures than the uncrosslinked PVA, that is, PVA-TMC membranes are more thermally stable. This will be discussed further later.

3.3.5 Thermal Stability and Degradation

Thermogravimetric analysis (TGA) was conducted in a helium atmosphere. The TGA thermograms

and the derivative thermogravimetric (DTG) curves of the uncrosslinked PVA film and PVA-TMC membranes are presented in Figure 3.8.

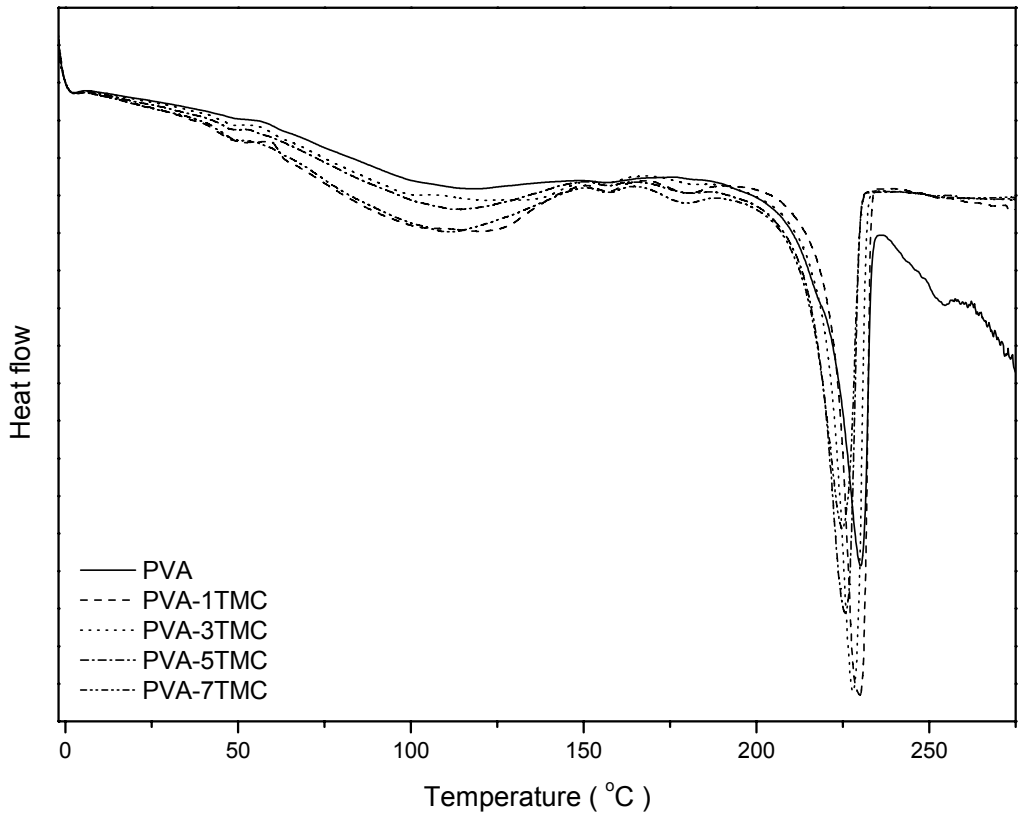

Figure 3.7 DSC curves of the uncrosslinked PVA and PVA-TMC membranes

TGA thermograms give a direct view of thermal degradation. T_ds for 5 % and 10 % weight losses, T_d onset and residual weights were read directly from the TGA curves and are listed in Table 3.3. The degradation temperature T_d reveals that TMC moieties can improve the thermal stability of PVA membranes. The T_d 5 %, for instance, increases from 247.6 °C to above 330 °C. For membranes of a high degree of crosslinking, *i.e.* PVA-3TMC, PVA-5TMC and PVA-7TMC, there is no significant difference among their T_ds 5 % which are about 90 °C higher than that of the uncrosslinked PVA. However, PVA-1TMC, with a lower degree of crosslinking, shows a small increase in T_d 5 %. The TMC moiety, in the form of trimesoyl ester in the crosslinked PVA membranes, contributes to the

improvement in thermal stability. The difference between the residual weights of the crosslinked and uncrosslinked PVA membranes is also believed to be caused by the TMC moiety.

Table 3.3 T_m onset temperature from DSC and weight changes of materials from TGA

Membranes	T_m onset (°C)	T_d 5 % wt. Loss (°C)	T_d 10 % wt. Loss (°C)	T_d onset (°C)	Residual wt. (%)
PVA	206.01	247.6	255.5	250.5	9.7
PVA-1TMC	216.40	259.2	271.0	250.6	9.4
PVA-3TMC	212.04	334.9	349.7	349.6	1.7
PVA-5TMC	211.30	339.7	353.8	352.8	2.8
PVA-7TMC	209.19	331.4	347.5	347.3	3.9

In an inert atmosphere, pyrolysis of PVA occurs mainly in two steps: Decomposition begins with a rapid chain-stripping elimination of water below 350 °C to form polyene, followed by breakage of the main chain [Gilman *et al.* 1994; McNeill 1997]. Detailed pyrolysis reactions were proposed by Gilman *et al.* [1994]. DTG was conducted to study the degradation reactions [Agherghinei 1996; Kim and Park 1995; Wilburn 1999]. All peak data from the DTG plots are listed in Table 3.4. In the DTG of the uncrosslinked PVA, two maximum values of $\Delta wt./\Delta T$ can be found at around 270 and 435 °C. There are three peaks in the DTG of PVA-1TMC, at approximately 275, 353 and 437 °C. The other three membranes with high degrees of crosslinking show no big difference between their DTG thermograms, with peaks at around 378 and 444 °C. The first DTG peak of the uncrosslinked PVA represents the thermal elimination of water, and the second is caused by the further degradation of the main chain. The mechanism of water elimination can be illustrated in Figure 3.9 (a).

The classic ester pyrolysis is a syn-elimination at a temperature above 300 °C to yield alkenes and the corresponding carboxylic acids. The cyclic transition states can be achieved in the presence of the β-H atoms if the steric environment is not too demanding. Consequently, as shown in Figure 3.9 (b), the ester pyrolysis mechanism is proposed for the elimination of trimesic acid from PVA-TMC. The produced polyenes continue to decompose to small molecules, which is represented by the second DTG peak.

Three peaks are observed in the DTG diagram of PVA-1TMC, which can also be interpreted with the pyrolysis mechanism proposed above. The first step is the elimination of water to form double bonds in the main chains. The intermediate, as shown in Figure 3.9 (c), can readily decompose further

following the ester pyrolysis mechanism at a lower temperature. This is because polyene, a more stable conjugated structure, can be formed this way. With continuous heating, chain breakage occurs.

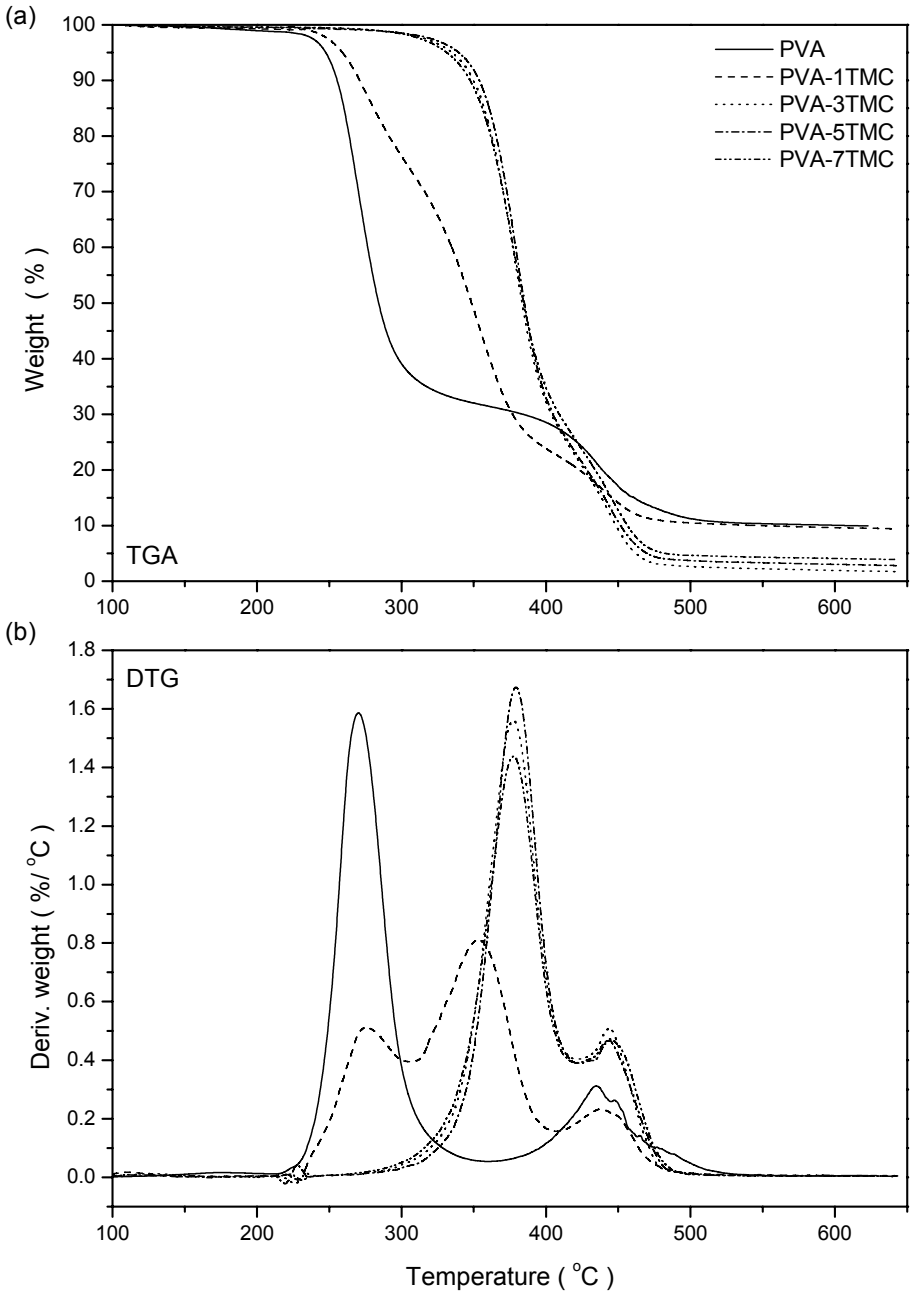

Figure 3.8 TGA and DTG curves of the PVA and PVA-TMC membranes

Therefore, generally speaking, with a higher degree of crosslinking, that is, a higher content of TMC moieties in PVA-TMC, the residual weights should be less. However, if the content of TMC moiety is too high, the presence of TMC moiety changes the uniformity of the main chain, and the polyene cannot fully degrade. This phenomenon can be observed from the data of the residual weights in Table 3.3.

Table 3.4 Peak values of DTG

Membranes	1st Peak (°C)	2nd Peak (°C)	3rd Peak (°C)
PVA	270.4	–	434.5
PVA-1TMC	275.0	352.7	437.0
PVA-3TMC	–	377.7	442.9
PVA-5TMC	–	379.0	444.2
PVA-7TMC	–	377.1	444.1

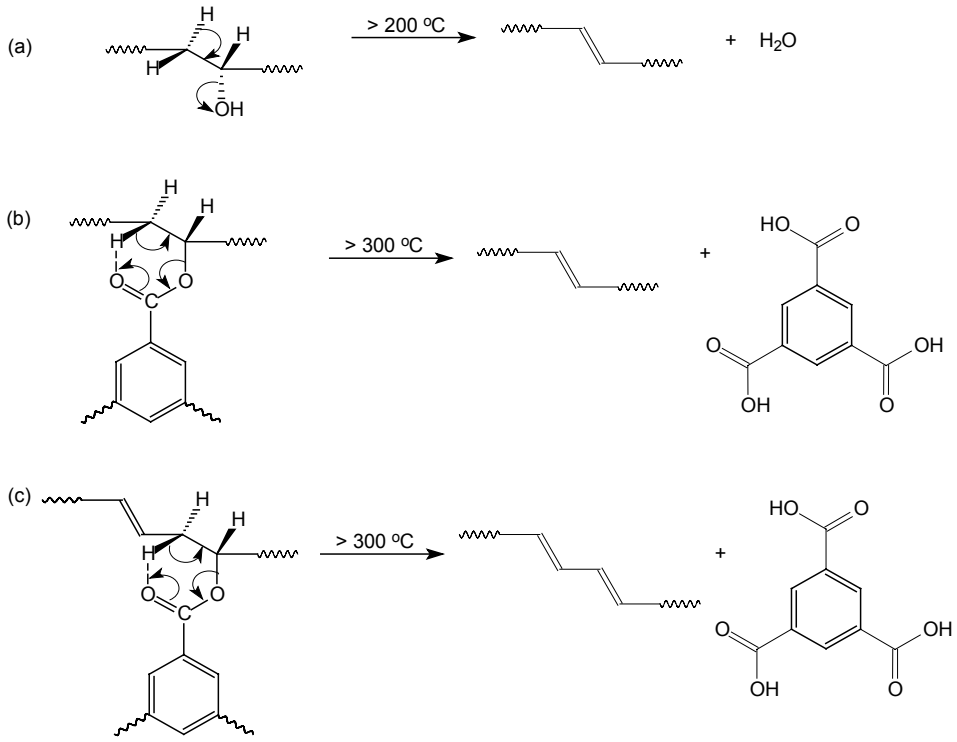

Figure 3.9 Pyrolysis reactions of PVA and PVA-TMC

3.3.6 Pervaporation Properties of PVA-TMC Membranes

3.3.6.1 Water Permeation through PVA-TMC Membranes

The relationship between water permeation and the operating temperature was investigated by conducting pervaporation with pure water at different temperatures. As shown in Figure 3.10, the water flux increases with an increase in the operating temperature. However, the temperature dependencies of the four PVA-TMC membranes are different. Since PVA chains are easily form crystallites at an elevated temperature, the crosslinked PVA with a lower degree of crosslinking, e.g., PVA-1TMC, produces more resistance for the permeation of water and isopropanol. Therefore, from 40 to 50 °C, the permeation flux of PVA-1TMC did not change significantly as the other membranes.

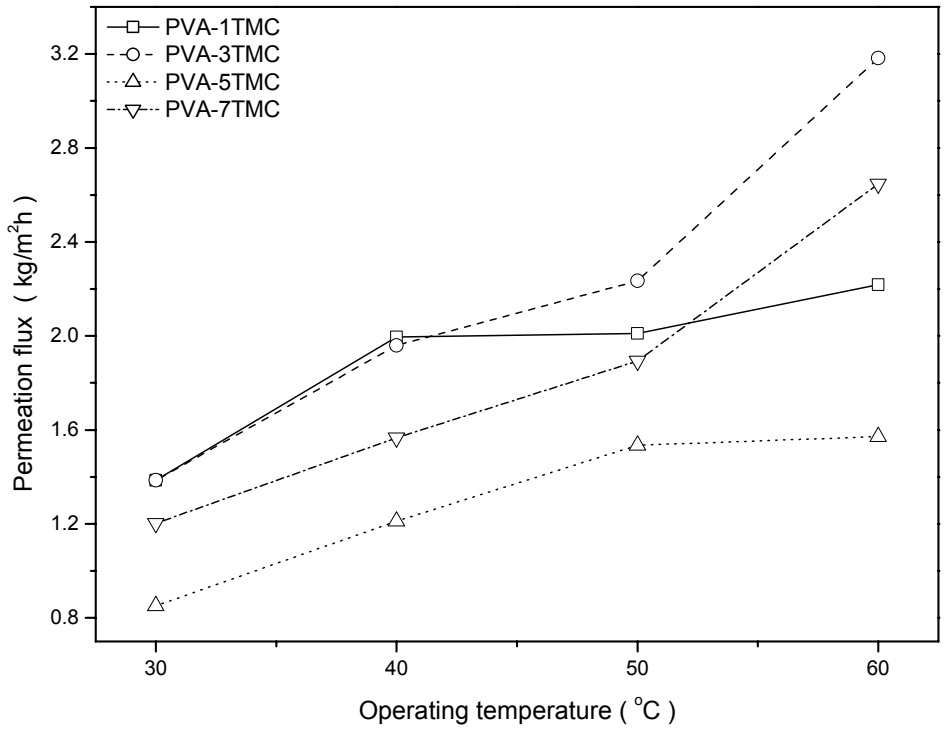

Figure 3.10 Pure water permeation at different temperatures

The Arrhenius equation can be used to study the effect of temperature on the permeation flux [Rhim *et al.* 1998; Yu *et al.* 2002].

$$F = A \cdot e^{-\frac{E_p}{RT}} \tag{3.4}$$

where A is the pre-exponential factor, E_p is the apparent permeation activation energy, R is the universal gas constant, and T is the temperature.

Since permeation depends on solubility and diffusivity of the permeant in the membrane, E_p is determined by the sorption and diffusion properties. The E_p data are listed in Table 3.5. PVA-1TMC has a smaller value of E_p, because crosslinking of the PVA matrix produces more resistance for the permeation of water, while for the other membranes, the larger values of E_p indicate that the static effect of TMC and the hydrophilicity of the residual $-$COOH groups facilitate water permeation. Such a conclusion agrees with the result of the degree of crosslinking discussed in 3.3.3.

Table 3.5 Activation energies of pure water permeation and water/isopropanol permeation

Membranes	E_p (pure water) (kJ/mol)	$E'_{p,w}$ [a] (kJ/mol)	$E'_{p,a}$ [a] (kJ/mol)
PVA-1TMC	13.5 ± 1.5	32.5 ± 1.7	31.9 ± 4.5
PVA-3TMC	23.0 ± 1.6	28.5 ± 0.6	43.8 ± 2.6
PVA-5TMC	24.1 ± 2.3	29.0 ± 5.1	28.6 ± 4.0
PVA-7TMC	22.2 ± 0.5	26.8 ± 2.1	27.3 ± 1.7

[a] The feed water content is ~20 wt. %.

3.3.6.2 Temperature Effect on Pervaporation

Temperature is an important factor influencing water permeation through the membrane. From Equations 3.3 and 3.4, the following equations can be obtained for pervaporation of binary feed mixtures [Svang-Ariyaskul *et al*. 2006]:

$$y_w = [1 + \frac{A_a}{A_w} \cdot e^{\frac{E'_{p,w} - E'_{p,a}}{RT}}]^{-1} \tag{3.5}$$

$$\alpha_{w/a} = \frac{x_a}{x_w} \cdot \frac{A_w}{A_a} \cdot e^{-\frac{E'_{p,w} - E'_{p,a}}{RT}} \tag{3.6}$$

The permeate water content and separation factor are directly affected by the activation energies for permeation, *i.e.* ($E'_{p,w} - E'_{p,a}$), as well as the pre-exponential factors.

Figure 3.11 show the total permeation flux at different temperatures. Compared with data in Figure 3.10, PVA-7TMC shows a higher permeation flux than PVA-5TMC. The E_p data for water and isopropanol permeation are shown in Table 3.5. PVA-3TMC has a large negative value of ($E'_{p,w} - E'_{p,a}$), but the others close to 0. This tells that the permeate water content of PVA-3TMC will increase when increasing temperature, and PVA-3TMC has a trend to produce a higher selectivity towards water/isopropanol than the other membranes. Therefore, from Figure 3.12, the effects of temperature on the permeate water content and separation factor for different membranes can be observed. It is obvious that PVA-3TMC had the best separation performance for pervaporation dehydration of isopropanol/water mixtures, especially at relatively lower temperatures.

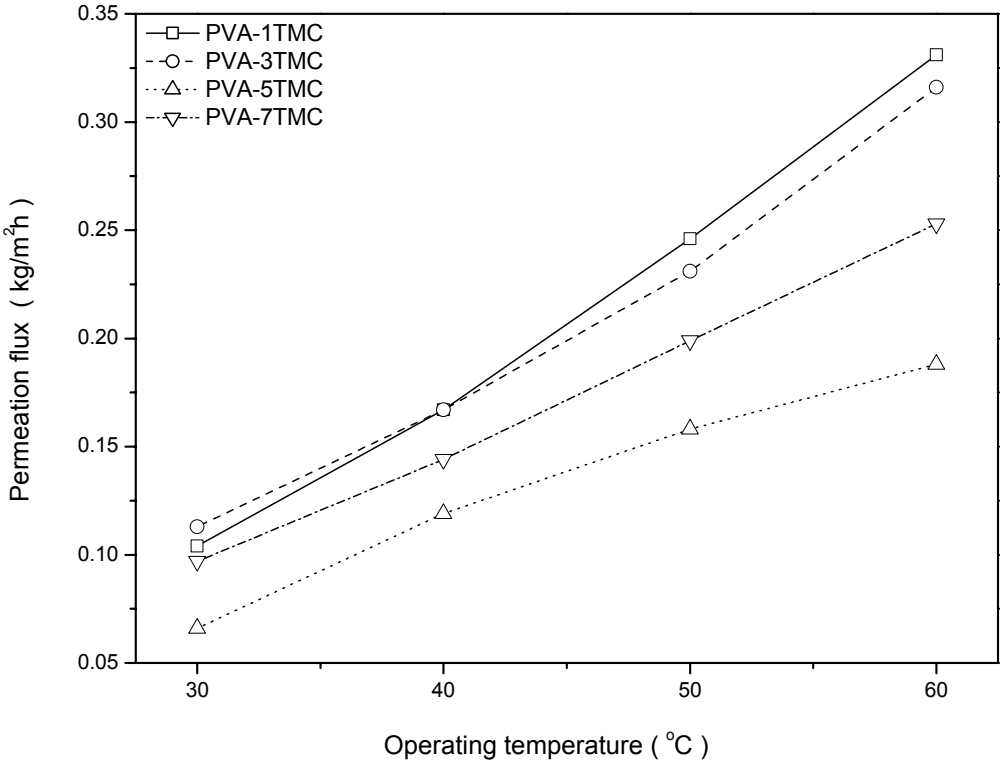

Figure 3.11 Total permeation flux at different temperatures (20 wt. % water in the feed)

3.3.6.3 Effect of Concentration on Pervaporation

Pervaporation experiments were conducted with different feed water contents at 60 °C. Figure 3.13 shows the relationship between the permeation flux and the feed concentration. The PVA-TMC

membranes in general have a higher flux with an increase in the feed water content. However, PVA-5TMC and PVA-7TMC have a lower permeation flux than PVA-1TMC and PVA-3TMC when the feed water content is sufficiently high.

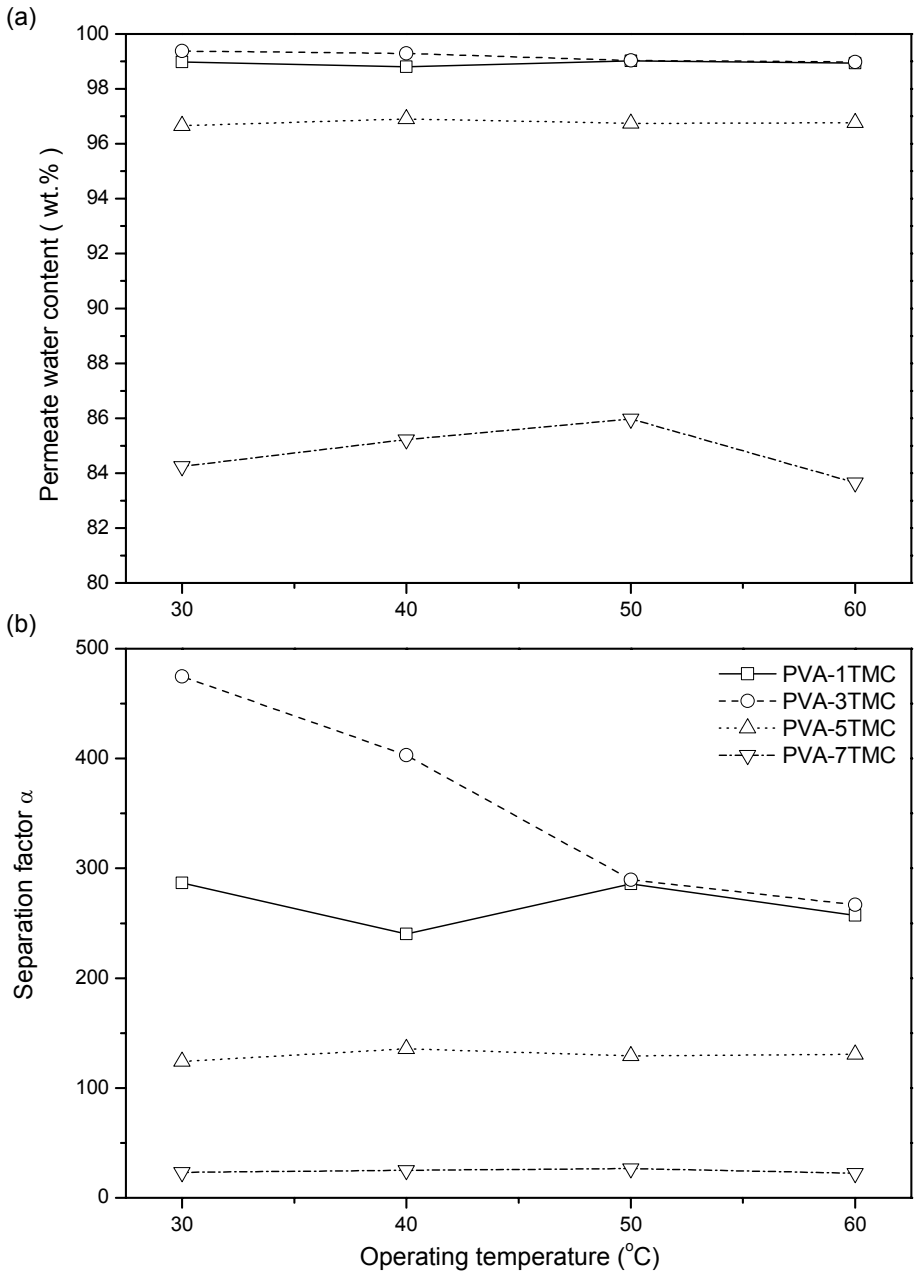

Figure 3.12 Permeate water contents and separation factors of water/isopropanol at different temperatures (20 wt. % water in the feed)

The permeation of water and isopropanol through PVA-TMC membranes depends on the membrane swelling. With a higher degree of crosslinking, the polymer chains are confined in a crosslinked matrix with less free volume, which allows less water to permeate. However, insertion of the large size moiety of TMC into the interchain space produces larger passageways for penetrants in the matrix. On the other hand, the ester groups formed from the crosslinking reaction will facilitate more isopropanol to permeate. In addition, the hydrophilic –COOH groups produced by the residual acid chloride groups of TMC will help increase the permeation of water through the membranes with a higher degree of crosslinking. Consequently, an increase in the degree of crosslinking may increase or decrease the membrane permeability, depending on which aspect is dominating.

The permeate water content and separation factor at different feed concentrations are plotted in Figure 3.14.

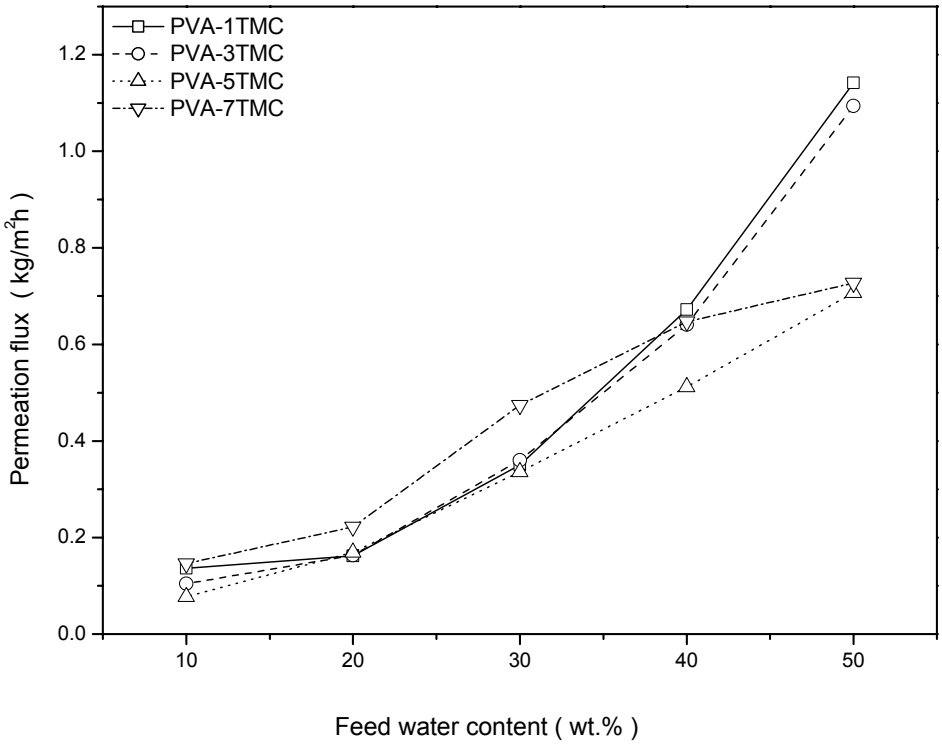

Figure 3.13 Effects of feed water contents on permeation flux at 60 °C

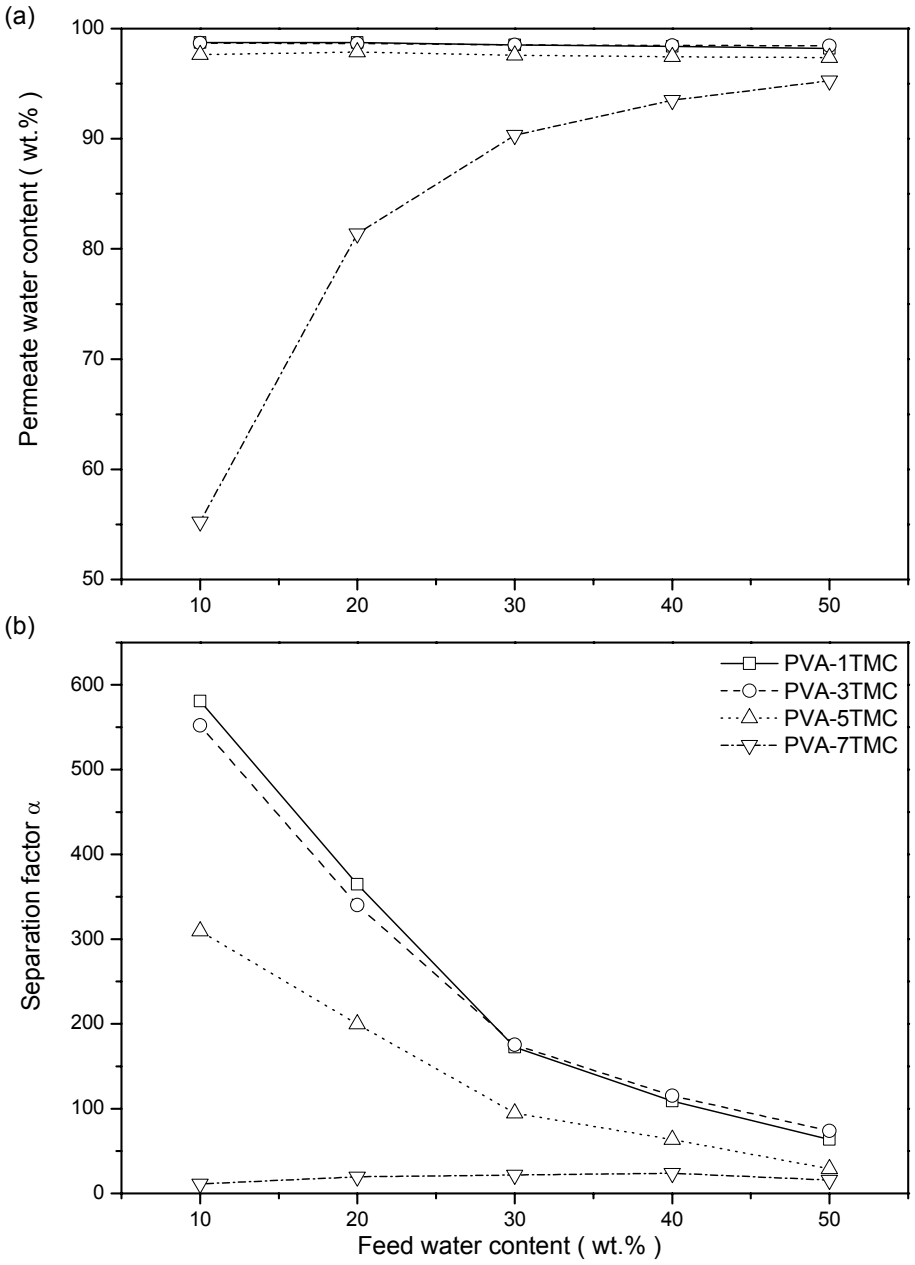

Figure 3.14 Effects of feed water contents on permeate water contents and separation factors of water/isopropanol at 60 °C

All PVA-TMC membranes show a decrease in selectivity and an increase in permeation flux with an increase in the feed water content. PVA-TMC membranes, except PVA-7TMC, are very selective

to water permeation at different feed concentrations. The high content of the TMC moiety in PVA-7TMC facilitates the permeation of both water and isopropanol as discussed before. Therefore, when the isopropanol content in the feed is high enough, isopropanol can also permeate more easily.

Note that aqueous isopropanol can form an azeotrope at 12.6 wt. % water. The vapor-liquid equilibrium shown in Figure 1.2 indicates that the equilibrium water content in the vapor phase is higher than that in the liquid phase when the water content in the liquid is below 12.6 wt. %.

3.3.6.4 Comparison of Pervaporation Performance with Other PVA Membranes

From pervaporation properties shown above, it can be found that among the four PVA-TMC membranes, PVA-3TMC shows the best overall pervaporation properties. In Table 3.6, PVA-3TMC is compared with other PVA crosslinked membranes for pervaporation separation of water/isopropanol mixtures at 60 °C. The permeate concentration and permeation flux are summarized in Table 3.6. Though the permeation flux of PVA-3TMC, 0.11 kg/m^{2}h (at a feed water content of 10 wt.%) at 60 °C is lower than other membranes, the permeate water content of PVA-3TMC is still comparable with the PVA-CM membrane [Nam *et al.* 1999], and better than the crosslinked PVA membranes that were crosslinked using the traditional methods such as thermal and glutaraldehyde crosslinking [Yu *et al.* 2002; Svang-Ariyaskul *et al*. 2006].

Table 3.6 Comparison of pervaporation performance of PVA-3TMC with those of other PVA crosslinked membranes for water/isopropanol mixtures at 60 °C

Membranes [a]	Feed water contents (wt.%)	Permeate water contents (wt.%) [b]	Permeation flux (kg/m^{2}h) [c]	References
PVA-SSA	10	~99.6	~0.33	Rhim *et al*.[1998]
PVA-CM	15	~99	~0.43	Nam *et al*. [1999]
PVA-GA	10	~95.5	~0.15	Yu *et al*. [2002]
PVA-Ceramic	5	~87	~0.3	Peters *et al*. [2006]
PVA-Thermal	10	~95	~0.21	Svang-Ariyaskul *et al*. [2006]
PVA-3TMC	10	~99	0.11	This work
PVA-3TMC	20	~99	0.32	This work

[a] The membrane preparation details can be found in the corresponding references.

[b] Permeate water contents were calculated from separation factors or estimated from plots.

[c] Permeation flux data were estimated from plots.

3.4 Conclusions

Trimesoyl chloride was used to crosslink PVA dry membranes on their top surfaces, and the crosslinked PVA-TMC membranes with different degrees of crosslinking were successfully prepared for pervaporation dehydration of isopropanol.

The degrees of crosslinking of the membranes were investigated with FTIR-ATR for these membranes by using the peak integration method. Loss of the hydroxyl groups was used to estimate the degree of crosslinking, which was in the range of 13–20 %. The membranes had different degrees of crosslinking on each side of the membranes. Therefore, they had asymmetric structures.

PVA-3TMC had the lowest degree of swelling in water at room temperature, and PVA-7TMC had the highest. The crosslinking and steric effects of TMC, as well as the hydrophilicity of the residual $-COOH$ groups from TMC, contributed to the swelling behavior of PVA-TMC membranes.

TGA and DSC thermograms revealed that PVA-TMC membranes had better thermal stability than the uncrosslinked PVA film. TGA and DTG curves were analyzed to provide an understanding of the mechanism of thermal pyrolysis for PVA-TMC membranes, which consisted of elimination of water and/or trimesoyl acid and breakage of the main chain. The PVA-TMC membranes with a lower degree of crosslinking degraded by elimination of water, while those with a higher degree of crosslinking degraded by elimination of TMC.

Pure water permeation and dehydration of isopropanol/water mixtures with PVA-TMC membranes at different temperatures and feed concentrations were studied. An appropriate degree of crosslinking was helpful to the stable flux and good membrane selectivity. The PVA-3TMC membrane had the best overall pervaporation performance for dehydration of isopropanol among the four PVA-TMC membranes. At a feed water content of 20 wt. %, an overall permeation flux of 0.32 kg/m^2h and a permeate water content of 99 wt. % were observed at an operating temperature of 60 °C. Further study of PVA-3TMC membrane can be found in Chapter 4.

Chapter 4

Trimesoyl Chloride Crosslinked Poly(vinyl alcohol) Membranes for Pervaporation Dehydration of Isopropanol. II. Sorption Properties and Pervaporation Behaviors under Different Operating Conditions*

Pervaporation and sorption properties of the TMC crosslinked PVA membrane (PVA-3TMC) were investigated. Temperature and concentration dependencies of sorption properties were studied through equilibrium water uptake and preferential sorption tests. The effects of water/isopropanol on the PVA-TMC matrix and the possible change of the degree of crystallinity induced by the sorbed water are believed to account for the differences of sorption properties at different temperatures and feed compositions. Permeation flux did not change significantly in the heating-cooling cycle when conducting water permeation and performing pseudo-steady-state pervaporation dehydration of isopropanol. However, the formation of crystallites during the heating run could improve the membrane selectivity. At a given feed concentration, the permeation flux and separation factor did not change in the diluting and concentrating runs at 60 °C. Permeate concentrations did not change significantly with time in the batch pervaporation process.

4.1 Introduction

The solution-diffusion model is widely accepted for describing mass transport in pervaporation [Shao and Huang 2007]. According to this model, the mass transport across the membrane consists of three steps [Ho and Sirkar 1992; Huang 1990]: sorption at the feed side surface, diffusion through the membrane under the chemical potential gradient, and desorption from the membrane at the permeate side. The desorption is usually regarded as a non-selective step when the partial pressure in the permeate side is much lower than the partial saturated vapor pressure of the penetrant. Hence, the permeation is mainly governed by the sorption and diffusion properties. In pervaporation, the sorption step is usually studied through the equilibrium sorption that can be easily conducted by equilibrating

* Portions of this work have been published in *Journal of Membrane Science*, vol. 302 (2007), pp. 36–44.

the membrane in a liquid mixture or in the vapor phase [Park *et al.* 1998]. Furthermore, the overall and the preferential sorption properties can be used directly to predict the sorption selectivity for a particular feed mixture [Freger *et al.* 2000; Oh *et al.* 2001]. The diffusivity of the penetrant can be calculated from the permeability and solubility data using an appropriate model equation, or alternatively be obtained from the time-lag measurements of transient permeation [Shah *et al.* 2006; Clement *et al.* 2004].

The separation performance is essentially determined by the interactions between the membrane and the species to be separated. The temperature and concentration dependencies of permeation flux and selectivity are usually studied when a membrane is selected for the separation of a liquid mixture, based on which optimization may be made to find appropriate operating conditions. In addition, the operating "history", including membrane conditioning and thermal/concentration cycles, may have an impact on the pervaporation performance, especially for glassy or crystalline polymer membranes. Yeom *et al.* [1996] proposed a qualitative model for the relaxation behavior of glassy membranes in pervaporation in order to illustrate the flux changes through a sodium alginate membrane in heating-cooling cycles. The glass transition of the swollen membrane and the occurrence and relaxation of the stress formed in the polymer matrix were suggested to be the intrinsic reason for the thermal hysteresis. Guo and Chung [2005] observed a thermal hysteresis in pervaporation in two thermal cycles for Matrimid® 5218 asymmetric membranes, and pointed out that the interactions between the feed molecules and the membrane, the non-equilibrium nature of the selective dense skin, and the asymmetric membrane swelling were the main factors that contributed to the thermal hysteresis. The feed concentration influences permeation flux and selectivity, and as such for conditioned membranes or in dynamic pervaporation processes, the concentration history may also have an impact on the hysteresis behavior. Rautenbach and Hommerich [1998] studied the dynamic mass transfer in pervaporation with PVA/PAN commercial membranes. And results showed that the time dependence of the permeation flux on sudden changes in the feed concentration was not significant and the mass transport could be considered to be at the "pseudo-steady" state.

However, investigations above mainly dealt with the hysteresis behaviors of permeation flux, and the temperature/concentration effects on selectivity as well as the correlation with sorption properties were not addressed. In Chapter 3, trimesoyl chloride crosslinked poly(vinyl alcohol) membranes showed some potentials to be pervaporation membranes for dehydration of isopropanol, but further study should be performed. Therefore, this work is also to study the trimesoyl chloride crosslinked poly(vinyl alcohol) membranes for pervaporation, with an emphasis on the swelling/sorption

properties and pervaporation performances under different operating conditions. Pseudo-steady-state and dynamic pervaporation tests were conducted to better understand the pervaporation behaviors of the membrane in dehydration of isopropanol.

4.2 Experimental

4.2.1 Materials and Membrane Preparation

All materials used were the same as described in 3.2.1.The membranes used in this chapter were named as PVA-3TMC in Chapter 3, and preparation and crosslinking conditions can be found in Table 3.1 [Xiao *et al.* 2006]. The thicknesses of the membranes were measured with a micrometer to be in the range of 50–60 μm.

4.2.2 Pervaporation Experiments

The pervaporation apparatus consists of two parts: the pervaporation cell (Figure 4.1) and the permeate collection system (Figure 4.2). The membrane was mounted in the pervaporation cell with the support of a porous stainless steel plate. The effective area of the membrane was 1.59×10^{-3} m^2. The feed chamber (Ø45 mm × 200 mm) was equipped with a magnetic stirrer, a thermal couple and a N_2 purge inlet. The pervaporation cell was immersed in a water bath. A magnetic stirrer was placed right beneath the water bath to guarantee sufficient mixing in the feed side, and consequently to minimize the concentration polarization. The vaporous permeate was condensed and collected in liquid nitrogen cold traps. A vacuum pump was used to provide the driving forces for permeation. The permeate collection system was also used in the desorption tests to collect the sorbed penetrants. A Varian CP-3800 Gas Chromatograph equipped with a TCD detector was utilized to determine the compositions of the permeate and sorbate samples. All pervaporation experiments were repeated with different membranes to verify the reproducibility.

4.2.2.1 Water Permeation

The water permeation was carried out in a thermal cycle, where the feed water was heated from 30 to 60 °C and then cooled from 60 to 30 °C. The water permeation flux was determined.

4.2.2.2 Pseudo-Steady State Pervaporation

The membrane was first conditioned by running water permeation at 30 °C for at least 0.5 h. An

isopropanol/water mixture (water content 18.9 ± 0.6 wt. %) was charged into the pervaporation system. The pervaporation was conducted in a thermal cycle from 30 to 60 °C and then from 60 to 30 °C. The pervaporation continued at 60 °C with feed water contents varying from 10 to 50 wt. % and then from 50 to 10 wt. %.

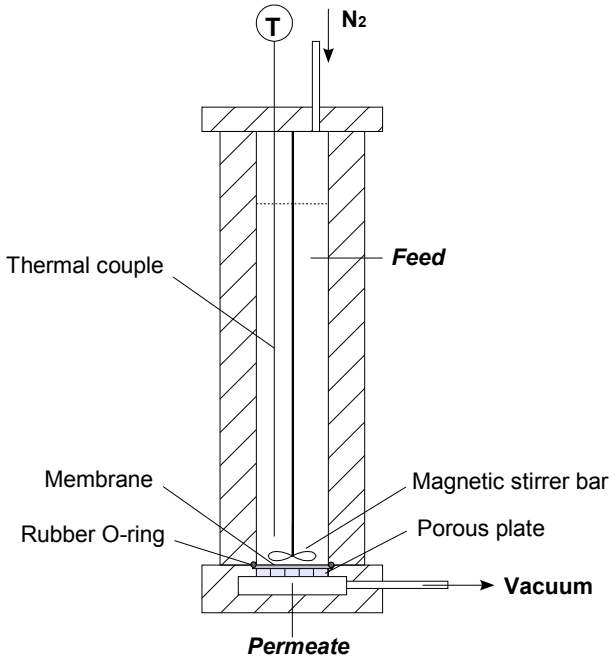

Figure 4.1 Schematic pervaporation cell

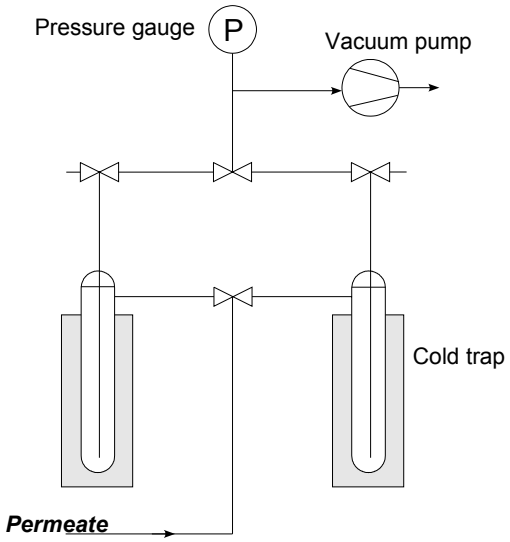

Figure 4.2 Schematic permeate collection system

4.2.2.3 Batch Pervaporation Process

About 25 mL of aqueous isopropanol (water content 20 wt. %) was admitted to the pervaporation system at 60 °C. The feed was maintained at 1.5 kPag with N_2. The batch pervaporation experiment was operated for 11 h, and the permeate sample was collected, weighed and analyzed. The average permeation flux and selectivity over the sampling period were calculated.

4.2.3 Swelling and Sorption Experiments

Membranes were fully dried *in vacuo* at 70 °C overnight before use. The membranes were soaked in pure water at a given temperature for at least 10 h to reach sorption equilibrium, and then the swollen membrane were treated with the same procedures as in 3.2.4.

The sorption experiments were also conducted with water/isopropanol mixtures (water contents 19.5 ± 0.3 wt. %) at different temperatures. To determine the sorption selectivity, the membrane sample containing sorbed penetrants was transferred into a container which was subjected to vacuum at 90 ± 5 °C for at least 1.5 h, and the desorbed species were collected in cold traps. Sorption tests were also carried out at 60 °C with aqueous isopropanol solutions of various water contents. The tests were repeated with different membranes to guarantee reproducibility

The degree of swelling (*SD*) can be calculated from Equation 3.1, and the sorption selectivity α_S is defined as

$$\alpha_S = \frac{y'_w / y'_a}{x'_w / x'_a} \tag{4.1}$$

where y'_w and y'_a represent the concentrations of the water and isopropanol in the adsorbate, respectively, and x'_w , x'_a are the water and isopropanol concentrations in the feed mixture, respectively.

4.3 Results and Discussion

4.3.1 Effect of Temperature on Sorption Properties

4.3.1.1 Temperature Dependence of the Degree of Swelling

The degrees of swelling for membranes in water and water/isopropanol mixtures at different temperatures were determined, and the results are shown in Table 4.1. In the temperature range of 30–

60 °C, the degree of swelling varied from 210 % to 310 % for sorption in water, and from 18.5 to 16.5 % for sorption in water/isopropanol mixtures. The water contents in the water-swollen PVA-TMC membranes were also calculated to be in the range of 68–76 wt. %.

Table 4.1 Parameters calculated for sorption in water and sorption in water/isopropanol at different temperatures

Sorption temperature (°C)	Sorption in water		Sorption in water/isopropanol [b]
	Degrees of swelling (%)	Water fraction [a] (wt. %)	Degree of swelling (%)
30	212	68	18.3
40	260	72	17.7
50	275	73	18.0
60	314	76	16.5

[a] Weight fraction of water in the swollen membranes.

[b] Water contents were 19.5 ± 0.3 wt. % in the feed mixtures of water/isopropanol.

The degrees of swelling of PVA-TMC in water indicate the high affinity to water. PVA is highly hydrophilic because of the strong H-bonding between water and –OH groups. The presence of water in the polymer matrix can be divided into three states: nonfreezing water (strongly bound to –OH), freezable bound water (weakly bound to polymer chains or to the nonfreezing water), and free water (with the same properties as bulk water) [Hodge *et al.* 1996a]. PVA is a semicrystalline polymer, and crosslinking with TMC decreases the uniformity of the structure, hence reducing the degree of crystallinity. However, in the DSC curve of PVA-TMC, T_m can be observed [Xiao *et al.* 2006]. When the uncrosslinked PVA undergoes the sorption test, water molecules penetrate mainly into the amorphous region to swell PVA, and will gradually affect the crystalline region and even dissolve the uncrosslinked PVA at high temperatures [Sperling 2001]. For PVA-TMC, the crosslinked polymer chains cannot be dissolved by water, but the polymer matrix can hold a large amount of water. Therefore, the PVA-TMC membranes show a very high degree of swelling in water.

Table 4.1 also shows that PVA-TMC membranes have a higher degree of swelling for sorption in water at higher temperatures, which can be interpreted by the changes in the mobility of polymer chains and the free volumes of the PVA-TMC matrix. Hodge *et al.* [1996a, 1996b] studied the degree of crystallinity of water-swollen PVA films, and found that the more water in the PVA matrix, the lower the degree of crystallinity, and when the water content was above 62 wt. %, the swollen PVA

was in an amorphous state. Therefore, it is highly likely that the water-swollen PVA-TMC membranes were non-crystalline. The movement of polymer chains is enhanced at a higher temperature, which requires more space in the polymer matrix. In other words, more free volume is produced based on the Fox-Flory free volume theory [Sperling 2001; Van den Beukel and Sietsma 1990; Gibbs and DiMarzio 1958; Turnbull and Cohen 1961], and the polymer matrix can accommodate more penetrant molecules, resulting in a higher degree of swelling.

The degree of swelling for sorption in water/isopropanol mixtures is much lower than in water, which is caused by the two opposite effects of water and isopropanol on the polymer matrix. Isopropanol is a non-solvent of PVA, and it can hardly swell PVA. The water-swollen PVA-TMC membrane will lose the flexibility when contacting with isopropanol. In the water/isopropanol sorption tests, water penetrates into the PVA-TMC matrix and opens some paths for the penetrant molecules. However, the unfavorable non-solvent effect of isopropanol severely restricts the amounts of the sorbed penetrants in the polymer matrix.

Additionally, the degrees of swelling for sorption in water/isopropanol at different temperatures do not change significantly. It was expected that at a higher temperature, more isopropanol and water molecules went inside the PVA-TMC matrix because of the more free volume formed. However, as the temperature increases, crystallites will be formed because of the high mobility of the segmental chains, which will decrease the free volume of the polymer matrix. As a result, the degree of swelling is not dramatically affected by the sorption temperature.

4.3.1.2 Temperature Dependence of Sorption Selectivity

The water contents in the water/isopropanol-swollen membranes and the sorption selectivities are shown in Figure 4.3. The sorbed water contents in the membrane varied in the range of 94–96 wt. %, and the sorption selectivity was found to be 63–100. Increasing the sorption temperature will increase isopropanol uptake in the membrane initially, and when the temperature is high enough, a further increase in the temperature will tend to reduce isopropanol uptake. From Figure 4.3, the minimum sorbed water content and/or sorption selectivity are expected.

4.3.2 Effect of Feed Concentration on Sorption Properties

4.3.2.1 Concentration Dependence of the Degree of Swelling

Dry membranes were soaked in water/isopropanol mixtures with different water contents at 60 °C,

and the degrees of swelling were determined. The results are shown in Figure 4.4. The degree of swelling increased from 9 to 88 % as the feed water content increased from 12 to 54 wt. %.

Since PVA is a hydrophilic material and isopropanol has an unfavorable non-solvent effect on PVA swelling, increasing water contents (*i.e.* decreasing isopropanol contents) in the sorption mixtures will facilitate water penetration into the polymer matrix. At the same time, the change in the degree of crystallinity is another cause for the higher degree of swelling when the feed water content increases. If only a small amount of water was sorbed in the membrane, the crystalline region in the polymer matrix was not be affected; however, if the swollen membrane contains a large amount of water, the crystalline region will be partially destroyed, which will provide more space to the penetrants.

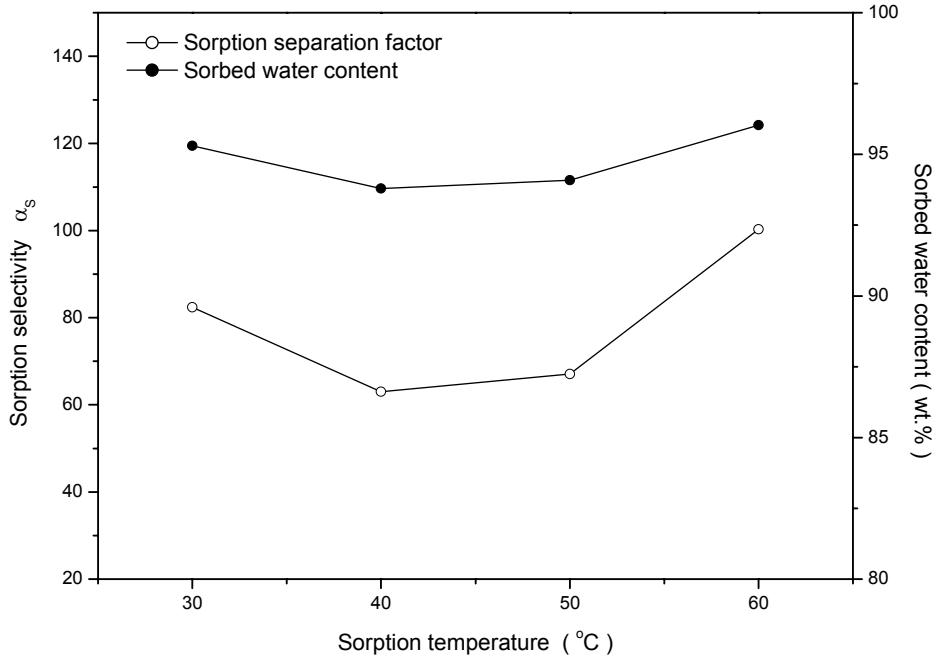

Figure 4.3 Sorption selectivities and sorbed water contents for membranes in water/isopropanol sorption mixtures at 19.5 ± 0.3 wt. % water

4.3.2.2 Concentration Dependence of Sorption Selectivity

The degree of swelling represents the total amount of the sorbed penetrants in the membrane. However, no details are known about the interactions of water and isopropanol with the polymer matrix. Therefore, the weight ratios of the sorbed species to the membrane material were evaluated, as

shown in Figure 4.5.

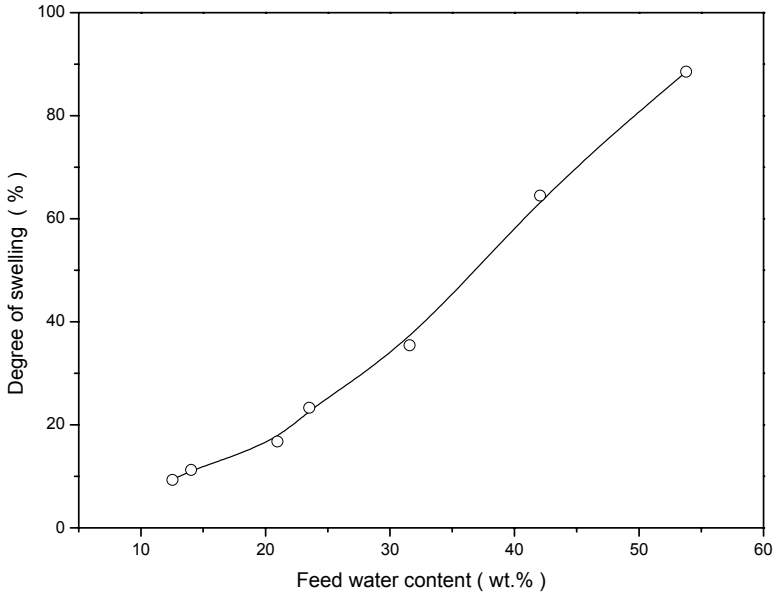

Figure 4.4 Degree of swelling for the membrane in water/isopropanol mixtures at 60 °C

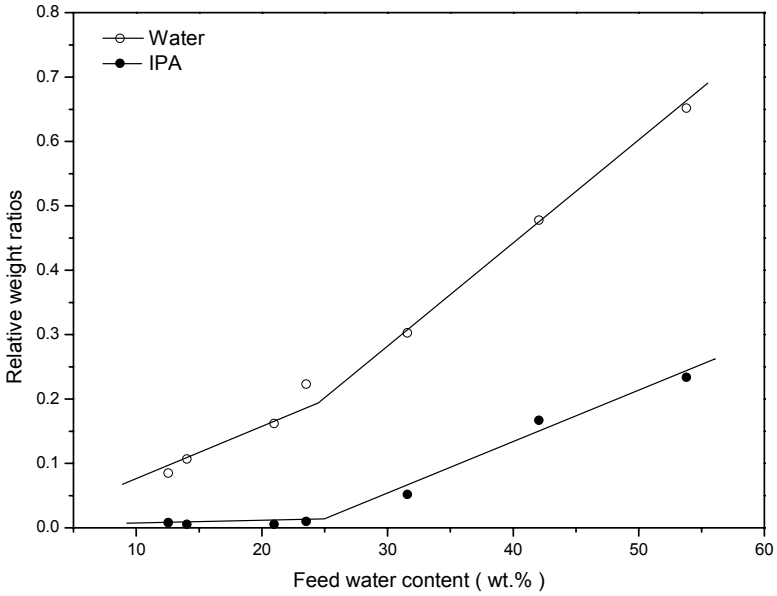

Figure 4.5 Weight ratios of the sorbed water and isopropanol to the membrane material in swollen membranes at 60 °C

Obviously, the increase in the sorbed water and isopropanol follows roughly a linear relationship when feed water contents are below and above the region of 20–30 wt. %. From the slopes of the lines, it is observed that water uptake is more sensitive to the feed water content than isopropanol uptake. This indicates that PVA-TMC membranes have a higher affinity to water than to isopropanol. When the feed water content is below 20 wt. %, there is little isopropanol in the adsorbate and the sorption uptake of isopropanol increases only slightly as the feed water content increases. When the water content in the liquid phase is greater than 30 wt. %, both uptake rates of water and isopropanol are higher. The slope change in Figure 4.5 indicates the opposite effects of water and isopropanol on the polymer matrix, and furthermore, the water-induced change in the degree of crystallinity is another possible factor [Jang and Lee 2003]. Accordingly, this change can also be found in sorption selectivity of the membrane.

Figure 4.6 shows the sorbed water content and the sorption selectivity at different feed water concentrations. The two curves have similar shapes, but the sorbed water content shows a maximum of 96.8 wt. % at a feed water content of ~21 wt. %, and the sorption selectivity tends to be the highest at a feed water content of ~14 wt. %. Note that aqueous isopropanol can form an azeotrope at a water content of 12.6 wt. %. The vapor-liquid equilibrium indicates that the equilibrium water content in the vapor phase is higher than that in the liquid phase when the water content in the liquid is below 12.6 wt. %, which helps contribute to the peak values of the sorption selectivity and sorbed water content in the membrane.

4.3.3 Pervaporation Behavior in a Thermal Cycle

Pure water permeation and pervaporation dehydration of isopropanol were performed from 30 to 60 °C, then back from 60 to 30 °C, and the thermal cycles were referred to as “heating” and “cooling”, respectively, in the following discussion.

4.3.3.1 Water Permeation in a Thermal Cycle

Figure 4.7 shows the permeation flux of pure water in a heating/cooling cycle. No significant difference in permeation flux was observed. The activation energies for water permeation were calculated for both the heating and cooling steps, and the results are shown in Table 4.2. Regardless of the heating and cooling processes, the activation energy for pervaporation appears to be the same. These results clearly show that the permeation properties of the PVA-TMC membrane were not affected by water. It is concluded that the polymer matrix undergoes fast relaxation, which renders the

polymer matrix to reach the new state easily in the thermal cycle [Yeom *et al.* 1996; Shafee and Naguib 2003].

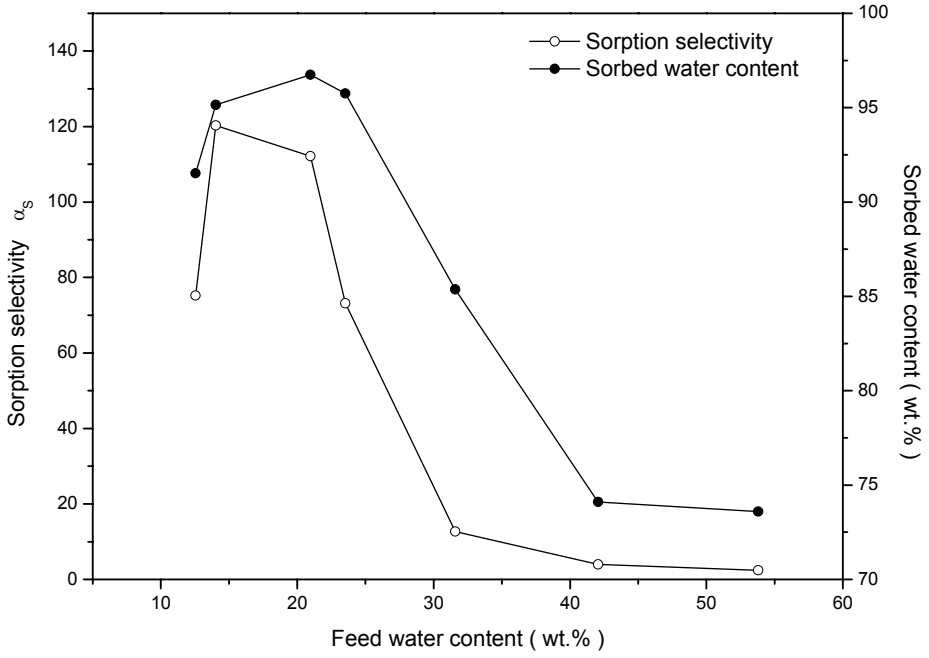

Figure 4.6 Sorption selectivity and sorbed water content for the membrane in water/ isopropanol at 60 °C

4.3.3.2 Dehydration of Isopropanol in a Thermal Cycle

The dehydration of isopropanol by pervaporation was carried out with water/isopropanol mixtures (18.9 ± 0.6 wt. %) at steady states of permeation. The permeation flux, separation factor and permeate water content in the thermal cycle are shown in Figure 4.8.

In the heating-cooling runs, the permeation flux remained unchanged, while the separation factor showed a significant increase in the cooling run. The change in the separation factor was due to the increase of the permeate water content in the cooling run.

Table 4.2 also shows the activation energies for permeation of the binary water/isopropanol mixtures in the thermal cycle. The activation energy for water permeation shows no distinct change in the heating and cooling runs, while the activation energy for isopropanol permeation varies from ~56 kJ/mol (in the heating run) to ~84 kJ/mol (in the cooling run). Since the cooling run started from the

end of the heating run, it can be seen that in the cooling run isopropanol encounters a greater resistance to permeate through the membrane than in the heating run, whereas the resistance to water permeation in the two runs does not differ much. This is contributed to the increase in the chain packing density and the loss of the free volume in the membrane. Considering the crystallinity properties of the PVA-TMC membrane, some crystallites are formed in the membrane during the heating run. The crystallites are usually considered to be impermeable and act as crosslinked regions [Gref *et al.* 1993]. Therefore, both the transport of water and isopropanol in the non-crystalline region will be affected. However, the mass transport resistance of isopropanol in the PVA-TMC matrix is more significant because of the larger size of the isopropanol molecules than water. Consequently, as shown in Figure 4.8, the permeate water concentration and thus the membrane selectivity are improved in the cooling run. Though the activation energy for isopropanol permeation increases in the cooling run, the activation energy for the overall permeation changes only slightly from 40.8 to 42.7 kJ/mol, and that for water permeation decreases from 44.2 to 43.1 kJ/mol.

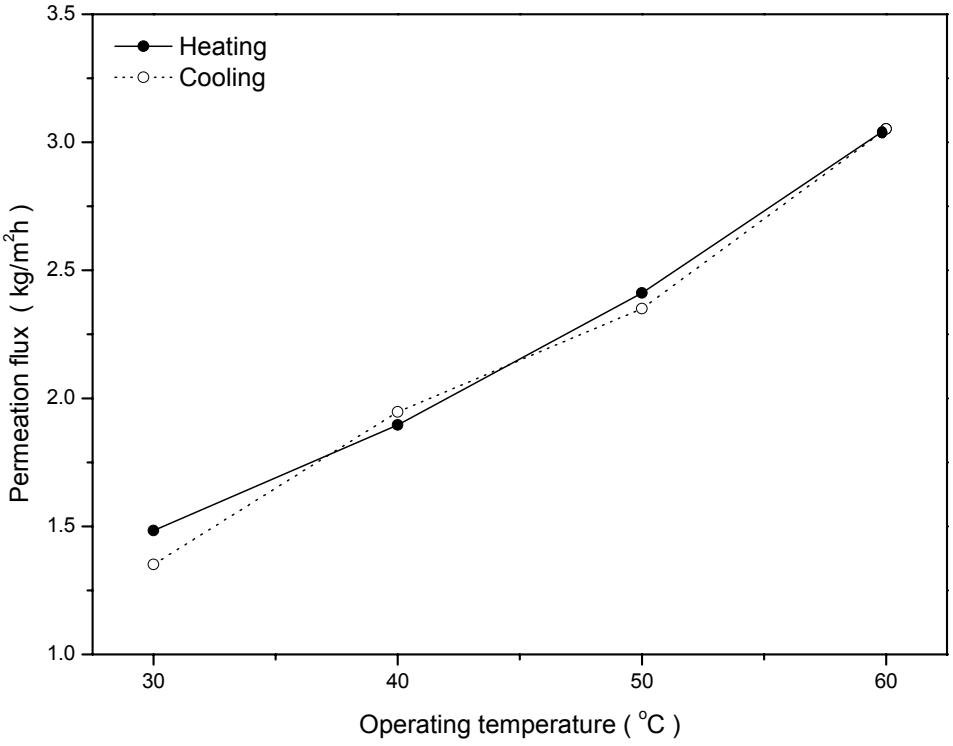

Figure 4.7 Pure water permeation in a thermal cycle

Table 4.2 Permeation activation energies in the heating/cooling runs, for water permeation and for total flux and water/isopropanol individual flux

Thermal cycle	Water permeation [c]	Pervaporation dehydration [d]		
	E_w (kJ/mol)	$E_{p,t}$ (kJ/mol)	$E'_{p,w}$ (kJ/mol)	$E'_{p,a}$ (kJ/mol)
Heating [a]	19.4 ± 1.0	40.8 ± 0.7	44.2 ± 2.3	55.9 ± 1.7
Cooling [b]	19.3 ± 1.1	42.7 ± 0.3	43.1 ± 0.6	83.7 ± 3.2

[a] Operating temperatures varied from 30 to 60 °C.

[b] Operating temperatures varied from 60 to 30 °C.

[c] Pure water permeation.

[d] The water contents in feed mixtures were kept to be 18.9 ± 0.6 wt. % during pervaporation processes.

From the solution-diffusion model, diffusion selectivity α_D can be determined from pervaporation selectivity α and sorption selectivity α_S [Wang *et al.* 2000a; Sun *et al.* 2006], based on the assumption of equilibrium sorption on the membrane surface at the feed side [Shao and Huang 2007].

$$\alpha_D = \alpha / \alpha_S \tag{4.2}$$

Based on Equation 4.2, the diffusion selectivity was evaluated, as shown in Figure 4.9. The diffusion selectivity for the heating runs is in the range of 1.5–3.5, and larger values (1.5–8.5) are observed for the cooling run, which supports the hypothesis of the "crosslinking" effect of the crystallites formed during the heating runs. Compared with the sorption selectivity of 63–100 shown in Figure 4.3, the diffusion selectivity is much smaller. It appears that the sorption step is dominant in pervaporation in the thermal cycle, and the overall membrane performance will be thus controlled by the sorption step.

4.3.4 Pervaporation in a Concentration Cycle

Pervaporation dehydration of isopropanol was conducted at 60 °C by changing the feed water contents from 10 to 50 wt. % (diluting), and then from 50 to 10 wt. % (concentrating). Figure 4.10 presents the permeation flux, separation factor and permeate water concentration in the concentration cycle.

There is no significant difference in the permeation flux and selectivity in the diluting and concentrating runs. Apparently, the membrane permeability is not influenced by the concentration history, which indicates the quick response of the polymer matrix to the concentration changes in the

feed. Furthermore, at 60 °C, the degree of crystallinity and the free volume of the non-crystalline regions in the PVA-TMC matrix can be restored. The restorability of the PVA-TMC membrane in the diluting and concentrating runs is attributed to its crosslinked structure [Sperling 2001].

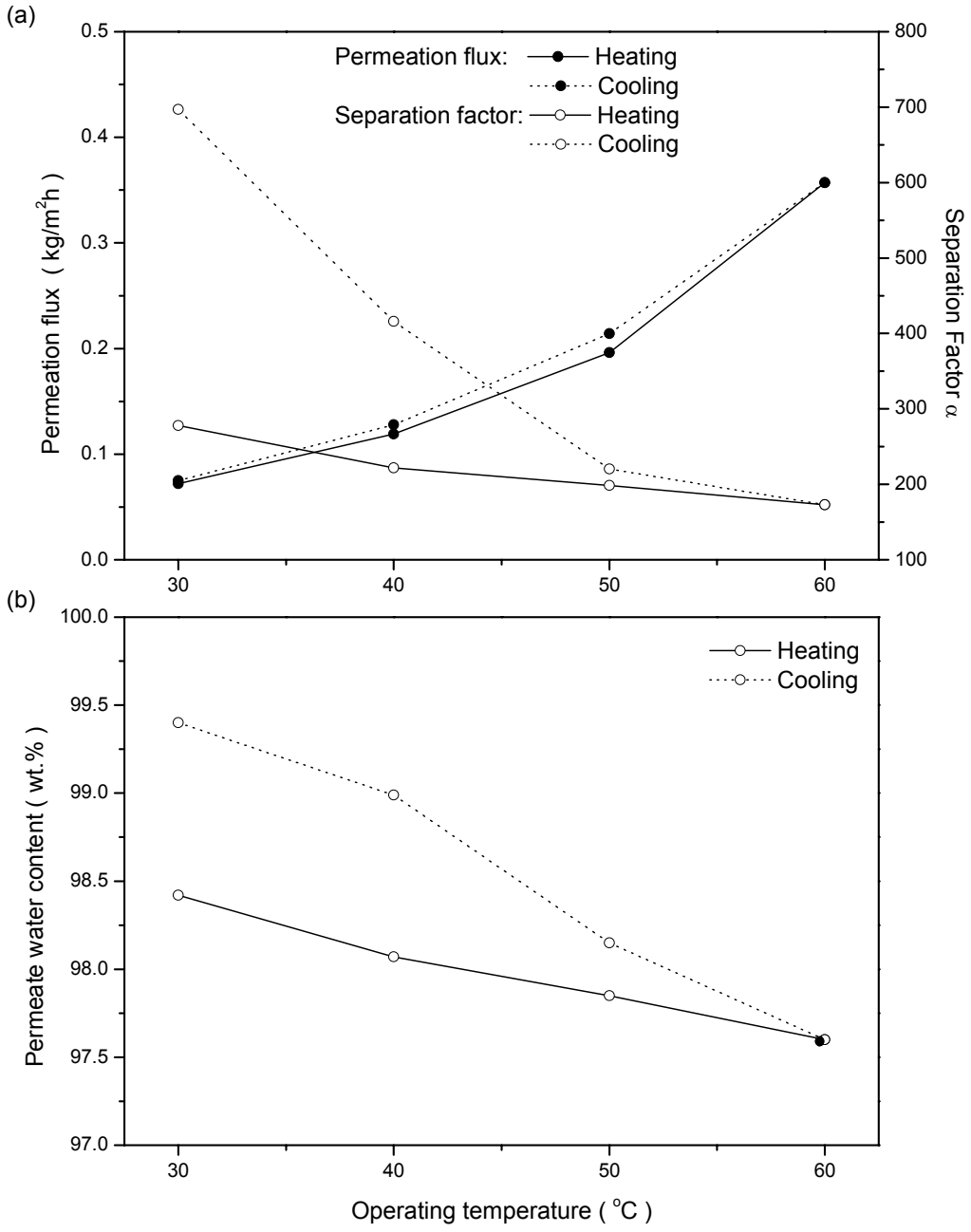

Figure 4.8 Pervaporation dehydration of isopropanol in a thermal cycle
(a) Permeation flux and separation factor (b) Permeate water content

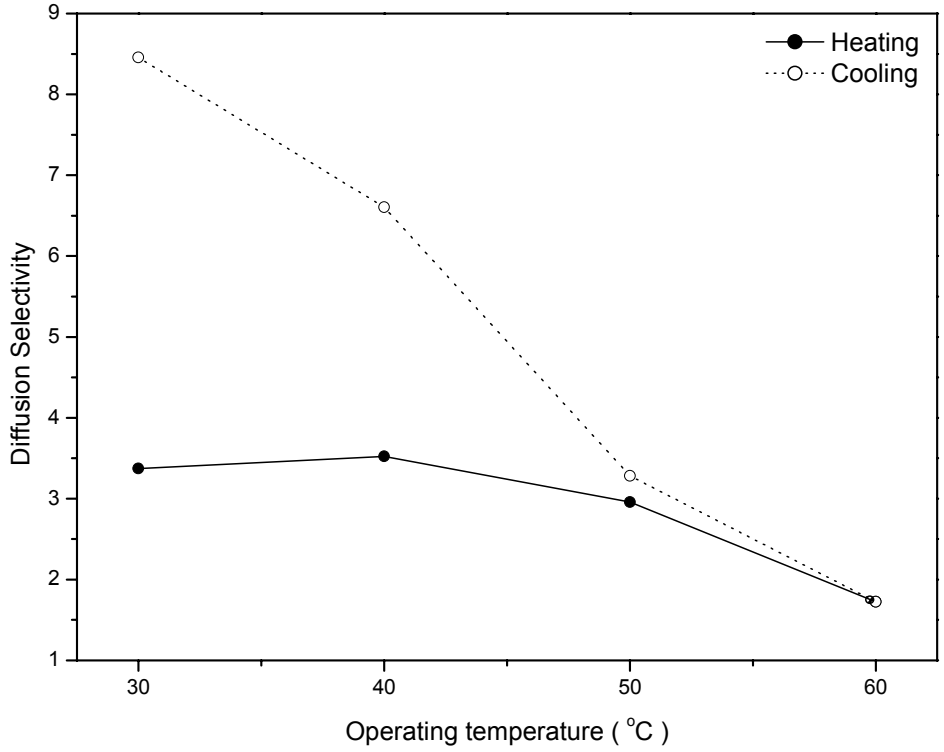

Figure 4.9 Diffusion selectivity for pervaporation in a thermal cycle

Figure 4.10 (b) shows that the permeate water concentration does not change significantly as the feed water concentration varies from 10 to 50 wt. %. This is interesting because the feed water concentration only affects permeation flux. This feature will be very useful especially in batch operations where the feed concentration will change with time.

The diffusion selectivity, calculated using Equation 4.2, is shown in Figure 4.11. The diluting and concentrating runs have no remarkable influence on the diffusion selectivity. A comparison of diffusion selectivity (7–14) with the sorption selectivity (45–2) as shown in Figure 4.6 is still unclear which step, sorption or diffusion, is more dominating for the pervaporation process at 60 °C in the concentration cycle. However, a simple observation is made based on the values of the sorption/diffusion selectivities: sorption is more important at low feed water concentrations, while diffusion is more controlling at high feed water concentrations.

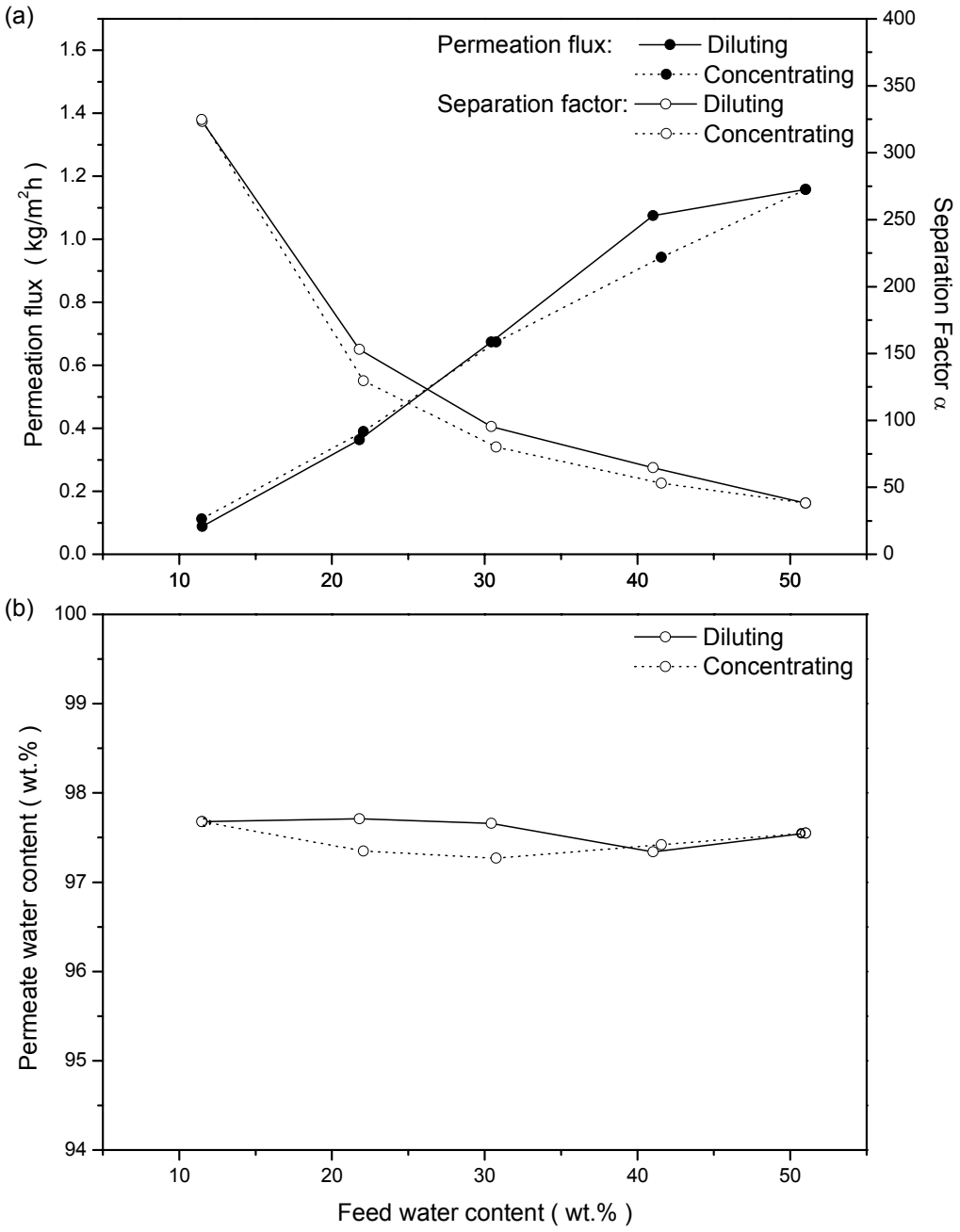

Figure 4.10 Pervaporation dehydration of isopropanol in a concentration cycle (a) Permeation flux and separation factor (b) Permeate water content

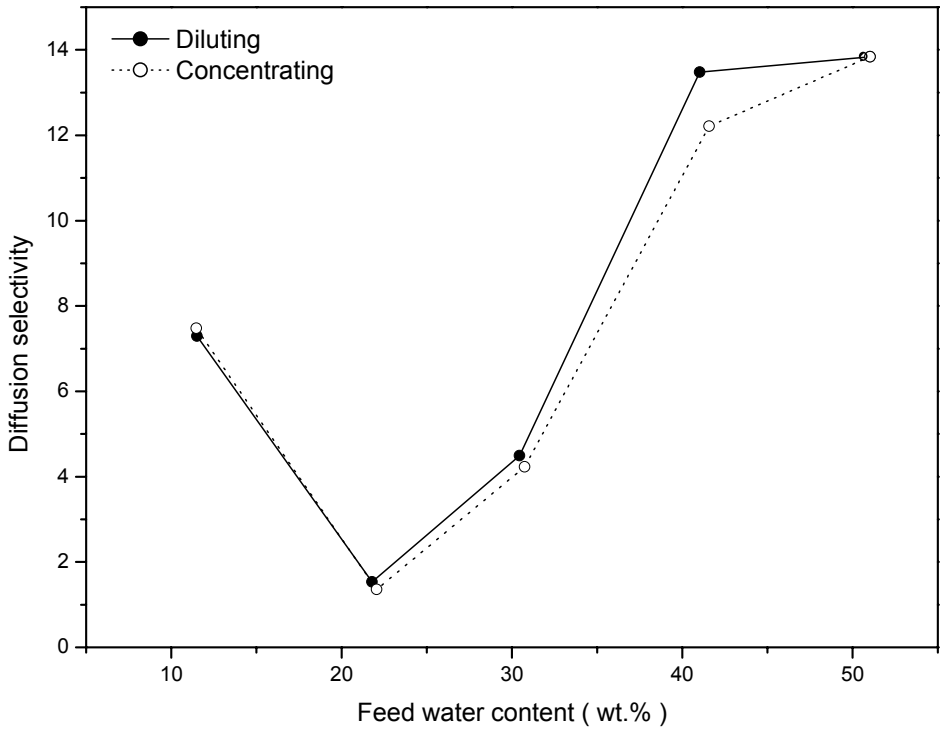

Figure 4.11 Diffusion selectivity for pervaporation in a concentration cycle at 60 °C

4.3.5 Dynamic Pervaporation Process

To verify the effect of the feed concentration on pervaporation performance of the PVA-TMC membrane, batch pervaporation was performed at 60 °C.

Figure 4.12 (a) shows the water contents of the feed and permeate during the batch operation. The feed concentration continuously decreases with time, and the permeate concentration reaches a "steady-state" within 1 h. As the feed water concentration decreases, there is no significant change in the permeate water concentration, which is consistent with the results of pervaporation in a concentration cycle. From Figure 4.12 (b), it is observed that the permeation flux decreases with time, whereas the selectivity increases.

The batch pervaporation process covers a feed concentration range of 9–20 wt. % water that includes the azeotropic concentration of the aqueous isopropanol (12.6 wt. % water). Experimental results showed that the PVA-TMC membrane was stable for pervaporation dehydration of

water/isopropanol mixtures at concentrations close to the azeotrope. One potential application of the membrane is to break the azeotrope in distillation separation of water/isopropanol mixtures.

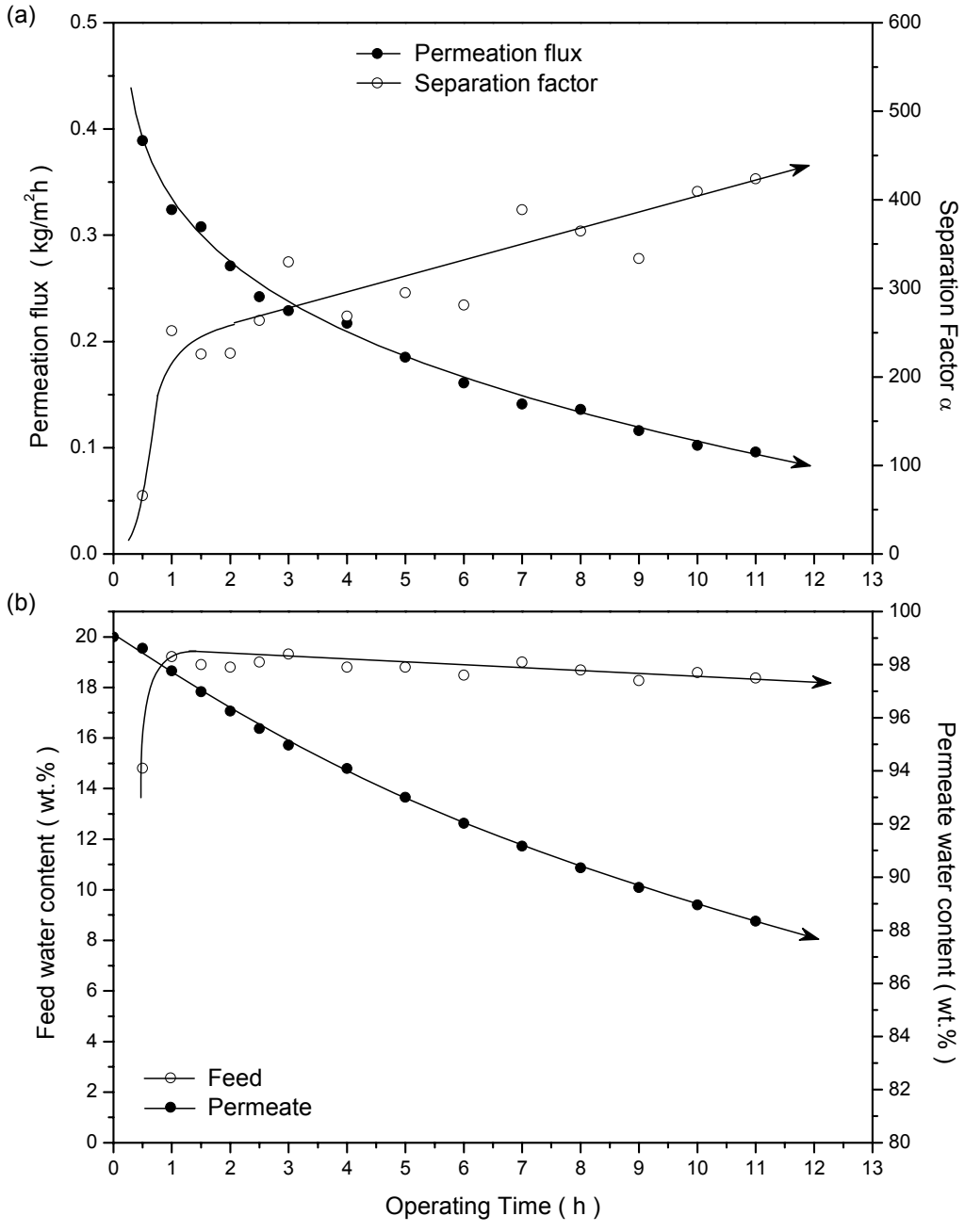

Figure 4.12 Batch operation of pervaporation dehydration of isopropanol
(a) Water contents in the feed and permeate (b) Permeation flux and separation factor

4.4 Conclusions

This work is a further study of the crosslinked PVA-3TMC membrane in Chapter 3. Equilibrium water uptake and preferential sorption tests were carried out and the sorption selectivity towards water and isopropanol was evaluated. The pervaporation performance was investigated by means of pseudo-steady-state and batch pervaporation processes.

The degree of swelling in water was found to vary in the range of 210 % (at 30 °C) to 310 % (at 60 °C). However, membrane swelling was suppressed substantially in water/isopropanol mixtures (~19.5 wt. % water). At a water content of 21 wt. %, the sorbed water content reached a maximum of 96.8 wt. %, and the sorption selectivity had the highest value of 120 at the water content of 14 wt. %.

No significant difference was observed in the permeation flux of pure water as well as pseudo-steady-state pervaporation of water/isopropanol mixture in the heating-cooling cycle. However, the "crosslinking" effect of the crystallites formed during the heating run caused more diffusion resistance for isopropanol, and increased the permeation activation energies for isopropanol, leading to a higher selectivity in the cooling run.

Pervaporation in the concentration cycle did not show significant changes in flux and the permeate water content in the diluting and concentrating runs. In the batch operation of pervaporation dehydration of isopropanol, there were no substantial changes in the permeate water contents at the feed water concentration of 9–20 wt. %.

Chapter 5

Trimesoyl Chloride Crosslinked Chitosan Membranes: Gas Separation and Pervaporation Properties*

Crosslinked chitosan membranes were prepared from interfacial crosslinking of chitosan membranes in trimesoyl chloride/hexane. A higher degree of swelling was observed for the membrane with a higher degree of crosslinking when swollen in water at room temperature. Membranes were characterized with DSC and TGA, and a two-stage thermal decomposition mechanism was proposed. Pure gas permeation was performed with CO_2 and N_2 at room temperature, and CS-TMC-2 membrane showed the best selectivity towards CO_2/N_2, with CO_2 permeability of ~163 Barrer and the CO_2/N_2 permeability ratio of ~42. Pervaporation was carried out for dehydration of isopropanol with the unconditioned and conditioned membranes, and CS-TMC-3 membrane showed the best pervaporation properties. The crosslinking-induced changes in the relaxation behavior and mobility/packing properties of polymer matrices were attributed to the changes in pervaporation and gas permeation performances.

5.1 Introduction

Chitosan is the deacetylation product of chitin. With the aid of an acid, usually a dilute acetic acid, chitosan can dissolve in water to form a viscous solution of maximum ~2 wt. %, and thus it has found more applications than chitin in membrane technologies.

Some attempts were made to prepare porous chitosan membranes with conventional fabrication techniques such as the phase inversion method, but the mechanical property of the membranes was not satisfactory [Zeng and Ruckenstein 1996b]. However, the porosity-controlling method with silica [Zeng and Ruckenstein 1996a] and the cryogenic-induced phase inversion method [Gu *et al.* 2001] have been developed to prepare macro-porous chitosan membranes with good mechanical properties. In addition, chitosan could also be used as a coating on a porous substrate for ultrafiltration

* Portions of this work will be published in *Journal of Membrane Science*, available online on August 17, 2007. doi:10.1016/j.memsci.2007.08.021

membranes [Musale *et al.* 1999; Yoon *et al.* 2006]. Applications are also found for non-porous chitosan membranes in gas separation and pervaporation.

The gas permeation properties of chitosan membranes were reported in a few papers [Duan *et al.* 2006; Kouketsu *et al.* 2007; Krasemann and Tieke 1999; Tual *et al.* 2000]. Chitosan membranes are dense and rigid in the fully dry state, and they show very low permeabilities to gases. However, higher permeation rates can be achieved if they are swollen by water. Based on the interactions between CO_2 and the amino groups of chitosan as well as the hydroxyl groups, selective permeation of CO_2 is expected for water-swollen chitosan membranes. Therefore, CO_2/N_2 separation is one of the potential applications of chitosan membranes. The permeabilities of CO_2 and N_2 were measured for the uncrosslinked and crosslinked chitosan membranes in this work.

The application of chitosan membranes in pervaporation has attracted extensive research interest, and studies were conducted for dehydration and separation of organic solvents with chitosan membranes. Extensive swelling of the membrane in pervaporation will lower the membrane selectivity, and crosslinking is often used to suppress membrane swelling. Though in some research pervaporation was performed with uncrosslinked chitosan membranes [Feng and Huang 1996b; Won *et al.* 2002], crosslinking of chitosan membranes for improved long-term stability remains a focus of research. The aqueous solutions of sulfuric acid [Won *et al.* 2003], glutaraldehyde [Huang *et al.* 1999], 1,6-hexamethylene diisocyanate [Nawawi and Huang 1997], sulfosuccinic acid [Jegal and Lee 1999] and epichlorohydrin [Wei *et al.* 1992] have been used as crosslinking agents. Since chitosan is a hydrophilic material and the hydroxyl/amino groups can form H-bonding with water molecules, water acts as a carrier for the crosslinking agents when chitosan membranes are crosslinked by the aforementioned crosslinking agents. Water first diffuses from the surface into the chitosan matrix, and the membrane becomes swollen. Then the crosslinking agent is dispersed within the polymer matrix. Crosslinking reactions occur during both stages, and the obtained membrane will be uniformly crosslinked if the crosslinking agent is not of high reactivity, and a long period of crosslinking is also essential in such a case.

Different from crosslinking in aqueous solutions, crosslinked chitosan membranes can also be prepared with 2,4-toluylene diisocyanate (TDI) in hexane [Devi *et al.* 2005; Biduru *et al.* 2005]. Trimesoyl chloride/hexane was used as the crosslinking medium for PVA in our previous work [Xiao *et al.* 2006]. Hexane, as a non-solvent, can hardly penetrate the chitosan matrix through direct contact. However, the crosslinking agent facilitates the diffusion of hexane by means of swelling the polymer

matrix, which contributes to further crosslinking in the matrix during the interfacial crosslinking reaction [Xiao *et al.* 2006].

In this work, interfacially crosslinked chitosan membranes were prepared for CO_2/N_2 separation and pervaporation dehydration of isopropanol, based on the crosslinking method developed in Chapter 3. For convenience of discussion, an uncrosslinked chitosan membrane was also tested.

5.2 Experimental

5.2.1 Preparation of CS-TMC Membranes

Chitosan (flakes, 99 % *N*-deacetylated, MW 100,000) was supplied by Kyowa Technos, Chiba, Japan. Acetic acid (glacial, ACS reagent, ≥ 99.7 %) and sodium hydroxide (pellets, ACS reagent, ≥ 97.0 %) were provided by Fisher Scientific and EMD Chemicals, respectively. All materials were used directly as obtained.

Homogeneous chitosan membranes were prepared from the following procedures. Chitosan, acetic acid and water were mixed with a weight ratio of 1:5:94 to form a viscous solution. The solution was filtered under moderate vacuum to remove the undissolved impurities, followed by degassing for at least 10 h to remove air bubbles. The solution (20 mL) was poured into a glass O-ring (Ø75 mm) on a polyethylene sheet, and then dried at ambient conditions. Dry membranes were peeled off from the polyethylene sheets, and then immersed into a sodium hydroxide aqueous solution (1 mol/L) for at least 10 h to neutralize acetic acid. The membranes were soaked/rinsed with deionized water for at least 5 times. The obtained chitosan membranes were fully dried at ambient conditions and were kept in a desiccator for further treatments.

Crosslinked CS-TMC membranes were prepared by crosslinking the chitosan membranes in trimesoyl chloride/hexane solution. Dry membranes were first immersed in a large volume of TMC/hexane solution (2 w/v %) for various periods of time as shown in Table 5.1. Then the crosslinked membranes were rinsed with water and isopropanol for at least 10 times before being soaked in isopropanol for 24 h. The crosslinked membranes were preserved in water for later use. The designations of these membranes and their dry thicknesses are listed in Table 5.1; the uncrosslinked membrane is denoted as CS-TMC-0.

5.2.2 DSC and TGA Measurements

Membrane samples were dried *in vacuo* at 85 °C overnight before thermal analyses. DSC thermograms were recorded from 0 to 300 °C at a heating rate of 10 °C/min in a helium atmosphere. TGA curves were obtained by heating the samples from 100 to 650 °C at a heating rate of 10 °C/min in helium.

Table 5.1 Crosslinking time and dry thicknesses of membranes

CS-TMC membranes	Crosslinking time [a] (min)	Dry thickness [b] (μm)
CS-TMC-0 [c]	0	120
CS-TMC-1	20	145
CS-TMC-2	40	120
CS-TMC-3	60	140
CS-TMC-4	80	130

[a] in TMC/hexane (2 w/v %) at room temperature.

[b] average thickness, measured with a micrometer.

[c] uncrosslinked chitosan membranes.

5.2.3 Water Uptake

Water uptake tests were performed as described in 3.2.4, and the degree of swelling was determined from Equation 3.1.

5.2.4 Pure N_2/CO_2 Permeation

Gas permeation was carried out with pure N_2 and CO_2 at room temperature with the setup shown in Figure 5.1. Membranes (swollen in water before use) were placed in the permeation cell (Figure 3.2), and tested with N_2 first and then CO_2. The effective area of the membrane for permeation was 2.38×10^{-3} m^2. The feed gas was allowed to flow through a humidifier before entering the permeation cell at given pressures, and the gas permeation rate was measured by a bubble flow meter. The permeate side was kept at an atmospheric pressure. For steady state permeation, the gas permeability can be calculated using the equation:

$$P = \frac{q(\mathrm{STP}) \cdot l}{S \cdot \Delta p} \tag{5.1}$$

where P is the permeability coefficient, in terms of unit Barrer [Stern 1968], $10^{-10}\ \frac{\mathrm{cm^3(STP)\cdot cm}}{\mathrm{s\cdot cm^2\cdot cmHg}}$

($1\,\mathrm{Barrer} = 7.5\times10^{-15}\,\mathrm{m^3(STP)\,m\,m^{-2}\,s^{-1}\,kPa^{-1}}$). $q(\mathrm{STP})$ is the volumetric flow rate at standard conditions which has passed through the membrane with an effective area S (cm^2) and a thickness l (cm). Δp is the pressure difference across the membrane and is expressed in cmHg.

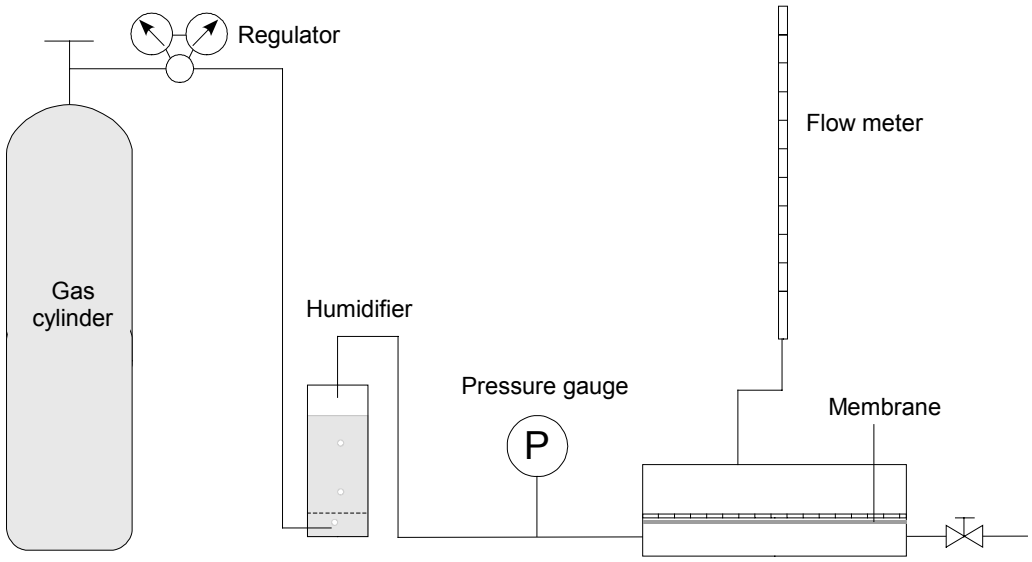

Figure 5.1 Gas permeation setup

The permeability ratio α_{CO_2/N_2} is defined as the ratio of the permeabilities of the two pure gases:

$$\alpha_{\mathrm{CO_2/N_2}} = \frac{P_{\mathrm{CO_2}}}{P_{\mathrm{N_2}}} \tag{5.2}$$

5.2.5 Pervaporation Dehydration of Isopropanol

Water swollen CS-TMC membranes were placed in the pervaporation cell (Figure 3.2) with an effective area of 2.38×10^{-3} m^2. Figure 3.1 shows the schematic setup for pervaporation experiments.

Pervaporation dehydration experiments were first conducted for isopropanol/water mixtures with a water content of 12 wt. % at 30–60 °C, and then the experiments were run at 60 °C with feed mixtures containing 10–40 wt. % water. The membranes were then conditioned in water overnight followed by water permeation at room temperature for 0.5 h. The conditioned membranes were tested

again for dehydration of isopropanol, (1) at feed water content of 12 wt. % and temperatures ranging from 30 to 60 °C, and (2) the feed water contents varying from 10 to ~40 wt. % at 60 °C.

As described previously, the permeation flux and the separation factor are important parameters to characterize permeability and selectivity. In this work, permeation flux normalized by the membrane thickness is used for easy comparison with gas permeability:

$$Normalized\ flux = F \cdot l = \frac{Q \cdot l}{S \cdot t} \tag{5.3}$$

where Q (kg) is the total amount of permeate through a membrane with an effective area S (m^2) and a thickness l (μm) over a period of operating time t (h). Thus the unit of the normalized total flux is kg·μm /m^2h accordingly.

5.3 Results and Discussion

5.3.1 Crosslinking in a Non-solvent

TMC is a well-known crosslinking agent in interfacial polymerization, where it reacts at the liquid interface with amino groups. Recently, attempts have also been made to achieve crosslinking at the liquid/solid interface [Devi *et al.* 2005; Biduru *et al.* 2005; Xiao *et al.* 2006], and the results showed that the molecules of the crosslinking agents could penetrate the solid matrix and react with the active groups inside the matrix.

In chitosan, dissociated amino groups were formed from neutralization of the acetic acid-containing membranes with sodium hydroxide. When the dried chitosan membrane was immersed in TMC/hexane, the solid surface was in direct contact with TMC. The acyl chloride groups of TMC reacted with the amino groups to form amide linkages between chitosan chains. Hexane acted as the dispersion agent for TMC. When TMC reacted with the amino groups at the surface, TMC molecules were "inserted" between the polymer chains from the surface, and a "looser" structure was formed. Hexane molecules, therefore, could enter the matrix. At the same time, the penetration of TMC was facilitated by the hexane molecules residing within the chitosan matrix. However, hexane is a non-solvent for chitosan, and will not induce membrane swelling. As a result, both hexane and TMC could not deeply penetrate the polymer matrix. Therefore, chitosan membranes were interfacially crosslinked. A schematic structure of the crosslinked chitosan is illustrated in Figure 5.2. The formation of amide is known as a fast reaction, and it is supposed to control the crosslinking of chitosan. Crosslinking can also occur between TMC and hydroxyl groups when chitosan membranes

were soaked in TMC/hexane, because TMC can react slowly with hydroxyl groups in chitosan since the hydroxyl groups are active enough to react with TMC [Xiao *et al.* 2006].

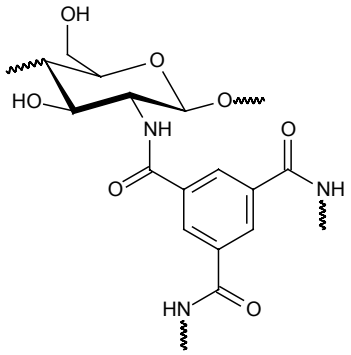

Figure 5.2 Schematic diagram of the crosslinked structure of CS-TMC membranes

5.3.2 Effect of Crosslinking on Thermal Properties

Thermal analysis provides information on thermal stabilities and thermal transitions of polymer materials, and offers an alternative approach to studying the structure of the polymer network as well. Figure 5.3 shows the DSC plots of the uncrosslinked chitosan membrane (CS-TMC-0) and TMC-crosslinked chitosan membranes. Figure 5.4 shows their TGA and DTG plots. The characteristic data of the thermal diagrams are listed in Table 5.2.

DSC measures heat flow required to increase the temperature of the sample. When the sample undergoes a physical transformation such as a phase transition, a change in heat flow will occur to maintain the sample at a specific heating rate. Glass transitions can be possibly observed in the DSC diagrams when the polymers are heated to cause a change from the glassy state to the rubbery state. Unfortunately, the glass transition of chitosan was difficult to detect because of its hydroscopicity [Dong *et al.* [2004]. The T_g values of chitosan were determined from DSC, DMTA, TSC and DIL [Dong *et al.* 2004] to be in a range of 140–150 °C. However, the DSC curve of chitosan (CS-TMC-0) in Figure 5.3 shows only two slope-change regions at 130–160 °C and 260–280 °C. Obviously, the first region (130–160 °C) covers the glass transition temperature of chitosan. Therefore, it is reasonable to use the transition onset temperature to "represent" the T_g of chitosan (CS-TMC-0) when T_g cannot be clearly determined. As shown in Table 5.2, no significant difference can be observed between the onset temperatures of the crosslinked and uncrosslinked chitosan membranes. This reveals that the interfacial crosslinking of chitosan with TMC does not affect the glass transition significantly, and on the other hand, it indicates that the degree of crosslinking is not high. The second region (260–280 °C) appears in all DSC curves of crosslinked chitosan membranes. It is part of the

exothermal peak of chitosan's decomposition [Guinesi and Cavalheiro 2006], whose counterparts can be found in the TGA curves in Figure 5.4 (a).

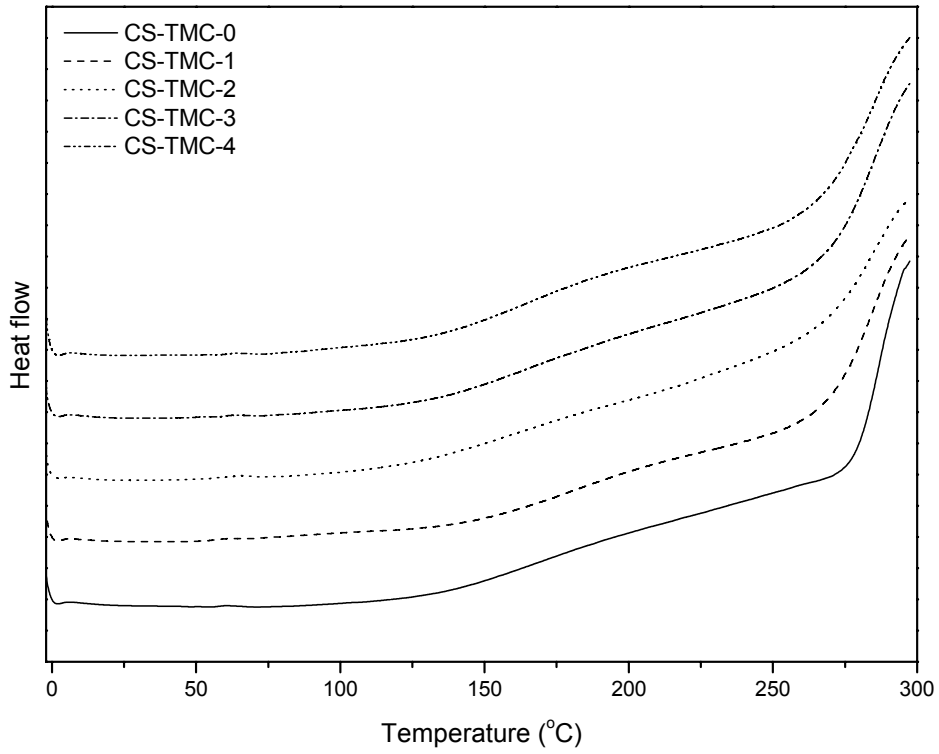

Figure 5.3 DSC plots of CS-TMC membranes

As shown in Table 5.2, T_d onset drops from 279 °C (chitosan) to ~270 °C (crosslinked membranes). With an increase in the crosslinking time, T_d onset is lowered, indicating that crosslinking leads to a depression in the thermal stability. T_ds for 5 % and 10 % weight losses show similar trends, decreasing from 278 °C (chitosan) to 260 °C (CS-TMC-4), and from 286 °C (chitosan) to 275 °C (CS-TMC-4), respectively. The effect of crosslinking on the thermal stability appears to result from the change of the polymer network structure. Since chitosan is a polymer with linear chains, membranes prepared from solvent evaporation processes have a well-packed network structure due to the intermolecular H-bonding between –OH groups as well as $–NH_2$ groups. On the other hand, the structural regularity of a polymer material, contributing to the crystallinity, is also involved in the properties of thermal stability. The insertion of TMC moieties into the chitosan matrix can change the regularity of the polymer network, and to some extent, decreases the thermal stability. In addition, the amide structure formed in the crosslinking reaction has good thermal stability, which

leads to a lower decomposition rate of the membrane. The effect of the amide groups is also reflected in the residual weights of the membranes in TGA. At 650 °C, 38.8 % was left for chitosan, whereas 43.2 % for CS-TMC-4.

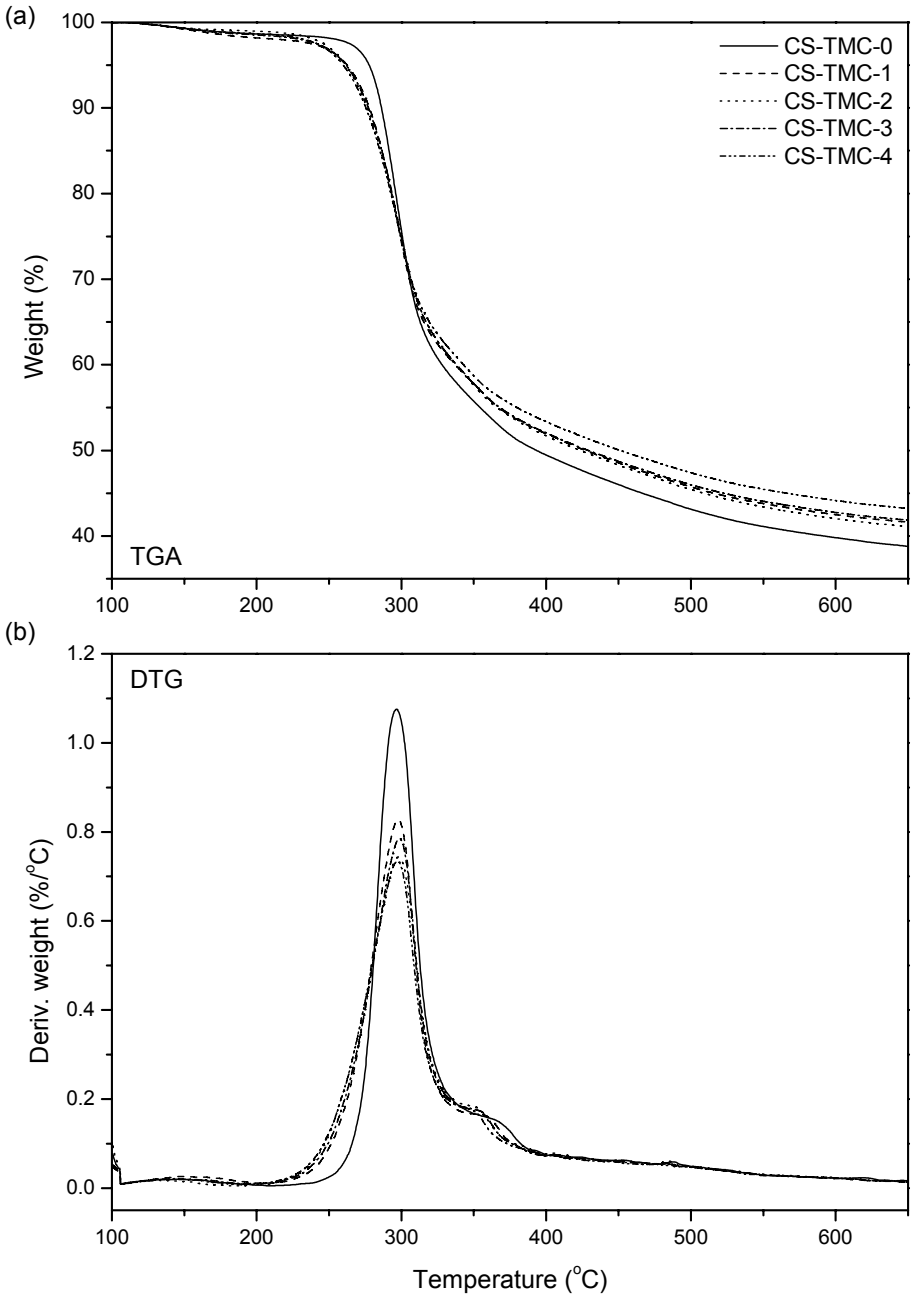

Figure 5.4 TGA and DTG plots of CS-TMC membranes

Table 5.2 Thermal analysis data

Membrane	DSC onset [a] (°C)	T_d 5 % wt. loss [b] (°C)	T_d 10 % wt. loss [b] (°C)	Residual wt. at 650 °C [b] (%)	T_d onset [c] (°C)	DTG peak [d] (°C)
CS-TMC-0	134	278	286	38.8	279	297
CS-TMC-1	144	263	278	41.6	271	298
CS-TMC-2	125	262	277	41.1	266	298
CS-TMC-3	128	262	277	41.9	270	298
CS-TMC-4	131	260	275	43.2	266	297

[a] Onset temperature of the transitions was obtained from the first slope change in DSC curve at approximately 130-160 °C (heating at a rate of 10°C /min in helium).

[b] All values were read directly from TGA plots (heating at a rate of 10 °C /min in helium).

[c] Decomposition onset temperature was determined from TGA curve with the aid of DTG curves.

[d] DTG peak values were read directly from DTG plots.

Broido [1969] developed a graphical method for processing TGA data to find the activation energy for the decomposition. The plot of $\ln\ln(1/y)$ *vs.* $1/T$ yields a straight line whose slope is related to the decomposition activation energy.

$$\ln\ln(1/y) = -(E_d / R)\cdot(1/T) + const. \tag{5.4}$$

where $y = (W_t - W_\infty)/(W_o - W_\infty)$, W_o is the initial weight of the sample, W_t is the weight at time *t*, W_∞ is the weight of the residual, whereas E_d is the activation energy of thermal decomposition, *R* is the gas constant, and *T* is the temperature.

The TGA curves in Figure 5.4 (a) exhibit two distinct decomposition stages, one at 200–320 °C and the other at > 400 °C. The first stage (200–320 °C) is supposed to be the elimination of –OH and $–NH_2$ groups from the cyclic structure in the structural unit of chitosan, while the second stage (> 400 °C) is probably the breakage of the main chains. The apparent activation energies for the thermal decompositions were calculated from Equation 5.4, and the results are listed in Table 5.3. In the first stage, the activation energy of chitosan (CS-TMC-0) is much higher than that of the crosslinked CS-TMC membranes, while in the second stage, the crosslinked CS-TMC membranes have higher activation energies. Hence it can be easily concluded that the crosslinked CS-TMC membranes have poor thermal stability in the first stage (200–320 °C), and good thermal stability in the second stage (> 400 °C). This result is probably due to the effect of the amide structure and the change of the polymer chain-packing properties of the CS-TMC membranes.

Table 5.3 Apparent activation energies for thermal decomposition and pervaporation

Membrane	$E_{d,1}$ (kJ/mol) [a]	$E_{d,2}$ (kJ/mol) [b]	$E_{p,o}$ (kJ/mol) [c]	$E_{p,c}$ (kJ/mol) [d]
CS-TMC-0	216 ± 1	18.4 ± 0.1	21.1 ± 2.0	34.0 ± 1.7
CS-TMC-1	135 ± 1	19.4 ± 0.1	26.5 ± 1.2	27.0 ± 2.1
CS-TMC-2	123 ± 1	19.9 ± 0.1	26.3 ± 2.9	26.3 ± 0.8
CS-TMC-3	127 ± 1	19.0 ± 0.1	26.6 ± 1.1	26.3 ± 0.1
CS-TMC-4	120 ± 1	19.1 ± 0.1	31.7 ± 3.2	31.8 ± 1.9

[a] Apparent activation energies for thermal decomposition at the first stage of 275–300 °C.

[b] Apparent activation energies for thermal decomposition at the second stage of 400–630 °C.

[c] Pervaporation activation energies for the unconditioned membranes.

[d] Pervaporation activation energies for the conditioned membranes.

No significant difference can be observed in the characteristic decomposition temperatures (DTG peak temperatures in Table 5.2), since the maximum decomposition rates of all samples occur at ~298 °C. Furthermore, in Figure 5.4 (a), all TGA curves go through the same point at ~298 °C, and thus the areas under the DTG curves in the range of 200–298 °C, as shown in Figure 5.4 (b), are equal, because the area under a DTG peak is proportional to the weight loss of the sample. The small plateaus in DTG curves at 330–380 °C, as mentioned in the discussion of TGA curves, indicate the second stage of thermal decomposition.

5.3.3 Membrane Swelling in Water

The degree of crosslinking cannot be easily determined through routine analytical methods for crosslinked membranes, especially for the surface-crosslinked membranes with a low degree of crosslinking [Xiao *et al.* 2006]. Therefore, swelling tests, which are easy to perform, are utilized to characterize the degree of crosslinking. In this work, water uptake was conducted for membranes at room temperature. The membranes were tested before and after the separation experiments and the degrees of swelling are shown in Figure 5.5.

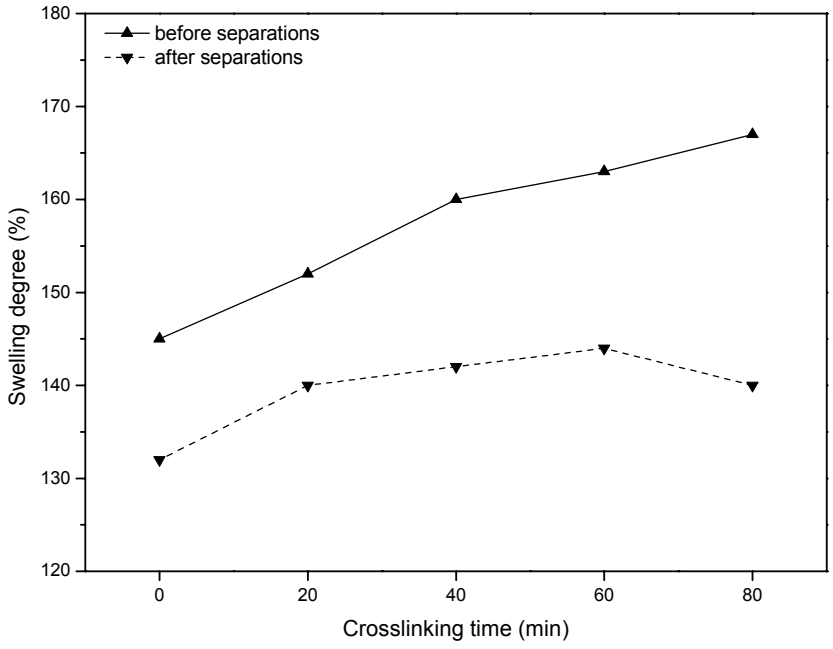

Figure 5.5 The degree swelling of CS-TMC membranes in water at room temperature

After neutralization with sodium hydroxide, chitosan membranes could not dissolve in water, but the hydrophilic –OH and $–NH_2$ groups could still form H-bonds with water molecules. This resulted in a degree of swelling of 145 % for the uncrosslinked membrane. The degree of swelling was shown to increase from 145 % to 167 % when the crosslinking time increased from 0 to 80 min. Such a result seems to contradict with the common perception that the degree of swelling decreases as the degree of crosslinking increases, since the crosslinked polymer network limits the space for the sorbed species during the course of swelling. Note that the interfacially crosslinked CS-TMC membranes were not highly crosslinked. Furthermore, as described in the interfacial crosslinking mechanism, TMC moieties are inserted between chitosan chains, and more space is formed to accommodate the sorbed water. Therefore, it is reasonable to witness a higher degree of swelling for CS-TMC membranes with a higher degree of crosslinking.

5.3.4 Gas Permeation Properties

Gas permeation occurs when gas molecules pass the transient gaps caused by the motion of the segmental chains under the pressure gradients across the dense membrane [Koros and Fleming 1993]. Though different from the permeation of gas mixtures as encountered in the actual separation processes, pure gas permeation can provide information on the interactive effects between gas molecules and the polymer matrix. Therefore, when studying the gas transport properties of a membrane, pure gas permeation is often performed.

In chitosan membranes, there exist hydroxyl groups and amino groups that can form H-bonds. The strong intermolecular H-bonding can lead to the dense packing of polymer chains. The dry chitosan membrane appears to be rigid, because chitosan has a glass transition temperature above 130 °C, and it is in the glassy state at room temperature. However, the water-swollen chitosan membranes appear to be pliable. Within the chitosan matrix, water acts as a plasticizer, and decreases the T_g of the chitosan network. As a result, the membrane will be changed from a glassy state to a rubbery state. Research shows that gas permeability of the dry chitosan membrane is very low, but the water-swollen chitosan membranes have good permeability to gases [Ito *et al.* 1997]. Therefore, in gas permeation experiments, a humidifier was used to humidify the gas.

Figure 5.6 (a) and Figure 5.6 (b) show the permeabilities of CO_2 and N_2 through the water-swollen membranes, respectively. No significant difference can be observed in N_2 permeability, which was found to be ~4 Barrer as shown in Figure 5.6 (b). However, it should be noted that CS-TMC-1 (crosslinking time 20 min) has the lowest permeability of ~3.7 Barrer, whereas CS-TMC-4

(crosslinking time 80 min) has the highest (~4.4 Barrer) for the permeation of N_2. As exhibited in Figure 5.6 (a), CS-TMC membranes show much higher permeability (155–170 Barrer) to CO_2.

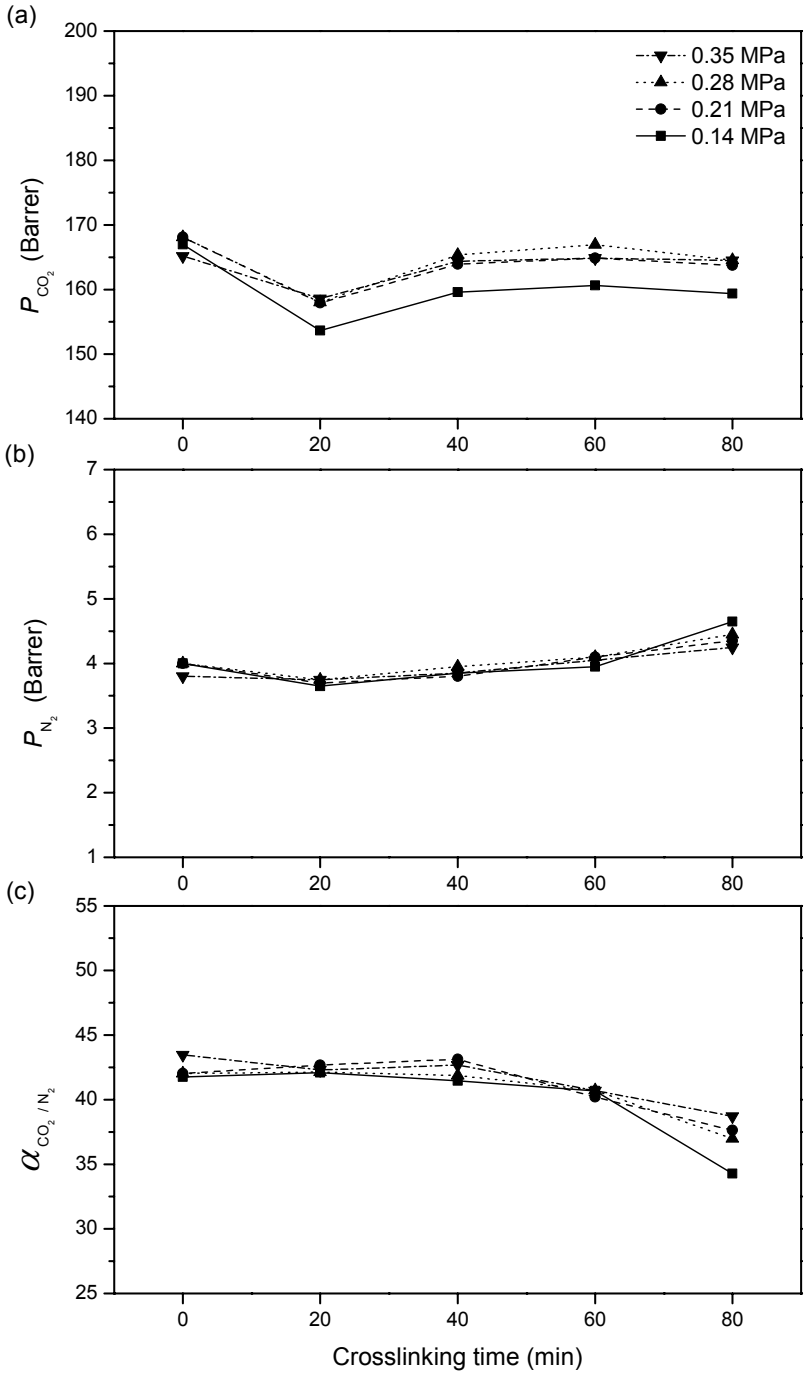

Figure 5.6 Gas permeabilities to CO_2 and N_2 and CO_2/N_2 permeability ratios

The transport of a gas in a membrane is a process where gas molecules move along the transient gaps formed by the thermal movement of polymer segments. Hence gas permeation is governed by the dimensions of the penetrants and the inter-chain transient gaps, the mobility of the polymer chains, as well as the interactions between the penetrants and the polymer matrix. The operating temperature and the water content in the membrane account for the flexibility and mobility of the polymers, but in this work, these two parameters were set to be the constant for the permeation of N_2 and CO_2. Considering the kinetic sieving diameters of CO_2 (0.33 nm) and N_2 (0.36 nm) [Koros and Fleming 1993], CO_2 should have a permeation rate a little higher than N_2 based on the sizes of the gas molecules. However, the transient gaps for the transport of gas molecules in the polymer matrix are different from the fine pores in molecular sieving membranes, and the role of the sizes of gas molecules is not crucial in the permeation of N_2 and CO_2. CO_2, an acidic gas, can react with the amino groups in the water-swollen membranes, which greatly influences the sorption properties of the chitosan membrane. In addition, two effects are attributed to the existence of CO_2 in the chitosan matrix: the interaction between CO_2 and $–NH_2$ can accelerate the hopping of CO_2 between the transient gaps in the matrix, and at the same time, the sorbed CO_2 molecules function as a plasticizer, and enhance the mobility of the polymer chains and enlarge the gaps within the matrix. Therefore, from Figure 5.6 (a), it can be observed that the CO_2 permeability at 0.14 MPa is apparently lower than that at higher pressures. However, the amount of the sorbed CO_2 and the effect of plasticization will reach maximum within the chitosan matrix under a high pressure. This is probably the reason why the permeability of CO_2 remains unchanged at 0.21–0.35 MPa, but only a rapid change is observed from 0.14 to 0.21 MPa for CO_2 permeation through CS-TMC membranes.

From Figure 5.6 (a) and Figure 5.6 (b), it is found that with an increase in the crosslinking time, the gas permeabilities decrease first (for CS-TMC-1), and then increase for both N_2 and CO_2. Particularly for CS-TMC-4 with a higher degree of crosslinking (longer time of crosslinking), the CO_2 permeability is lower and the N_2 permeability is higher, compared with CS-TMC-3. The decrease in the permeabilities of CO_2 and N_2 for CS-TMC-1 compared with the uncrosslinked chitosan membrane indicates that crosslinking occurs at the surface of the membranes, and crosslinking with TMC restricts the mobility of chitosan segmental chains, and the activation energy gap for the permeation of penetrants is enlarged. In other words, the size of the transient gaps for gas permeation is reduced. However, the permeation of N_2 is not affected that much as the permeation of CO_2 because the favorable amino groups for CO_2 are consumed by TMC, which has no influences on N_2. Compared with CS-TMC-1, the increases in the permeabilities of CO_2 and N_2 for CS-TMC-2 and CS-TMC-3 suggest a steric influence of the TMC moiety: TMC, with a large molecular size, is

inserted into the matrix and enlarges the inter-chain space, though as a crosslinking agent, it reduces the extent of the segmental movement. N_2 molecules do not have strong interactions with the polymer matrix, and the membranes show a continuous increase in permeability as the crosslinking time increases. However, for the permeation of CO_2 in CS-TMC-4, because more $–NH_2$ groups are consumed by TMC, the favorable effect from the interactions between CO_2 and $–NH_2$ groups is reduced. Again, it should be noted that this has little impact on N_2 permeability. Consequently, CS-TMC-4 shows a higher N_2 permeability and a lower CO_2 permeability than CS-TMC-3.

Permeability ratios were calculated from the permeabilities of pure CO_2 and N_2, and the results are shown in Figure 5.6 (c). The uncrosslinked chitosan membrane (CS-TMC-0), and the crosslinked membranes CS-TMC-1 and CS-TMC-2 show a similar selectivity of ~42 towards CO_2/N_2, but the selectivity drops to ~37 for membranes with higher degrees of crosslinking (*i.e.* CS-TMC-3 and CS-TMC-4). To draw a conclusion, an appropriate degree of crosslinking can improve the membrane stability and maintain a good selectivity in gas separations, and the CS-TMC-2 membrane appears to have the best performance for CO_2/N_2 separation among the membranes studied.

5.3.5 Pervaporation Properties

Membranes were tested in pervaporation dehydration of isopropanol. Pervaporation experiments were first carried out with the unconditioned membranes (right after swelling in water), and another set of trials was performed by running pervaporation after soaking the membranes in water overnight followed by water permeation for 0.5 h.

5.3.5.1 Effects of Temperature and Conditioning

Figure 5.7 shows the normalized total flux at different operating temperatures for the unconditioned and conditioned membranes. There appears to be a decrease in the flux of the uncrosslinked chitosan membrane (CS-TMC-0) if the membrane is conditioned, while the crosslinked CS-TMC membranes exhibit an increase in the flux if the membrane is conditioned. This can be explained through the effects of conditioning on the polymer matrices. The membranes had a high degree of swelling during the sorption tests in water, but when they were used in pervaporation, the sorbed water contents decreased. Accordingly, the structure of the membrane under pervaporation conditions was different from those under swelling conditions. However, the water-swollen matrices need “some time” for the

segmental chains to change the conformation from the fully swollen state in sorption to the asymmetrically swollen state in pervaporation, *i.e.* relaxation is needed.

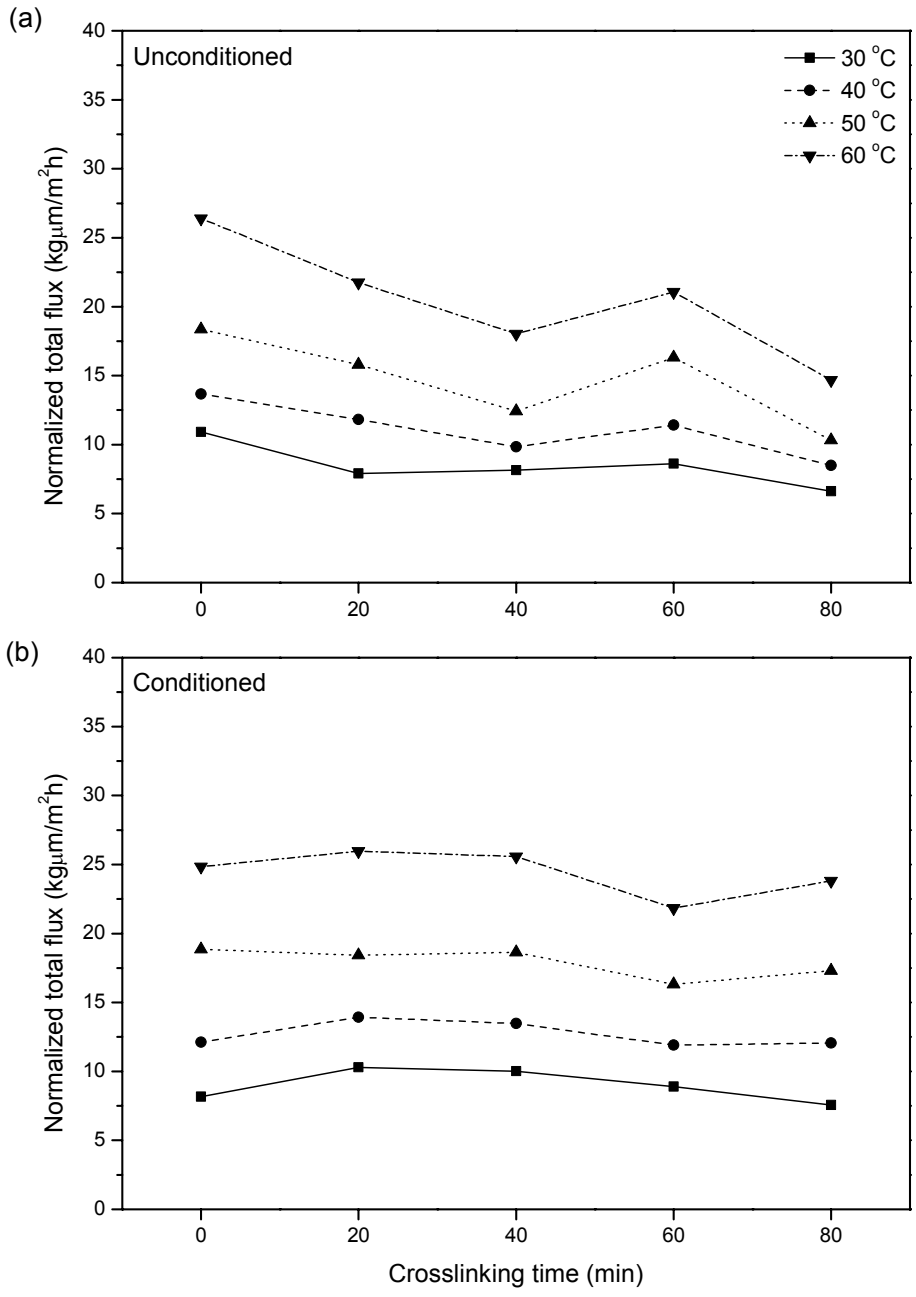

Figure 5.7 Effect of temperature on the normalized flux of CS-TMC membranes for pervaporation of water/isopropanol mixtures

The polymer matrix of the unconditioned chitosan membrane (CS-TMC-0) shrank when the membrane was in contact with isopropanol solutions, but could not achieve the same orderly conformation as the dry chitosan membrane, and more inter-chain space was left favorable to the permeation of penetrants. While in the pervaporation with the conditioned chitosan membrane, the polymer matrix packed more densely and more orderly after sorption in water followed by water permeation, resulting in more resistance to the penetrants. Therefore, the permeation flux of the unconditioned chitosan membrane is higher than that of the conditioned chitosan membrane, as shown in Figure 5.7.

In the crosslinked CS-TMC membranes, TMC moieties and the polymer chains of chitosan formed intermolecular networks within the polymer matrices. In a water-swollen crosslinked membrane, the sorbed water occupied the free volume in the network, but did not change the conformation of the polymer matrix substantially. In pervaporation, the chain segments of the unconditioned membrane easily fell into the positions in the polymer matrix when isopropanol solution was applied to the membrane. More free volume was formed due to the swelling by water after soaking the membrane in water and performing water permeation. Therefore, as shown in Figure 5.7, the conditioned CS-TMC membranes (especially CS-TMC-4 that has a higher degree of crosslinking) had a higher flux than the unconditioned membranes.

Figure 5.7 also shows that all membranes had higher flux at a higher temperature. To discuss the temperature effect, the activation energies for permeation through the CS-TMC membranes were calculated, and the results are shown in Table 5.3. By comparing the permeation activation energies $E_{p,o}$ (for pervaporation with the unconditioned membranes) and $E_{p,c}$ (for pervaporation with the conditioned membranes), it is found that there is a significant difference between $E_{p,o}$ and $E_{p,c}$ for the uncrosslinked chitosan membrane (CS-TMC-0), which is very different form the crosslinked CS-TMC membranes. As mentioned above, for the uncrosslinked membranes, the relaxation of the polymer chains during conditioning led to less inter-chain space for the penetrants, hence yielding more resistance for pervaporation with the conditioned membrane. For the crosslinked membranes, the conditioning processes did not transform the conformation of the crosslinked matrices significantly, and therefore, permeation activation energies remained unchanged. A comparison of $E_{p,o}$ and $E_{p,c}$ for different membranes showed that both that the unconditioned and the conditioned CS-TMC-4 membranes exhibit remarkably higher activation energies, which is believed to result from its higher degree of crosslinking. TMC moieties reduce the flexibility of chitosan and produce

more permeation resistance in the matrix, and therefore, the membrane with a higher degree of crosslinking is supposed to show a higher activation energy for permeation.

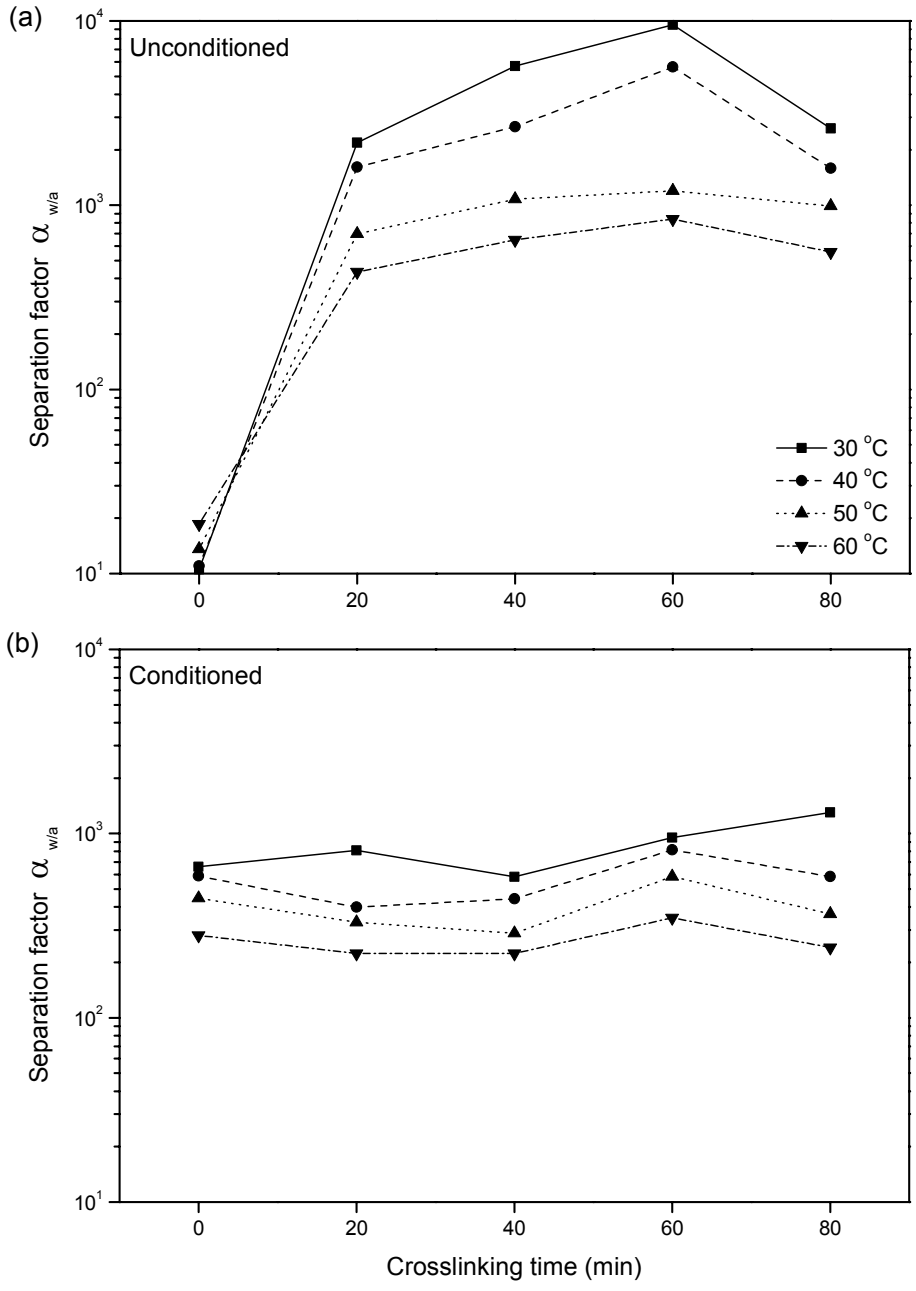

Figure 5.8 Effect of temperature on separation factor of CS-TMC membranes for water/isopropanol separation by pervaporation

The relationship between operating temperature and selectivity for membranes with different degrees of crosslinking is shown in Figure 5.8. Except the unconditioned chitosan membranes (CS-TMC-0), all membranes showed a higher selectivity at a lower temperature. The unconditioned chitosan membrane exhibited a high flux due to the loose packing of the matrix. However, isopropanol could also permeate easily, resulting in a lower water/ isopropanol selectivity. Since the uncrosslinked matrix is an unstable structure that will undergo densification due to the thermal movement of the polymer chains at a higher temperature, the selectivity, therefore, tends to increase at an elevated temperature. However, when the uncrosslinked membrane was conditioned, the more stable structure of the matrix was formed, and as a result, no great deviation could be found in selectivity between the conditioned chitosan membrane and the conditioned CS-TMC membranes.

As shown in Figure 5.8, the unconditioned CS-TMC membranes showed a higher pervaporation selectivity, but the unconditioned membranes exhibited less stable selectivity than the conditioned CS-TMC membranes. As discussed before, the inter-chain space of the conditioned membranes was expanded by water swelling during the conditioning processes, which resulted in a reduction in the selectivity.

Based on the data in Figure 5.7 and Figure 5.8, it can be concluded that the CS-TMC-3 membrane has the best overall pervaporation performance at different temperatures, considering the permeation flux and selectivity.

5.3.5.2 Effects of Feed Concentration and Conditioning

After the pervaporation tests with a feed mixture of ~12 wt. % water from 30 to 60 °C, experiments were conducted with the same membranes by gradually changing the feed water content. The normalized permeation flux and separation factor for pervaporation with the unconditioned and the conditioned membranes are presented in Figure 5.9 and Figure 5.10, respectively.

Diluting the feed mixtures can be considered as a process that allows relaxation of the polymer chains in the membrane. Since the mobility of the polymer chains was enhanced by the strong interactions with water molecules, the unconditioned and conditioned membranes had no great difference in the inter-chain space for the permeation of penetrants. Therefore, as shown in Figure 5.9, the total flux of the unconditioned membranes only appears to be a little lower than that of the conditioned membranes when diluting the feed. Moreover, the conditioned CS-TMC membranes showed less variation in flux than the unconditioned CS-TMC membranes. Interestingly, with a

higher water content in the feed, the CS-TMC-2 membrane showed a lower flux than the other membranes, while CS-TMC-3 had the highest flux. The opposite effects of crosslinking that limits the mobility of the chains and the steric effect from TMC moieties on the matrix, as discussed before, contribute to these results.

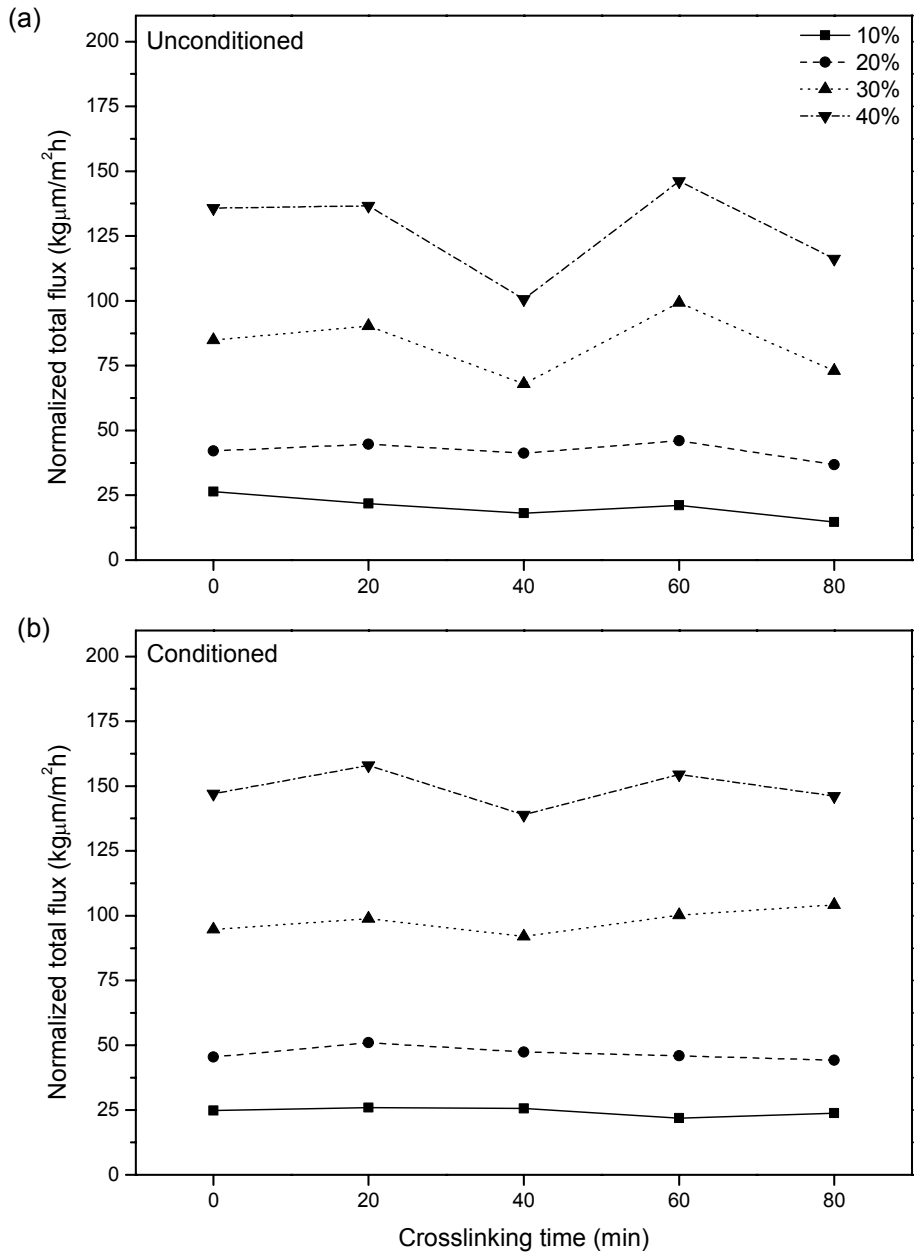

Figure 5.9 Effect of the feed water content on the normalized flux of the water/isopropanol through CS-TMC membranes

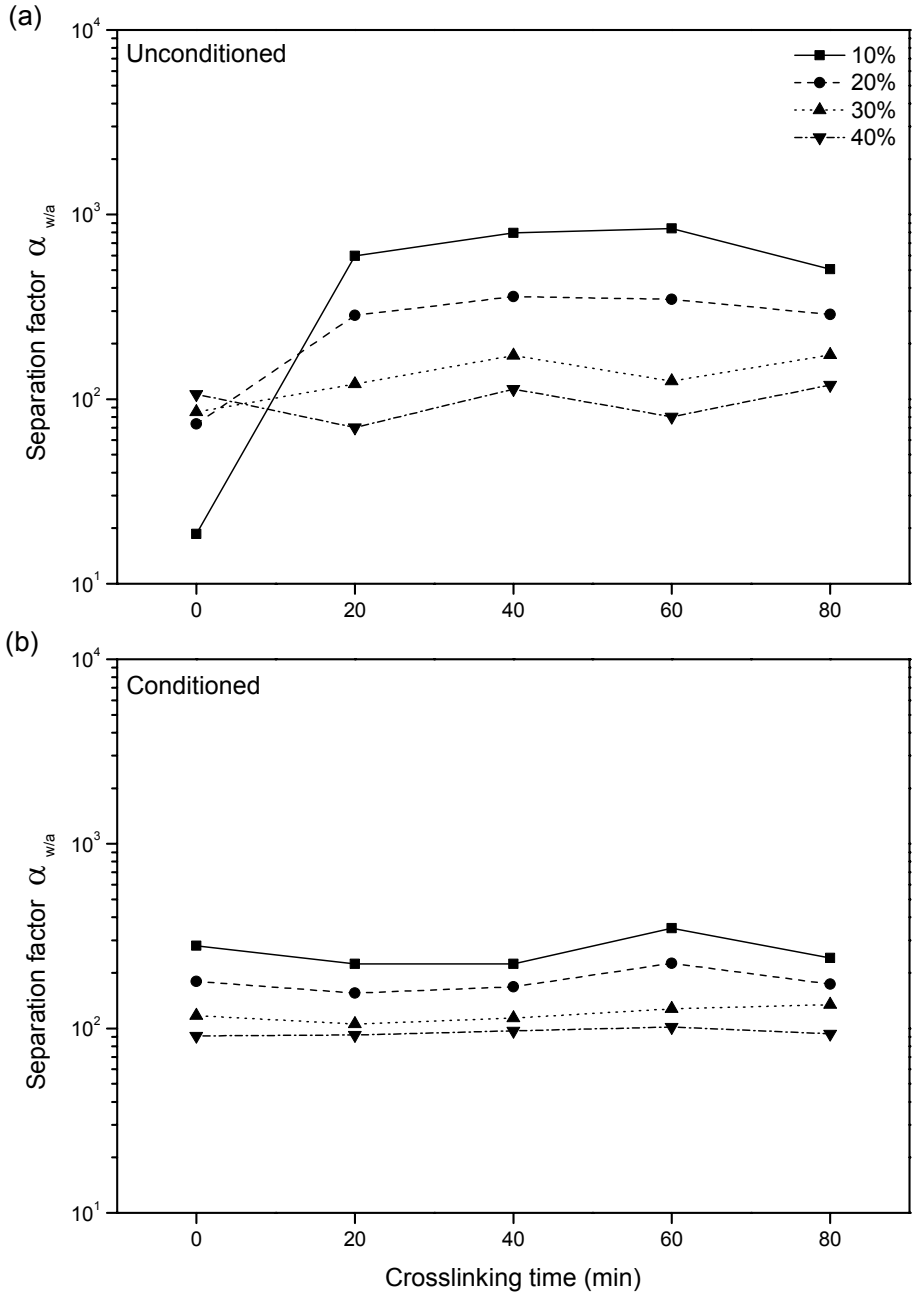

Figure 5.10 Effect of feed water content on separation factor of water/isopropanol through CS-TMC membranes

As shown in Figure 5.10, the unconditioned chitosan membrane (CS-TMC-0) exhibited a higher selectivity towards water/isopropanol when the feed mixture was diluted, but the selectivity was not

comparable with the crosslinked membranes until the feed water content reached 30 wt. %. This gives some hints on the change of the inter-chain space in the polymer matrix. When the swollen chitosan membrane was in contact with an isopropanol solution, polymer chains were fixed to some positions in the matrix from its swollen state as a response to the non-solvent effect from isopropanol. However, when more water was added into the feed, polymer chains regained some mobility and tried to pack more densely and orderly in the matrix. Therefore, fewer isopropanol molecules could permeate through, but the permeation of water was not affected significantly. Consequently, a higher selectivity was achieved when the feed water content was increased for the uncrosslinked chitosan membrane.

It is observed from Figure 5.10 that the unconditioned CS-TMC membranes had a higher selectivity than the conditioned CS-TMC membranes, especially when the water content in the feed was low. This suggests that the relaxation behavior of the unconditioned membranes is much more remarkable than the conditioned membranes. Though all crosslinked CS-TMC membranes show very similar selectivity towards water/isopropanol, the CS-TMC-3 membrane still has the best overall pervaporation performance.

5.3.6 Comparison of Separation Properties with Other Membranes

5.3.6.1 Gas Separation Membranes

A key consideration involved in the development of membranes for gas separation is to maximize the permeability P_i and selectivity (in terms of the permeability ratio $\alpha_{i/j} = P_i / P_j$) for the desired gases. However, generally speaking, increasing the permeability often leads to a decrease in selectivity. Robeson [1991] studied this "trade-off" relationship for gas separations, and found out that the plot of $\log \alpha_{i/j}$ *vs.* $\log P_i$ yielded an upper bound line for each pair of gases.

$$\alpha_{i/j} \propto P^{1/m} \tag{5.5}$$

Furthermore, the slope of the upper bound line was found to be related to the kinetic diameter difference of the gas pairs.

$$-1/m \propto \Delta d_k \tag{5.6}$$

where m is the slope of the upper bound line and Δd_k is the kinetic diameter difference of the gas pair.

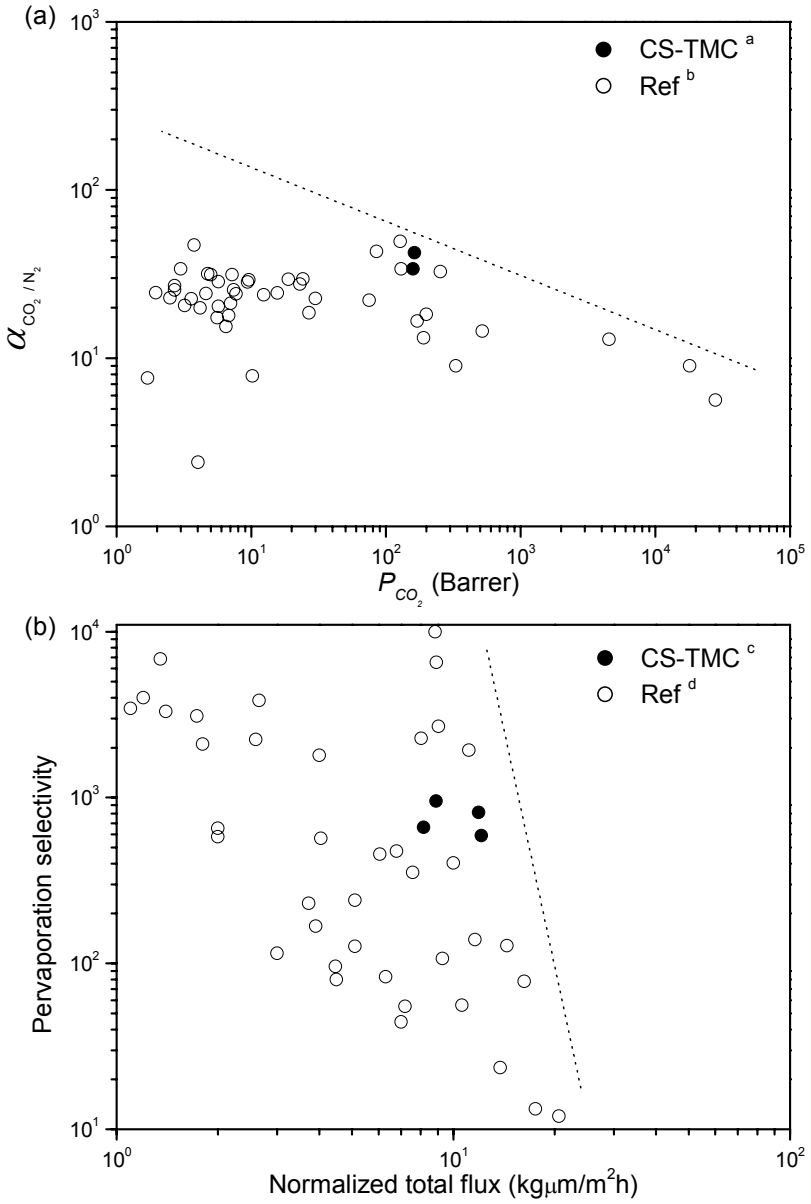

Figure 5.11 The CO_2/N_2 gas separation and water/isopropanol pervaporation performance of chitosan membranes as compared with other membranes reported in the literature

[a] Chitosan membrane and CS-TMC-2 membrane;
[b] Data from Ref. [Ayala *et al.* 2003; Du *et al.* 2007; Hyun *et al.* 1999; Kazama *et al.* 2002; Lehermeier *et al.* 2001; Liu *et al.* 2004; Maier 1998; Stern 1994; Wu and Yuan 2002] ;
[c] Chitosan membrane and CS-TMC-3 membrane;
[d] Data from Ref. [Aminabhavi *et al.* 2005; Devi *et al.* 2005; Huang *et al.* 2001b; Liu *et al.* 2005; Qiao *et al.* 2006; Shen *et al.* 2007; Toti and Aminabhavi 2004; Xiao *et al.* 2006].

Figure 5.11 (a) is a plot of log α_{CO_2/N_2} vs. log P_{CO_2} for CS-TMC membranes in this work along with the membranes reported in the literature [Maier 1998; Stern 1994; Du *et al.* 2007; Wu and Yuan 2002; Lehermeier *et al.* 2001; Liu *et al.* 2004; Ayala *et al.* 2003; Hyun *et al.* 1999; Kazama *et al.* 2002]. The upper bound line was drawn with the slope value calculated from Equations 5.5 and 5.6. The experimental data points of this work are located close to the upper bound line, indicating the overall high permselectivity of CS-TMC membranes for CO_2/N_2 separation.

5.3.6.2 Pervaporation Membranes

Xu *et al.* [2003] applied the same concept of the upper bound for gas separation to the study of pervaporation. Normalized flux was utilized instead of the permeabilities in gas separation. Figure 5.11 (b) presents a plot of pervaporation selectivity (separation factor) vs. normalized flux for pervaporation dehydration of isopropanol. Data of the chitosan membrane (CS-TMC-0) and CS-TMC-3 membrane at 30 °C and 40 °C were plotted among literature data [Aminabhavi *et al.* 2005; Devi *et al.* 2005; Huang *et al.* 2001b; Liu *et al.* 2005; Qiao *et al.* 2006; Shen *et al.* 2007; Toti and Aminabhavi 2004; Xiao *et al.* 2006]. Though the separation factor of CS-TMC membranes for water/isopropanol is lower than 1000, the data points are still close to the upper bound. The high permeation flux is of great interest for the potential application of the membranes to separate water from isopropanol.

5.4 Conclusions

Crosslinked chitosan membranes were prepared by interfacially crosslinking chitosan membranes in TMC/hexane solution, and the degree of crosslinking was controlled by the reaction time. The membranes with a higher degree of crosslinking showed a higher degree of swelling in water due to the steric effect of TMC and the hydrophilicity of the residual $-COOH$ groups from TMC, and the degree of swelling decreased after the gas separation and pervaporation tests.

The TMC moieties changed the thermal properties of the chitosan membranes, and a two-stage thermal decomposition mechanism was proposed for the CS-TMC membranes.

Gas permeation properties of CS-TMC membranes were influenced by the steric effect of TMC and the content of amino groups in the membranes. For the membrane with a lower degree of crosslinking, *i.e.* CS-TMC-1 membrane, the densification effect of crosslinking and the consumption

of amino groups by TMC at the surface greatly decreased the permeation of CO_2, but the permeation of N_2 was not significantly affected. For membranes with a higher degree of crosslinking, more free volume was formed by the insertion of TMC, and more amino groups were consumed by TMC, hence resulting in an enhanced permeability to N_2, but no great change to the permeability to CO_2. CS-TMC-2 showed the best permselectivity towards CO_2/N_2, with a CO_2 permeability of ~163 Barrer and a CO_2/N_2 permeability ratio of ~42.

For the conditioned uncrosslinked chitosan membrane, the polymer chains were packed more densely and orderly after conditioning, resulting in an increased resistance to the penetrants. For the crosslinked CS-TMC membranes, conditioning did not show significant effects on the permeation of penetrants, but TMC moieties reduced the flexibility of the matrix and increased its resistance to permeation. The CS-TMC-3 membrane showed the best overall pervaporation properties among the CS-TMC membranes studied.

In general, the crosslinked CS-TMC membranes were found to be favorably comparable with other membranes reported in the literature for CO_2/N_2 separation and pervaporation dehydration of isopropanol.

Part II
Synthetic Polyimide Membranes for Pervaporation and Gas Separation

The first polyimides were synthesized in 1908, but more research interest in preparation and application of polyimides was attracted since 1955 when high molecular weight polyimides were successfully obtained through the two-step method [Ohya *et al.* 1996]. Because of their excellent thermal stability, superior mechanical strength and good chemical resistance properties, polyimides found applications in many industrial fields [Wilson *et al.* 1990]. The evolution of membrane separation technologies in the past few decades stimulated investigations on the separation performance of polyimide membranes. The correlations of the chemical structure of polyimides with their separation properties have become a critical concern for the solution-diffusion membrane processes, such as gas separation and pervaporation [Park and Paul 1997; Robeson *et al.* 1997]. The high performance polyimide membranes have shown outstanding advantages over the conventional membranes, such as poly(vinyl alcohol) and chitosan, in harsh operating conditions.

The solubility parameters of some representative polyimides are shown in Appendix A, and these polyimides have some affinity to water. Therefore, 4,4'-(hexafluoroisopropylidene) diphthalic anhydride (6FDA)-based and 2,2-bis[4-(3,4-dicarboxyphenoxy) phenyl]propane dianhydride (BPADA)-based polyimides were synthesized and characterized as membrane materials for pervaporation dehydration of isopropanol. The gas permeation properties were also studied. A linear moiety contribution method was proposed for gas permselectivities, and it was also used to correlate polymer structures with pervaporation performance.

Chapter 6

4,4'-(Hexafluoroisopropylidene) Diphthalic Anhydride (6FDA) - 4-Aminophenyl Ether (ODA) - Based Polyimide Membranes for Gas Separation and Pervaporation. I. Polyimides Containing Side Groups or Functional Groups*

Copolyimides were prepared from one-step polymerization with 6FDA and ODA, and diamines 2,4-diaminobenzenesulfonic acid (DBSA), 3,5-diaminobenzoic acid (DABA), 2,6-daminopyridine (DAPy) and 1,5-diaminonaphthalene (DANT) as the third monomer. Polymers were characterized with Gel Permeation Chromatography (GPC), Nuclear Magnetic Resonance spectroscopy (NMR), FTIR, DSC and TGA. Surface free energies and the membrane-water interfacial free energies were calculated from contact angles, and results indicated that DABA, DBSA and DAPy moieties helped increase the hydrophilicity of the membrane. Gas permeation was measured with N_2, O_2, H_2, He and CO_2. A linear moiety contribution method was proposed to study the moiety effects on gas selectivities. The permselectivities towards O_2/N_2, H_2/N_2, and He/N_2 were significantly affected by the steric effects from the monomer moieties, but the permeability of CO_2 was mainly determined by its solubility in the polymer as well as the interactions with the functional groups. Water permeation and dehydration of isopropanol were carried out in the pervaporation mode. The linear moiety contribution method was used to quantitatively compare the effects of monomer moieties. Functional groups changed the liquid sorption and diffusion properties in pervaporation, and the moiety contribution factors indicated that feed concentrations mainly affected sorption properties, whereas the temperature influenced diffusion properties.

6.1 Introduction

Molecular design and modification of polyimides have been used to improve the permselectivity of the membranes for pervaporation and gas separation. Synthesis of new polyimides and incorporation

* Portions of this work have been published in *Polymer*, vol. 48 (2007), pp. 5355–5368.

of functional groups (such as sulfonic acid and carboxylic acid groups) and bulky side groups in the aromatic polyimides have been attempted [Okamoto *et al.* 1992; Kang *et al.* 1993].

For gas permeation membranes, side groups (such as sulfonic acid and methyl groups) have been introduced into the polyimide main chain for enhanced gas permeation properties. Piroux *et al.* [2002b] prepared sulfonated polyimides from 1,4,5,8-naphthalene tetracarboxylic dianhydride (NTDA), 4,4'-diamino-2,2'-biphenyl disulfonic acid (BDSA) and some non-sulfonated diamines. The gas permeation properties were shown to be greatly dependent on the structures of the non-sulfonated diamines of the copolyimides. To reveal the effects of sulfonic acid groups on membrane properties, Tanaka *et al.* [2006] synthesized polyimides from NTDA and 2,2-bis[4-(4-aminophenoxy)phenyl] hexafluoropropane disulfonic acid, and their gas permeabilities were compared with those of the non-sulfonated polyimides having the same backbone structure. It was shown that the sulfonated polyimide had a higher selectivity for H_2 over CH_4 without loss of H_2 permeability. Al-Masri *et al.* [2000] prepared polyimide membranes from methyl-substituted diamine monomers, and it was suggested that the introduction of methyl groups into the polymer main chain created large free volume for gas transport. Pinel *et al.* [2002] synthesized polyimides with trifluoromethyl and methoxyl side groups, and the chain cohesion properties were found to decrease while the void space available for gas diffusion increased by the trifluoromethyl substituents, but the methoxy substituents did not show significant steric effects on gas permeation.

Polyimides with functional groups were also used for pervaporation membranes. However, considering the difference between gas separation and pervaporation, the same substituent may affect the separation properties of the membranes differently. Kang *et al.* [1993] used 3,5-diaminobenzoic acid (DABA) to hydrophilically modify the polyimide from pyromellitic dianhydride (PMDA) and 4,4’-oxydianiline (ODA). A higher flux and higher water/ethanol selectivity were achieved, resulting from the hydrogen bonding between water and the carboxylic acid in DABA. Further studies showed that the diffusivity of the penetrants mainly dominate the pervaporation performance rather than the solubility. Xu *et al.* [2003] investigated the effect of DABA contents in the main chain of the polyimides synthesized from 4,4'-(hexafluoroisopropylidene) diphthalic anhydride (6FDA) and 4,6-trimethyl-1,3-phenylendiamine (DAM) on pervaporation separation of toluene/iso-octane mixtures. It was concluded that the polarity of DABA promoted membrane selectivity, but the smaller size of DABA and the interaction between carboxylic acid and the polymer main chains decreased the fractional free volume and facilitated packing of the segmental chains. As a result, the membrane swelling was reduced and the diffusivity selectivity increased.

Since pervaporation and gas separation follow the solution-diffusion mechanism, it is reasonable to investigate how the functional groups and monomer structures behave in the mass transport of both gas permeation and pervaporation, and to find out to what extent they may change the permeability and selectivity of the membranes. Therefore, the present work is focused on gas separation and pervaporation properties of 6FDA-ODA-based copolyimides. Because of the structural similarity, diamine monomers DBSA, DABA, DAPy and DANT were used as the third monomers in the synthesis of copolyimides, and their effects on the membrane properties for gas permeation and pervaporation were quantitatively analyzed.

6.2 Experimental

6.2.1 Materials

4,4'-(Hexafluoroisopropylidene) diphthalic anhydride (6FDA, > 98 %) was provided by TCI. 4-Aminophenyl ether (ODA, 98 %), 2,4-diaminobenzenesulfonic acid (DBSA, 97 %), 3,5-diaminobenzoic acid (DABA, 98 %), 2,6-diaminopyridine (DAPy, 98 %), 1,5-diaminonaphthalene (DANT, 97 %), *m*-cresol (97 %), isoquinoline (97 %), tetrahydrofuran (THF, 99.5 %) and pyridine (> 99 %) were obtained from Acros Organics. Glycerol (SigmaUltra grade, ≥ 99 %), formamide (SigmaUltra grade, ≥ 99 %) and diiodomethane (ReagentPlus® grade, ≥ 99 %), ethanol (99.5 %), isopropanol (anhydrous, 99.5 %) were supplied by Sigma-Aldrich. DAPy was recrystallized from water/ethanol followed by drying *in vacuo*. Other reagents and materials were used directly as received.

6.2.2 One-Step Polymerization

The monomers used in this work are listed in Figure 6.1. Polyimides (as shown in Table 6.1) were synthesized by the one-step polymerization as illustrated in Figure 6.2. The synthesis procedures are outlined as follows, using 6FDA-8ODA-2DAPy as an example:

6FDA 1.795 g (4.0 mmol), ODA 0.654 g (3.2 mmol), and DAPy 0.088 g (0.8 mmol) were charged into a 100 mL three-neck flask equipped with a mechanical stirrer, a Dean-Stark trap, a condenser and nitrogen inlet/outlet. *m*-cresol 12.5 mL was added into the flask to afford a concentration of 20 w/v %, and additional *m*-cresol 1.5 mL and a catalytical amount of isoquinoline were also charged into the system. The solution was allowed to react at 75 °C for 2 h, and then the temperature was slowly increased to 185 °C. Polymerization lasted for 20–24 h, and during this time,

1.5 mL of *m*-cresol was distilled out through the trap. The viscous solution was cooled to below 120 °C, and then precipitated into an excess of ethanol to get a white polymer. The polymer was collected and washed with ethanol in a Soxhlet extractor for at least 10 h to extract the residual *m*-cresol. The final product 6FDA-8ODA-2DAPy was dried *in vacuo* at 150 °C for 20 h.

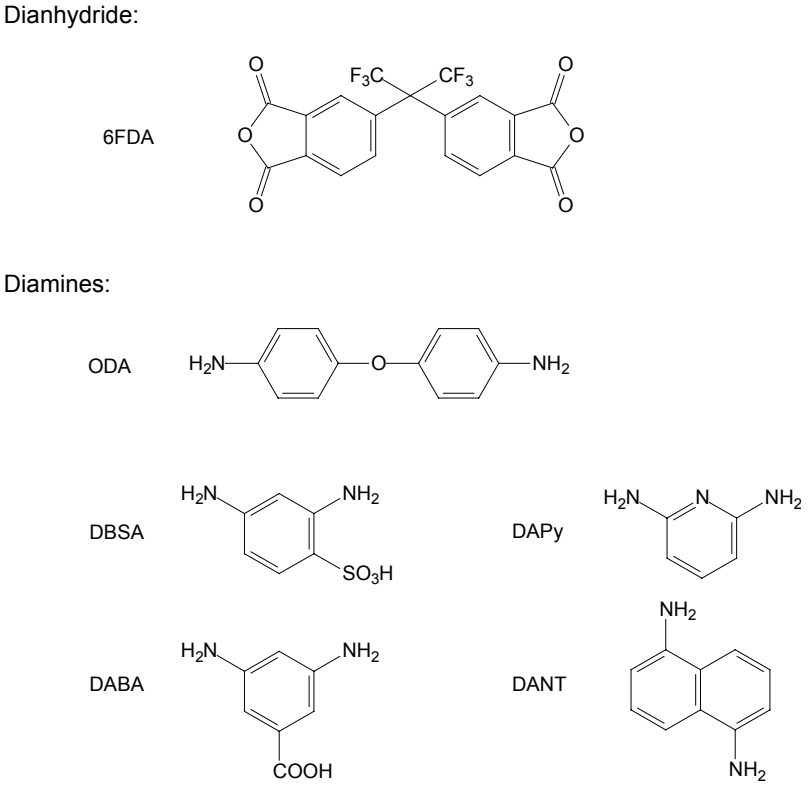

Figure 6.1 Monomers of polyimides

6.2.3 Characterization

Samples were dried *in vacuo* at 120 °C overnight before thermal analyses. The DSC thermograms were recorded from 250 to 370 °C at a heating rate of 10 °C/min in helium. The DSC baseline was obtained from running DSC with an empty aluminum sample pan. TGA was conducted by heating the samples from 100 to 650 °C at a heating rate of 10 °C/min in a helium atmosphere. FTIR was carried out with a Bio-Rad Excalibur 3000MX spectrometer for polymer films cast on NaCl crystals. Gel Permeation Chromatography (GPC) was conducted to obtain molecular weights and molecular weight distributions using a Waters GPC system with DAWN® DSP-F Laser Photometer, Waters 2410 Refractive Index Detector, and 3 PL gel 10 μm Mixed-B columns (300 × 7.5 mm). The GPC was calibrated with polystyrene standards and THF was used as the eluent. Nuclear Magnetic Resonance

spectroscopy (NMR) was performed with Bruker 300 MHz NMR to record ^{1}H and ^{19}F NMR spectra, using pyridine-*d5* as the solvent. A Tantec Contact Angle Meter was used to measure contact angles on the membrane with water, glycerol, formamide and diiodomethane at room temperature.

6.2.4 Polyimide Membranes

Polymers were dissolved in THF to form a 5 w/v % solution. PTFE syringe filters (pore size 0.45 μm) were used to filter the solution before casting the membrane on a glass plate at room temperature. The glass plate was placed in a dry clean chamber to prevent contamination by dust and also to slow the evaporation of the solvent THF. 6FDA-ODA had poor solubility in THF, and pyridine was used as a solvent to dissolve 6FDA-ODA as a 5 w/v % solution. After casting, the glass plate and the 6FDA-ODA/pyridine solution were kept in an oven at 40 °C. Transparent light brown membranes were prepared from the procedures above, and were easily peeled off from the glass plates. The thicknesses of the dense membranes were 8–15 μm.

6.2.5 Pure Gas Permeation

Gas permeation tests with N_2, O_2, H_2 and He were performed at room temperature followed by CO_2 permeation. A schematic gas permeation setup is shown in Figure 6.3. Membranes were placed on the porous plate in a permeation cell (shown in Figure 3.2) with an effective area of 2.38×10^{-3} m^2. Feed gas was controlled at specific pressures (0.14, 0.21, 0.28 and 0.35 MPa), while the permeate side was kept at atmospheric pressure and the permeation flux was determined with a bubble flow meter. At least 1 h purging of the permeate was allowed to guarantee a steady state for the pressure changes. The permeance was calculated using the equation:

$$J = \frac{q(\mathrm{STP})}{S \cdot \Delta p} \tag{6.1}$$

where J is the permeance in GPU, $10^{-6}\ \dfrac{\mathrm{cm}^3(\mathrm{STP})}{\mathrm{s} \cdot \mathrm{cm}^2 \cdot \mathrm{cmHg}}$ ($1\ \mathrm{GPU} = 7.5 \times 10^{-9}\ \mathrm{m}^3(\mathrm{STP})\ \mathrm{m}^{-2}\ \mathrm{s}^{-1}\ \mathrm{kPa}^{-1}$), q(STP) is the volumetric flow rate (cm^3/s) at standard conditions that has passed through a membrane with the effective area S (cm^2), and the pressure difference across the membrane is expressed in Δp (cmHg).

Table 6.1 6FDA-ODA copolyimides and their molecular weights

Polyimides	Monomers	Molar ratio	$\overline{M}_n$	$\overline{M}_w$	$\overline{M}_w / \overline{M}_n$	$\overline{DP}$
6FDA-ODA	6FDA : ODA	= 1 : 1	84150	89070	1.06	138
6FDA-8ODA-2DBSA	6FDA : ODA : DBSA	= 1 : 0.8 : 0.2	140200	205800	1.47	231
6FDA-6ODA-4DBSA	6FDA : ODA : DBSA	= 1 : 0.6 : 0.4	152800	165700	1.08	253
6FDA-8ODA-2DABA	6FDA : ODA : DABA	= 1 : 0.8 : 0.2	62750	89650	1.43	105
6FDA-6ODA-4DABA	6FDA : ODA : DABA	= 1 : 0.6 : 0.4	125600	166600	1.33	213
6FDA-9ODA-1DAPy	6FDA : ODA : DAPy	= 1 : 0.9 : 0.1	34560	48470	1.40	57
6FDA-8ODA-2DAPy	6FDA : ODA : DAPy	= 1 : 0.8 : 0.2	28690	37050	1.30	48
6FDA-9ODA-1DANT	6FDA : ODA : DANT	= 1 : 0.9 : 0.1	63730	72780	1.14	105
6FDA-8ODA-2DANT	6FDA : ODA : DANT	= 1 : 0.8 : 0.2	82110	90560	1.10	137

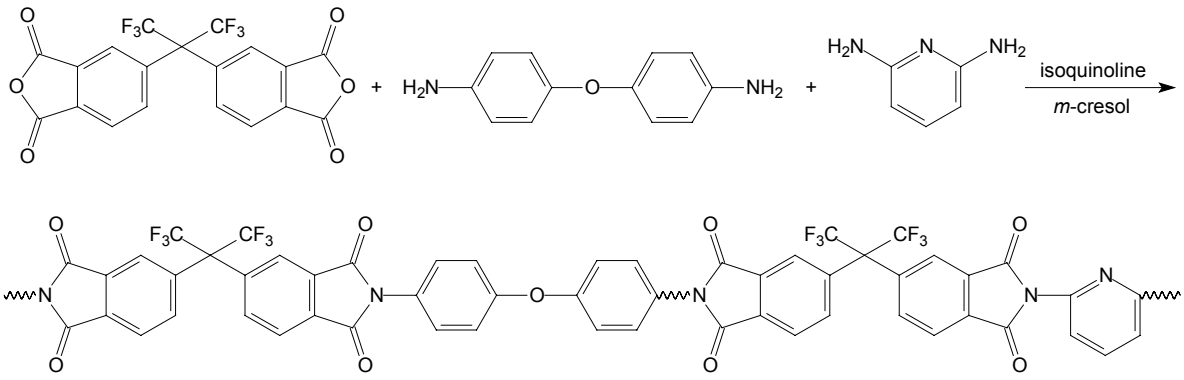

Figure 6.2 One-step polymerization of 6FDA-8ODA-2DAPy

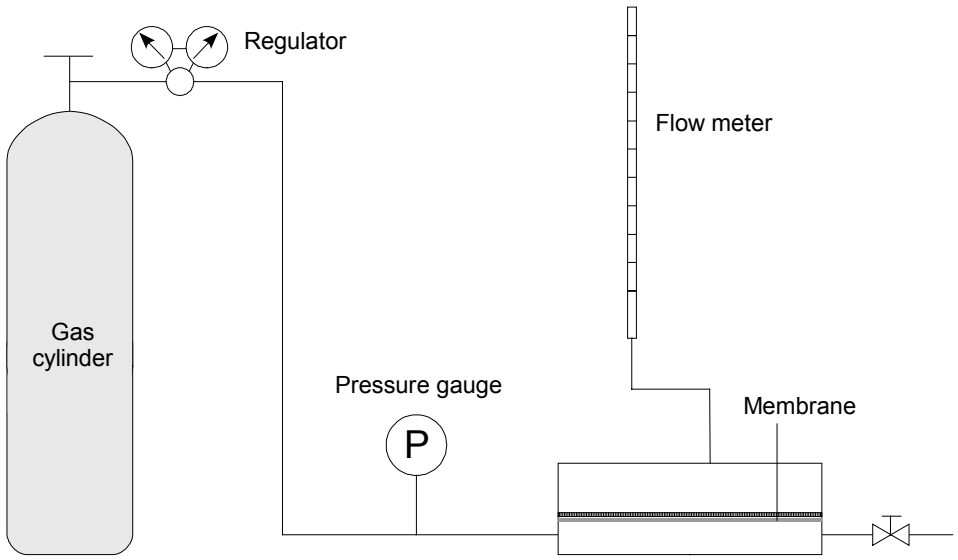

Figure 6.3 Gas permeation setup

The permeance ratio can be calculated from the equation

$$\alpha_{i/j} = \frac{J_i}{J_j} \tag{6.2}$$

where $\alpha_{i/j}$ is the permeance ratio for pure gases *i* and *j*, and J_i , J_j are permeances of pure gases *i* and *j*, respectively.

6.2.6 Pervaporation Tests

Pervaporation was carried out for pure water permeation and dehydration of isopropanol. A schematic pervaporation setup is shown in Figure 3.1. Pure water permeation was conducted at 30, 40, 50, 60 °C respectively, followed by dehydration of isopropanol: First, the feed water content was kept at ~20 wt. % as the feed temperature was varied from 30 to 60 °C. Second, the feed temperature was remained at 60 °C, and the feed water content was changed from 10 to 50 wt. %. Before permeate samples were collected for analysis, pervaporation was operated for at least 1 h to attain steady states. The feed and permeate concentrations were determined by a Varian CP-3800 Gas Chromatograph.

6.3 Results and Discussion

6.3.1 Synthesis of Polyimides

Figure 6.2 illustrates the polymerization of 6FDA-8ODA-2DAPy. DBSA, DABA and DANT were also used as the third monomer in preparation of 6FDA-ODA-based copolyimides using the same method. This one-pot polymerization method is based on the one-step high-temperature polycondensation. Its application is limited by the solubility of the products [Sroog 1965]. For those polyimides with rigid structures, coagulation or precipitation may occur in the reaction solutions. Therefore, a rigid structure and/or poor solubility will lead to a low molecular weight. In the one-step polycondensation, the dianhydride reacts with diamines in *m*-cresol at a low temperature (~80 °C) to form poly(amic acid)s, and thereafter at a high temperature (> 180 °C), the cyclodehydration reaction occurs to form polyimides in the presence of the catalyst isoquinoline.

Figure 6.4 shows ^{1}H NMR spectra of the polyimides. The coupled peaks at 7.91 and 7.31 ppm correspond to the protons of the ODA moiety. For 6FDA-6ODA-4DBSA, at 8.51 ppm, a peak appears for the proton attached to α-C of the sulfonic acid group, and for 6FDA-6ODA-4DABA, the proton attached to α-C of the carboxylic acid group has a chemical shift of 8.98 ppm. In the ^{1}H NMR spectrum of 6FDA-8ODA-2DAPy, the resonance peaks of the protons in the pyridine moiety shift to ~8.15 ppm (from 7.22 ppm in pyridine) and ~7.22 ppm (from 7.59 ppm in pyridine), respectively. The protons in naphthalene moieties are shown to have chemical shifts of 8.46, 8.25 and 7.74 ppm, respectively, in the ^{1}H NMR spectrum of 6FDA-8ODA-2DANT. The detailed NMR data can be found in Appendix A.

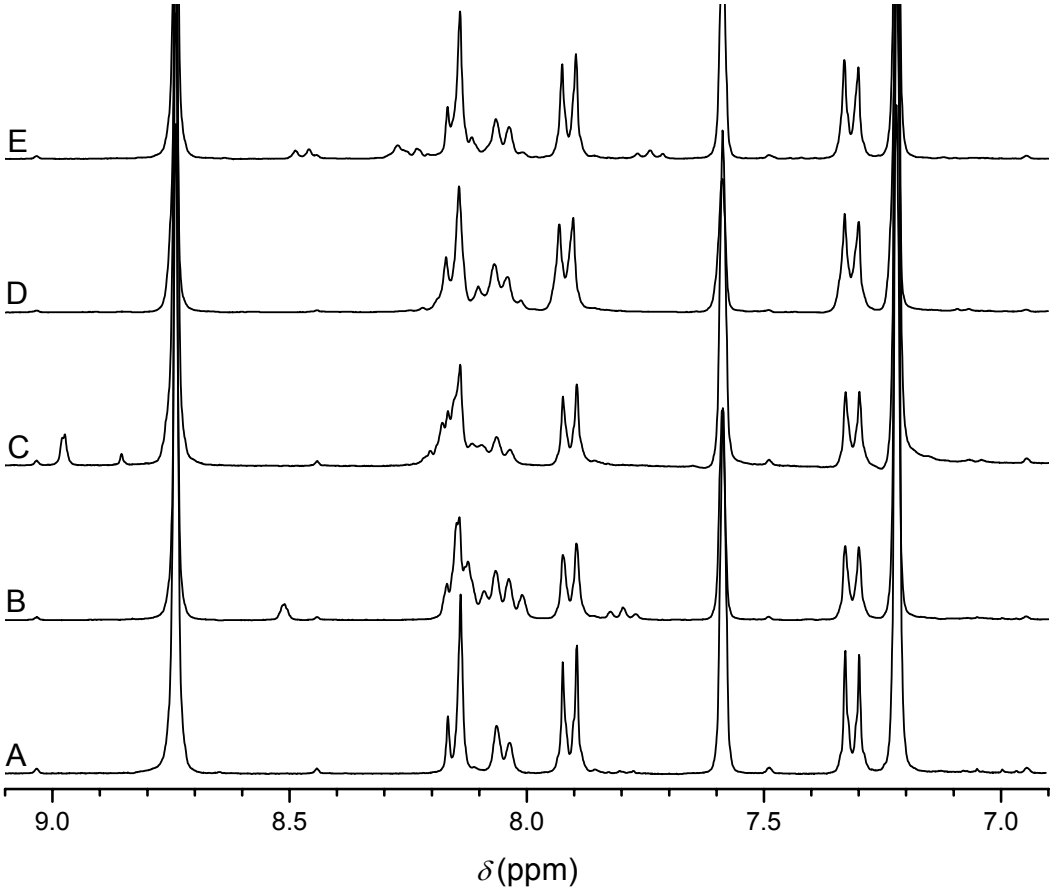

Figure 6.4 ^{1}H NMR spectra of polyimides

A: 6FDA-ODA, B: 6FDA-6ODA-4DBSA, C: 6FDA-6ODA-4DABA,
D: 6FDA-8ODA-2DAPy, E: 6FDA-8ODA-2DANT

In the FTIR spectra of the polyimides, a weak absorption band is shown at ~3494 cm^{-1}, which indicates the existence of the amino groups. These amino groups are the end groups of the polyimide chains from diamine monomers. At ~3070 cm^{-1}, aromatic C–H stretching band occurs. Figure 6.5 shows part of the FTIR spectra (1950–600 cm^{-1}) of the polyimides. Skeletal stretching of the aromatic rings produces absorption at ~1600 cm^{-1} and ~1500 cm^{-1}, and the weak absorption at 1015 cm^{-1} is due to the in-plane bending of the phenyl rings [Silverstein 1997]. The absorptions at 1785 cm^{-1} (C=O asymmetrical stretching, Imide I band), 1728 cm^{-1} (C=O symmetrical stretching, imide II band), 1110 cm^{-1} (imide III band), and 723 cm^{-1} (imide ring bending vibration, imide IV band), as well as 1380 cm^{-1} (C–N stretching) are the characteristic absorptions of imide rings [Dunson 2000;

Pramoda *et al.* 2002; Sroog *et al.* 1965]. Asymmetrical stretching vibration of $-CF_3$ groups produces absorption at ~1300 cm^{-1}. The ether bond in ODA moieties shows strong stretching absorption at ~1240 cm^{-1}. The detailed FTIR data can be found in Appendix A.

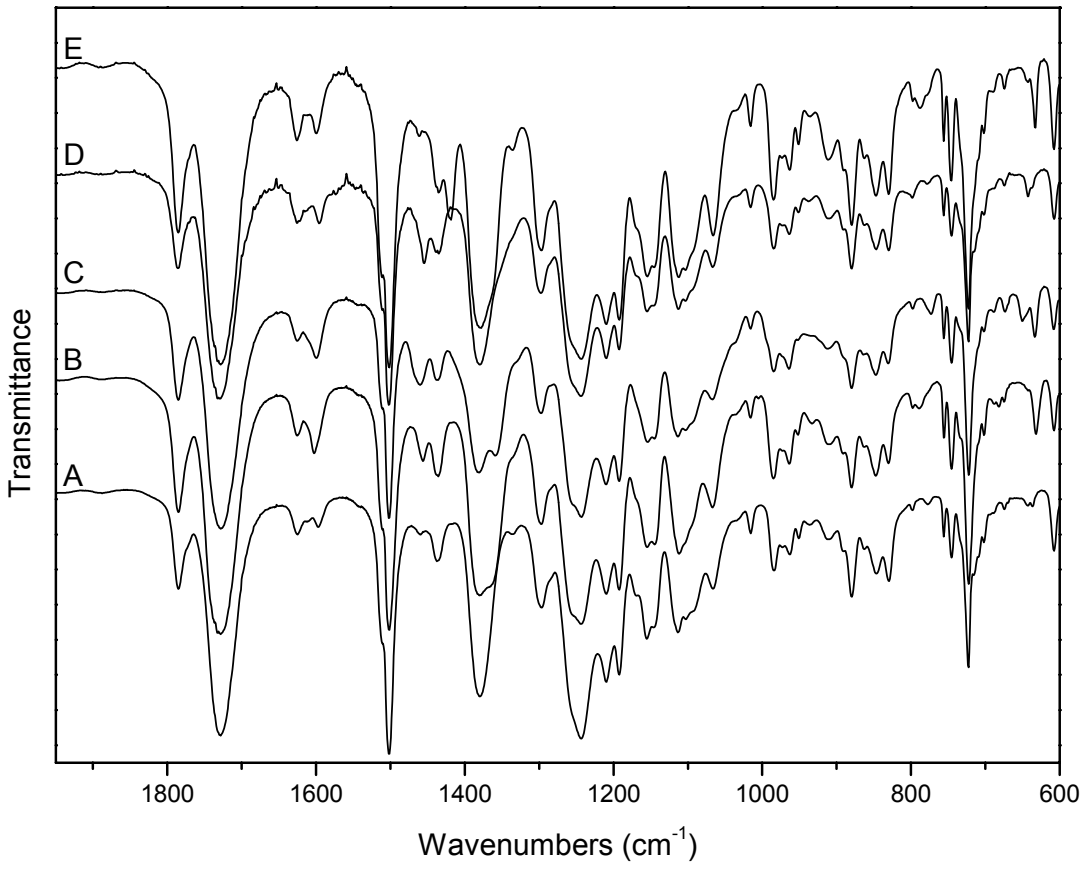

Figure 6.5 FTIR spectra of polyimides (film on NaCl)

A: 6FDA-ODA, B: 6FDA-6ODA-4DBSA, C: 6FDA-6ODA-4DABA,
D: 6FDA-8ODA-2DAPy, E: 6FDA-8ODA-2DANT

The molecular weights and polydispersity indexes ($\overline{M}_w / \overline{M}_n$) of the polyimides are shown in Table 6.1. 6FDA-8ODA-2DAPy and 6FDA-9ODA-1DAPy show lower molecular weights, while 6FDA-8ODA-2DBSA, 6FDA-6ODA-4DBSA and 6FDA-6ODA-4DABA have higher molecular weights. It is known that the rate of polycondensation is favored by the increased electron affinity of the dianhydrides and by the increased basicity of the diamines [Ohya 1996; Sroog 1991; Wilson *et al.*

1990]. In the present work, 5 diamine monomers were used in synthesis of the polyimides, and their basicity can be compared with the charges on the N-atom of the $–NH_2$ groups. Their Wang-Ford Charges obtained from MOPAC are in the following order: ODA (–0.940) > DABA (–0.930) > DANT (–0.920) > *p*- DBSA (–0.824) > DAPy (–0.760) > *o*- DBSA (–0.681). This sequence indicates the lower reactivity of the amino groups in DAPy, and the higher reactivity of the amino groups in DABA, which results in the lower and the higher molecular weights, respectively. These polyimides show narrow molecular weight distributions. The $\overline{M}_w / \overline{M}_n$ values are ~1.1 for 6FDA-ODA, 6FDA-6ODA-4DBSA, 6FDA-8ODA-2DANT and 6FDA-9ODA-1DANT, and 1.30–1.43 for the other polyimides. The small values of $\overline{M}_w / \overline{M}_n$ obtained from GPC result from the fractionation effect of the ethanol during the extraction of *m*-cresol.

6.3.2 Properties of Polyimides

6.3.2.1 Solubility

The solubility of polyimides was tested by putting small pieces of polyimides into a large amount of solvent. All polymers are readily soluble in THF and/or pyridine, and are also soluble in chloroform, *N*,*N*-dimethylacetamide (DMAc), *N*,*N*-dimethylformamide (DMF), *N*-methylpyrrolidone (NMP), acetone, and dimethyl sulfoxide (DMSO). They are insoluble in isopropanol, toluene and cyclohexane. However, a high concentration (> 3 w/v %) of 6FDA-ODA solution cannot be prepared using THF as the solvent, and thus when casting 6FDA-ODA membranes, pyridine was used as the solvent.

6.3.2.2 Thermal Properties

The characteristic temperatures obtained from the DSC and TGA measurements are listed in Table 6.2. The characteristic decomposition temperatures were determined as the peak temperature in the DTG plots.

The glass transition can be considered to occur when the expansion rate of free volume changes, and it is reflected in the density change of a material. In the thermal analysis, the glass transition is determined from the change in heat capacities [Sperling 2001]. However, in this work, the glass transitions of 6FDA-ODA-based polyimides were not observed in their first and second DSC runs, partially due to the incomplete conversion of poly(amic acid)s in imidization. The glass transition temperature (T_g) of 6FDA-ODA was determined to be 285.6 °C, when the DSC curve is subtracted by

a baseline obtained from an empty sample pan. This T_g value is very close to the bibliographic data [Sroog 1991]. Furthermore, the onset temperature from the modified DSC curve of 6FDA-ODA is close to the T_g. Based on this fact, the onset temperatures of the modified DSC curves are utilized as an estimation of glass transition temperatures for polyimides. The results are listed in Table 6.2. 6FDA-8ODA-2DANT shows the highest onset temperature, because the rigid naphthalene structure increases the transition temperature. The sulfonic acid group of the DBSA moiety and the carboxylic acid group of the DABA moiety change the packing densities of the polymer chains, possibly resulting in a slight decrease from the onset temperature of 6FDA-ODA.

The TGA plot records the weight change of the material when it is heated at a specific rate. T_ds 5 % and 10 % weight loss are usually used to characterize the thermal stability of a material. The derivative of the TGA curves, *i.e.* DTG, depicts the rate of pyrolysis. Figure 6.6 shows the TGA and DTG curves of the polyimides. The further conversion of poly(amic acid)s to polyimides can be found at about 200 °C. The DANT moiety contributes to the good thermal stability of 6FDA-8ODA-2DANT. Furthermore, the T_d 5 % and T_d 10 % of the polyimides demonstrate a sequence of thermal stability for the diamine moieties: DANT > DAPy > ODA > DBSA > DABA. The thermal stability is affected by the side groups, such as sulfonic acid and carboxylic acid. The pyrolysis of the carboxylic acid group occurs at a much lower temperature (T_d onset 372 °C), and consequently two stages of decomposition were observed in TGA onset and DTG peak temperatures. Except 6FDA-6ODA-4DABA, the polyimides have T_d 10 % about 20 °C higher than T_d 5 %. Read from the DTG plots of the polyimides, the maximum rates of degradation occur at ~556 °C. In the DTG curves, 6FDA-ODA shows a small peak at ~640 °C, and the –COOH decomposition peak is found at 417.8 °C for 6FDA-6ODA-4DABA.

6.3.2.3 Surface Free Energies

Contact angles of liquid drops (sessile drops) on horizontal membrane surfaces, as illustrated in Figure 6.7, were obtained at room temperature. The contact angles of several liquids on the polyimide membranes are presented in Table 6.3.

Good and van Oss [1991] defined the surface free energy as the sum of the Lifshitz-van der Waals apolar (LW) component γ_i^{LW} and the Lewis acid-base (AB) component γ_i^{AB}.

Table 6.2 Characteristic temperatures from DSC, TGA and DTG

Polyimides	DSC [a] (°C)	T_d 5 % wt. loss (°C)	T_d 10 % wt. loss (°C)	T_d onset [c] (°C)	DTG [e] (°C)
6FDA-ODA	293 285 [b]	511	538	521	557
6FDA-6ODA-4DBSA	293	505	536	522	557
6FDA-6ODA-4DABA	291	427	526	372 [d]	418 [d]
				524	557
6FDA-8ODA-2DAPy	295	517	539	520	557
6FDA-8ODA-2DANT	299	528	547	522	555

[a] DSC operating conditions: 10 °C/min in helium. Glass transition temperatures were not distinctly decided from the first and second runs of DSC. The onset temperatures were used as an estimation of their glass transition temperatures.

[b] Glass transition temperature of 6FDA-ODA.

[c] TGA operating conditions: 10 °C/min in helium.

[d] 6FDA-6ODA-4DABA showed two degradation stages in TGA. This temperature was obtained from the first stage degradation.

[e] These temperatures were obtained from DTG peak temperatures.

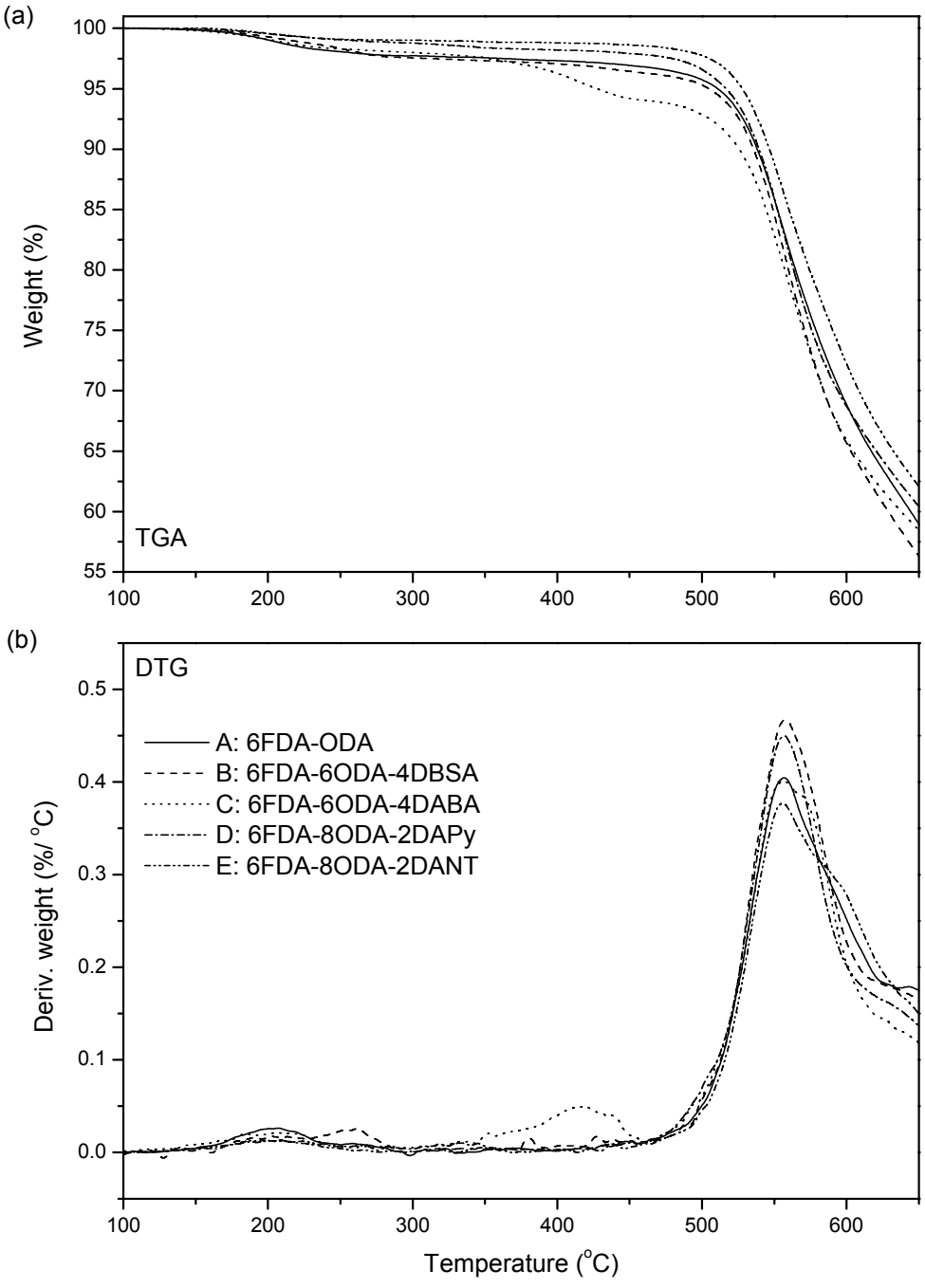

Figure 6.6 TGA and DTG curves of polyimides

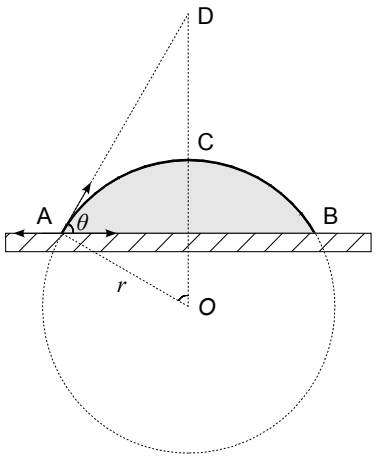

Figure 6.7 Determination of the contact angle from a sessile drop on a horizontal surface

Table 6.3 Contact angles of liquids on polyimide membranes at room temperature

Membranes	Water (°)	Glycerol (°)	Formamide (°)	Diiodomethane (°)
6FDA-ODA	77.5 ± 1.0	67.4 ± 2.4	54.3 ± 2.0	26.0 ± 0.6
FDA-6ODA-4DBSA	76.1 ± 0.7	60.8 ± 0.7	51.5 ± 0.6	30.0 ± 1.4
6FDA-6ODA-4DABA	77.5 ± 1.1	63.8 ± 1.4	48.4 ± 1.1	36.8 ± 2.0
6FDA-8ODA-2DAPy	77.4 ± 2.5	66.7 ± 3.1	54.8 ± 1.1	34.3 ± 1.4
6FDA-8ODA-2DANT	78.2 ± 0.9	66.6 ± 0.5	55.7 ± 1.3	29.5 ± 2.3

All results are given as means with the 95 % confidence intervals.

$$\gamma_i = \gamma_i^{LW} + \gamma_i^{AB} \tag{6.3}$$

$$\gamma_i^{AB} = 2\sqrt{\gamma_i^- \gamma_i^+} \tag{6.4}$$

The Lifshitz-van der Waals component γ_i^{LW} is the apolar component related to Lifshitz-van der Waals interactions including London dispersion forces, Debye-polarization and Keesom forces, and it can be determined from measurement of the contact angles of an apolar liquid on the solid surface. The acid-base component γ_i^{AB} is associated with the acid-base interactions including hydrogen bonding, π-bonds and ligand formation in a bipolar system. γ_i^{AB} was further split into two mono-polar surface parameters: Lewis acid (electron-acceptor) component γ^+ and Lewis base (electron-

donor) component γ^-. A substance can be considered to be apolar if both the acidic and basic components are negligible.

In this work, the γ_s^{LW} of the membranes was calculated from contact angles by using an apolar liquid diiodomethane (DIM) from Equation 6.5. Three polar liquids, water, glycerol and formamide were used in the measurement of contact angles on the polyimide membrane, and their surface free energy components are listed in Table 6.4. The values of γ_s^+ and γ_s^- can be obtained from Equation 6.6 using least squares regression [De Bartolo *et al.* 2004].

$$\gamma_s^{LW} = \frac{\gamma_{DIM}^{LW}(1+\cos\theta_{DIM})^2}{4} \tag{6.5}$$

$$\gamma_l(1+\cos\theta) = 2\left(\sqrt{\gamma_s^{LW}\gamma_l^{LW}} + \sqrt{\gamma_s^+\gamma_l^-} + \sqrt{\gamma_s^-\gamma_l^+}\right) \tag{6.6}$$

Free energy of the interfacial interaction ΔG_{sl}^{IF} can be evaluated using Equation 6.7 [De Bartolo *et al.* 2004], and thus the water-membrane interfacial free energies ΔG_{sw}^{IF} can be calculated.

$$\Delta G_{sl}^{IF} = -2\left(\sqrt{\gamma_s^{LW}} - \sqrt{\gamma_l^{LW}}\right)^2 - 4\left(\sqrt{\gamma_s^+\gamma_s^-} + \sqrt{\gamma_l^+\gamma_l^-} - \sqrt{\gamma_s^+\gamma_l^-} - \sqrt{\gamma_s^-\gamma_l^+}\right) \tag{6.7}$$

Table 6.4 Surface free energy components (in mJ/m^2) of liquids used in measurement of contact angles at room temperature

Liquids	γ_l^{LW}	γ_l^+	γ_l^-	γ_l^{AB}	γ_l
Water	21.8	25.5	25.5	51.0	72.8
Glycerol	34.0	3.92	57.4	30.0	64.0
Formamide	39.0	2.28	39.6	19.0	58.0
Diiodomethane	50.8	0	0	0	50.8

The contact angles of the polyimide membranes are shown to be in the order: water > glycerol > formamide >> diiodomethane. Since diiodomethane is considered as the apolar liquid, the smaller contact angle with diiodomethane reflects the affinity of the polyimides to apolar liquids, and the larger contact angle with water reflects hydrophobicity of the membranes.

Table 6.5 shows the membrane surface free energies and water-membrane interfacial free energies from the calculations. The values of Lifshitz-van der Waals components γ_i^{LW} appear to be in the range of 41–46 mJ/m^2, and they make the predominant contributions to the total surface free

energies of γ_s. The great difference in the values of Lewis acid-base (AB) components γ_i^{AB} mainly results from the deviations in the values of the electron-acceptor (Lewis acid) components γ^+. The acidity of DBSA and DABA moieties in the polymers contributes to a larger value of the acid components γ^+, whereas the basicity of the DAPy moieties favors the basic components γ_s^-. If γ^+ and γ_s^- are compared, all polyimide membranes show the properties of electron-donicity, which is probably due to the residual amino groups in the polyimides. The values of γ_s are not significantly affected by the variations in the values of γ_s^{AB}, and all the membranes have a surface free energy between 43–46.5 mJ/m^2. ΔG_{sw}^{IF} can be used to compare the affinity of the membranes to water since a negative value of ΔG_{sw}^{IF} represents hydrophobicity of the surface [Van Oss and Giese 1995]. Hence, 6FDA-based membranes are hydrophobic membranes, but 6FDA-6ODA-4DABA and 6FDA-8ODA-2DAPy show more hydrophilicity than the other polyimides studied here.

Table 6.5 Surface free energy components (mJ/m^2) and membrane-water interfacial free energies (mJ/m^2) of polyimides at room temperature

Membranes	γ_s^{LW}	γ_s^+	γ_s^-	γ_s^{AB}	γ_s	ΔG_{sw}^{IF}
6FDA-ODA	45.79	0.0001	6.16	0.05	45.84	–60.67
6FDA-6ODA-4DBSA	44.22	0.2072	5.49	2.13	46.35	–57.60
6FDA-6ODA-4DABA	41.18	0.4428	4.68	2.88	44.06	–56.71
6FDA-8ODA-2DAPy	42.35	0.0431	6.54	1.06	43.41	–55.05
6FDA-8ODA-2DANT	44.43	0.0063	5.97	0.39	44.82	–59.79

6.3.3 Gas Permeation Properties

The gas permeability of 6FDA-ODA and the copolyimides was measured with 5 gases at room temperature. Because very thin membranes (8–15 μm) were used in gas permeation, it was decided to use permeance instead of permeability in the discussion of gas permeabilities to minimize the experimental errors from thickness measurements. The gas permeances (in GPU) of the polyimide membranes are shown in Table 6.6. Figure 6.8 shows the permeance ratios of 6FDA-ODA and 4 copolyimide membranes for O_2, H_2, He and CO_2 over N_2 at different pressures. It is observed that membrane selectivity is independent of pressures, and therefore, the average permeance ratios (listed in Table 6.6) are used for the polyimide membranes in later work.

Table 6.6 Gas separation properties of polyimide membranes at room temperature

Membranes	Permeances (GPU) [a]					Permeance ratios			
	J_{N_2}	J_{O_2}	J_{H2}	J_{He}	J_{CO_2}	α_{O_2/N_2}	α_{H_2/N_2}	α_{He/N_2}	α_{CO_2/N_2}
6FDA-ODA	0.03	0.14	0.99	1.26	1.45	5.1	35.5	44.9	52.0
6FDA-8ODA-2DBSA	0.02	0.14	0.95	1.07	1.34	5.5	38.8	43.3	54.3
6FDA-6ODA-4DBSA	0.02	0.13	1.40	1.90	0.90	6.0	63.9	85.0	40.2
6FDA-8ODA-2DABA	0.02	0.13	1.69	1.54	1.16	5.7	75.4	68.9	51.7
6FDA-6ODA-4DABA	0.03	0.20	0.58	2.10	0.95	7.3	21.5	74.3	35.2
6FDA-9ODA-1DAPy	0.02	0.07	0.38	0.44	0.86	3.6	18.8	21.8	42.5
6FDA-8ODA-2DAPy	0.05	0.22	2.24	3.25	1.83	4.5	50.2	67.6	38.1
6FDA-9ODA-1DANT	0.03	0.14	0.93	1.07	1.51	4.8	32.2	37.1	55.6
6FDA-8ODA-2DANT	0.02	0.10	0.54	0.60	1.35	4.7	24.8	27.6	61.9

[a] Average data of gas permeances at 0.14, 0.21, 0.28 and 0.35 MPa.

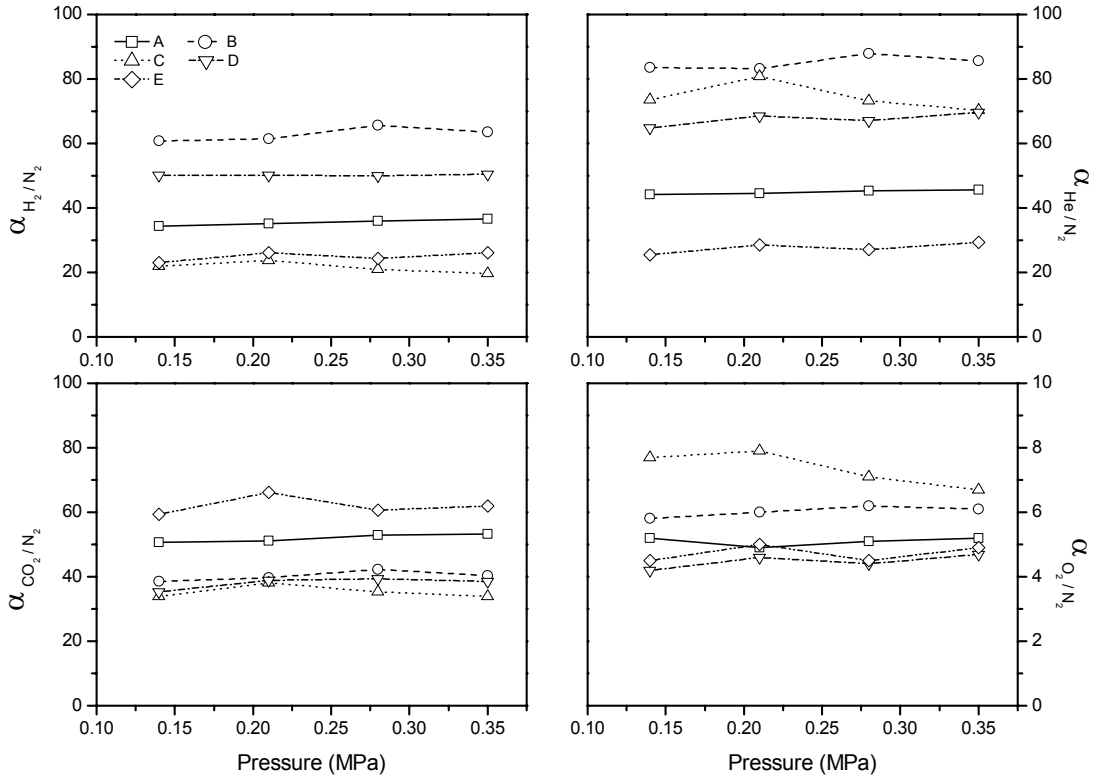

Figure 6.8 Permeance ratios of gas pairs for membranes at different pressures

A: 6FDA-ODA, B: 6FDA-6ODA-4DBSA, C: 6FDA-6ODA-4DABA,
D: 6FDA-8ODA-2DAPy, E: 6FDA-8ODA-2DANT

6.3.3.1 Gas Transport through Polyimides

Gas permeation in polymers is governed by the solution-diffusion mechanism [Baker 2004]. Sorption occurs on the upstream side of the membrane, and gas molecules diffuse through the membrane under the pressure difference across the membrane [Ho and Sirkar 1992]. The solubility of gases in a membrane is related to their critical temperatures. Gases with higher critical temperatures are much easier to condense and are more soluble in the membrane [Koros and Fleming 1993]. Based on the difference in their critical temperatures: CO_2 (304.1K) > O_2 (154.6K) > N_2 (126.2K) > H_2 (33.2K) > He (5.19K), a solubility selectivity of 1.35–1.89 for O_2/N_2 can be achieved at room temperature [Koros and Fleming 1993]. The experimental data show that α_{O_2/N_2} is in the range of 3.6–7.3 for the

polyimide membranes studied. This suggests that the diffusivity selectivity plays a significant role in the permeation selectivity towards O_2/N_2.

In the non-porous membrane, gas molecules move through the transient gaps produced from the segmental movement of the polymer matrix [Koros and Fleming 1993; Perry *et al.* 2006]. The transient gaps are related to the free volume [Ho and Sirkar 1992]. Polymer chains in glassy polymers are confined in the matrix, and the whole matrix acts as a molecular sieve in gas permeation. The diffusion selectivity towards O_2/N_2 can be achieved up to 5 by rigid glassy polymers [Koros and Fleming 1993]. Considering the difference in the kenetic diameters of the gases, N_2 (0.364 nm) > O_2 (0.346 nm) > CO_2 (0.33 nm) >H_2 (0.289 nm)> He (0.26 nm) [Perry *et al.* 2006], H_2 and He are supposed to have much higher diffusivity selectivity than O_2. The experimental data in Table 6.6 show that $\alpha_{He/N_2} > \alpha_{H_2/N_2} > \alpha_{O_2/N_2}$, and for all membranes, α_{CO_2/N_2} has values much greater than α_{O_2/N_2}, mainly due to the higher solubility selectivity towards CO_2/N_2 than that towards O_2/N_2.

6.3.3.2 Moiety Contributions

The polymer structure is critical to the selectivity for gases. Relationships between polymer structures and gas separation performances were investigated [Ohya *et al.* 1996; Kim *et al.* 1988], but they were not quantitatively described to account for the effects of the functional groups and polymer chains. The group contribution methods for prediction of gas permeabilities were developed. Salame [1986] proposed a group contribution method for the first time to predict gas permeability *P*, but this method may result in the same selectivity for gases in different polymers [Robeson *et al.* 1997].

$$P = Ae^{-s\pi} \text{ and } \pi = \frac{1}{n}\sum \pi_i \tag{6.8}$$

where *A* and *s* are constants for a particular gas, π_i is the contribution from the group *i*, and *n* is the number of groups per structural unit.

Jia and Xu [1991] developed a method based on molecular structures for prediction of gas permeabilities using the molar free volume V_f and the molar cohesive energy E_{coh}:

$$\log P = a + b(\frac{V_f}{E_{coh}}) \tag{6.9}$$

where *a* and *b* are constants for a given penetrant. However, the accuracy of the method is limited.

Park and Paul [1997] correlated the gas permeabilities with fractional free volume:

$$P = Ae^{-B/FFV} \tag{6.10}$$

where A and B are constants for a particular gas and FFV is the fractional free volume. In this method, overlaps of the free volumes of different units were neglected because it was assumed that the free volume of a specific group remained the same as in all polymers [Robeson *et al.* 1997].

Robeson *et al.* [1997] simplified the group contribution method using the volume fractions of structural groups:

$$\ln P = \sum \phi_i \ln P_i \tag{6.11}$$

where ϕ_i is the volume fraction of a specific group *i* comprising the polymer repeating structure and P_i is the permeability contribution of the specific group *i*. The simplicity of this method lies in that the permeability of a membrane was divided into partial permeabilities of the structural units. As a matter of fact, Equation 6.11 deals with the local concentrations of the structural groups.

The transport of non-condensable gases in glassy polymers, mainly controlled by diffusivity properties, is much simpler than that of condensable gases, and thus predictions of permeabilities can be made with good agreement with experimental data. Nevertheless, the prediction of permeabilities of condensable gases through glassy polymers remains a problem because in these cases the solubility aspect is more dominating than the diffusivity aspect. Therefore, if the prediction method can combine both the solubility and diffusivity aspects of mass transport, more conclusions will be obtained.

In this work, a linear moiety contribution method is proposed to predict the membrane selectivities. For simplicity, the moiety contributions are assumed to be linear. The general form of the linear moiety contribution method is expressed as

$$f = \sum_i (a_i \cdot X_i) + \sum_j (b_j \cdot Y_j) \tag{6.12}$$

where *f* is the parameter characterizing the membrane property (it can be the permeance ratio for gas separation), a_i and b_j are the molar fractions of dianhydride moieties and diamine moieties, respectively, $\sum_i a_i = 1$, $\sum_j b_j = 1$, X_i and Y_j are moiety contribution factors for dianhydride moieties and diamine moieties in the polyimide, respectively.

This method is purely empirical, and parameters do not have clear physical meanings. Statistical analysis cannot be done meaningfully because of the limited data available here. Results from least

squares regression of permeance ratios of gas pairs (shown in Table 6.6) are listed Table 6.7. The calculation procedures can be found in Appendix D.

Table 6.7 Contribution of monomer moieties to the membrane selectivity

Moieties of monomers	α_{O_2/N_2}	α_{H_2/N_2}	α_{He/N_2}	α_{CO_2/N_2}
6FDA	3.6	29.4	36.4	33.8
ODA	0.6	–0.4	–2.7	9.6
DBSA	5.9	79.5	101.2	13.2
DABA	8.2	31.1	113.6	1.5
DAPy	–2.9	20.7	58.8	–28.4
DANT	3.6	–10.6	–20.5	108.0

Values were calculated from 6FDA-based polyimides using least squares regression method. Calculations should be based on the overall molar ratio of dianhydrides/diamines of 1:1.

The molecular sieving effect on the non-condensable gases of O_2, He and H_2, can be seen from the contributions of the monomer moieties. The moieties of 6FDA, DBSA and DABA contribute positively to the selectivities towards O_2/N_2, He/N_2 and H_2/N_2, and their contributions are enhanced by the size difference in the gas molecules. The $–CF_3$ groups in 6FDA, $–SO_3H$ groups in DBSA and –COOH groups in DABA occupy more space in the matrices, and thus the polymer chains can pack more loosely [Pandey and Chauhan 2001]. Gas molecules of smaller sizes and lower solubility in the membrane can easily pass through, resulting in a higher selectivity against N_2. The smaller size and more rigid structure of the DAPy moiety decrease the mobility of O_2 (possibly N_2 as well), but the mobility of He and H_2 is not significantly affected, and at the same time the local concentration of 6FDA moieties is enhanced by the introduction of DAPy. The ODA moiety behaves differently, because it decreases the effects of 6FDA moieties in the main chain on the local moiety concentration, in spite of a positive contribution that is merely favorable to the diffusion of O_2 other than N_2, probably due to the flexible ether bond. The DANT moiety is different from the others, and the rigid naphthalene structure that is larger than the DAPy moiety produces more space for O_2, but limits the mobility of H_2 and He in the polymer matrix. The contributions of monomer moieties for α_{CO_2/N_2} reflect their overall influences on CO_2 solubility and diffusivity in the polymers. It is interesting that the pyridine structure with the Lewis-base property decreases α_{CO_2/N_2}. The lone electron pair is supposed to be a cause of the solubility change of CO_2 in the polymers [Lin and Freeman, 2005].

Figure 6.9 shows a comparison of the experimental data with the predicted permeance ratios for the polyimide membranes. The predicted α_{O_2/N_2} and α_{CO_2/N_2} agree with the experimental data better than α_{He/N_2} and α_{H_2/N_2}. More data are required for more reliable predictions using this method.

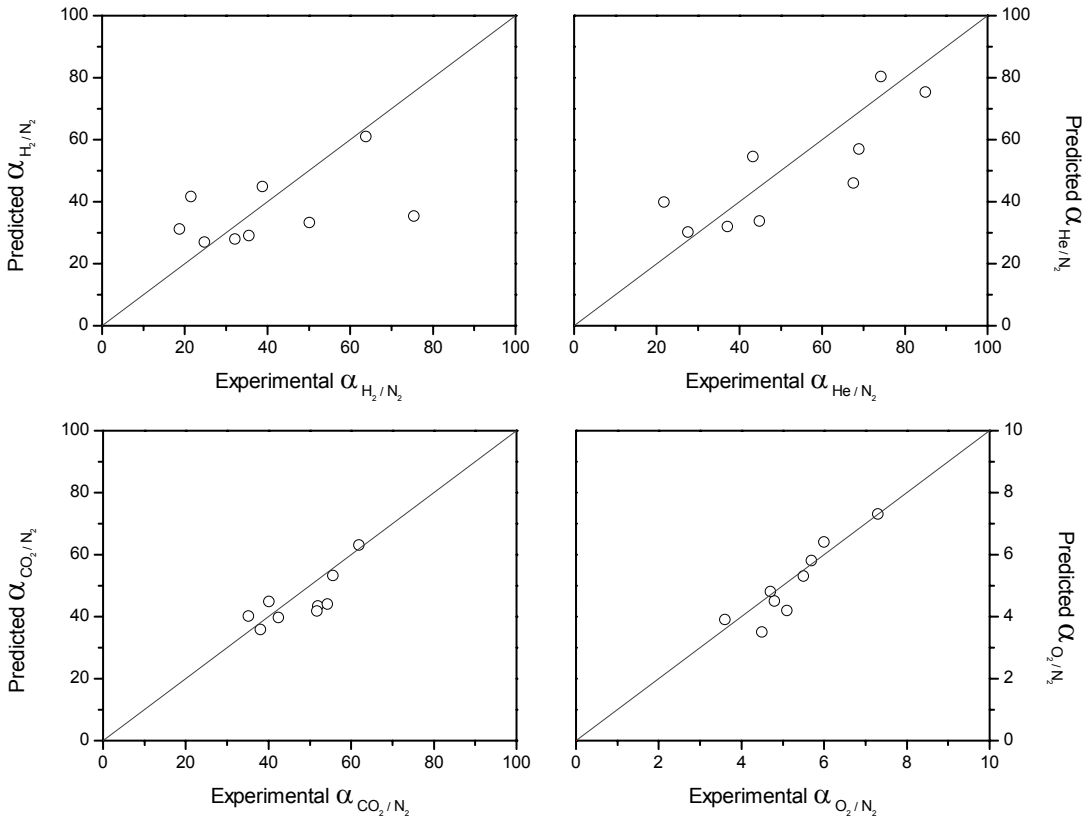

Figure 6.9 Comparison of experimental data with the predicted permeance ratios for polyimide membranes

6.3.4 Pervaporation Properties

Pervaporation experiments were carried out for pure water permeation and dehydration of isopropanol. The temperature and feed concentration dependencies of permeation flux and selectivity were studied.

6.3.4.1 Mass Transport

In pervaporation, the liquid components of the feed mixture selectively permeate through the membrane, to produce a vaporous product with the aid of vacuum or the purge gas at the downstream side. Based on the solution-diffusion model, sorption occurs at the feed side surface of the membrane, and the penetrants diffuse across the membrane, followed by evaporation/desorption of the components into the permeate [Shao and Huang 2007]. Desorption is usually considered as a fast step, and the sorption and diffusion properties of the penetrants in the membrane are of great importance.

As discussed for gas separation, the molecular size of the penetrant and the dimension of the transport paths arising from thermal transient gaps in the membrane are critical parameters that determine the diffusivity of the penetrants in glassy polymers. Isopropanol has a molecular diameter (0.43 nm) larger than water (0.265 nm) [Perry *et al.* 2006; Kuznicki *et al.* 2002], which means that isopropanol has a lower diffusivity than water. The high glass transition temperature and the rigidity of aromatic imide moieties result in the low mobility of the polyimide segmental chains, thereby restricting the diffusivity of isopropanol and water. The packing properties of the polyimide matrices are attributed to the regularity of the polymer chains as well as the steric effects of side groups, which also influence the diffusivity of the penetrant [Pandey and Chauhan 2001]. The DAPy and DANT moieties in the copolyimides change the regularity of the polymer chains, and the DABA and DBSA moieties bear bulky groups. All these will help improve the diffusivity of the penetrant. Besides the steric effects, the pyridine moiety (from DAPy) and the functional groups (e.g. sulfonic acid groups from DBSA and carboxylic acid groups from DABA), have some favorable diffusional effects derived from their physiochemical interactions with isopropanol and/or water. These interactions possibly change the physical properties of the polymer matrices, such as packing densities and glass transition temperatures. As a matter of fact, most of these interactions are essentially related to the solubility of the penetrants in the polymers, or in other words, the sorption properties of the membranes.

Sorption of the penetrants in polymer membranes can be considered as the formation of polymer solutions where polymers are the “solvents” for the penetrants. Functional groups play an important role in the sorption properties because of their interactions with the penetrants. The acyl groups in imide rings can form hydrogen bonds with water, and the hydrophilic groups (e.g. sulfonic acid groups and carboxylic acid groups) are favorable to the sorption of water. However, the pyridine moiety has a positive effect on isopropanol, and the aromatic properties of the polyimide membranes

also promote the solubility of isopropanol. In 6FDA-based polyimides, the $-CF_3$ groups show unfavorable effects on the solubilities of the penetrants, but it is beneficial to the flexibility of the polymer matrices that will lead to a higher diffusivity.

6.3.4.2 Effects of Functional Groups on Selectivity

Polyimide membranes show fairly good selectivity for water. As shown in Figure 6.10, most polyimide membranes have a permeate water content higher than 90 wt. %. It is also observed that by introducing a third monomer into the main chains of 6FDA-ODA, the membrane selectivity undergoes substantial changes.

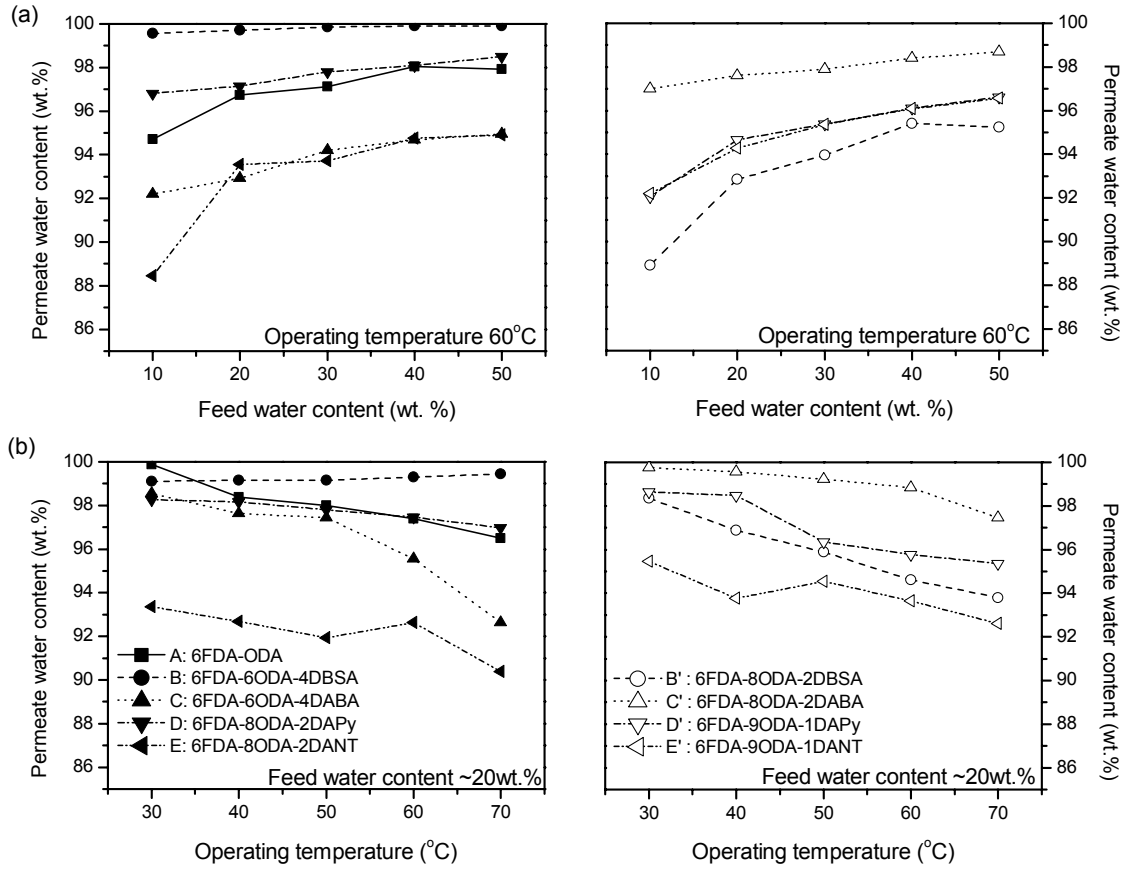

Figure 6.10 Permeate water contents of polyimide membranes in pervaporation dehydration of isopropanol (a) operating temperature 60 °C (b) feed water content ~20 wt. %

It should be pointed out that the 6FDA-ODA membrane was cast from a pyridine solution, and the solvent may affect the chain packing properties. Furthermore, 6FDA-ODA has better regularity in the main chain than the copolyimides, and the higher packing density can lead to the lower permeability to both water and isopropanol.

DBSA and DAPy moieties have similar effects on permeation selectivity. When a small amount of DBSA and DAPy is introduced to substitute ODA, the loose packing of the polymer matrices will occur because of the irregularity of the main chains. With an increase in the content of the third monomer in copolymers, more water can permeate selectively, probably due to the higher solubility in the matrices. However, the DABA moiety has reverse effects compared with DBSA and DAPy moieties. Generally speaking, the DABA moiety has two effects: hydrogen bonding effect (favorable to water permeation) and size-induced steric effect (favorable to both isopropanol and water). Thus a small number of DABA moieties lead to a higher water content in permeate; however, the opposite will hold when the main chains contain a large number of DABA moieties. The DANT moiety in 6FDA-ODA-based copolyimides show affinity to isopropanol, resulting in a decrease in the permeate water content.

6.3.4.3 Effects of the Feed Concentration

Figure 6.10 (a) exhibits the effects of the feed concentration on the permeate water content in pervaporation dehydration of isopropanol. For all membranes, the permeation flux increases with an increase in the feed water concentration.

Based on the experimental data, the effect of feed concentration on permeation flux can be described by an empirical equation when the feed concentration is below 50 wt. %:

$$F(x_w) = k \cdot x_w^n \tag{6.13}$$

where $F(x_w)$ is the total permeation flux at a feed water content of x_w (mass fraction), n is an exponential parameter, and it is defined as the "*concentration coefficient*" for total flux, and k is a parameter related to the membrane material and thickness as well as the operating temperature. The parameter k is considered to be a constant for the same membrane at the same operating temperature.

The values of n were determined from total flux by curve fitting. Results are listed in Table 6.8. Most of the coefficients of determination are greater than 0.99, indicating good qualities of fit achieved by the regression.

Table 6.8 Concentration coefficients and permeation activation energies for pervaporation

Membranes	n [a]	E_p (pure water) [b] (kJ/mol)	E_p (total flux) [c] (kJ/mol)
6FDA-ODA	0.22	15.7 ± 0.8	46.1 ± 2.8
6FDA-8ODA-2DBSA	0.37	17.7 ± 2.5	40.9 ± 2.4
6FDA-6ODA-4DBSA	0.39	36.1 ± 1.4	37.4 ± 1.8
6FDA-8ODA-2DABA	0.35	28.6 ± 0.9	53.6 ± 2.8
6FDA-6ODA-4DABA	0.44	32.1 ± 1.7	59.6 ± 2.7
6FDA-9ODA-1DAPy	0.33	31.9 ± 2.7	49.4 ± 4.7
6FDA-8ODA-2DAPy	0.37	34.0 ± 2.6	55.6 ± 3.1
6FDA-9ODA-1DANT	0.32	15.2 ± 1.1	34.4 ± 3.0
6FDA-8ODA-2DANT	0.36	12.7 ± 0.5	30.1 ± 1.8

[a] Obtained from curve fitting, r^2=0.92–0.99.

[b] Apparent activation energies for pure water permeation.

[c] Apparent activation energies for total permeation flux with feed water content ~20 wt. %.

By using the linear contributions approach proposed as Equation 6.12, the moiety contributions of the monomers were calculated (calculation details as shown in Appendix E). The results are listed in Table 6.9. In Equation 6.13, a lager value of n will result in a smaller value of x_w^n at a given feed concentration x_w ($0 < x_w < 1$). It is observed that the hydrophilic moieties of DBSA and DABA have greater n values. This is possibly because the sorption properties of the membranes do not change significantly considering the "fixed space" for the sorbed penetrants in the glassy matrices. However, for the ODA moiety, sorption is enhanced with a high concentration of water in the feed, resulting in an improved total flux. The DANT moiety with a rigid naphthalene structure has "less space" for the sorbed penetrants, especially for isopropanol. Furthermore, no functional groups in the DANT moiety can facilitate possible interactions with water. As a result, the total flux of the polyimide membrane containing DANT moieties does not increase significantly as the feed water content is increased.

Figure 6.11 (a) shows the comparison of concentration coefficients from experimental data with those from predictions. The validity of the method is confirmed from these results.

6.3.4.4 Effects of the Operating Temperature

Figure 6.10 (b) shows the permeate water contents for pervaporation dehydration of isopropanol at different operating temperatures. Activation energies for pure water permeation were calculated using Equation 3.4, and the results are listed in Table 6.8.

The linear contributions approach was applied to the activation energies to study the effect of monomer moieties on the temperature dependency of permeation flux. The moiety contribution factors for activation energies were calculated from the least squares regression (calculation details are shown in Appendix E), and are presented in Table 6.9.

Table 6.9 Moiety contributions to concentration coefficients and permeation activation energies

Moieties of monomers	n	E_p (pure water) (kJ/mol)	E_p (total flux) (kJ/mol)
6FDA	0.25	24.1	35.6
ODA	0.03	–6.7	7.1
DBSA	0.37	33.0	0.7
DABA	0.41	33.7	51.6
DAPy	0.18	98.0	27.0
DANT	0.41	–30.2	–60.3

It is much more complicated to study the effects of functional groups/moieties on permeation activation energies, because temperature can not only increase the mobility of the segmental chains of polymers, but also change the sorption properties. In some cases, sorption properties are crucial for permeation flux. The moiety contributions to activation energies appear to be in the following sequences (negative signs included), for pure water permeation: DAPy > DABA > DBSA > 6FDA > ODA(–) > DANT(–), and for total flux: DABA > 6FDA > DAPy > ODA > DBSA > DANT(–). The negative contributions from ODA and DANT moieties are acceptable because both the activation energy of diffusion and the heat of sorption (can be positive or negative) contribute to the apparent permeation activation energies. The negative contribution from DANT indicates that the effects of the rigid structure offset the increase in flux caused by the moieties of 6FDA and ODA in the main chain. A great difference is observed in the contributions of the DBSA moiety to the activation energies of pure water permeation and the total flux. It results from the interactions between isopropanol and the DBSA moiety, because shrinkage of the polymer matrices occurs when introducing DBSA moiety to

the polyimides. This offsets the positive effect from the increase of segmental mobility at elevated temperatures, leading to a lower flux but a higher selectivity. As seen in Figure 6.10 (b), when increasing operating temperature, 6FDA-6ODA-4DBSA shows a higher selectivity and a higher flux.

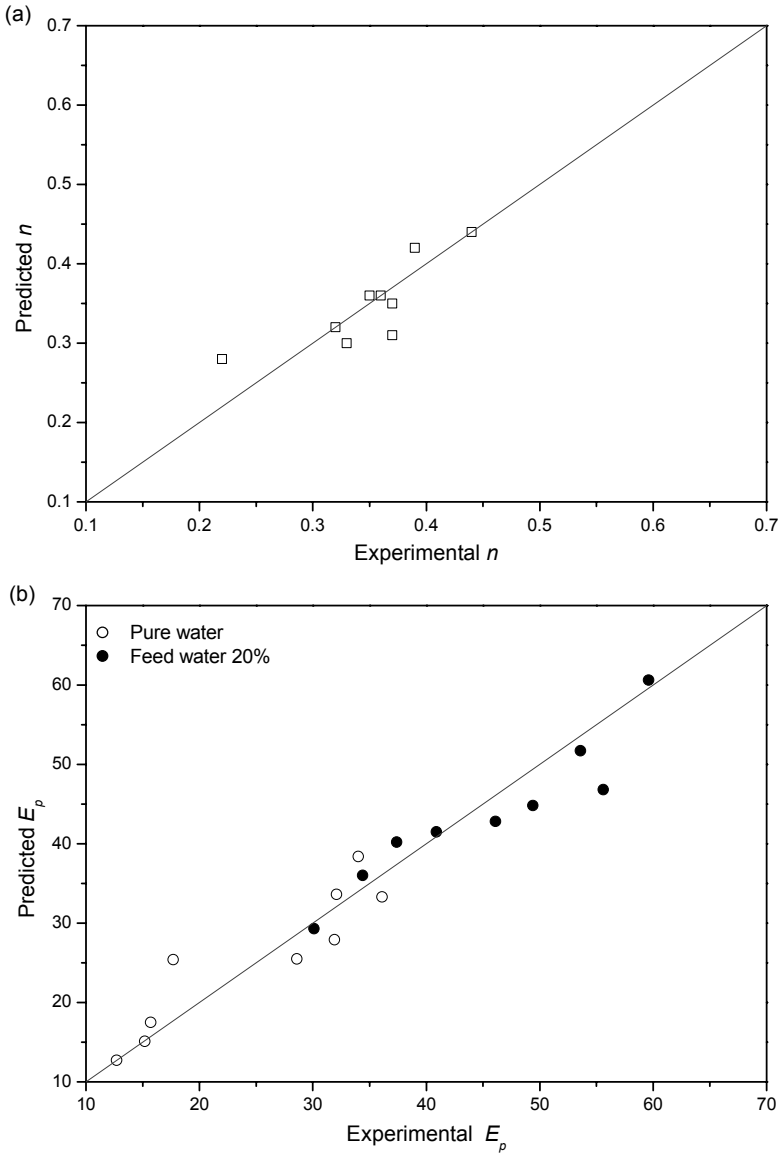

Figure 6.11 Comparison of the concentration coefficients and permeation activation energies from predictions using linear moiety contributions with those from experimental data

Permeation activation energies were recalculated from the moiety contribution factors using the linear contribution method (Equation 6.12). As shown in Figure 6.11 (b), the predicted values are compared with those calculated from the experimental data,. The reasonableness of the linear moiety contributions is suggested by the agreement between the experimental results and the calculated results.

6.4 Conclusions

6FDA-ODA-based copolyimides of high molecular weights were prepared from one-step polymerization of 6FDA and ODA, and a diamine (*i.e*. DBSA, DABA, DAPy and DANT) as a third monomer. Their chemical structures were confirmed by FTIR and NMR spectra. The polyimides showed good thermal stabilities.

The surface free energy and the membrane-water interfacial free energy were calculated from contact angles, and it was found that DABA, DBSA and DAPy moieties helped increase the hydrophilicity of 6FDA-ODA-based membranes.

Gas permeation was measured with N_2, O_2, H_2, He and CO_2. A linear moiety contribution method was proposed to study the moiety effects on gas selectivities. Introduction of a third monomer in 6FDA-ODA main chains increased the rigidity and limited the segmental mobility, but the side groups in DABA and DBSA provided more space for gas transport due to the loose packing of the polymer chains. Permeability of N_2, O_2, H_2 and He and the corresponding selectivities were significantly affected by the steric effects of the monomer moieties, but the permeation of CO_2 was mainly determined by its solubility in the polymer as well as the interactions with the functional groups.

Water permeation and dehydration of isopropanol were carried out in pervaporation processes. An empirical relation was proposed to represent the effect of the feed concentration on permeation flux, and the temperature dependence of permeation flux was also studied. The linear moiety contribution method was applied to quantitatively compare the influences of monomer moieties on the temperature and feed concentration dependencies of the permeation flux. It is indicated that the functional groups in the membranes affect their pervaporation properties: the feed concentration significantly influences the sorption properties of the membranes, and the effect the temperature leads to changes in diffusion properties of the penetrants.

Chapter 7

4,4'-(Hexafluoroisopropylidene) Diphthalic Anhydride (6FDA) - 4-Aminophenyl Ether (ODA) - Based Polyimide Membranes for Gas Separation and Pervaporation. II. Polyimides Containing Moieties with Different Chain Structures

Copolyimides were synthesized from 6FDA and ODA with diamines 4-Aminophenyl sulfone (DDS), 4,4'-methylenedianiline (MDA), 4,4'-bis(3-aminophenoxy)diphenyl sulfone (BADS), 4,4'-bis(3-aminophenoxy) benzophenone (BABP) and 2,6-bis(3-aminophenoxyl)benzonitrile (DABN) as the third monomer. Diamine monomers showed different reactivities in the one-step polycondensation, but they did not change thermal properties of the resulting polyimides significantly. Surface free energies and interfacial free energies were calculated for comparison of the membrane hydrophilicity. Gas permeation was carried out with N_2, O_2, H_2, He and CO_2, and the moiety contributions to membrane selectivity were calculated. DDS and BADS moieties contribute negatively to the selectivities towards O_2/N_2, H_2/N_2 and He/N_2, and the DABN moiety is favorable for improving CO_2/N_2 selectivity. Water permeation and dehydration of isopropanol were performed, and the linear moiety contribution method was applied to study the effects of the monomer structures on the temperature and feed concentration dependencies of the permeation flux. The steric effects of DDS and BADS moieties, as well as the interactions of BABP and DABN moieties with water, account for the differences in pervaporation properties of the membranes.

7.1 Introduction

Relationships between the gas permeability and the chemical structure of membrane materials were studied in the early years [Park and Paul 1997; Robeson *et al.* 1997], and new polyimides with special structural features were prepared for gas separation, enriching the knowledge of chemical structure vs. separation properties. Kim *et al.* [1988] studied the gas separation properties of a series of polyimides. The polymer segmental mobility and the packing properties were used to explain the difference in membrane permeabilities: a lower density and larger *d*-spacing of the membranes could

lead to a higher permeability. Stern *et al.* [1989] investigated gas permeabilities of different polyimide membranes, and found out that segmental mobility, interchain distance, and charge transfer complexes formed in membranes determined gas permeabilities. Highly soluble and O_2 permeable polyimides were synthesized from twisted biphenyl dianhydrides and spirobifluorene diamines by Kim *et al.* [2005]. The characteristic structures of the dianhydrides and the diamines caused a decrease in the degrees of molecular packing and crystallinity, and the restricted segmental mobility resulted in high permeabilities to O_2.

Due to the complexity of interactions between the membrane and the liquid mixture to be separated, polyimide pervaporation membranes were not explored intensively in terms of structure-property relationships. Xu *et al.* [2006] studied the pervaporation properties of some polyimide membranes. The permeation flux was found to be in agreement with the orders of *d*-spacing and free volume of the polymers. High rigidity of the polymer chains was supposed to help increase pervaporation selectivity, while low packing density of the segmental chains led to high flux [Xu *et al.* 2006].

Membrane permeabilities are governed by sorption and diffusivity of the penetrants in the membranes. From the results mentioned above, it can be summarized that diffusion properties are greatly influenced by the steric effects and the mobility of polymer chains. However, the steric effects of segmental chains also partially account for the sorption properties, leading to a complicated mix-up. If the effects of monomer moieties on separation properties are quantitatively outlined, a better understanding and a deeper insight can be achieved.

In Chapter 6, 6FDA-ODA-based copolyimides from the diamine monomers with side substituents (or functional groups) were synthesized and their separation properties were studied. However, the structure of the main chains also has some effects on the membrane performance. Therefore, the diamine monomers having similar main chains but different steric configurations were used to prepare copolyimides, and their moiety contributions to separation properties were investigated.

7.2 Experimental

4-Aminophenyl sulfone (DDS, 97 %), 4,4'-methylenedianiline (MDA, 97 %), 4,4'-bis(3-aminophenoxy)diphenyl sulfone (BADS, 97 %), 2,6-difluorobenzonitrile (97 %), 3-aminophenol (99 %), 4,4'-difluorobenzophenone (99 %), potassium carbonate (K_2CO_3, anhydrous, > 99 %) and *N*, *N*-

dimethylacetamide (DMAc, >99 %) were provided by Acros Organics. All other materials are the same as in 6.2.1. All experiments, unless stated otherwise, were carried out as described in 6.2.

7.2.1 Synthesis of Monomers

The two monomers 2,6-bis(3-aminophenoxyl)benzonitrile (DABN) and 4,4'-bis(3-aminophenoxy) benzophenone (BABP) were synthesized from nucleophilic substitution reactions of 3-aminophenol with 2,6-difluorobenzonitrile and 4,4'-difluorobenzophenone, respectively [Heath and Wirth 1972; Tanabe *et al.* 1986]. The procedures for DABN synthesis (shown in Figure 7.1) were summarized as follows:

To a 1 L three-neck flask with a mechanical stirrer, a Dean-Stark trap, a condenser and nitrogen inlet/outlet, 2,6-difluorobenzonitrile 28 g (0.2 mol), 3-aminophenol 80 g (0.6 mol), anhydrous potassium carbonate 170 g (1.2 mol) and DMAc 300 mL, toluene 50 mL were added under f nitrogen. The mixture was stirred and heated to about 150 °C to allow toluene to reflux. Water was distilled out to the trap in the form of toluene/water azeotrope. Toluene was kept refluxing and water was continuously removed for 10 h. Then the reaction temperature was increased to 165 °C, and meanwhile toluene was blown out through the trap. The reaction lasted for 14 h before the dark brown mixture was cooled to about 100 °C and poured into hot water. The mixture was filtered when cooled to obtain the crude product. The pure product was obtained from recrystallization in isopropanol. The final product 2,6-bis(3-amino phenoxyl)benzonitrile (DABN) was dried under vacuum at 40 °C for 20 h.

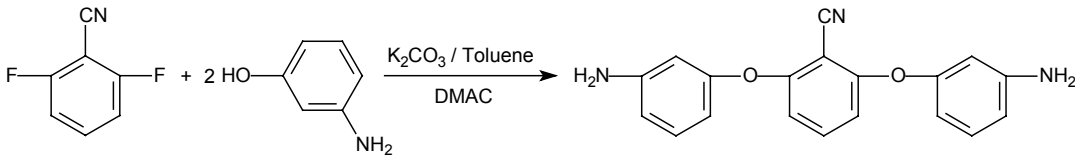

Figure 7.1 Synthesis of DABN

7.2.2 Polymers and Membranes

Copolyimides (shown in Table 7.1) were synthesized from 6FDA and ODA with diamines DDS, MDA, BADS, BABP or DABN as the third monomer (shown in Figure 7.2), and procedures were outlined in 6.2.2. Polyimide membranes (15–30 μm thick) were prepared from 5 w/v % polyimide THF solutions.

Table 7.1 6FDA-ODA copolyimides and molecular weights

Polyimides	Monomers	Molar ratio	$\overline{M}_n$	$\overline{M}_w$	$\overline{M}_w / \overline{M}_n$	$\overline{DP}$
6FDA-8ODA-2DDS	6FDA : ODA : DDS	= 1 : 0.8 : 0.2	44510	58270	1.31	72
6FDA-6ODA-4DDS	6FDA : ODA : DDS	= 1 : 0.6 : 0.4	50410	62810	1.25	80
6FDA-8ODA-2MDA	6FDA : ODA : MDA	= 1 : 0.8 : 0.2	54320	74930	1.38	89
6FDA-6ODA-4MDA	6FDA : ODA : MDA	= 1 : 0.6 : 0.4	63460	74680	1.18	104
6FDA-8ODA-2BADS	6FDA : ODA : BADS	= 1 : 0.8 : 0.2	133900	171500	1.28	205
6FDA-6ODA-4BADS	6FDA : ODA : BADS	= 1 : 0.6 : 0.4	118200	160800	1.36	169
6FDA-8ODA-2BABP	6FDA : ODA : BABP	= 1 : 0.8 : 0.2	164300	275100	1.67	254
6FDA-6ODA-4BABP	6FDA : ODA : BABP	= 1 : 0.6 : 0.4	128300	204500	1.59	187
6FDA-8ODA-2DABN	6FDA : ODA : DABN	= 1 : 0.8 : 0.2	46990	62280	1.33	74
6FDA-6ODA-4DABN	6FDA : ODA : DABN	= 1 : 0.6 : 0.4	89560	124800	1.39	137

Dianhydride:

6FDA

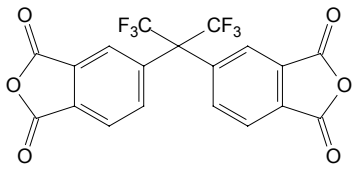

Diamines:

ODA

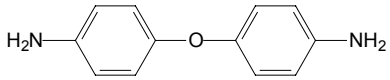

DDS

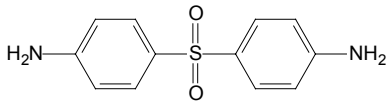

MDA

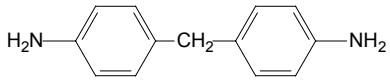

BADS

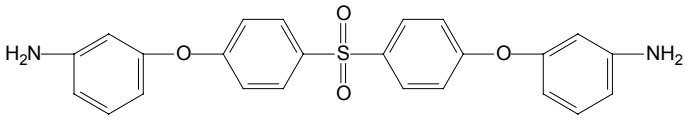

BABP

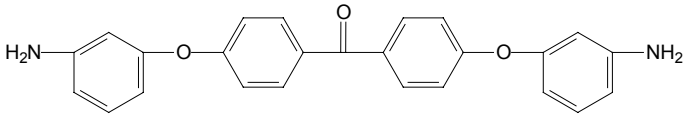

DABN

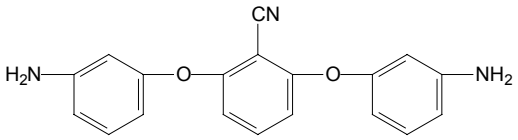

Figure 7.2 Monomers of polyimides

7.3 Results and Discussion

7.3.1 Preparation of Monomers and Polymers

7.3.1.1 BABP and DABN

Monomers BABP and DABN were synthesized from nucleophilic substitution reactions. The phenolic salt was formed when 3-aminophenol reacted with K_2CO_3 in the first step, and it acted as the

nucleophilic agent to attack the electrophilic site of the activated halide compounds (*i.e.* 2,6-difluorobenzonitrile and 4,4'-difluorobenzophenone). The reaction ended when the new σ-bond formed to the nucleophile and the former σ-bond was broken to form the leaving group, *i.e*. halide anions.

Details of FTIR and NMR data are shown in Appendix A. In the FTIR spectra of BABP and DABN, the asymmetrical and symmetrical stretching vibrations of amino groups absorb at 3470 cm^{-1} and 3370 cm^{-1}, respectively. The C–N stretching absorption occurs at ~1285 cm^{-1}. Skeletal vibrations of the phenyl rings are found to be in the region of 1570–1590 cm^{-1}. The aryl ether bonds show asymmetrical stretching vibration at 1226 cm^{-1} for BABP and symmetrical stretching vibration at 1027 cm^{-1} for DABN, respectively [Silverstein *et al.* 1997]. In the spectrum of DABN, the characteristic absorption of the nitrile groups occurs at 2231 cm^{-1}, and the stretching vibration of nitrile groups absorbs at 1625 cm^{-1}. In FTIR of BABP, the absorption at 1635 cm^{-1} is assigned to C=O stretching vibration, and it shifts to a lower wavenumber because of the two phenyl rings [Silverstein *et al.* 1997; Nakanishi and Solomon 1977]. Figure 7.3 (a) shows NMR spectra of BABP and DABN in DMSO-*d6*. H_a, H_b and H_d in BABP and DABN have their chemical shifts at the same positions, and the resonance peaks at ~5.3 ppm are assigned to the protons in the amino groups in BABP and DABN, respectively.

7.3.1.2 Copolyimides

Copolyimides were synthesized from one-step high-temperature polycondensation of 6FDA and ODA with the third monomers. As shown in Figure 7.2, DDS and MDA have molecular structures similar to ODA, and the only difference lies in the sulfonyl group and the methylene bond, respectively, instead of the ether bond in ODA, while BADS, BABP and DABN have 3-aminophenyl moieties in the molecules. Though the one-step polycondensation is different from the two-step procedures for preparing polyimides, it still can be considered to consist of two stages. In the first stage, the dianhydride monomer reacts with diamines in *m*-cresol at a low temperature (~80 °C) to form poly(amic acid)s, and in the second stage at a high temperature (~200 °C), imidization reaction occurs with isoquinoline as the catalyst to form polyimides.

In the FTIR spectra of the copolyimides, a very weak absorption band at ~3493 cm^{-1} representing the "free" asymmetrical N–H stretching modes [Silverstein *et al.* 1997], is observed for amino groups, possibly including the uncyclized amino groups and the polyimide end groups. Aromatic C-H stretching band occurs at ~3075 cm^{-1} for all polyimides. Figure 7.4 shows part of the FTIR spectra

(2300–600 cm^{-1}) of the copolyimides. At ~1600 cm^{-1} and ~500 cm^{-1}, the spectra show two absorption bands of the skeletal stretching of aromatic rings. The five characteristic absorption bands of the imide ring occur at 1785 cm^{-1} (C=O asymmetrical stretching), 1728 cm^{-1} (C=O symmetrical stretching), 1380 cm^{-1} (C–N stretching), 1110 cm^{-1} (imide III band), and 723 cm^{-1} (imide ring bending vibration) [Dunson 2000; Pramoda *et al.* 2002; Sroog1965; Kim *et al.* 1993a]. The asymmetrical stretching vibration of $–CF_3$ groups produces absorption at ~1300 cm^{-1}, and the stretching absorption of the ether bond in ODA moieties appears at ~1245 cm^{-1}. The very weak absorption at 1331 and 1326 cm^{-1} for 6FDA-6ODA-4DDS and 6FDA-6ODA-4BADS, respectively, is due to the asymmetrical stretching vibration of sulfonyl groups [Silverstein *et al.* 1997]. The vibration of aromatic-aromatic ketone produces absorptions at 1658 and 1655 cm^{-1} in the spectra of 6FDA-8ODA-2BABP and 6FDA-6ODA-4BABP, respectively. Sharp absorption peaks can be observed for 6FDA-8ODA-2DABN and 6FDA-6ODA-4DABN at 2232 cm^{-1}, which is attributed to the vibration of nitrile groups in the polymer chains.

Figure 7.3 (b) shows the ^1H NMR spectra of the copolyimides. The coupled peaks at 7.91 and 7.31 ppm are assigned to the protons of the ODA moiety. The chemical shifts of protons in the 6FDA moiety are located at 8.2–8.0 ppm. The protons attached to α-C of the sulfonyl groups in DDS and BADS show peaks at 8.45 and 8.19 ppm, respectively, while the protons attached to β-C of the sulfonyl groups produce peaks at ~8.14 and ~7.18 ppm, respectively. The methylene groups of MDA moieties in 6FDA-6ODA-4MDA show a peak at 4.09 ppm, and the two peaks coupled at 7.83 and 7.48 ppm are assigned to the protons attached to the phenyl rings. In the NMR spectra of 6FDA-6ODA-4DABN and 6FDA-ODA-BABP, chemical shifts of H_e and H_f do not shift too far away from their monomers DABN and DABP, as shown in Figure 7.3 (a), but the chemical shifts of $H_{a–d}$ show great difference between the monomers and the polymers, which also indicates the formation of imide bonds in the polymer chains.

The molecular weights and molecular weight distributions of the copolyimides are listed in Table 7.1. Four polyimides, 6FDA-8ODA-2BABP, 6FDA-6ODA-4BABP, 6FDA-8ODA-2BADS and 6FDA-6ODA-4BADS, have higher molecular weights than the others. The molecular weight distributions are calculated from $\overline{M}_n$ and $\overline{M}_w$, and the values vary in the range of 1.18–1.67. The small values of $\overline{M}_w / \overline{M}_n$ obtained from GPC result from the fractionation effect of the ethanol during the extraction of *m*-cresol.

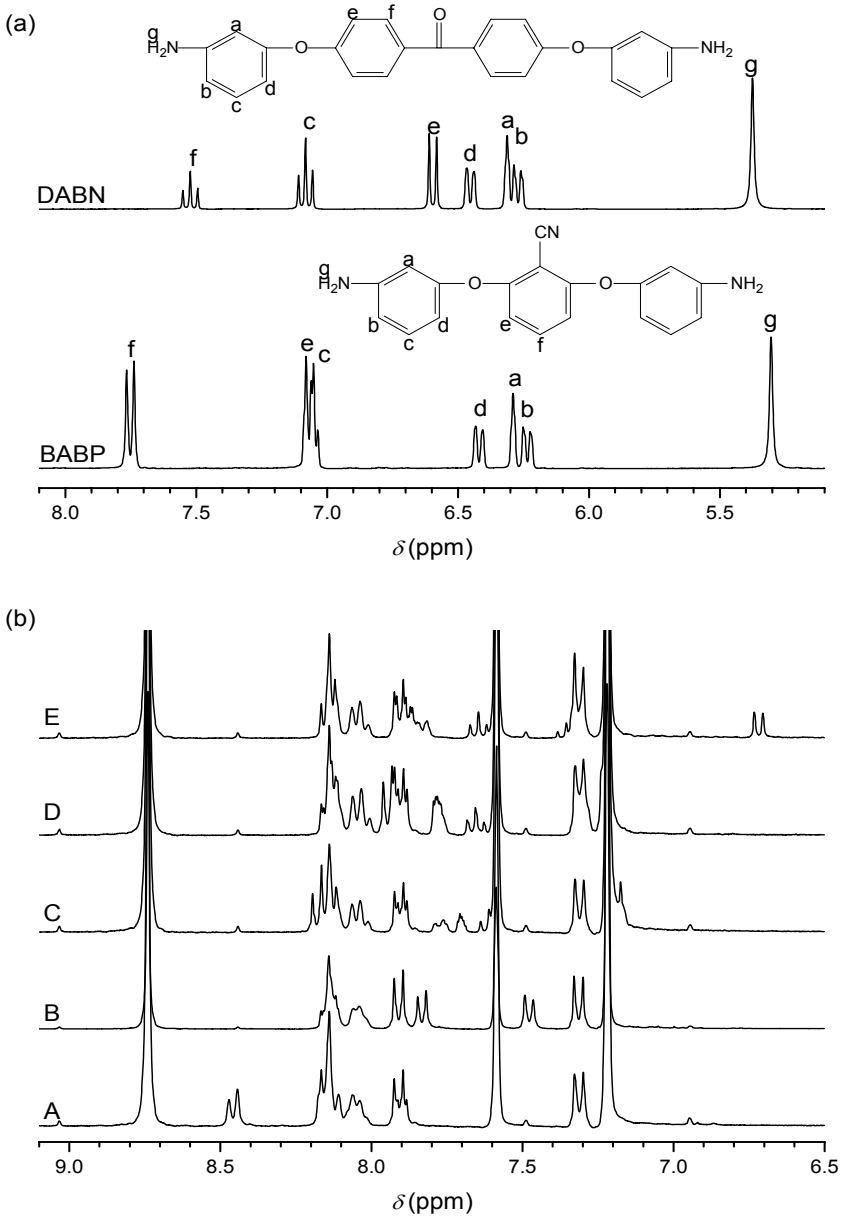

Figure 7.3 ^{1}H NMR spectra (a) BABP and DABN, and (b) 6FDA-ODA-based copolyimides

A: 6FDA-6ODA-4DDS, B: 6FDA-6ODA-4MDA, C: 6FDA-6ODA-4BADS,
D: 6FDA-6ODA-4BABP, E: 6FDA-6ODA-4DABN

Since these copolyimides were synthesized from the same procedures and under the same conditions, the difference in the molecular weight is supposed to result from the difference in the monomer reactivities. It is known that synthesis of polyimides is favored by the basicity of the diamines. Therefore, comparison of the charges on N-atom of the $-NH_2$ groups can lead to a better

understanding of the basicity of the diamines and thus their reactivities. Using MOPAC, Wang-Ford charges were determined: ODA (–0.940) > BABP (–0.932), BADS (–0.931), DABN (–0.930) > MDA (–0.926) > DDS (–0.920). This sequence indicates the charge densities on N-atoms and the monomer reactivities. 6FDA-8ODA-2DDS and 6FDA-6ODA-4DDS have lower molecular weights, and this is also consistent with the sequence of Wang-Ford charges.

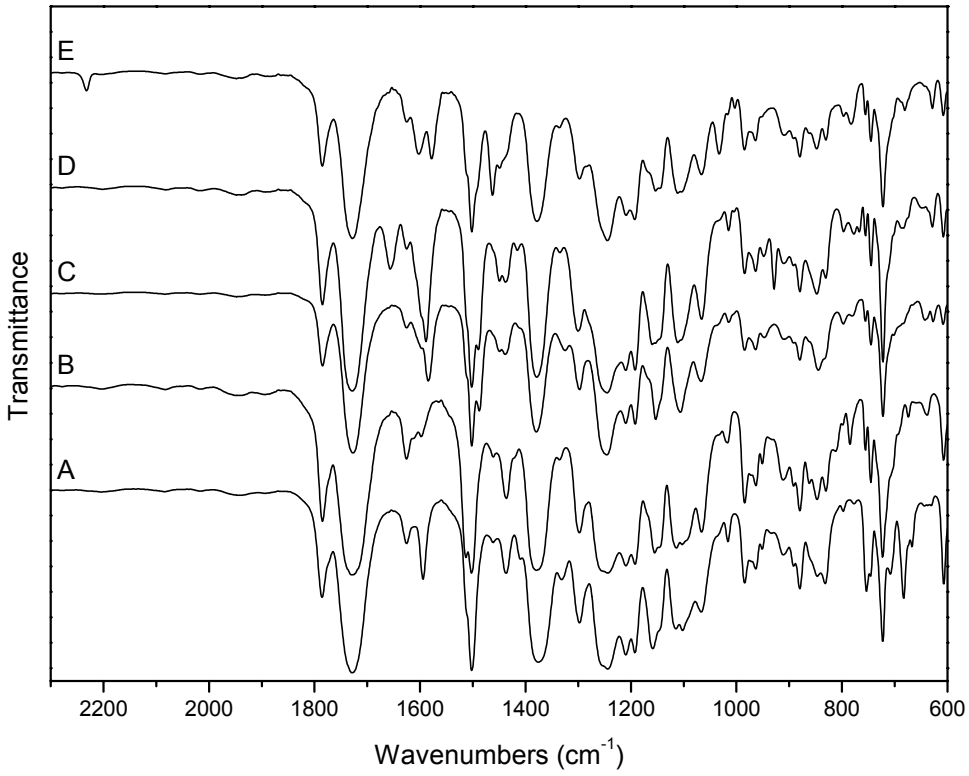

Figure 7.4 FTIR spectra of 6FDA-ODA-based copolyimides

A: 6FDA-6ODA-4DDS, B: 6FDA-6ODA-4MDA, C: 6FDA-6ODA-4BADS, D: 6FDA-6ODA-4BABP, E: 6FDA-6ODA-4DABN

7.3.2 Properties of Polyimides

7.3.2.1 Solubility

All polymers are readily soluble in THF and pyridine, and they can dissolve in chloroform, DMAc, DMF, NMP, acetone, and DMSO, but they are insoluble in isopropanol, toluene and cyclohexane. THF was used as the solvent to prepare polyimide solutions when casting membranes.

7.3.2.2 Thermal Properties

The DSC onset temperature, as presented in Table 7.2, was used to estimate the glass transition temperature. From the known T_gs of 6FDA-ODA (285°C), 6FDA-MDA (291°C) and 6FDA-DDS (336°C) [Ohya *et al.* 1996], the T_gs of the copolyimides can be roughly calculated using the Fox equation [Fox 1956]. The estimated T_gs are 287 °C for 6FDA-6ODA-4MDA and 305 °C for 6FDA-6ODA-4DDS. The DSC onset temperatures are comparable to these estimated values. The experimental results also show that sulfonyl and ketone groups as well as nitrile groups are favorable structures in polyimides that can help remain a high T_g.

TGA and DTG curves are plotted in Figure 7.5 and the characteristic values are listed in Table 7.2. The further conversion of poly(amic acid)s to polyimides can be found at about 200 °C. 6FDA-6ODA-4BABP has the highest T_d 5 % and T_d 10 % (which are ~521 and ~543 °C, respectively) whereas T_d 5 % and T_d 10 % of the other polyimides are in the range of 502–508 °C and 534–537 °C, respectively. The degradation onset temperatures show no significant difference, which are all in the range of 513–518 °C, with a maximum decomposition rate (DTG peak temperature) at ~557 °C for all polyimides. These results indicate the outstanding thermal stabilities for the copolyimides.

Table 7.2 Characteristic temperatures from DSC, TGA and DTG

Polyimides	DSC [a] (°C)	T_d 5 % wt. loss (°C)	T_d 10 % wt. loss (°C)	T_d onset [b] (°C)	DTG [c] (°C)
6FDA-6ODA-4DDS	296	508	535	514	557
6FDA-6ODA-4MDA	293	510	537	516	556
6FDA-6ODA-4BADS	290	502	534	514	557
6FDA-6ODA-4BABP	298	521	543	518	558
6FDA-6ODA-4DABN	289	507	538	517	558

[a] DSC operating conditions: 10 °C/min in helium. Glass transition temperatures were not distinctly decided from the first and second runs of DSC. The onset temperatures were used as an estimation of their glass transition temperatures.

[b] TGA operating conditions: 10 °C/min in helium.

[c] These temperatures were obtained from DTG peak temperatures.

7.3.2.3 Surface free energies

Table 7.3 shows the contact angles of various liquids on the copolyimide membranes at room temperature. The surface free energies and interfacial free energies are calculated using the methods shown in 6.3.2.3, and results are listed in Table 7.4.

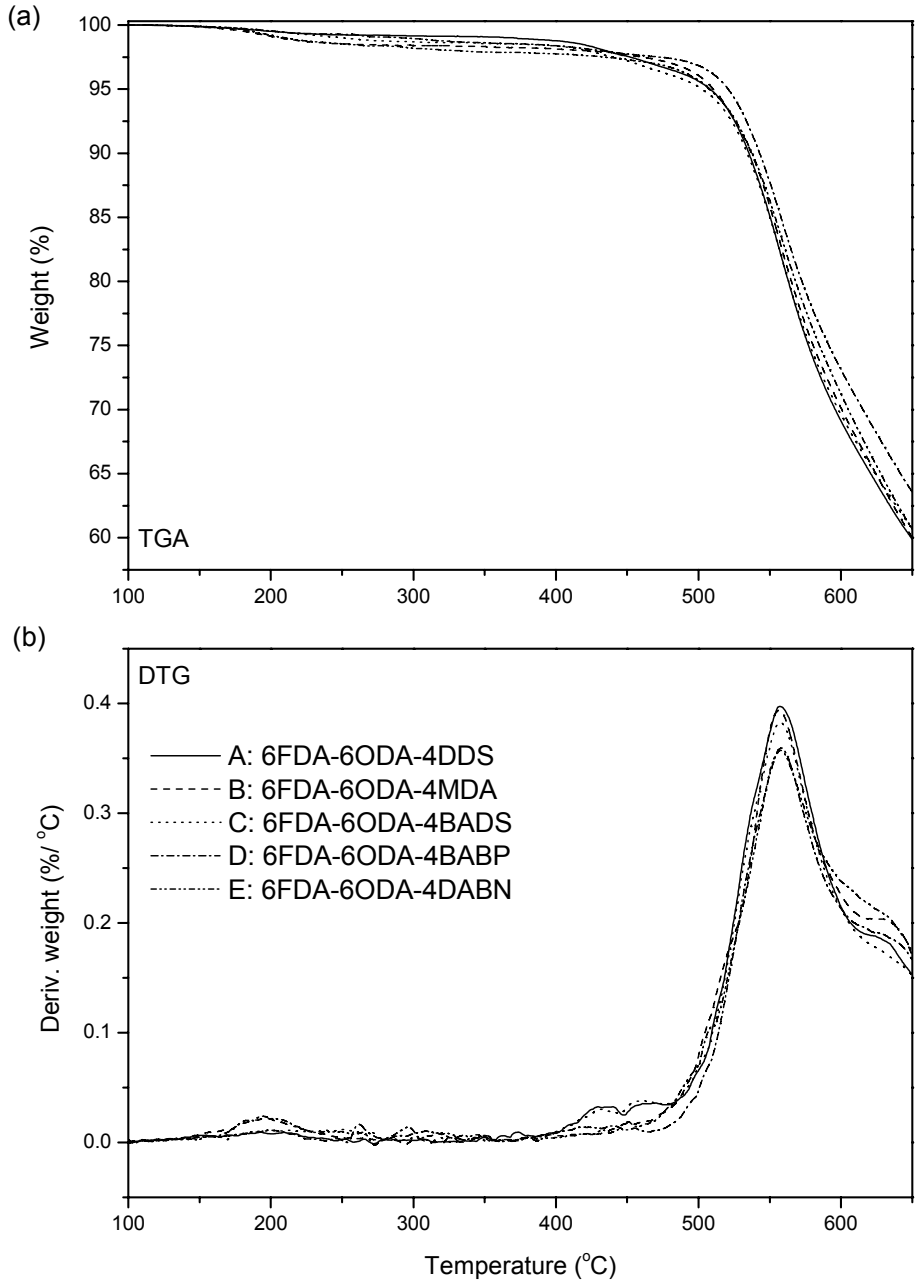

Figure 7.5 TGA and DTG curves of polyimides

Since contact angles are directly related to the affinity of membranes toward the testing liquids, a rough judgment can be made from Table 7.3 that 6FDA-based membranes show great hydrophobicity

based on the contact angles with water, but more evidences from contact angles with other liquids are still required.

Table 7.3 Contact angles of liquids on polyimide membranes at room temperature

Membranes	Water (°)	Glycerol (°)	Formamide (°)	Diiodomethane (°)
6FDA-6ODA-4DDS	78.6 ± 0.9	66.0 ± 1.9	53.8 ± 1.2	21.3 ± 1.2
6FDA-6ODA-4MDA	75.9 ± 2.1	65.0 ± 0.9	54.0 ± 0.8	28.0 ± 0.5
6FDA-6ODA-4BADS	77.3 ± 1.1	65.5 ± 0.7	59.9 ± 0.2	34.1 ± 0.8
6FDA-6ODA-4BABP	82.9 ± 0.5	67.4 ± 0.6	56.5 ± 1.9	26.7 ± 0.8
6FDA-6ODA-4DABN	68.4 ± 2.1	61.2 ± 2.7	45.8 ± 2.1	32.2 ± 0.5

All results are given as means with the 95 % confidence intervals.

Table 7.4 Surface free energy components (mJ/m^2) and membrane-water interfacial free energies (mJ/m^2) of polyimides at room temperature

Membranes	γ_s^{LW}	γ_s^+	γ_s^-	γ_s^{AB}	γ_s	ΔG_{sw}^{IF}
6FDA-6ODA-4DDS	47.39	0.0002	5.09	0.06	47.45	–66.07
6FDA-6ODA-4MDA	45.03	0.0086	7.13	0.50	45.52	–55.51
6FDA-6ODA-4BADS	42.44	0.0043	7.38	0.35	42.80	–53.34
6FDA-6ODA-4BABP	45.53	0.0182	2.99	0.47	45.99	–73.91
6FDA-6ODA-4DABN	43.29	0.1427	11.54	2.57	45.85	–38.20

As shown in Table 7.4, the LW components γ_s^{LW} have much larger values than the AB components γ_s^{AB}. Thus it is reasonable to say that the apolar interactions play an important role in the surface free energies, however, the effects of acid-base interactions are more essential. A smaller value of γ_s^+ is an indication of residual hydration [Van Oss *et al.* 1997], and a larger value of γ_s^- suggests higher hydrophilicity [Van Oss and Giese 1995]. The predominant monopolar Lewis base behavior of the polyimide membranes is also due to the residual amino groups in the polymers. Among the membranes tested, 6FDA-6ODA-4DABN has a smaller γ_s^{LW}, but both γ_s^+ and γ_s^- are larger than the other membranes. Therefore, 6FDA-6ODA-4DABN is supposed to be the most hydrophilic membrane. The water-membrane interfacial free energies ΔG_{sw}^{IF} offer a direct view of the affinity of membrane surfaces toward water. Van Oss and Giese [1995] found a boundary value of the

interfacial free energies for clay materials, and pointed out that a negative value of ΔG_{sw}^{IF} represented hydrophobicity of the surface. Therefore, results from this work reveal that 6FDA-based membranes show great hydrophobicity, and this is not surprising because of the presence of F-atoms in the polymer chains. However, the hydrophobicity can be reduced by the incorporation of functional groups, such as the nitrile groups in DABN moieties.

7.3.3 Gas Permeation Properties

Pure gas permeation was performed at room temperature at different feed pressures. As shown in Figure 7.6, the membrane selectivities at different pressures did not show substantial changes for the same membranes. Therefore, the average values of permeance ratios were utilized in further studies. Table 7.5 shows the average gas permeances and permeance ratios for O_2/N_2, H_2/N_2, He/N_2 and CO_2/N_2. 6FDA-6ODA-4BABP and 6FDA-6ODA-4DABN showed the best selectivities towards O_2/N_2, H_2/N_2 and He/N_2, while 6FDA-8ODA-2DABN and 6FDA-6ODA-4DABN exhibited the best separation performances for CO_2/N_2.

From the linear moiety contribution method, the contributions of monomer moieties to the permeance ratios were calculated (shown in Appendix D) and are listed in Table 7.6. The contributions of monomer moieties to α_{CO_2/N_2} are very complicated because they are combinations of diffusivity effects and solubility effects. It is observed that the BADS moiety shows a negative effect on α_{CO_2/N_2}, and the DABN moiety is very helpful in promoting α_{CO_2/N_2}.

From Table 7.6, it is observed that 6FDA, MDA, BABP and DABN moieties have positive contributions to all the permeance ratios, while ODA, DDS and BADS contribute negatively to α_{H_2/N_2} and α_{He/N_2}. It is easy to track the contributions of monomer moieties simply from their structures. It is believed that $-CF_3$ (in 6FDA) and methylene (in MDA) groups are beneficial to increase the flexibility of the polymer main chains, and C=O (in BABP), –CN (in DABN) as well as $-CF_3$ (in 6FDA) groups provide more space for gas transport in the membranes. The contribution of the ODA moiety indicates that the flexible ether bond produces transient gaps that are only more favorable to O_2, but the great change in local concentration of 6FDA moieties offsets the increase in gas diffusivity. The effects of the BADS moiety are analogous with the ODA moiety, but the sulfonyl groups have an entirely different impact on the diffusion of gases. The moiety of phenyl sulfone exerts enormous steric effect, and huge inter-chain space is created within the matrix, resulting in a great increase in the diffusivities of gases including N_2. The flexibility of the ether bonds in the

BADS moiety counteracts part of the steric effects from the moiety of phenyl sulfone (*i.e.* the DDS moiety) in regards to the contributions to the selectivities towards O_2/N_2, H_2/N_2 and He/N_2.

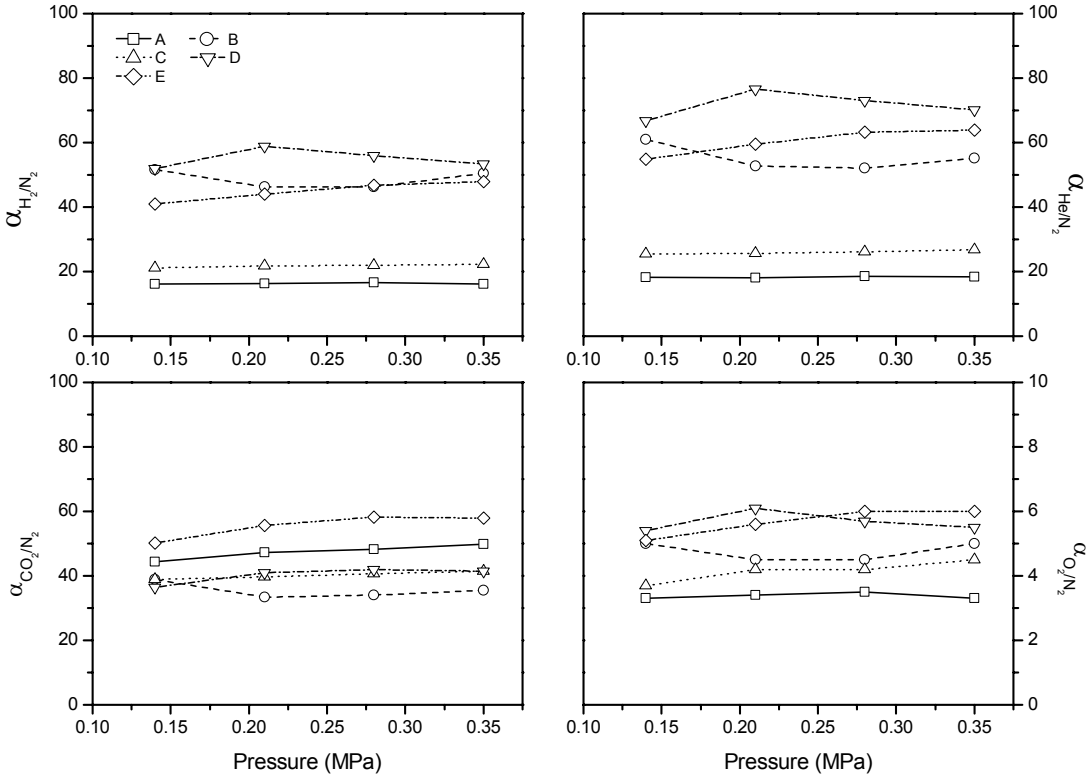

Figure 7.6 Permeance ratios of gas pairs for membranes at different pressures

A: 6FDA-6ODA-4DDS, B: 6FDA-6ODA-4MDA, C: 6FDA-6ODA-4BADS,
D: 6FDA-6ODA-4BABP, E: 6FDA-6ODA-4DABN

Comparisons of the membrane selectivities with the predicted permeance ratios from the linear moiety contribution method are made for the copolyimide membranes, as shown in Figure 7.7. The predicted data can match the experimental data, and α_{O_2/N_2} and α_{CO_2/N_2} show better agreement than α_{He/N_2} and α_{H_2/N_2}.

Table 7.5 Gas separation properties of polyimide membranes at room temperature

Membranes	Permeances (GPU) [a]					Permeance ratios			
	J_{N_2}	J_{O_2}	J_{H2}	J_{He}	J_{CO_2}	α_{O_2/N_2}	α_{H_2/N_2}	α_{He/N_2}	α_{CO_2/N_2}
6FDA-8ODA-2DDS	0.03	0.10	0.47	0.52	1.37	3.6	17.4	19.0	50.1
6FDA-6ODA-4DDS	0.03	0.10	0.49	0.54	1.41	3.4	16.3	18.3	47.4
6FDA-8ODA-2MDA	0.02	0.08	0.47	0.49	0.90	4.1	22.7	24.1	44.1
6FDA-6ODA-4MDA	0.06	0.27	2.75	3.12	2.00	4.8	48.6	55.0	35.3
6FDA-8ODA-2BADS	0.01	0.05	0.32	0.32	0.50	4.0	25.1	25.5	40.0
6FDA-6ODA-4BADS	0.04	0.16	0.82	0.97	1.50	4.2	21.8	26.0	40.2
6FDA-8ODA-2BABP	0.03	0.10	0.52	0.54	1.29	3.6	18.7	19.7	46.7
6FDA-6ODA-4BABP	0.01	0.07	0.73	0.95	0.53	5.7	54.9	71.5	40.2
6FDA-8ODA-2DABN	0.09	0.50	3.11	3.03	5.68	5.3	33.3	32.4	60.7
6FDA-6ODA-4DABN	0.02	0.12	0.96	1.29	1.18	5.7	44.8	60.1	55.3

[a] Average data of gas permeances at 0.14, 0.21, 0.28 and 0.35 MPa.

Table 7.6 Contributions of monomer moieties to permeance ratios

Moieties of monomers	α_{O_2/N_2}	α_{H_2/N_2}	α_{He/N_2}	α_{CO_2/N_2}
6FDA	3.6	29.4	36.4	33.8
ODA	0.6	–0.4	–2.7	9.6
MDA	1.7	9.7	5.1	12.1
DDS	–1.7	–37.3	–48.3	24.3
BADS	0.3	–18.6	–26.4	–0.2
BABP	2.9	41.2	58.8	6.5
DABN	4.6	35.6	48.7	50.7

Values were calculated from 6FDA-based polyimides using least squares regression method. Calculations should be based on the overall molar ratio of dianhydrides/diamines of 1:1.

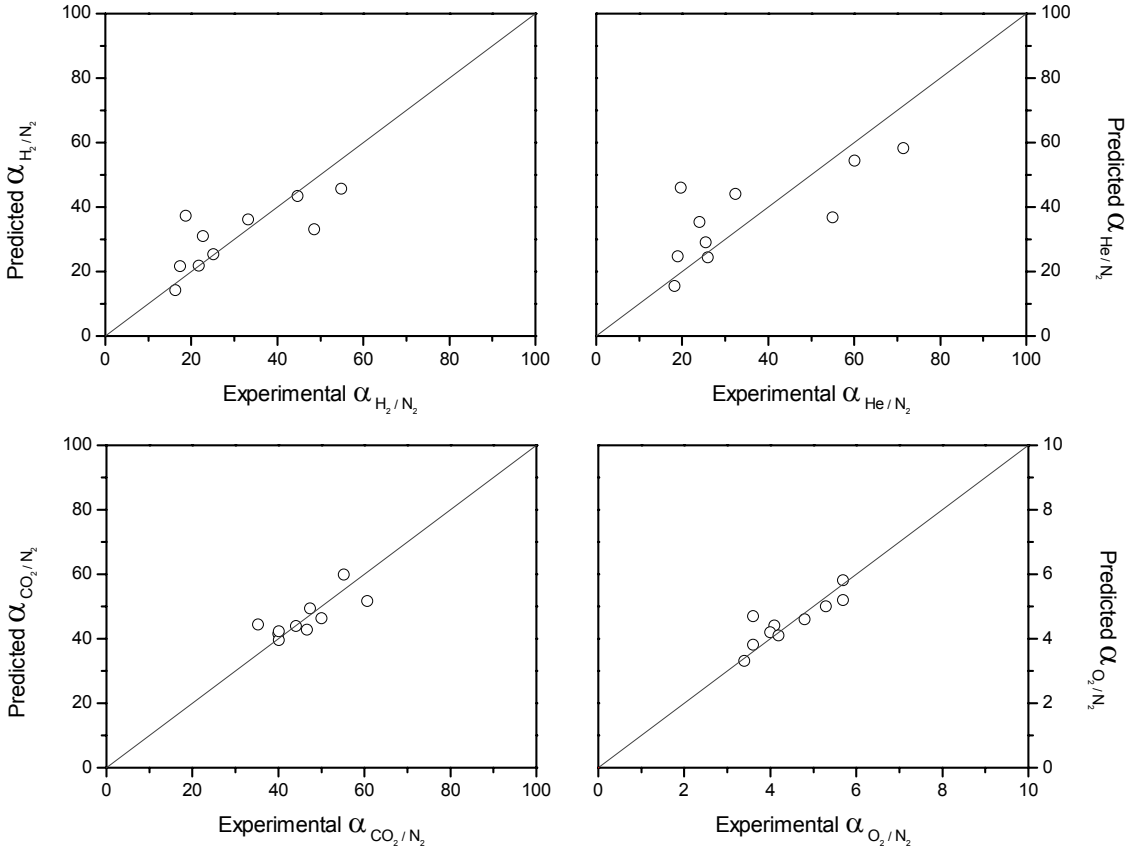

Figure 7.7 Comparison of experimental permeance ratios with the predicted values for polyimide membranes

7.3.4 Pervaporation Properties

7.3.4.1 Effects of Monomer Structure on Selectivity

Figure 7.8 shows the permeate water content for pervaporation with various feed water contents and at different operating temperatures. The membrane selectivity can be directly compared from the permeate water contents.

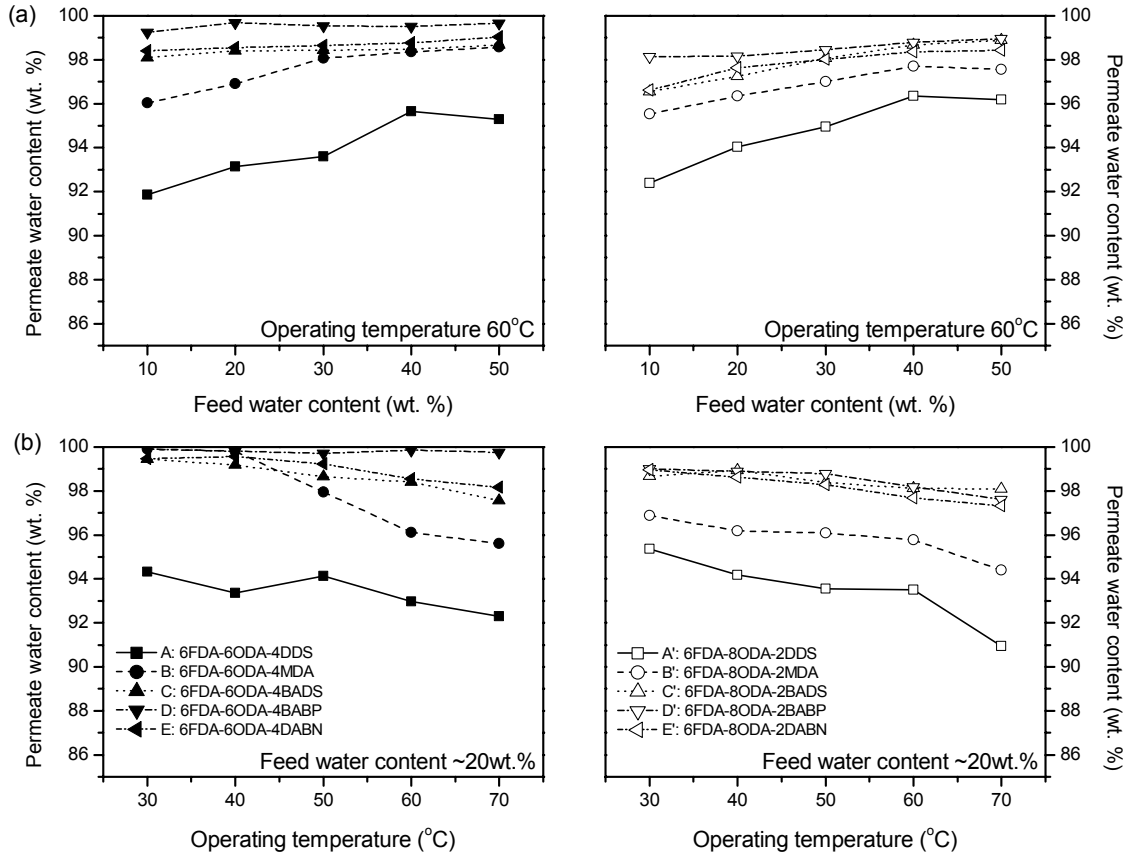

Figure 7.8 Permeate water contents of polyimide membranes in pervaporation dehydration of isopropanol

Based on Figure 7.8, a rough sequence of monomer contributions to the pervaporation selectivity can be obtained for the monomers used in this work: DDS (–) < MDA < BADS and DABN < BABP, the negative sign for DDS means that a negative contribution was made by the DDS moiety to the pervaporation selectivity. It is known that the MDA moiety has more affinity to isopropanol but less

to water. However, the flexible methylene groups in the MDA moiety cause the polymer chains to pack more densely if compared with ODA. Thus, the MDA moieties in membranes will lead to a high permeate water content. However, the selectivity of MDA moiety-containing membranes is still lower than the other membranes. As discussed in gas separation, larger inter-chain space in the polymer matrix can be produced because of the steric effects of the sulfonyl groups in DDS and BADS. More isopropanol and water can pass through the membranes containing DDS and BADS moieties, even though the sulfonyl groups interact with water molecules and the better sorption can be achieved for water. In BADS moieties, however, the flexible ether bonds reduce the steric effect of the sulfonyl groups. Therefore, the BADS moiety still has a positive contribution to the membrane selectivity, while the DDS moiety shows a negative contribution. Hydrogen bonding between water and BABP moieties is stronger than the van der Waals forces between water and the nitrile groups in DABN moieties. Accordingly, higher selectivities are observed for the membranes having BABP moieties than those containing DABN moieties.

7.3.4.2 Effects of the Feed Concentration

As shown in Figure 7.8 (a), with a higher feed water content, most membranes produce higher permeation flux and a higher water content in the permeate, but the DDS moiety-containing membranes show the highest permeate water contents at the feed water contents of 40 wt. %.

The *concentration coefficient* defined in 6.3.4.3 reflects the intrinsic properties of the pervaporation membranes. Good regressions were achieved in curve fitting with Equation 6.13, and Table 7.7 shows the n values. Obviously, the n values are related to the numbers of the monomer moieties. Therefore, the linear moiety contribution method was applied to the n values, and least squares regression was made with the n values of 6FDA-based membranes (calculations as shown in Appendix E). The moiety contribution factors are listed in Table 7.8. From the obtained moiety contribution factors, *concentration coefficients* were recalculated using Equation 6.12, and were compared with those from curve fitting. As shown in Figure 7.9 (a), the two sets of n values can match well for most of the membranes.

ODA, MDA and DABN moieties have smaller n values, which means that the permeation flux of the membranes containing these moieties are more sensitive to the change in the feed water content. This is probably attributed to the moiety contributions to the sorption properties of the membranes. It is known that the improved sorption properties can promote the permeation of penetrants. BABP moieties can form favorable interactions with water, and a better sorption can be achieved. However,

the sorption saturation in the polymer matrix is easy to reach, and it can lead to no significant increase in total flux. BABP moieties do so, resulting in a larger *n* value. The structures of DDS and BADS moieties provide more inter-chain space, and their membranes can accommodate the more sorbed penetrants. But similarly to BABP moieties, the saturation in sorption leads to larger *n* values for DDS and BADS moieties. As for 6FDA moieties, the combination of the favorable effect from imide rings and the unfavorable effect from $-CF_3$ groups contributes to the *n* value of 0.25.

Table 7.7 Concentration coefficients and permeation activation energies for pervaporation

Membranes	n [a]	E_p (pure water) [b] (kJ/mol)	E_p (total flux) [c] (kJ/mol)
6FDA-8ODA-2DDS	0.50	21.6 ± 3.6	36.2 ± 2.7
6FDA-6ODA-4DDS	0.60	21.6 ± 3.1	34.0 ± 2.9
6FDA-8ODA-2MDA	0.31	26.6 ± 0.3	38.5 ± 1.1
6FDA-6ODA-4MDA	0.41	30.0 ± 2.9	48.7 ± 2.8
6FDA-8ODA-2BADS	0.37	16.8 ± 4.9	30.8 ± 0.6
6FDA-6ODA-4BADS	0.44	19.5 ± 1.1	38.7 ± 1.3
6FDA-8ODA-2BABP	0.27	22.1 ± 1.3	39.1 ± 2.2
6FDA-6ODA-4BABP	0.41	30.0 ± 0.2	49.1 ± 3.3
6FDA-8ODA-2DABN	0.28	27.8 ± 2.0	41.9 ± 0.5
6FDA-6ODA-4DABN	0.30	30.3 ± 3.7	43.5 ± 3.6

[a] Obtained from curve fitting, r^2=0.92–0.99.

[b] Apparent activation energies for pure water permeation.

[c] Apparent activation energies for total permeation flux with feed water content ~20 wt. %.

Table 7.8 Moiety contributions to concentration coefficients and permeation activation energies

Moieties of monomers	n	E_p (pure water) (kJ/mol)	E_p (total flux) (kJ/mol)
6FDA	0.25	24.1	35.6
ODA	0.03	–6.7	7.1
MDA	0.07	16.9	6.3
DDS	0.88	5.7	–17.0
BADS	0.43	–3.3	–13.0
BABP	0.27	23.0	16.1
DABN	0.06	29.3	7.7

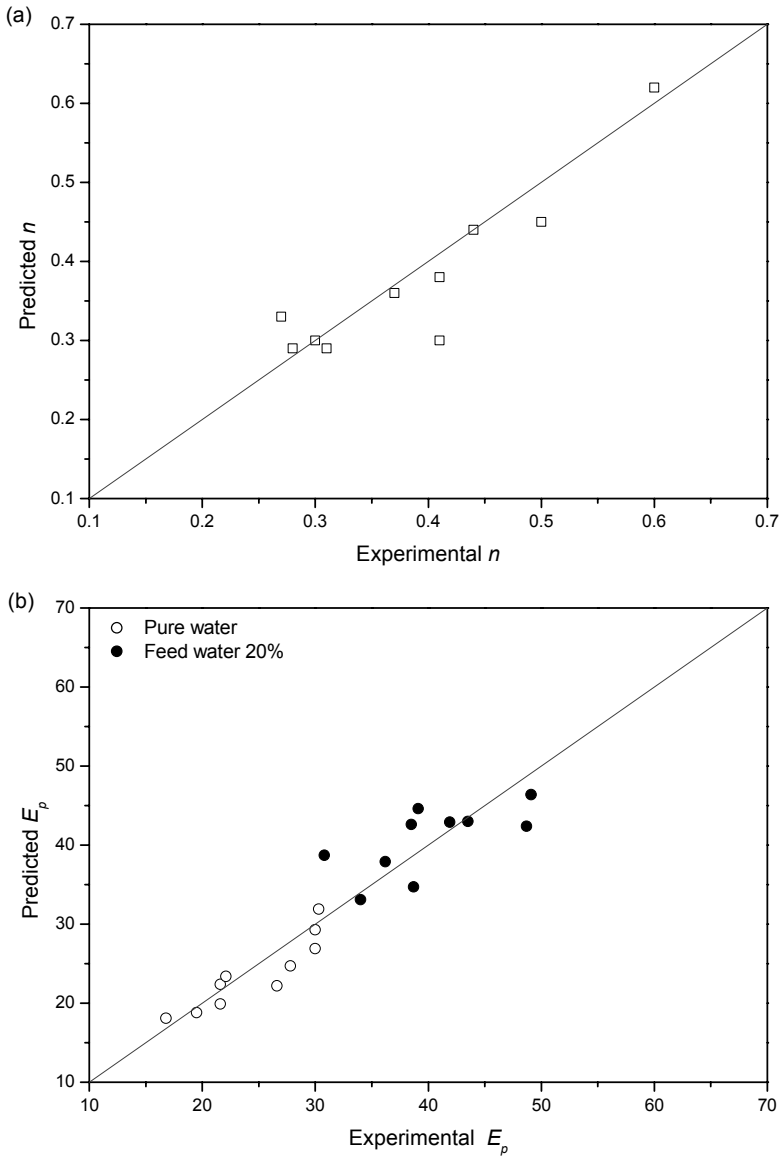

Figure 7.9 Comparison of concentration coefficients and permeation activation energies from predictions with those from experimental data

7.3.4.3 Effects of the Operating Temperature

As shown in Figure 7.8 (b), permeate water contents decrease at a higher temperature when the feed concentration is kept unchanged. 6FDA-6ODA-4BABP has the best pervaporation selectivity in dehydration of isopropanol. The permeation activation energies were calculated for water permeation and dehydration of isopropanol, as listed in Table 7.7.

The moiety contribution factors were calculated from least squares regression of the permeation activation energies for 6FDA-based polyimide membranes using the linear moiety contribution method (shown in Appendix E), and results are listed in Table 7.8. Comparison is made in Figure 7.9 (b) between the activation energies from Arrhenius equation and those recalculated from the linear moiety contribution method.

With regard to the 6FDA and ODA moieties, activation energies for pure water permeation are lower than those for total flux, while the other moieties act in a completely different way, which is an indication of the hydrophobicity of 6FDA and ODA moieties in the membranes. The negative contributions to activation energies from DDS and BADS moieties possibly benefit from their steric effects. The flexibility of MDA, BABP and DABN moieties, as well as the favorable interactions with water, accounts for the large contribution factors to the activation energies.

7.4 Conclusions

Copolyimides were synthesized from 6FDA and diamine monomers with different structures. The diamine monomers showed different reactivities in polycondensation, and led to great differences in molecular weights of the copolyimides. However, due to the structural similarity, the thermal properties did not show a considerable difference. Good solubility was observed, and the membranes were cast from their THF solutions. 6FDA-6ODA-4DABN showed the best hydrophilicity among the copolyimide membranes from contact angles and surface free energies.

In gas permeation, by employing the linear moiety contribution method to permeance ratios, the contributions of the monomer moieties were obtained. Attributed to steric effects of the sulfonyl groups, DDS and BADS moieties had negative contributions to the selectivities of O_2/N_2, H_2/N_2 and He/N_2. The DABN moiety was found to be favorable for improving the CO_2/N_2 selectivity.

In pervaporation, the linear moiety contribution method was applied to the *concentration coefficients* and activation energies for the permeation flux. DDS and BADS moieties influenced the sorption properties when changing feed concentrations. The interactions between water and the moieties of BABP and DABN contributed to the high activation energies.

Chapter 8

4,4'-(Hexafluoroisopropylidene) Diphthalic Anhydride (6FDA) - 4,4'-Methylenedianiline (MDA) - Based Polyimide Membranes for Gas Separation and Pervaporation*

6FDA-MDA-based polyimides were synthesized from one-step polymerization, and were characterized with GPC, FTIR, NMR, DSC and TGA. Dense membranes were prepared from their THF solutions. Surface free energies and interfacial free energies were calculated from contact angles, and the membrane hydrophilicity was compared. Gas permeation was conducted with N_2, O_2, H_2, He and CO_2, and gas separation properties were investigated using the linear moiety contribution method on permeance ratios. Pervaporation was carried out for dehydration of isopropanol and pure water permeation. The moiety contribution method was applied to the *concentration coefficients* and the activation energies. The contribution factors of the dianhydride and diamine moieties for gas separation and pervaporation were compared based on the steric effects, flexibility and the interactions with penetrants.

8.1 Introduction

To study the effect of the dianhydride and diamine moieties on gas separation and pervaporation properties, 6FDA-MDA-based copolyimides were synthesized from 6FDA and MDA, the dianhydrides (BTDA, NTDA and BPADA) and the diamines (DBSA and DAPy) as the third monomer. The polyimides were characterized, and the separation properties of the membranes were investigated using the linear moiety contribution method.

8.2 Experimental

2,2-Bis[4-(3,4-dicarboxyphenoxy) phenyl]propane dianhydride (BPADA), 3,3',4,4'-benzophenon-tetracarboxylic anhydride (BTDA, 96 %) and naphthalene-1,4,5,8-tetracarboxylic dianhydride

* Portions of this work will be published in *Macromolecular Chemistry and Physics*, available online on Oct. 2, 2007. DOI: 10.1002/macp.200700328

(NTDA, > 93 %) were provided by Polysciences, Acros Organics and TCI, respectively. All other materials are the same as listed in 6.2.1 and 7.2.

Diamine and dianhydride monomers used in this work are listed in Figure 8.1. Polyimides (shown in Table 8.1) were synthesized from one-step polymerization, and procedures are outlined in 6.2.2. Polyimide membranes (15–30 μm thick) were prepared from 5 w/v % polyimides THF solutions.

All experiments, unless stated otherwise, were carried out as described in 6.2.

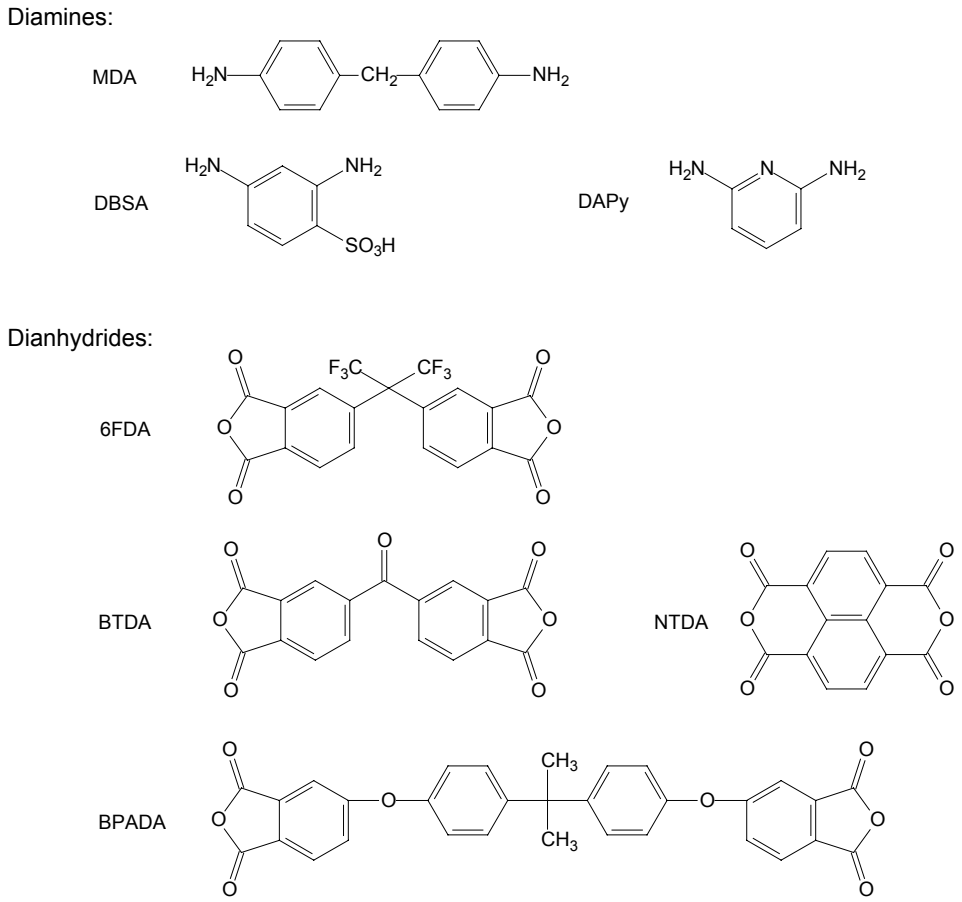

Figure 8.1 Monomers of 6FDA-MDA-based polyimides

Table 8.1 Polyimides and molecular weights

Polyimides	Monomers	Molar ratio	$\overline{M}_n$	$\overline{M}_w$	$\overline{M}_w / \overline{M}_n$	$\overline{DP}$
6FDA-MDA	6FDA : MDA	= 1 : 1	53630	73030	1.362	88
6FDA-8MDA-2DBSA	6FDA : MDA : DBSA	= 1 : 0.8 : 0.2	142100	168100	1.183	235
6FDA-8MDA-2DAPy	6FDA : MDA : DAPy	= 1 : 0.8 : 0.2	71720	90920	1.268	122
6FDA-10MDA-1BTDA	6FDA : MDA : BTDA	= 0.9 : 1 : 0.1	85840	124300	1.448	144
6FDA-10MDA-1NTDA	6FDA : MDA : NTDA	= 0.9 : 1 : 0.1	162800	207900	1.277	277
6FDA-10MDA-1BPADA	6FDA : MDA : BPADA	= 0.9 : 1 : 0.1	48080	59830	1.244	78

8.3 Results and Discussion

8.3.1 Polymerization and Polymers

The one-step polymerization method is limited by the solubility of the products. Polyimides with a rigid structure, such as the BTDA moiety, may coagulate or precipitate from the reaction solution. As a result, only low molecular weight polymers can be obtained. Table 8.1 shows 6FDA-MDA-based polyimides and their molecular weights. The molecular weights vary in a wide range, but the small values of $\overline{M}_w / \overline{M}_n$ obtained from GPC are believed to result from the fractionation effect of the ethanol during the extraction of *m*-cresol.

The electron affinity of dianhydrides and the basicity of diamines also have significant influence on the molecular weights. The basicity of diamines can be compared with the charges on the N-atom of the $–NH_2$ groups. Wang-Ford Charges on the N-atoms were obtained from MOPAC and are shown in such an order: MDA (–0.926) > *p*- DBSA (–0.824) > DAPy (–0.760) > *o*- DBSA (–0.681). The electron affinity of the dianhydrides depends on their chemical structures: BTDA (1.55 eV) > BPADA (1.12 eV) [Bessonov *et al.* 1987]. The electron affinity decreases with electron donor (e.g. the ether bond in BPADA), and therefore, a relationship can be found for the electron affinity of the dianhydrides: NTDA > BPADA. Thus, taking into account of the basicity of the diamines and the electron affinity of the dianhydrides, it is reasonable to anticipate the lowest molecular weight for the copolyimide with BPADA moieties.

In the FTIR spectra, at ~3490 cm^{-1}, a very weak absorption peak is observed, which is likely to be attributed to the asymmetrical stretching vibration of amino groups, because the polyimides with low molecular weights bear amino groups as end groups of the main chains. At ~3040 cm^{-1}, the absorption of aromatic C–H bending vibration can be found [Silverstein *et al.* 1997]. Figure 8.2 gives a close view of the FTIR spectra in the range of 1950–600 cm^{-1}. The characteristic absorption bands of the imide rings occur at 1784 cm^{-1} (C=O asymmetrical stretching, Imide I band), 1726 cm^{-1} (C=O symmetrical stretching, imide II band), 1103 cm^{-1} (imide III band), and 722 cm^{-1} (imide ring bending, imide IV band), and 1376 cm^{-1} (C–N stretching) [Dunson 2000; Pramoda *et al.* 2002; Sroog *et al.* 1965]. The absorption peaks of skeletal stretching of aromatic rings appear at ~1600 and ~1500 cm^{-1}. Bending vibration of $–CH_2$ produces absorption at about 1435 cm^{-1}, and symmetrical stretching of $–CF_3$ shows a weak peak at 1298 cm^{-1} [Nakanishi and Solomon 1977]. The peak at 1255 cm^{-1} is probably due to the amide C–N stretching mixed with N–H bending vibration (amide III band)

[Nakanishi and Solomon 1977], and these amide groups in polyimide chains result from the incomplete imidization reactions. Detailed FTIR data are shown in Appendix A.

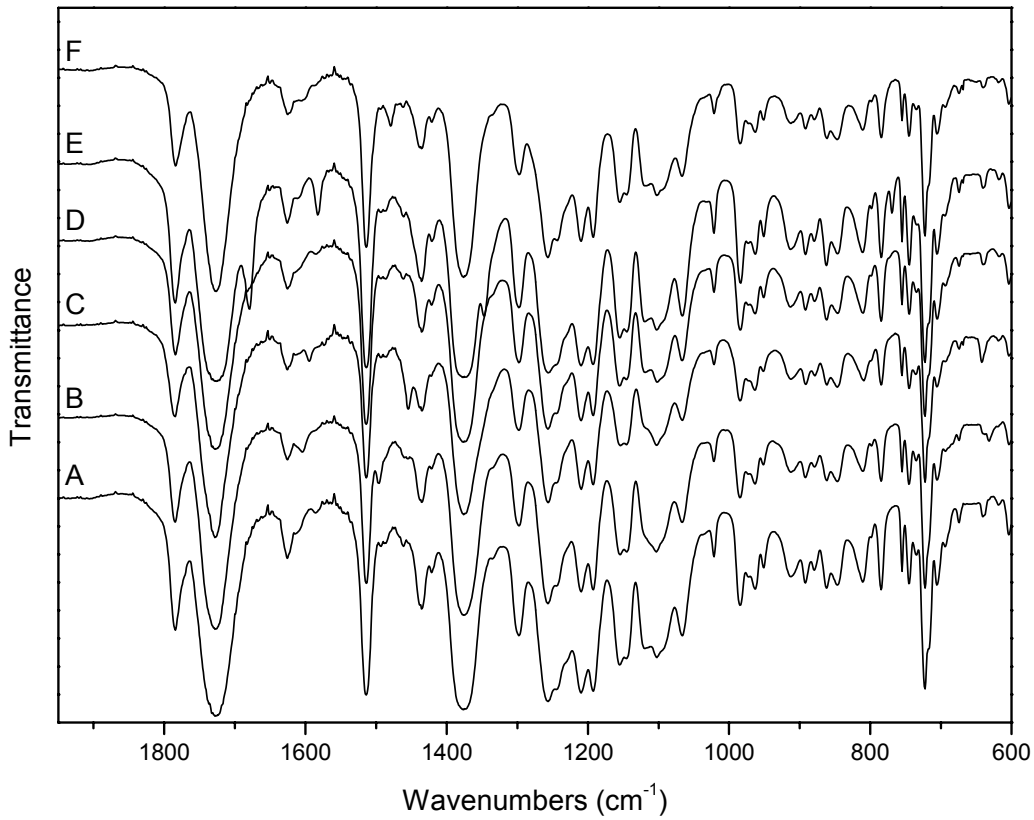

Figure 8.2 FTIR spectra of polyimides

A: 6FDA-MDA, B: 6FDA-8MDA-2DBSA, C: 6FDA-8MDA-2DAPy,
D: 6FDA-10MDA-1BTDA, E: 6FDA-10MDA-1NTDA, F: 6FDA-10MDA-1BPADA

In ^{1}H NMR spectra of the polyimides, the protons in $–CH_2$ groups of the MDA moieties have a chemical shift of 4.09 ppm. The $–CH_3$ groups of BPADA moieties show a peak at 1.74 ppm in the NMR spectrum of 6FDA-10MDA-1BPADA. Figure 8.3 shows the ^{1}H NMR spectra (9.1–6.9 ppm) of the polyimides. The resonance peaks of protons in MDA moieties occur at 7.83 and 7.48 ppm, and the peaks of protons in 6FDA moieties appear at 8.13–8.01 ppm (4H) and 8.04–8.01 ppm (2H). The protons in DBSA moieties have chemical shifts of 8.51 and 8.1–8.0 ppm as shown in the spectrum of 6FDA-8MDA-2DBSA, while the peaks at ~8.16 and ~7.23 ppm are assigned to the protons of DAPy moieties in 6FDA-8MDA-2DAPy. For 6FDA-10MDA-1BTDA, the chemical shifts of protons on

BTDA moieties are 8.48, 8.38, and ~8.18 ppm, respectively. In the NTDA moiety, only one type of protons exists, and the resonance peak is located at 8.93 ppm in the NMR spectrum of 6FDA-10MDA-1NTDA. Except the $-CH_3$ groups in BPADA moieties, there are another 5 types of protons in the phenyl rings. As seen in the ^1H NMR spectrum of 6FDA-10MDA-1BPADA, the protons on the phenyl ring of the BPA structure have chemical shifts of 7.44 and 7.27 ppm, while the other 3 protons adjacent to the imide ring show peaks at 7.65, 7.40 and 7.94 ppm, respectively. Details of the NMR data can be found in Appendix A.

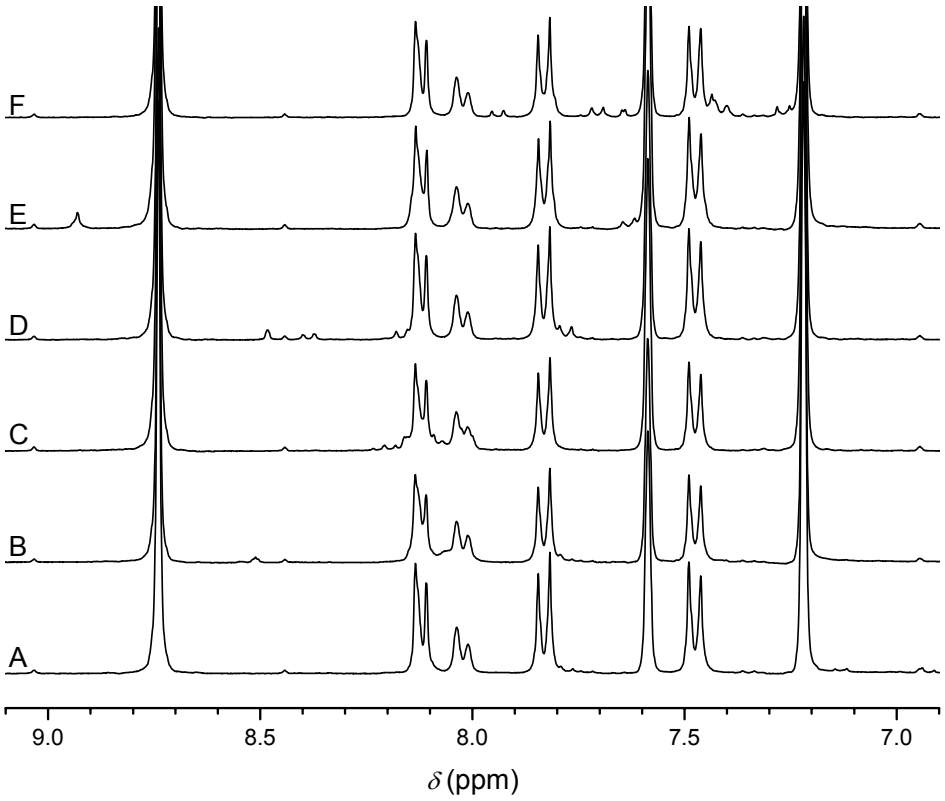

Figure 8.3 ^1H NMR spectra of polyimides

A: 6FDA-MDA, B: 6FDA-8MDA-2DBSA, C: 6FDA-8MDA-2DAPy,
D: 6FDA-10MDA-1BTDA, E: 6FDA-10MDA-1NTDA, F: 6FDA-10MDA-1BPADA

8.3.2 Properties of Polyimides

8.3.2.1 Solubility

All polyimides are readily soluble in THF and pyridine, and they are soluble in chloroform, DMAc,

DMF, NMP and DMSO. Isopropanol, toluene and cyclohexane are not solvents for the polyimides. 6FDA-9MDA-1NTDA is partially soluble in acetone, while the others can dissolve in acetone. When casting membranes for separation processes, THF was used as the solvent.

8.3.2.2 Thermal Properties

DSC and TGA (as shown in Figure 8.4) were performed at a heating rate of 10 °C/min in helium. The characteristic data are listed in Table 8.2.

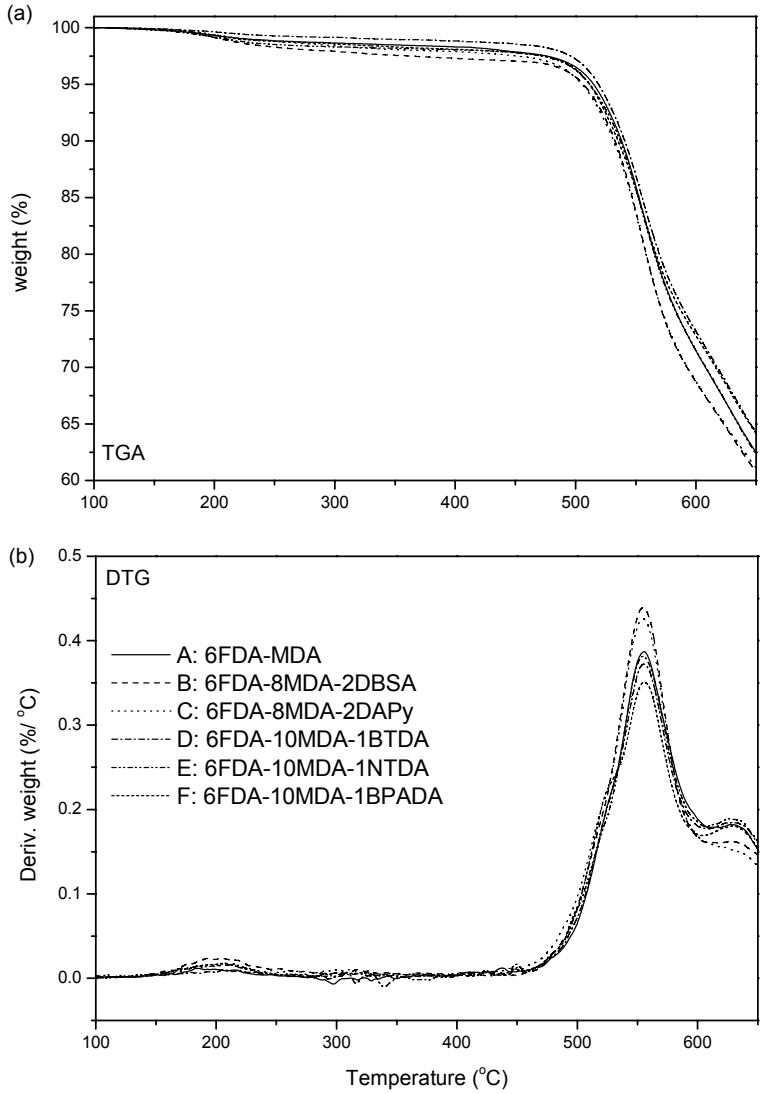

Figure 8.4 TGA and DTG curves of polyimides

Table 8.2 Characteristic temperatures from DSC, TGA and DTG

Polyimides	DSC [a] (°C)	T_d 5 % wt. loss (°C)	T_d 10 % wt. loss (°C)	TGA onset [b] (°C)	DTG [c] (°C)
6FDA-MDA	292	515	538	517	556
6FDA-8MDA-2DBSA	291	507	533	518	555
6FDA-8MDA-2DAPy	292	506	532	515	555
6FDA-10MDA-1BTDA	290	519	541	518	555
6FDA-10MDA-1NTDA	297	512	537	515	555
6FDA-10MDA-1BPADA	286	512	535	513	556

[a] DSC operating conditions: 10 °C/min in helium. Glass transition temperatures were not distinctly decided from the first and second runs of DSC. The onset temperatures were used as an estimation of their glass transition temperatures.

[b] TGA operating conditions: 10 °C/min in helium.

[c] These temperatures were obtained from DTG peak temperatures.

Introduction of a third monomer into the polymer main chain destroys the structural uniformity, possibly leading to a decrease in the thermal stability, However, if the third monomer has a higher thermal stability, it will improve the thermal stability of the polymer. The BPADA moiety contains an alkyl bond, and the degradation temperature (T_d onset 513 °C) of 6FDA-10MDA-1BPADA appears to be lower. The degradation of polyimides occurs at a very high temperature (> 500 °C). T_d 10 % is about 25 °C higher than T_d 5 %, and all the characteristic decomposition temperatures (DTG peak temperatures) are about 555 °C.

8.3.2.3 Surface Free Energies

Contact angles of various liquids on the polyimide membranes are listed in Table 8.3. The surface free energies and the water-membrane interfacial free energies ΔG_{sw}^{IF} were calculated, and are presented in Table 8.4.

The LW components γ_s^{LW} of surface free energies are in the range of 40–27 mJ/m^2, and they are much larger than the AB components γ_s^{AB}. The electron-donicity behavior can be seen from the two parameters of γ_s^{AB}: Lewis base (electron-donor) parameters γ^- are much larger than Lewis acid (electron-acceptor) parameters γ^+. A large value of γ^- is due to the hydrophilicity of the surface [Van Oss and Giese 1995]. The residual amino groups in polyimide are a contribution to the electron-donicity of the AB components γ_s^{AB}. 6FDA-10MDA-1BPADA that has the smallest contact angle

with water shows the largest value of γ^-. Van Oss and Giese [1995] pointed out that a negative value of ΔG_{sw}^{IF} represents hydrophobicity of the surface. Therefore, it can be concluded from the ΔG_{sw}^{IF} data: 6FDA-10MDA-1BPADA shows more hydrophilicity, and 6FDA-10MDA-1BTDA appears to be more hydrophobic.

Table 8.3 Contact angles of liquids on polyimide membranes at room temperature

Membranes	Water (°)	Glycerol (°)	Formamide (°)	Diiodomethane (°)
6FDA-MDA	81.5 ± 2.4	67.6 ± 1.1	54.4 ± 1.0	35.6 ± 0.8
6FDA-8MDA-2DBSA	78.1 ± 3.1	59.0 ± 2.2	43.2 ± 2.3	27.5 ± 0.7
6FDA-8ODA-2DAPy	80.2 ± 1.9	68.5 ± 1.4	50.9 ± 0.7	39.4 ± 1.0
6FDA-10MDA-1BTDA	81.4 ± 0.4	65.8 ± 1.6	54.1 ± 1.3	23.4 ± 0.8
6FDA-10MDA-1NTDA	80.6 ± 1.4	54.8 ± 1.0	52.0 ± 0.7	28.2 ± 1.7
6FDA-10MDA-1BPADA	78.5 ± 0.8	70.6 ± 1.5	56.8 ± 0.3	33.1 ± 0.7

All results are given as means with the 95 % confidence intervals.

Table 8.4 Surface free energy components (in mJ/m^2) of liquids used in measurement of contact angles at room temperature

Membranes	γ_s^{LW}	γ_s^+	γ_s^-	γ_s^{AB}	γ_s	ΔG_{sw}
6FDA-MDA	41.75	0.1483	3.66	1.47	43.22	–64.96
6FDA-8MDA-2DBSA	45.22	0.7063	2.67	2.75	47.97	–65.97
6FDA-8ODA-2DAPy	39.91	0.2815	4.22	2.18	42.09	–59.60
6FDA-10MDA-1BTDA	46.71	0.0295	3.24	0.62	47.33	–72.81
6FDA-10MDA-1NTDA	44.95	0.7531	1.79	2.32	47.27	–70.40
6FDA-10MDA-1BPADA	42.89	0.0001	6.42	0.05	42.94	–57.87

8.3.3 Gas Permeation Properties

Pure gas permeation was tested at room temperature, and gas permeances are listed in Table 8.5 together with the permeance ratios calculated from the average permeances. Figure 8.5 shows the permeance ratios calculated separately from gas permeances at difference pressures. Since these permeance ratios are shown to be independent from feed pressures, the average permeance ratios are utilized to represent the membrane selectivities.

Contributions of monomer moieties to the membrane selectivities were calculated based on the linear moiety contribution method (calculations shown in Appendix D), and the results are listed in Table 8.6. It should be noted that the data for BTDA, NTDA and BPADA moieties were calculated directly from the contribution factors of 6FDA and MDA, and may contain errors.

Except DAPy, the monomer moieties contribute positively to α_{CO_2/N_2}. The size of CO_2 molecules is close to that of O_2, which indicates similar effects of the penetrant mobility, but CO_2 has much higher solubility than O_2 because of the huge difference between their critical temperatures. Therefore, the difference between the contribution factors for α_{O_2/N_2} and α_{CO_2/N_2} can be used to compare the contributions from the solubility of CO_2. The following sequence can be found for the moiety contributions to the solubility of CO_2: BPADA > NTDA > BTDA > 6FDA > MDA > DBSA > DAPy. The acidic group $-SO_3H$ in DBSA and the lone electron pair in DAPy are supposed to be the possible factors that cause the low solubility of CO_2 [Lin and Freeman, 2005].

6FDA, MDA and DBSA moieties contribute positively to α_{O_2/N_2}, α_{H_2/N_2}, and α_{He/N_2}, because 6FDA and MDA moieties benefit from the flexible bonds between the phenyl groups, and the DBSA moiety benefits from the bulky sulfonic acid group. The DAPy moiety has a smaller molecular size and a more rigid structure that only decrease the mobility of O_2 (possibly N_2 as well), but the mobility of H_2 and He is not greatly affected, because their sizes are much smaller than O_2. In addition, the local concentration of 6FDA moieties is also enhanced when DAPy moieties are introduced into the main chain. The rigid structures of BTDA and NTDA moieties lead to the negative contributions to α_{O_2/N_2}, α_{H_2/N_2}, and α_{He/N_2}. The flexible structure of the BPADA moiety has a positive effect on the selectivities, but the BPADA moiety also exerts a negative influence since the large molecular weight also decrease the local concentrations of 6FDA and MDA moieties.

8.3.4 Pervaporation Properties

Pervaporation dehydration of isopropanol was carried out at 60 °C with different feed water contents, and the permeation flux and the permeate water content are shown in Figure 8.6. Temperature effects on the permeation flux and the permeate water content were studied in pervaporation with ~20 wt. % water in the feed solutions, and results are presented in Figure 8.7.

Table 8.5 Gas separation properties of polyimide membranes at room temperature

Membranes	Permeances (GPU) [a]					Permeance ratios			
	J_{N_2}	J_{O_2}	J_{H2}	J_{He}	J_{CO_2}	α_{O_2/N_2}	α_{H_2/N_2}	α_{He/N_2}	α_{CO_2/N_2}
6FDA-MDA	0.02	0.13	1.22	0.99	1.18	5.1	49.4	40.1	48.0
6FDA-8MDA-2DBSA	0.06	0.33	2.38	2.62	2.12	5.2	37.5	41.2	33.3
6FDA-8MDA-2DAPy	0.04	0.16	1.79	1.38	1.58	4.4	48.9	37.7	43.2
6FDA-10MDA-1BTDA	0.01	0.04	0.17	0.17	0.48	4.2	17.1	17.7	49.3
6FDA-10MDA-1NTDA	0.08	0.30	2.81	2.04	4.21	3.9	36.7	26.6	54.9
6FDA-10MDA-1BPADA	0.05	0.22	2.15	1.64	3.36	4.8	46.3	35.5	72.5

[a] Average data of gas permeances at 0.14, 0.21, 0.28 and 0.35 MPa.

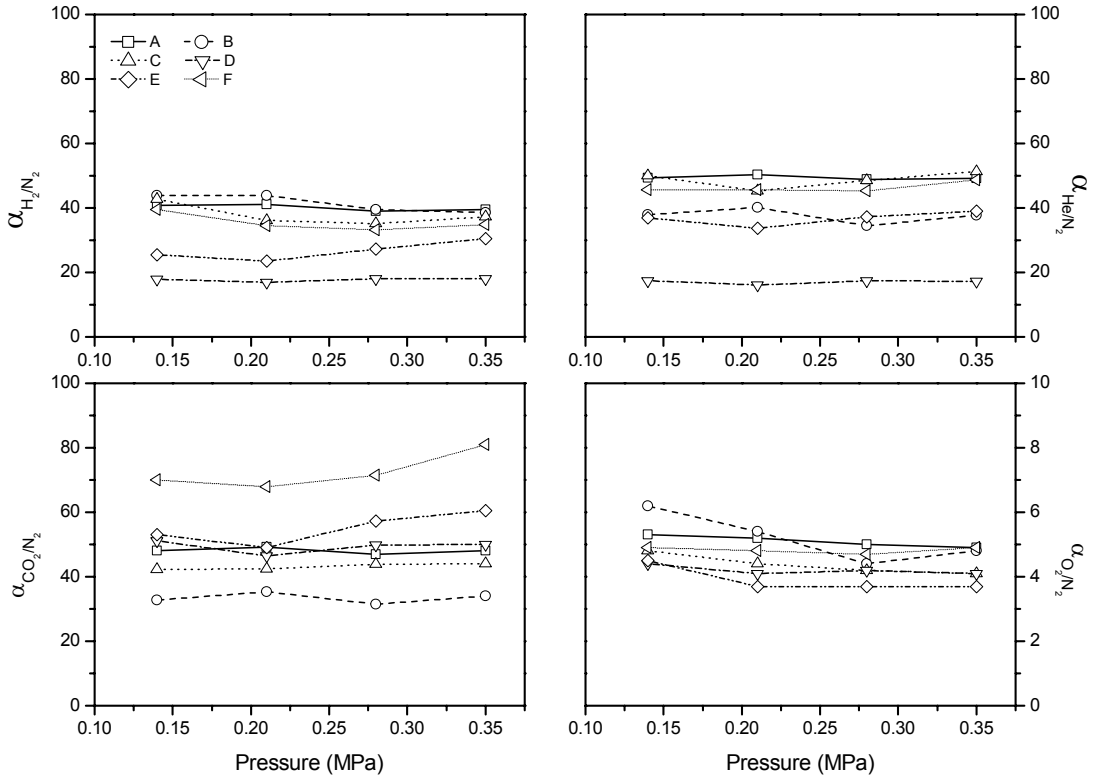

Figure 8.5 Permeance ratios of gas pairs for membranes at different pressures

A: 6FDA-MDA, B: 6FDA-8MDA-2DBSA, C: 6FDA-8MDA-2DAPy,
D: 6FDA-10MDA-1BTDA, E: 6FDA-10MDA-1NTDA, F: 6FDA-10MDA-1BPADA

Table 8.6 Contributions of monomer moieties to permeance ratios

Moieties of monomers	α_{O_2/N_2}	α_{H_2/N_2}	α_{He/N_2}	α_{CO_2/N_2}
6FDA	3.6	29.4	36.4	33.8
MDA	1.7	9.7	5.1	12.1
DBSA	5.9	79.5	101.2	13.2
DAPy	–2.9	20.7	58.8	–28.4
BTDA	–6.9	–184.1	–207.4	67.4
NTDA	–9.9	–95.1	–11.4	123.4
BPADA	–0.9	–6.1	84.6	299.4

Values were calculated from 6FDA-based polyimides using least squares regression method. Calculations should be based on the overall molar ratio of dianhydrides/diamines of 1:1.

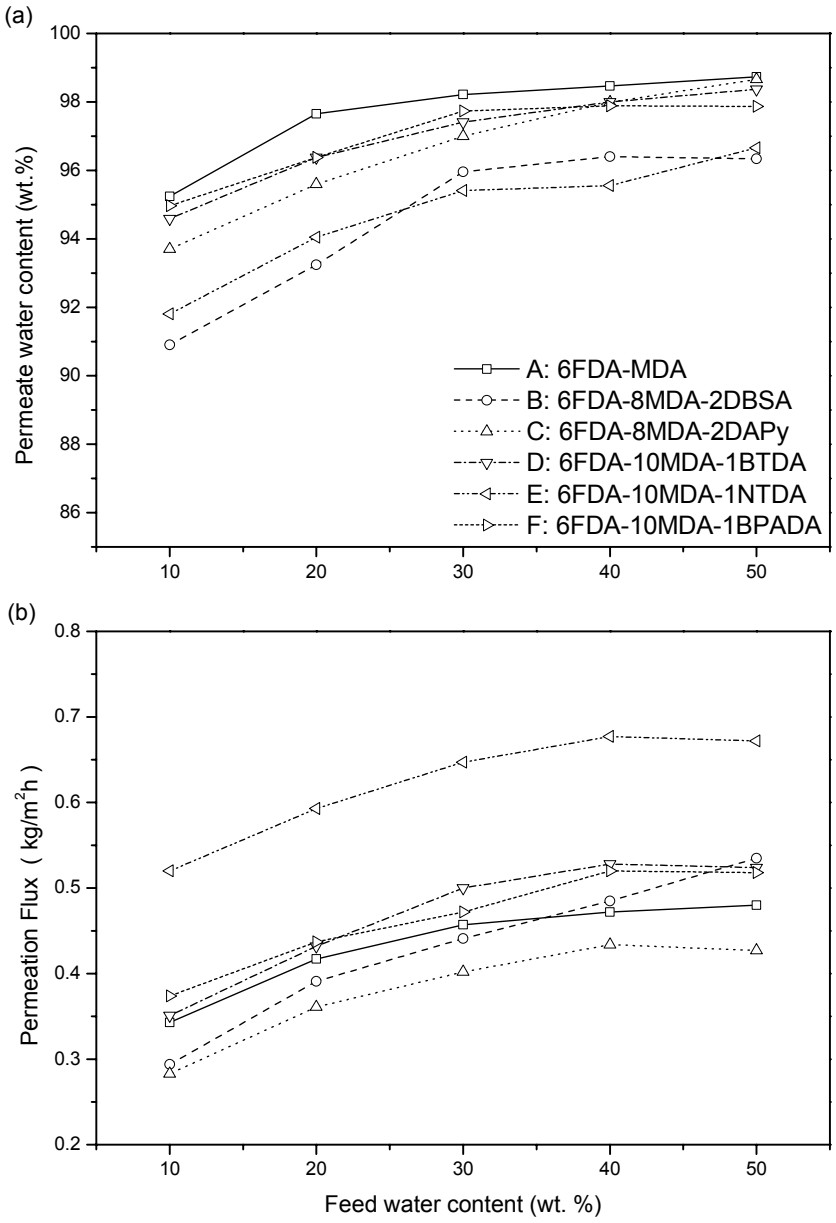

Figure 8.6 Permeate water contents in pervaporation dehydration of isopropanol with different feed water contents at 60 °C

8.3.4.1 Monomers vs. Pervaporation Selectivities

Figure 8.6 (a) shows that a higher permeate water content can be achieved when increasing the water content in the feed. Hydrogen bonding exists between the acyl groups of the imide rings and water,

and it is much stronger than the intermolecular van der Waals force between isopropanol and the polymer matrix. Therefore, better sorption can be achieved when the feed water content is increased, and the permeability of water is improved. Comparing the permeate water contents, it can be found that introduction of the third monomers into the 6FDA-MDA matrix leads to more changes in diffusivity properties than in the sorption of penetrants, when changing the water content of the feed. 6FDA-8MDA-2DBSA shows a lower selectivity than other membranes, because the sulfonic acid group produces more space for isopropanol to permeate, though the DBSA moiety is also favorable for improving the sorption of water. The smaller sizes of DBSA and DAPy moieties compared with the MDA moiety also increase the local concentration of the 6FDA moiety, hence decreasing the water sorption properties in polymer matrices. However, no bulky side groups are attached to the DAPy moiety, and thus a higher selectivity is observed for 6FDA-8MDA-2DAPy than 6FDA-8MDA-2DBSA. The rigid structures of BTDA and NTDA moieties cause a decrease in the mobility of polymer chains, so the lower selectivity is observed, even with less $–CF_3$ groups in the polymers. The contribution of the acyl group in the BTDA moiety to the sorption of water can be used to interpret the difference in the selectivities of 6FDA-10MDA-1BTDA and 6FDA-10MDA-1NTDA. In spite of the adverse effect on sorption, the flexibility and the large size of the BPADA moiety offer a good selectivity towards water/isopropanol to 6FDA-10MDA-1BPADA.

It can be observed in Figure 8.7 (a), with the same water content in the feed, permeate water contents deceased a little when the operating temperature was increased. In addition to the higher mobility of polymer chains, the possible changes in sorption properties can cause changes in selectivity at a higher operating temperature. The permeate with a low water content was produced by 6FDA-8MDA-2DAPy at 30 °C, which is attributed to the low mobility of the polymer chains and the weak sorption of water in the matrix.

8.3.4.2 Effects of the Feed Concentration on Total Flux

Figure 8.6 (b) shows the permeation flux of the pervaporation membranes with different water contents in the feed. The DBSA moiety is favorable for promoting the sorption of water and the diffusion of the penetrants, so the flux keeps increasing when increasing the water contents in the feed. However, the other membranes show the maximum flux when the feed water content is 40 wt. %, possibly due to the saturation state reached for the sorption of water within the polymer matrices with a high water content in the feed.

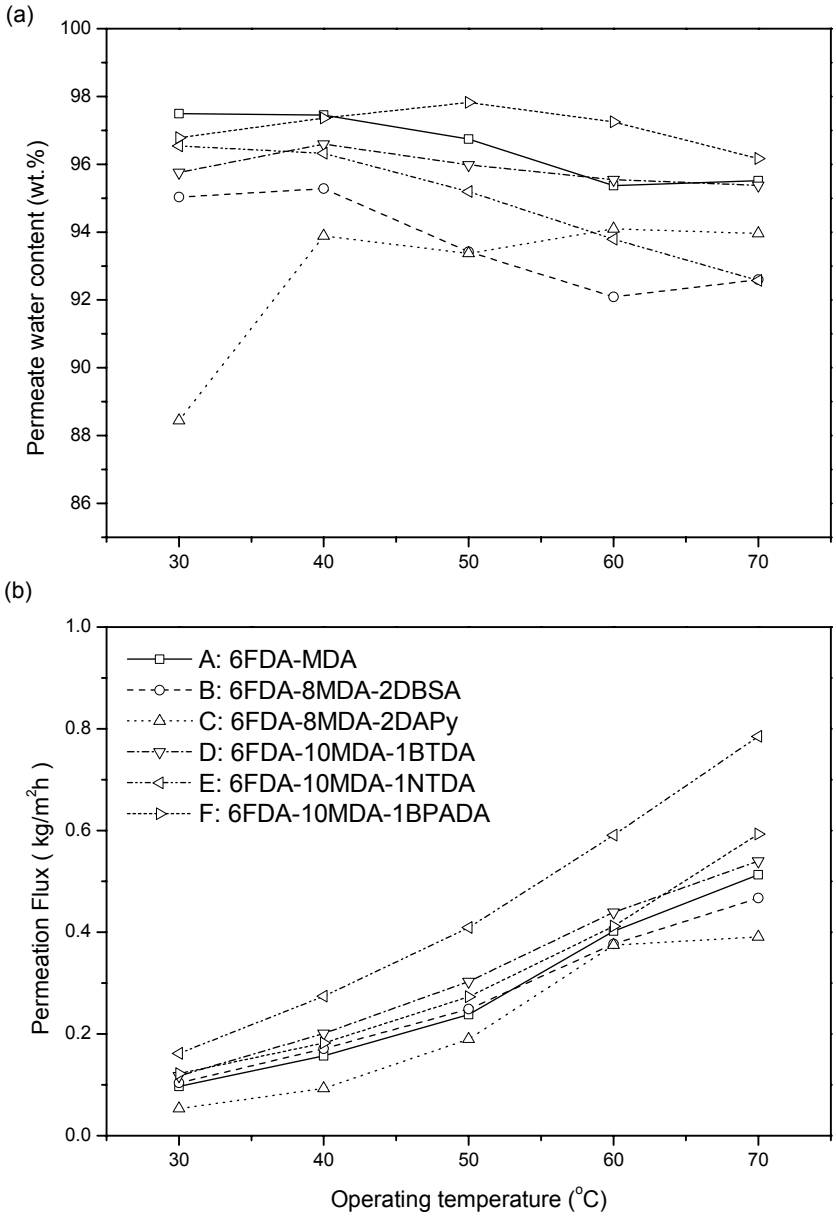

Figure 8.7 Permeate water contents in pervaporation dehydration of isopropanol with the water content of ~20 wt. %

The *n* values (defined as the *concentration coefficient*) were obtained from curve fitting, and are listed in Table 8.7. The differences between the *n* values for different membranes reflect the effects of the third monomers of the copolyimides.

The linear moiety contribution method was applied to obtain the moiety contribution factors for the *concentration coefficients* (listed in Table 8.8). Calculation details can be found in Appendix E.

Table 8.7 Concentration coefficients and permeation activation energies for pervaporation

Membranes	n [a]	E_p (pure water) [b] (kJ/mol)	E_p (total flux) [c] (kJ/mol)
6FDA-MDA	0.27	36.0 ± 2.3	39.8 ± 1.7
6FDA-8MDA-2DBSA	0.33	35.6 ± 1.5	33.7 ± 2.1
6FDA-8MDA-2DAPy	0.34	62.7 ± 9.5	44.1 ± 3.8
6FDA-10MDA-1BTDA	0.28	29.2 ± 0.9	32.8 ± 2.3
6FDA-10MDA-1NTDA	0.22	34.9 ± 1.2	34.2 ± 1.5
6FDA-10MDA-1BPADA	0.25	32.3 ± 0.8	34.5 ± 0.8

[a] Pervaporation dehydration of isopropanol at 60 °C. All values were obtained from curve fitting, r^2=0.95–0.99.

[b] Apparent activation energies for pure water permeation.

[c] Apparent activation energies for total permeation flux with feed water content ~20 wt. %.

Table 8.8 Moiety contributions to concentration coefficients and permeation activation energies

Moieties of monomers	n	E_p (pure water) (kJ/mol)	E_p (total flux) (kJ/mol)
6FDA	0.25	24.1	35.6
MDA	0.07	16.9	6.3
DBSA	0.37	33.0	0.7
DAPy	0.18	98.0	27.0
BTDA [a]	–0.18	–94.6	–55.8
NTDA [a]	–0.78	–37.6	–41.8
BPADA [a]	–0.48	–63.6	–38.8

[a] Contribution factors for BTDA, NTDA and BPADA moieties were obtained based on those for 6FDA and MDA moieties, and may contain some errors.

The hydrophilicity and the bulky side group of the DBSA moiety render a high permeation flux to 6FDA-8MDA-2DBSA even with a low water content in the feed, so that the increase in flux is not significant at higher feed water contents. As a result, the DBSA moiety has a large contribution to the n value. The DAPy moiety that is smaller in size decreases the free volume for sorption and diffusion, and therefore, the feed water content has a weak influence on flux. Thus the DAPy moiety has a

greater contribution to the *n* value of 6FDA-8MDA-2DAPy. Introduction of the dianhydride monomers BTDA, NTDA and BPADA weakens the influence of 6FDA moieties, resulting in the negative contributions to the *n* values, and the order BTDA > BPADA > NTDA also reflects their contributions to selectivity as previously discussed.

8.3.4.3 Effects of the Operating Temperature on Permeation Flux

At elevated operating temperatures, the permeation flux increased in pervaporation dehydration of isopropanol, as shown in Figure 8.7 (b). Such a trend was also observed for pure water permeation. The activation energies for water permeation and dehydration of isopropanol with feed water content of 20 wt. % were determined, and results are listed in Table 8.7.

By applying the linear moiety contribution method to the activation energies (shown in Appendix E), the moiety contribution factors for activation energies can also be obtained. The contribution factors for BTDA, NTDA and BPADA moieties were calculated directly from those for 6FDA and MDA moieties, since the least squares regression failed due to lack of data. Table 8.8 exhibits the calculated contribution factors for monomer moieties.

The DAPy moiety can narrow the transport path in the polymer matrix for the penetrants, which causes a decrease in the diffusivity of the penetrants. By increasing the operating temperature, the wider path will be formed and the higher flux can be observed. As a result, the DAPy moiety shows greater contributions to the activation energies for water permeation and dehydration of isopropanol. The greater contribution to the activation energy for water permeation can also be observed for the DBSA moiety, because the diffusion of water is facilitated by the larger transient gaps formed at a higher temperature. Isopropanol, as a penetrant and a non-solvent, has a negative effect on the mobility of the polymer chains, and therefore, smaller contributions to the activation energies are found for MDA, DBSA and DAPy moieties. The apparent permeation activation energy is composed of the activation energy of diffusion and the heat of sorption (which can be positive or negative). The negative contributions from BTDA, NTDA and BPADA moieties mean that the heats of sorption from BTDA, NTDA and BPADA moieties are more controlling. However, BTDA, NTDA and BPADA moieties act differently for the mass transport (diffusion) in the membranes. The mobility of the NTDA moiety is greatly limited by its rigidity, and thus, the diffusion of penetrants is limited. The interactions between BTDA moieties and water as well as the flexibility of BPADA moieties offer a high flux to the membranes containing BTDA and BPADA moieties even at a low temperature. As a result, BTDA and BPADA moieties show negative contributions. Furthermore, if the polymers are

BTDA-based or BPADA-based other than 6FDA-based, *i.e.* 6FDA acts as the third monomer, the moieties of BTDA and BPADA should have positive contributions to flux. More work has been done in Chapter 9 to find the contributions of the BPADA moiety to pervaporation properties.

8.4 Conclusions

6FDA-MDA-based polyimides were synthesized from various diamines and dianhydrides, and were characterized with FTIR, NMR, GPC, DSC and TGA. They were soluble in some organic solvents, and showed very good thermal stabilities. Due to the differences in the electron affinity of dianhydrides and the basicity of diamines, a wide range of molecular weights could be observed.

Interfacial free energies were calculated from surface free energies derived from contact angles. Effects of chemical structures of the dianhydride and diamine moieties on the hydrophilicity of the membranes were discussed. 6FDA-10MDA-1BPADA showed to be more hydrophilic, while 6FDA-10MDA-1BTDA appeared to be more hydrophobic.

Gas separation properties were tested with N_2, O_2, H_2, He and CO_2. The linear moiety contribution method was used to analyze the moiety contributions to gas selectivities. It was shown that transport of CO_2 in polyimide membranes were mainly controlled by its solubility, while the permeation properties of the other gases were greatly influenced by the steric effects and flexibility of the monomer moieties. The moiety contributions to the solubility of CO_2 in polyimides were suggested to be in such a sequence: BPADA > NTDA > BTDA > 6FDA > MDA > DBSA > DAPy.

The linear moiety contribution method was applied to study the effects of the feed concentration and the operating temperature on pervaporation dehydration performances. The differences in diffusion and sorption properties were attributed to the structures of the diamine and dianhydride monomers and the interactions between the penetrants and the polymer matrices. The moiety contributions of the dianhydride monomers showed to be in an order: BTDA > BPADA > NTDA. More work is needed to adjust the contribution factors of the BPADA moiety for pervaporation properties.

Chapter 9

2,2-Bis[4-(3,4-dicarboxyphenoxy) phenyl]propane dianhydride (BPADA) - Based Polyimide Membranes for Pervaporation Dehydration of Isopropanol: Characterization and Comparison with 4,4'-(Hexafluoroisopropylidene) Diphthalic Anhydride (6FDA) - Based Polyimide Membranes

Polyimides were synthesized from one-step polycondensation of BPADA and various diamines, and were characterized with GPC, FTIR, NMR, DSC and TGA. Polyimide membranes were prepared and surface free energies were calculated from contact angles. Pervaporation properties were investigated for dehydration of isopropanol, and comparisons were made between BPADA-based membranes and 6FDA-based membranes. The *concentration coefficients* were calculated to study the effects of the feed concentration on pervaporation properties. The effects of temperature on permeation flux were studied with permeation activation energies for total flux and water flux in the permeates. The moiety contribution factors of the monomer moieties were used to correlate separation properties and the chemical structures of polymers, and reasonable results were obtained for the BPADA moiety.

9.1 Introduction

To determine the contribution factors of the BPADA moiety for pervaporation properties, polyimides were prepared from BPADA and various diamine monomers, and their pervaporation properties were quantitatively compared with 6FDA-based membranes. Based on the moiety contribution factors, the influences of dianhydrides and diamines were discussed in details.

9.2 Experimental

The chemicals used in this work are the same as listed in 6.2.1 and. 8.2. Polyimides (listed in Table 9.1) were synthesized from one-step polymerization (similar procedures have been outlined in 6.2.2) of BPDADA monomers used this work are shown in Figure 9.1.

Table 9.1 Synthesis of BPADA copolyimides and molecular weights

Polyimides	Monomers	Molar ratio	$\overline{M}_n$	$\overline{M}_w$	$\overline{M}_w / \overline{M}_n$	$\overline{DP}$
BPADA-ODA	BPADA : ODA	= 1 : 1	65840	87500	1.33	96
BPADA-8ODA-2DAPy	BPADA: ODA : DAPy	= 1 : 0.8 : 0.2	57990	74960	1.29	87
BPADA-8ODA-2DABA	BPADA : ODA : DABA	= 1 : 0.8 : 0.2	141900	163800	1.15	210
BPADA-8ODA-2DBSA	BPADA : ODA : DBSA	= 1 : 0.8 : 0.2	197900	237500	1.20	290
BPADA-MDA	BPADA : MDA	= 1 : 1	70430	93810	1.33	103
BPADA-8MDA-2DAPy	BPADA : MDA : DAPy	= 1 : 0.8 : 0.2	75840	108900	1.44	114
BPADA-8MDA-2DABA [a]	BPADA : MDA : DABA	= 1 : 0.8 : 0.2	–	–	–	–
BPADA-8MDA-2DBSA [a]	BPADA : MDA : DBSA	= 1 : 0.8 : 0.2	–	–	–	–

[a] Poor mechanical properties and low molecular weights, and no further tests were carried out.

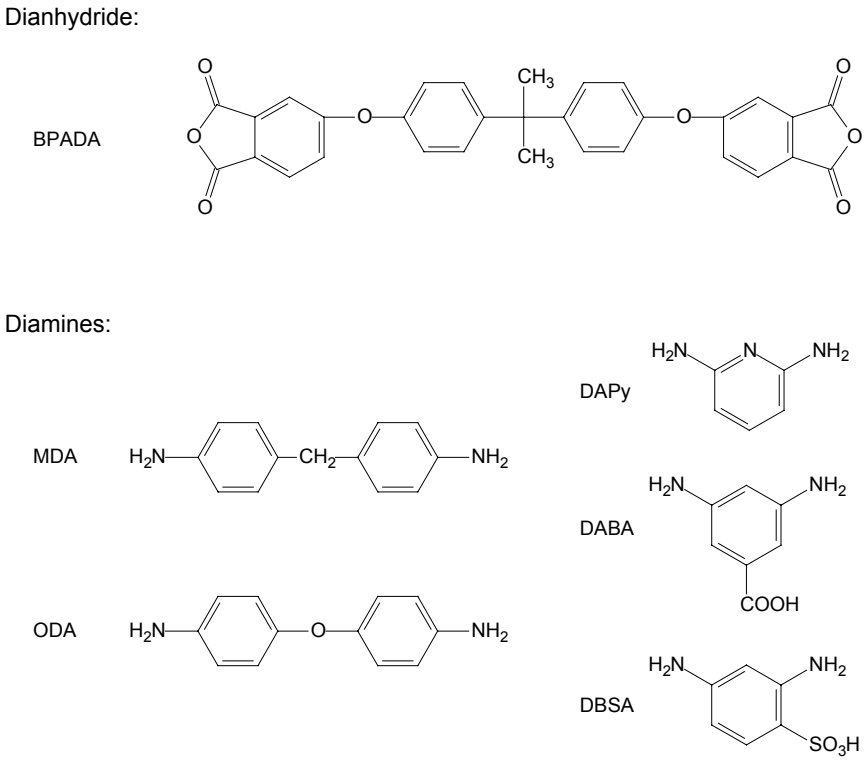

Figure 9.1 Chemical structures of monomers

BPADA-8MDA-2DABA and BPADA-8MDA-2DBSA showed low molecular weights and could not be used for further research as membranes. Polyimide membranes (15–25 μm thick) were prepared from 5 w/v % polyimides THF solutions as described in 6.2.4. GPC, FTIR, GPC and the contact angle measurements were carried out following the procedures described in 6.2.3. DSC was performed from 100 to 350 °C and TGA from 100 to 650 °C both at the heating rate of 10 °C·min^{-1} in a helium atmosphere.

Pervaporation dehydration of isopropanol was carried out to study the temperature and concentration effects on pervaporation properties. Experimental details have been outlined in 6.2.6.

9.3 Results and Discussion

9.3.1 BPADA-Based Polyimides

The dianhydride monomer BPADA was used to react with 5 diamine monomers in *m*-cresol at elevated temperatures in the presence of isoquinoline. Among the diamine monomers, DAPy, DABA and DBSA were used as the third monomer to prepare BPADA-ODA-based and BPADA-MDA-based copolymers. It failed to obtain BPADA-8MDA-2DABA and BPADA-8MDA-2DBSA films

with good mechanical properties from this method, and no further tests were conducted for these two polymers. Table 9.1 shows molecular weights of the polyimides, degrees of polymerization and their molecular weight distributions. BPADA-8ODA-2DABA and BPADA-8ODA-2DBSA have higher molecular weights than the others. The molecular weight distributions vary in the range of 1.15–1.44. The small values of $\overline{M}_w / \overline{M}_n$ obtained from GPC result from the fractionation effect of the ethanol during the extraction of *m*-cresol

In the FTIR spectra, the absorption peak of N–H asymmetrical stretching vibration can be observed at 3481 cm^{-1}, and the absorption of aromatic C–H bending vibration occurs at ~3050 cm^{-1} [Silverstein *et al.* 1997]. Figure 9.2 shows the FTIR spectra of the polymers in the range of 1950–600 cm^{-1}. The absorption peaks of skeletal vibrations, involving carbon-carbon stretching within the phenyl ring, appear at ~1600 cm^{-1} and ~1500 cm^{-1}. The in-plane bending of C–H on phenyl rings show a peak at 1014 cm^{-1}. Imide I band at 1776 cm^{-1} (C=O asymmetrical stretching), imide II band at 1722 cm^{-1} (C=O symmetrical stretching), imide III band at ~1078 cm^{-1}, and imide IV band at 744 cm^{-1} (imide ring bending vibration) occur in all FTIR spectra of BPADA-based polyimides [Dunson 2000; Pramoda *et al.* 2002]. The peaks at ~1380 cm^{-1} and ~605 cm^{-1} are also contributed to the imide structure of the polymers [Pramoda *et al.* 2002; Sroog *et al.* 1965]. Asymmetrical stretching vibration of the aryl-aryl ether produces absorption at 1240 cm^{-1}, and the absorption at 1276 cm^{-1} is probably due to stretching vibration of C–N in the unreacted amide groups [Nakanishi and Solomon 1977].

Figure 9.3 shows the ^{1}H NMR of BPADA-MDA. The protons on $–CH_2$ and $–CH_3$ groups have chemical shifts of 4.02 and 1.74 ppm, respectively. $H_{a'}$ and $H_{b'}$ are correlated, and H_d couples with H_e. The two protons H_b and H_g are located on two adjacent C-atoms. H_b is overlapped by H_d and $H_{a'}$. H_a shows no coupling relationship with other protons, and its chemical shift independently appears at 7.64 ppm. Figure 9.4 shows the ^{1}H NMR spectra of all BPADA-based polyimides. Compared with BPADA-MDA (E) and its proton assignment in Figure 9.3, the two protons of DAPy moieties in BPADA-8MDA-2DAPy can be identified to have chemical shifts of 7.80 ppm and ~7.40 ppm. Different from BPADA-MDA, the two protons of the ODA moiety in BPADA-ODA (A) have chemical shifts of 7.75 and ~7.24 ppm, respectively. Accordingly, from the coupling relationships and integration properties, chemical shifts can be assigned to different protons of the DAPy moiety in BPADA-8ODA-2DAPy (B), the protons of the DABA moiety in BPADA-8ODA-2DABA (C) and the protons of the DBSA moiety in BPADA-8ODA-2DBSA (D): ~7.77 and ~7.41 ppm for the DAPy moiety, 8.83 and 8.11 ppm for the DABA moiety, 8.28, 7.84 and 7.81 ppm for the DBSA moiety, respectively.

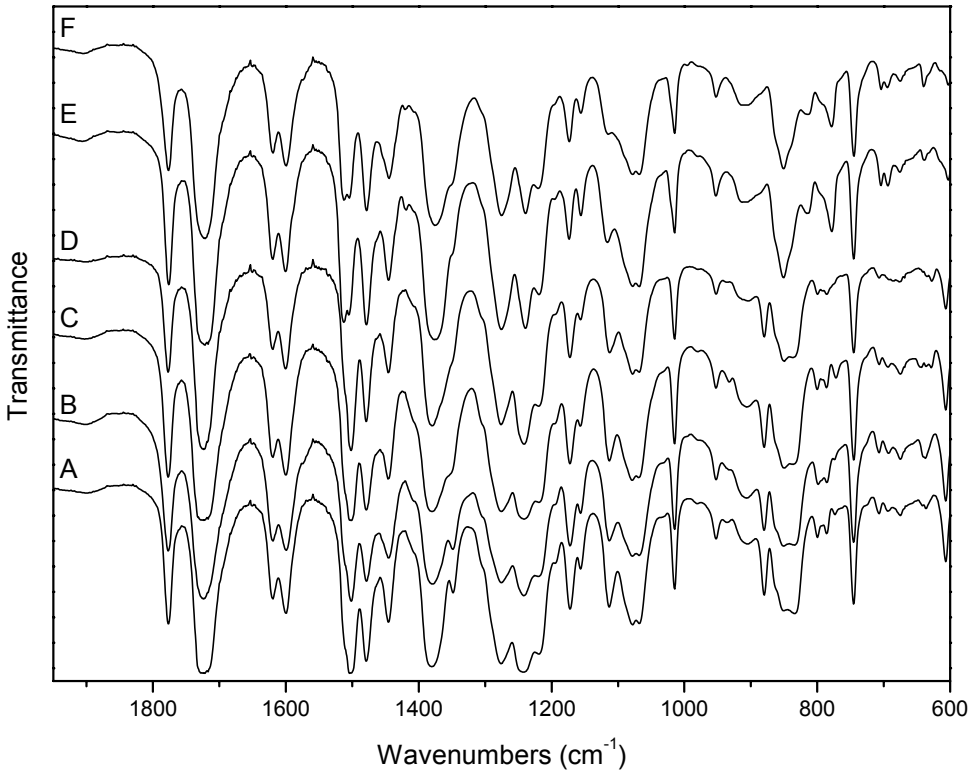

Figure 9.2 FTIR spectra of polyimides

A: BPADA-ODA, B: BPADA-8ODA-2DAPy, C: BPADA-8ODA-2DABA, D: BPADA-8ODA-2DBSA, E: BPADA-MDA, F: BPADA-8MDA-2DAPy

9.3.2 Properties of Polyimides

9.3.2.1 Solubility

All polymers are readily soluble in THF and pyridine, and they can get dissolved in chloroform, DMAc, DMF, NMP and DMSO, but they are insoluble in isopropanol, acetone, toluene and cyclohexane.

9.3.2.2 Thermal Properties

The DSC temperatures in Table 9.2 were read as DSC onset temperatures, and they are used to estimate the glass transition temperatures. According to the known T_gs of BPADA-ODA (215 °C), BPADA-MDA (217 °C) [Li *et al.* 1996], the estimated temperatures from DSC in Table 9.2 are

reasonably comparable. From the DSC onset temperatures, it is found that BPADA-8ODA-2DAPy > BPADA-8ODA-2DABA > BPADA-8ODA-2DBSA > BPADA-ODA. It results in a sequence of the contributions from the diamines to the glass transition temperatures: DAPy > DABA > DBSA > ODA. The flexible ether bonds in ODA moieties can decrease T_g, and thus the lowest onset temperature is observed for BPADA-ODA. The side groups of –COOH in DABA moieties and $-SO_3H$ groups in DBSA moieties change the uniformity and the packing density of polymer matrices, and can slightly lower the T_gs.

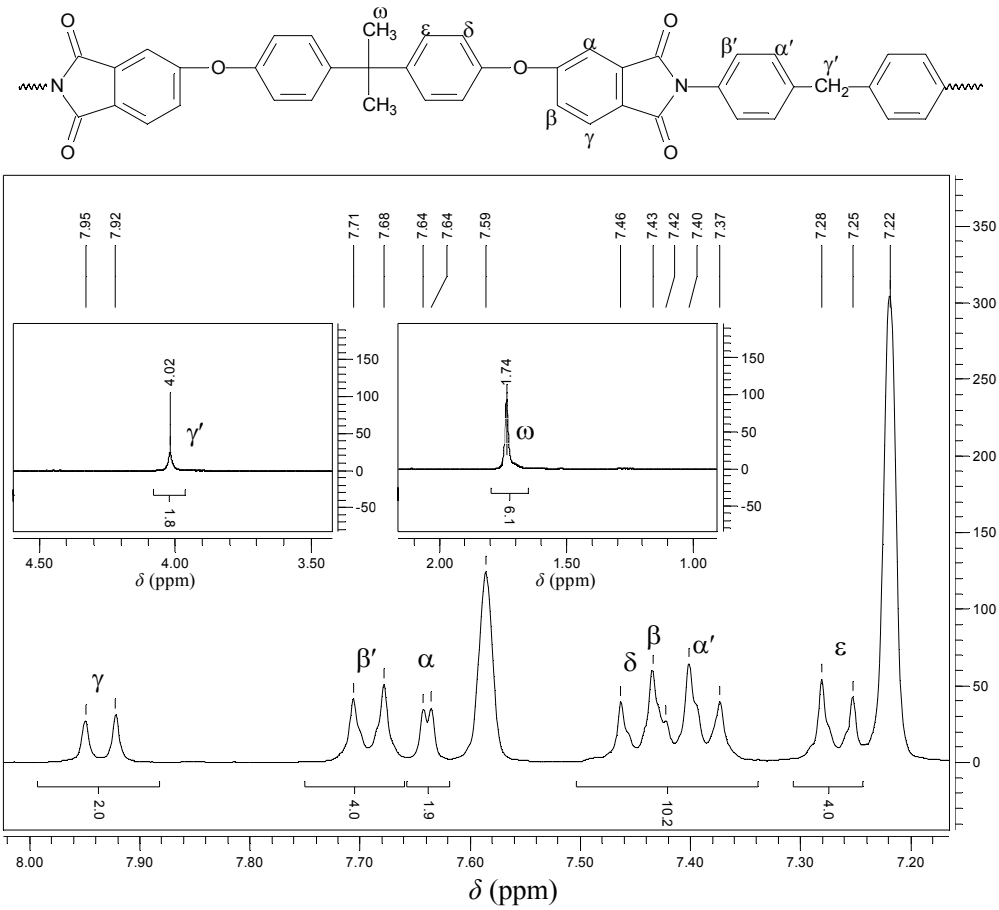

Figure 9.3 ^{1}H NMR of BPADA-MDA

TGA and DTG curves of the polyimides are displayed in Figure 9.5, and the characteristic temperatures are listed in Table 9.2. The further conversion of poly(amic acid)s to polyimides can be found at about 200 °C. BPADA-8ODA-2DABA undergoes two stages of degradation starting from ~350 and ~500 °C, respectively, and it has lower T_ds for 5 % and 10 % weight losses.

The apparent activation energies for thermal decomposition were calculated using Equation 5.4, and results are listed in Table 9.2. From TGA curves, it is observed that all curves of polyimides pass though the point of (560 °C, 64 %). The polymer with a larger value of activation energy appears to have a higher degradation rate when the temperature approaches up to 560 °C, and hence these polymers have better thermal stability below 560 °C. The huge difference in the values of activation energies reduces the possible error when these data are compared.

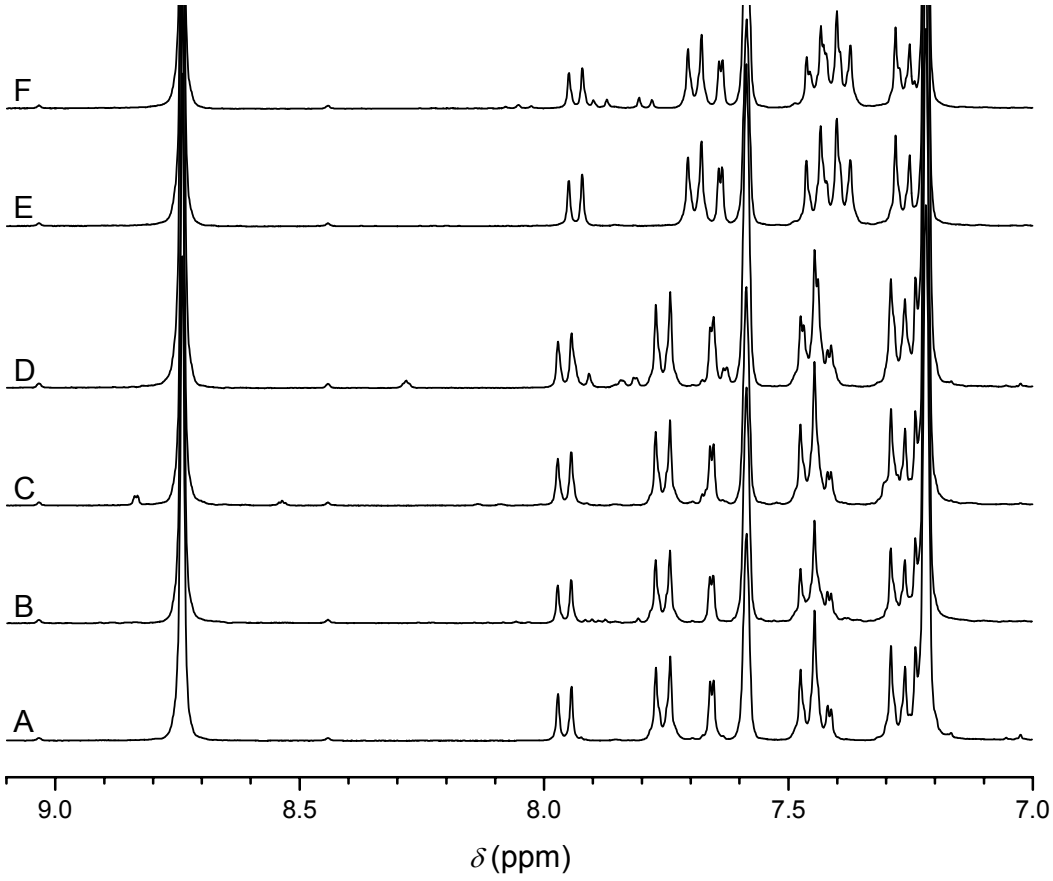

Figure 9.4 ^{1}H NMR spectra of BPADA-based polyimides

Table 9.2 Characteristic temperatures from DSC, TGA and DTG and estimated apparent activation energies for thermal decomposition

Polyimides	DSC [a] (°C)	T_d 5 % wt. loss (°C)	T_d 10 % wt. loss (°C)	T_d onset [b] (°C)	DTG [c] (°C)	E_d [d] (kJ/mol)
BPADA-ODA	219	517	531	522	543	350
BPADA-8ODA-2DAPy	234	508	522	512	536	300
BPADA-8ODA-2DABA	229	481	517	~350 [e]	420 [e]	–
				508	537	260
BPADA-8ODA-2DBSA	225	520	531	524	543	380
BPADA-MDA	226	490	512	500	528	250
BPADA-8MDA-2DAPy	229	485	504	492	524	190

[a] DSC operating conditions: 10 °C/min in helium. Glass transition temperatures were not distinctly decided from the first and second runs of DSC. The onset temperatures were used as an estimation of their glass transition temperatures.

[b] TGA operating conditions: 10 °C/min in helium.

[c] These temperatures were obtained from DTG peak temperatures.

[d] Estimated apparent activation energies for thermal decomposition in the range of ~520–550 °C, $r^2 = 0.99$.

[e] BPADA-8ODA-2DABA showed two degradation stages in TGA. This temperature was obtained from the first stage degradation.

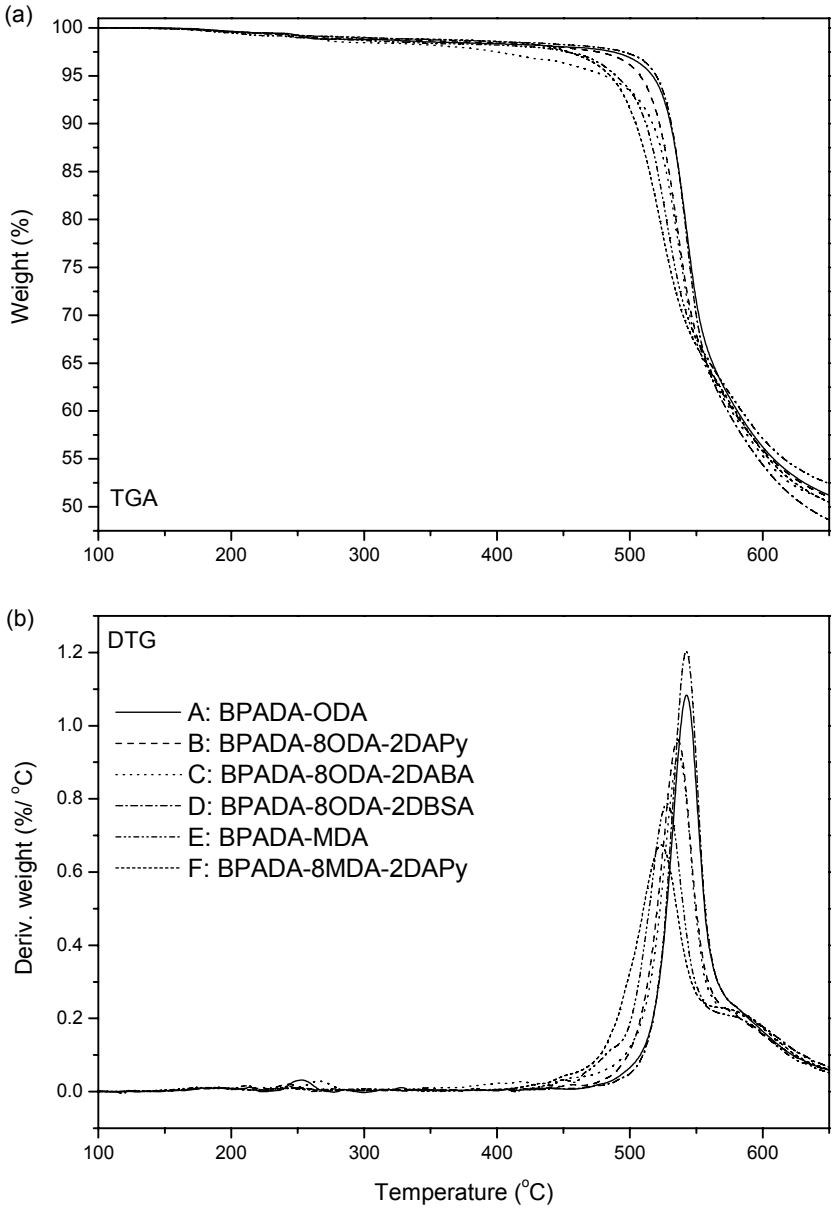

Figure 9.5 TGA (a) and DTG (b) curves of BPADA-based polyimides

9.3.2.3 Surface Free Energies

The contact angles of various liquids on polyimide membranes are listed in Table 9.3, and the surface free energies and the membrane-water interfacial free energies were calculated, and results are shown in Table 9.4.

Table 9.3 Contact angles of liquids on polyimide membranes at room temperature

Membranes	Water (°)	Glycerol (°)	Formamide (°)	Diiodomethane (°)
BPADA-ODA	83.6 ± 0.3	67.2 ± 0.3	57.4 ± 2.0	23.3 ± 1.0
BPADA-8ODA-2DAPy	77.7 ± 0.8	62.6 ± 0.5	56.8 ± 0.6	17.6 ± 0.9
BPADA-8ODA-2DABA	84.2 ± 0.8	60.5 ± 1.0	54.7 ± 1.4	19.8 ± 1.8
BPADA-8ODA-2DBSA	78.7 ± 1.0	65.8 ± 1.4	56.5 ± 0.6	19.9 ± 1.1
BPADA-MDA	70.2 ± 1.5	61.7 ± 1.0	52.4 ± 1.2	20.3 ± 1.0
BPADA-8MDA-2DAPy	82.2 ± 1.6	64.4 ± 0.4	55.2 ± 0.9	31.6 ± 0.8

All results are given as means with the 95 % confidence intervals.

Table 9.4 Surface free energy components (mJ/m^2) and membrane-water interfacial free energies (mJ/m^2) of polyimides at room temperature

Membranes	γ_s^{LW}	γ_s^+	γ_s^-	γ_s^{AB}	γ_s	ΔG_{sw}^{IF}
BPADA-ODA	46.74	0.0043	2.66	0.21	46.96	–77.54
BPADA-8ODA-2DAPy	48.45	0.0001	5.25	0.05	48.50	–66.22
BPADA-8ODA-2DABA	47.84	0.2187	1.18	1.02	48.86	–82.71
BPADA-8ODA-2DBSA	47.81	0.0001	4.68	0.04	47.86	–68.40
BPADA-MDA	47.69	0.0001	10.31	0.06	47.76	–47.14
BPADA-8MDA-2DAPy	43.55	0.1897	2.74	1.44	44.99	–70.09

The total surface energies γ_s of the polyimides vary in the range of 45–49 mJ/m^2. The LW components of surface free energies γ_s^{LW} appear between 43.5 and 48.5 mJ/m^2, and are predominantly greater than the AB components γ_s^{AB}. Looking at the components of γ_s^{AB}, it can be found that some γ_s^+ are close to zero, but γ_s^- have much larger values, indicating the electron-donicity of the membranes. This is suggested to result from the interactions between electron donating and accepting sites as well as the residual hydration [Van Oss *et al.* 1997]. For the polyimide membranes, the Lewis base components γ_s^- are probably influenced by the basicity of the polyimides from their residual amino groups.

Free energy of the interfacial interaction combines the surface properties of the liquid and the solid. The membrane-water interfacial free energies ΔG_{sw}^{IF} can be used directly to compare the hydrophilicity of the membranes. It is also known that hydrophobic membranes exhibit negative

values of ΔG_{sw}^{IF} [Van Oss and Giese 1995]. Therefore, BPADA-MDA is shown to be more hydrophilic than the others. This is consistent with the results of contact angles and the values of γ_s^-.

9.3.3 Pervaporation Properties

9.3.3.1 Effects of Feed Concentrations

Pervaporation dehydration of isopropanol was carried at 60 °C with the feed water content varying in the range of 10–50 wt. %. Permeation flux and the permeate water content are presented in Figure 9.6.

It is observed that with an increase in the feed water content, most of the membranes have an increase in the permeate water content, and a similar trend can be seen in permeation flux. These results are possibly attributed to the enhancement of water sorption in the polymer matrix. When water is sorbed in the polymer matrix, it swells the matrix, especially for the glassy polymers with flexible structures. Therefore, it is reasonable to observe an increase in flux and a decrease in the permeate water content for BPADA-ODA at the feed water content of 10–30 wt. %. BPADA-8ODA-2DBSA and BPADA-8ODA-2DABA membranes had good selectivity towards water/isopropanol, benefiting from the hydrophilicity of their functional groups. With the possible affinity to isopropanol, the polyimides containing DAPy moieties showed worse selectivities towards water/ isopropanol. Due to the flexibility of MDA moieties, BPADA-MDA and BPADA-8MDA-2DAPy yielded higher flux and higher isopropanol contents in the permeates.

The *concentration coefficients* were determined by curve fitting based on Equation 6.13 from total flux and water flux, respectively. The calculations are shown in Appendices C and D, and results are listed in Table 9.5. For the purpose of comparison, the *n* values of 6FDA-based polyimide membranes are also presented in Table 9.5.

Since BPADA-based polyimide membranes produced permeates of high water contents, the *n* values for total flux and water flux are very close. Compared with 6FDA-based polyimide membranes, most of BPADA-based polyimides have larger *n* values. The hydrophobicity of 6FDA moieties and the flexibility of BPADA moieties contribute to these differences. It should be noted that BPADA-8ODA-2DAPy has exceptional *n* values, possibly resulting from the high thickness of the membrane. This is because the great resistance and the low degree of expansion of the thick membrane can reduce the permeation flux with a high water content in the feed. So a question was

raised, could the reasonable *n* values of BPADA-8ODA-2DAPy be predicted from the *n* values of BPADA-based and 6FDA-based polyimide membranes?

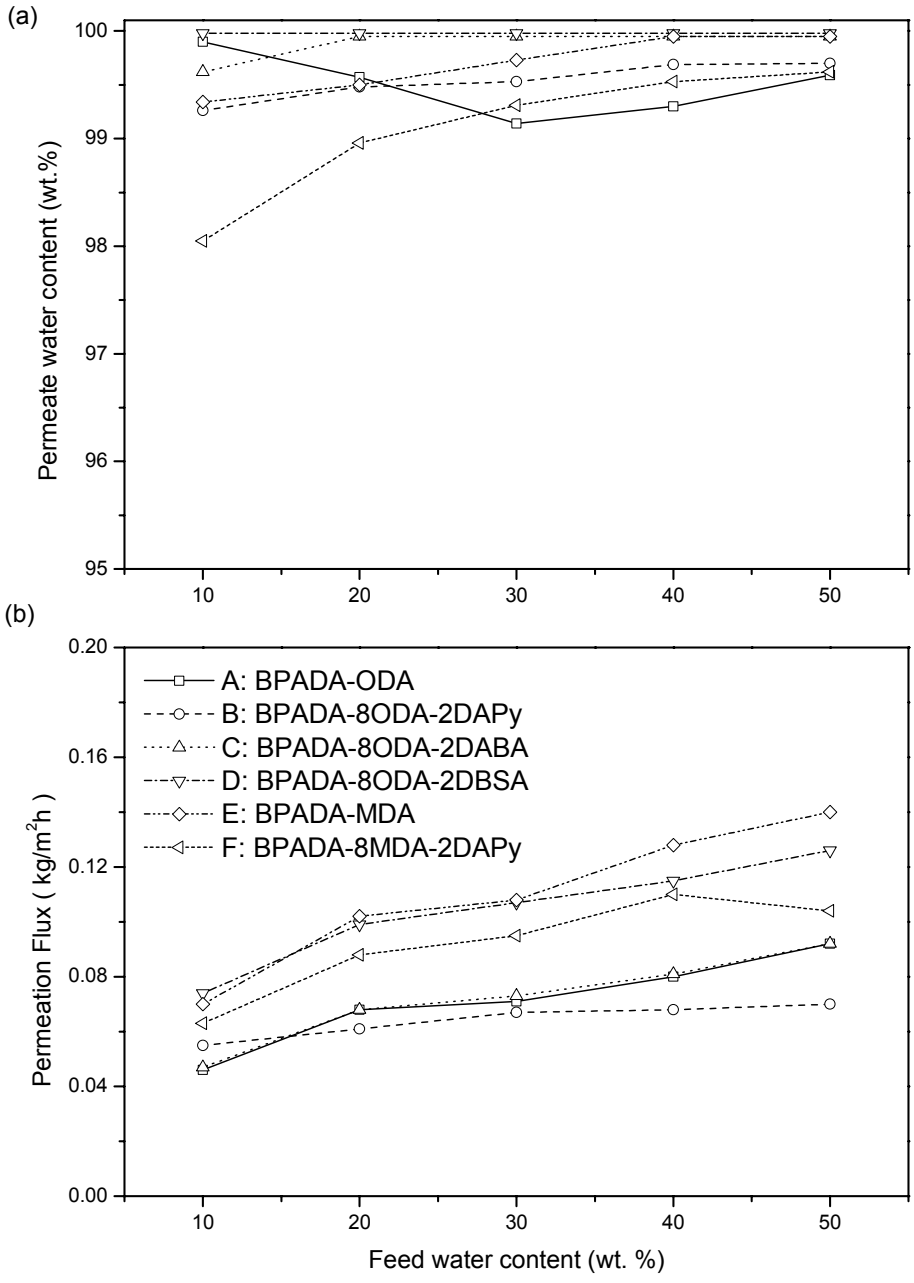

Figure 9.6 Permeation flux and permeate water contents for pervaporation dehydration of isopropanol at 60 °C

Table 9.5 Comparison of concentration coefficients and permeation activation energies for BPADA-based membranes and 6FDA-based membranes

Membranes	n [a]		E_p (kJ/mol) [b]	
	total flux	water flux	total flux	water flux
BPADA-ODA	0.43	0.42	37.9 ± 3.1	37.6 ± 3.0
BPADA-8ODA-2DAPy	0.18	0.18	38.6 ± 1.8	38.6 ± 1.9
BPADA-8ODA-2DABA	0.41	0.41	52.1 ± 0.6	52.2 ± 0.7
BPADA-8ODA-2DBSA	0.34	0.34	45.7 ± 3.3	45.9 ± 3.3
BPADA-MDA	0.43	0.43	55.6 ± 4.6	55.7 ± 4.6
BPADA-8MDA-2DAPy	0.44	0.45	36.9 ± 0.7	36.8 ± 0.8
6FDA-ODA	0.22	0.23	46.1 ± 2.8	45.6 ± 2.8
6FDA-8ODA-2DAPy	0.37	0.38	55.6 ± 3.1	55.4 ± 3.1
6FDA-8ODA-2DABA	0.35	0.40	53.6 ± 2.6	53.2 ± 2.7
6FDA-8ODA-2DBSA	0.37	0.42	40.9 ± 2.1	39.9 ± 2.1
6FDA-MDA	0.27	0.30	39.8 ± 1.7	40.7 ± 1.5
6FDA-8MDA-2DAPy	0.34	0.38	44.1 ± 3.8	45.3 ± 4.0

[a] Obtained from curve fitting, r^2=0.93–0.99.

[b] Apparent activation energies for total permeation flux with feed water content ~20 wt. %.

The moiety contribution factors for ODA, MDA, DBSA, DABA, DAPy and 6FDA moieties from the linear moiety contribution method (calculations shown in Appendices C and D) are listed in Table 9.6. By applying these moiety contribution factors to BPADA-based membranes, the average values of contribution factors of the BPADA moiety are found to be 0.30 (for total flux) and 0.29 (for water flux). The validity of the calculated n values of BPADA moiety is confirmed from the comparison with those of the 6FDA moiety. Since the BPADA moiety is more hydrophilic and more flexible than the 6FDA moiety, the larger n values are reasonable.

The n values of BPADA-based polyimide membranes can be calculated from Equation 6.12, and thus the n values of BPADA-8ODA-2DAPy are amended to be 0.36 (for total flux) and 0.35 (for water flux), respectively.

9.3.3.2 Effects of the Operating Temperature

Pervaporation was performed with aqueous isopropanol solutions (~20 wt. % water), and operating temperatures were controlled at 30–70°C. Figure 9.7 shows the total flux and the permeate water contents. Consistent with the behaviors in the study of the effects of feed concentrations, the membranes containing MDA moieties show lower water contents in the permeates. Higher permeate water contents are produced by BPADA-MDA, indicating a favorable effect on the permeation of water from the thermal movement of MDA moieties. The permeation of isopropanol is also enhanced in BPADA-ODA, which result from the higher sorption of isopropanol at elevated temperatures.

Activation energies for total flux and water flux were calculated and are listed in Table 9.5, together with the activation energies of 6FDA-based membranes, for the purpose of comparison. However, no distinct difference can be told between 6FDA-based membranes and BPADA-based membranes.

Linear moiety contribution method was also applied to the activation energies, and calculations are shown in Appendices C and D. The contributions of the BPADA moiety to the activation energies were calculated by deduction of the contributions of the other moieties from BPADA-based membranes. Average values of the contributions of the BPADA moiety were determined to be 35.0 kJ/mol (for total flux) and 34.9 kJ/mol (for water flux in permeates). Differences between the activation energies for total flux and those for water flux are not significant.

Table 9.6 Moiety contributions to concentration coefficients and permeation activation energies for total flux and water flux

Moieties of monomers	n		E_p (kJ/mol)	
	total flux	water flux	total flux	water flux
ODA	0.03	0.03	7.1	6.8
MDA	0.07	0.09	6.3	7.0
DAPy	0.18	0.17	27.0	28.9
DABA	0.41	0.32	51.6	50.7
DBSA	0.37	0.37	0.7	-0.1
6FDA	0.25	0.27	35.6	35.6
BPADA [a]	0.30	0.29	35.0	34.9

[a] Calculated with moiety contribution factors from 6FDA-based membranes.

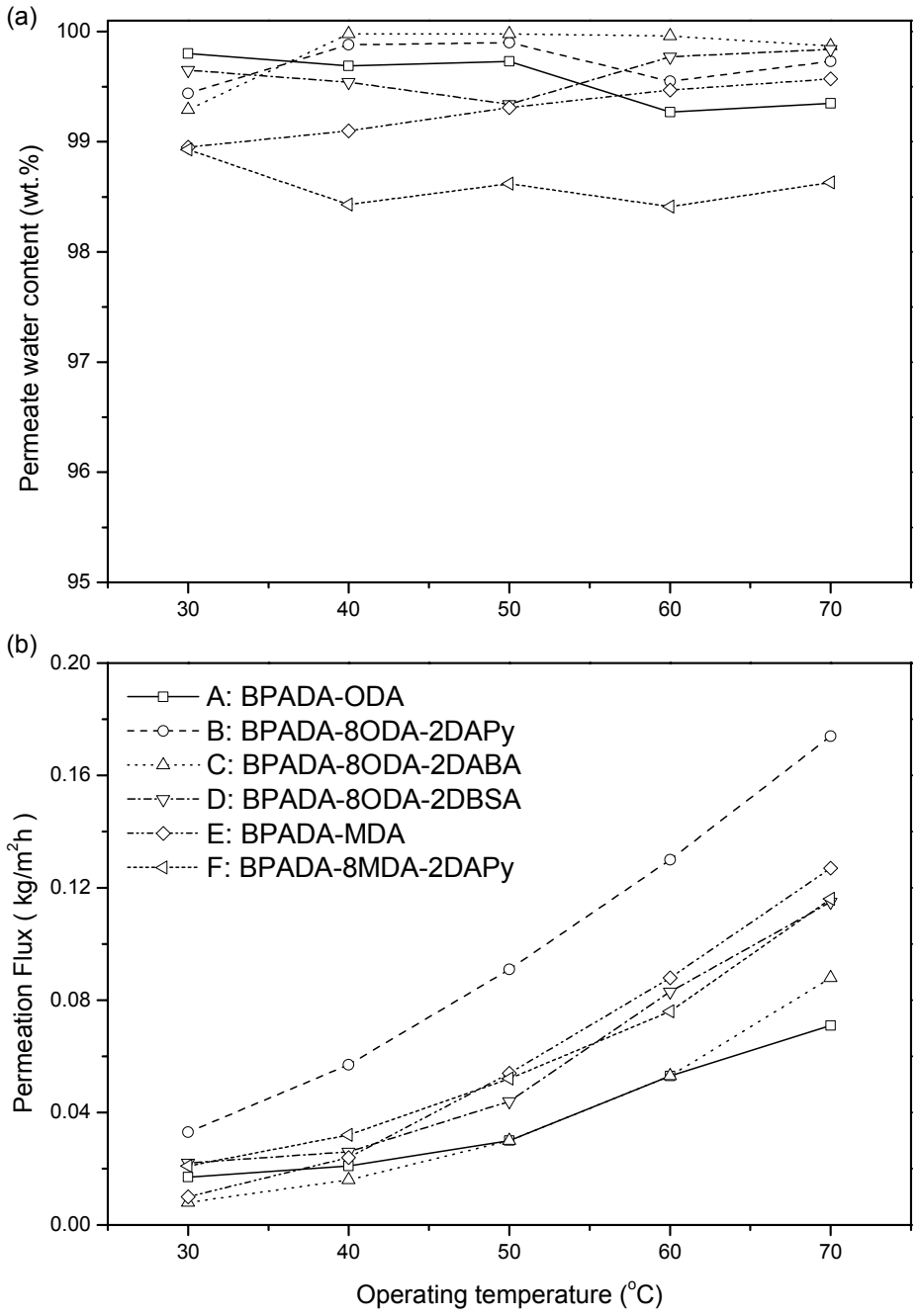

Figure 9.7 Total flux and permeate water contents for pervaporation with feed water contents of ~20 wt. %

9.4 Conclusions

Six polyimides with high molecular weights were successfully synthesized from BPADA and various diamines, and were characterized with GPC, DSC, FTIR, NMR, DSC and TGA.

DSC results showed that the contributions from the diamines to the glass transition temperatures were in an order: DAPy > DABA > DBSA > ODA. Polyimides showed good thermal stabilities, and the apparent activation energies for thermal decomposition were calculated.

Polyimide membranes were prepared from the THF solutions, and their hydrophilicity was estimated by contact angles and the water-membrane interfacial free energies. BPADA-MDA was more hydrophilic than the others.

Pervaporation properties were investigated for dehydration of isopropanol, and comparisons were made between BPADA-based membranes and 6FDA-based membranes. The linear moiety contribution method was applied to the *concentration coefficients* and activation energies. The contribution factors of the BPADA moiety for the *concentration coefficients* are found to be 0.30 (for total flux) and 0.29 (for water flux), respectively. The *concentration coefficients* of BPADA-8ODA-2DAPy are amended to be 0.36 (for total flux) and 0.35 (for water flux), respectively. The contribution factors of the BPADA moiety for activation energies were determined to be 35.0 kJ/mol (for total flux) and 34.9 kJ/mol (for water flux in permeates). The effects of monomer moieties on pervaporation properties were discussed based on the moiety contribution factors.

Chapter 10
Conclusions and Recommendations

10.1 General Contributions

In the thesis work, modified poly(vinyl alcohol) (PVA) / chitosan membranes (CS) and synthetic high-performance polyimide membranes were prepared and characterized for pervaporation dehydration of isopropanol. Gas permeation properties of the dense membranes were also investigated. The following conclusions can be drawn from this study:

10.1.1 Trimesoyl Chloride Crosslinked PVA Membranes

1) TMC/hexane proved to be a good crosslinking agent for PVA membranes. TMC reacted with the hydroxyl groups of PVA to form ester groups. The degrees of crosslinking of PVA-TMC membranes were estimated to be in the range of 13–20 % at room temperature, and degrees of crosslinking were found to be different at the two surfaces of the membranes.

2) PVA-TMC membranes had better thermal stability than the uncrosslinked PVA film. A thermal pyrolysis mechanism was proposed for PVA-TMC membranes: the PVA-TMC membranes with a lower degree of crosslinking degraded by elimination of water, while those with a higher degree of crosslinking degraded by elimination of TMC.

3) The crosslinking and steric effects of TMC, as well as the hydrophilicity of the residual $-COOH$ groups from TMC, contributed to the swelling behaviors of PVA-TMC membranes in water at room temperature: PVA-3TMC had the lowest degree of swelling, and PVA-7TMC had the highest. The degree of swelling of the PVA-3TMC membrane in water was in the range of 210 % (at 30 °C) – 310 % (at 60 °C). Membrane swelling of PVA-3TMC was suppressed substantially in water/isopropanol mixtures with different water contents and at different sorption temperatures, due to the non-solvent effect of isopropanol and the interactions between water and PVA matrix.

4) An appropriate degree of crosslinking was helpful to the stable flux and good membrane selectivity. The PVA-3TMC membrane showed the best overall pervaporation properties among the PVA-TMC membranes studied. In the permeation of pure water and pseudo-steady-state pervaporation of water/isopropanol mixture with PVA-3TMC in the heating-cooling cycle, the

permeation flux did not change significantly. However, crystallites of PVA were formed during the heating run, and produced more diffusion resistance for isopropanol, resulting in a higher selectivity in the cooling run. Pervaporation with PVA-3TMC in the concentration cycle did not show significant changes in flux and the permeate water content, and furthermore, the permeate water content did not show substantial changes in the batch operation of pervaporation dehydration of isopropanol at the feed water concentration of 9–20 wt. %.

10.1.2 Trimesoyl Chloride Crosslinked Chitosan Membranes

1) TMC/hexane was used to interfacially crosslink chitosan membranes. TMC mainly reacted with the amino groups of chitosan in the crosslinking reaction to form amide groups. Because of the steric effect of TMC and the hydrophilicity of the residual $-COOH$ groups from TMC, the chitosan membranes with a higher degree of crosslinking showed a higher degree of swelling in water.

2) When tested for CO_2 and N_2 permeation, because of the densification effect of crosslinking and the consumption of amino groups by TMC at the surface of the CS-TMC-1 membrane, the permeation of CO_2 decreased, while the permeation of N_2 was not significantly affected. However, at a higher degree of crosslinking, more free volume was formed by the insertion of TMC, and more amino groups were consumed by TMC. As a result, the permeation of N_2 was improved, while the permeation of CO_2 was not affected substantially. Therefore, to attain a high permselectivity, the degree of crosslinking must be controlled. CS-TMC-2 showed the best permselectivity towards CO_2/N_2, with a CO_2 permeability of ~163 Barrer and a CO_2/N_2 permeability ratio of ~42.

3) For pervaporation with the unconditioned and conditioned chitosan and CS-TMC membranes, the relaxation of the segmental chains in the chitosan matrix and the packing property of the matrix were influenced by the TMC moieties, which led to the differences in pervaporation flux and selectivity.

The polymer chains of the conditioned chitosan membrane (uncrosslinked) were packed more densely and orderly after the conditioning of sorption in water followed by water permeation, resulting in more resistance to the penetrants than the unconditioned chitosan membrane.

The conditioning processes of the crosslinked CS-TMC membranes did not significantly transform the conformation of the crosslinked matrices, and the permeation of penetrants was not affected, compared with the uncrosslinked chitosan membrane. TMC moieties in crosslinked CS-TMC membranes reduced the flexibility of the matrix and produced more permeation resistance in

the matrix, and therefore, the degree of crosslinking should be controlled to attain good pervaporation properties. The CS-TMC-3 membrane showed the best overall pervaporation properties among the CS-TMC membranes studied.

10.1.3 Synthetic Polyimide Membranes

1) 6FDA-based and BPADA-based copolyimides were synthesized from the one-step high-temperature polymerization in *m*-cresol with dianhydride and diamine monomers of different reactivities. The polyimides showed different thermal properties because of the different monomer moieties.

2) An empirical linear moiety contribution method was proposed for the permselectivities towards O_2/N_2, H_2/N_2, He/N_2 and CO_2/N_2. The effects of the dianhydride and diamine monomers on gas permeabilities were evaluated based on the moiety contribution factors.

Permeabilities of N_2, O_2, H_2 and He are significantly affected by the steric effects of the monomer moieties, but the CO_2 permeability is mainly determined by its solubility in the polymer as well as the interactions with the functional groups. Bulky side groups, flexibility of polymer main chains, structures of monomer moieties, and interactions between gas molecules and polymer chains are shown to affect gas permeabilities of the membranes. MDA, DABA, DBSA, BABP and DABN moieties are shown to help increase the selectivities towards O_2/N_2, H_2/N_2 and He/N_2, while BTDA and NTDA show negative effects. Attributed to the steric effects of sulfonyl groups, DDS and BADS moieties had negative contributions to the selectivities towards O_2/N_2, H_2/N_2 and He/N_2. DAPy and BADS moieties decreased the selectivity towards CO_2/N_2.

3) The moiety contribution method was also applied to pervaporation properties of polyimide membranes by linearly splitting the apparent permeation activation energies and the proposed *concentration coefficients*. Though these contribution factors are purely empirical, they still provide some information that can be used to correlate the moieties with pervaporation properties. The sorption and diffusion properties were studied based on the moiety contributions. The pervaporation performance was found to be determined by the interactions between penetrants and polymer matrices, as well as the steric effects of monomer moieties. However, additional work should be done to find better explanations of the contribution factors.

10.2 Recommendations for Future Work

Crosslinking of poly(vinyl alcohol) and chitosan with trimesoyl chloride and the linear moiety contribution method for gas separation and pervaporation processes were developed, and the membranes obtained from this work showed potentials for applications in pervaporation and gas separation. However, more work is needed to establish a structure-property relationship for the membranes. Several aspects should be explored if further studies are to be performed.

1) *Polymer Materials* For a specific mixture to be separated, choosing a membrane is the first consideration. The conventional membrane materials such as poly(vinyl alcohol) and chitosan, and the high-performance polyimides are good choices for pervaporation and gas separation processes. High permeation flux, good selectivities and the long-term stability are factors that have to be considered: if high flux is required for the hydrophilic membranes, one can choose poly(vinyl alcohol) and chitosan to prepare crosslinked membranes; if the membrane is to be used under harsh conditions (e.g., elevated temperatures and strong solvents), one can consider polyimide membranes.

2) *Molecular Design for Membrane Materials* Based on the relationship between chemical/ physical structures and membrane properties, synthesis or modifications should be conducted to improve the membrane performance. Surface free energies and moiety contribution factors from this work are helpful and may be utilized for tailoring the membrane materials.

3) *Crosslinking with Trimesoyl Chloride* The interfacial crosslinking of poly(vinyl alcohol) and chitosan with trimesoyl chloride showed to be useful, but it should be further studied to accurately control the degree of crosslinking.

4) *Pervaporation Processes* In this work, pervaporation experiments were conducted for dehydration of isopropanol, and crosslinked PVA and chitosan membranes showed fairly good separation performance. Other aqueous solutions (e.g., ethanol, glycol, acetone) may be tested for pervaporation dehydration as well. Separation of organic mixtures is challenging, and the trimesoyl chloride crosslinked PVA and CS membranes as well as the copolyimide membranes may be a good choice because of their good chemical stabilities.

5) *Gas Separation Processes* Pure gas permeation is often different from the actual mixture gas separation processes, and further investigations should be done with gas mixtures to evaluate the membrane performance for gas mixture separations.

6) *Linear Moiety Contribution* The linear moiety contribution method proposed in this work is an empirical model. It does not have a very clear physical meaning, but is only a simple mathematical

approach. Therefore, further studies should be done to correlate the moiety contribution factors with the chemical/physical parameters of the moieties.

Nomenclature

A	the pre-exponential factor of the Arrhenius equation
$\overline{DP}$	the degree of polymerization
E_d	the apparent activation energy for thermal decomposition
$E_{d,1}$	the apparent activation energies for thermal decomposition at the first stage
$E_{d,2}$	the apparent activation energies for thermal decomposition at the second stage
E_p	the apparent permeation activation energy
$E'_{p,a}$	the apparent permeation activation energy for isopropanol flux
$E_{p,c}$	the apparent permeation activation energy for the conditioned membrane
$E_{p,o}$	the apparent permeation activation energy for the unconditioned membrane
$E_{p,t}$	the apparent permeation activation energy for total flux
$E'_{p,w}$	the apparent permeation activation energy for water flux
E_w	the permeation activation energy for pure water permeation
F	the pervaporation flux
J	the gas permeation flux
k	a parameter related to the membrane and the operating temperature
l	the membrane thickness
m	the slope of the upper bound line for gas separation
$\overline{M}_n$	the number average molecular weight
$\overline{M}_w$	the weight average molecular weight
n	the concentration coefficient for pervaporation
p	the pressure
P	the permeability coefficient
q	the volumetric flow rate
Q	the amount of permeate
r^2	the coefficients of determination
R	the universal gas constant
S	the membrane area

SD	the degree of swelling
t	the operating time
T	the operating temperature
T_d	the decomposition temperature
T_g	the glass transition temperature
T_m	the melting temperature
W_o	the initial weight of the dry membrane
W_s	the weight of the swollen membrane at sorption equilibrium
W_t	the weight of the membrane at time t
W_∞	the weight of the residual
x_a	the isopropanol concentration in the feed for pervaporation
x'_a	the isopropanol concentration in the feed mixture for sorption
x_w	the water concentration in the feed for pervaporation
x'_w	the water concentration in the feed mixture for sorption
y_a	the isopropanol concentration in the permeate
y'_a	the concentration of isopropanol in the adsorbate
y_w	the water concentration in the permeate
y'_w	the concentration of water in the adsorbate

Greek symbols

α	the pervaporation separation factor
$\alpha_{w/a}$	the pervaporation separation factor for water and isopropanol
α_S	the sorption selectivity
α_D	the diffusion selectivity
$\alpha_{i/j}$	the permeance ratio for pure gases i and j
γ_i^{AB}	the Lewis acid-base (AB) component of the surface free energy
γ_i^{LW}	the Lifshitz-van der Waals component of the surface free energy
γ^+	the Lewis acid (electron-acceptor) component of the surface free energy

γ^-	the Lewis base (electron-donor) component of the surface free energy
Δd_k	the kinetic diameter difference of the gas pair
ΔG_{sw}^{IF}	the water-membrane interfacial free energy

Special Units for gas permeation

GPU Gas Permeation Unit, a non-SI unit for permeance, $10^{-6}\ \dfrac{\mathrm{cm^3(STP)}}{\mathrm{s\cdot cm^2\cdot cmHg}}$

$1\ \mathrm{GPU} = 7.5\times10^{-9}\ \mathrm{m^3(STP)\,m^{-2}\,s^{-1}\,kPa^{-1}}$

Barrer a non-SI unit for permeability, $10^{-10}\ \dfrac{\mathrm{cm^3(STP)\cdot cm}}{\mathrm{s\cdot cm^2\cdot cmHg}}$

$1\,\mathrm{Barrer} = 7.5\times10^{-15}\,\mathrm{m^3(STP)\,m\,m^{-2}\,s^{-1}\,kPa^{-1}}$

Abbreviations

6FDA	4,4'-(hexafluoroisopropylidene) diphthalic anhydride
BABP	4,4'-bis(3-aminophenoxy) benzophenone
BADS	4,4'-bis(3-aminophenoxy)diphenyl sulfone
BPADA	2,2-Bis[4-(3,4-dicarboxyphenoxy) phenyl]propane dianhydride
BTDA	3,3',4,4'-benzophenon-tetracarboxylic anhydride
CS	chitosan
DABA	3,5-diaminobenzoic acid
DABN	2,6-bis(3-aminophenoxyl)benzonitrile
DANT	1,5-diaminonaphthalene
DAPy	2,6-daminopyridine
DBSA	2,4-diaminobenzenesulfonic acid
DDS	4-aminophenyl sulfone
DMAc	*N*, *N*-dimethylacetamide
DMSO	dimethyl sulfoxide
MDA	4,4'-methylenedianiline
NTDA	naphthalene-1,4,5,8-tetracarboxylic dianhydride
ODA	aminophenyl ether
PVA	poly(vinyl alcohol)
THF	tetrahydrofuran
TMC	trimesoyl chloride

ATR	attenuated total reflectance spectroscopy
DSC	differential scanning calorimetry
DTG	the derivative thermogravimetry
FTIR	fourier transform infrared spectroscopy
GPC	gel permeation chromatography
IRE	the internal reflection element
NMR	nuclear magnetic resonance spectroscopy
TCD	thermal conductivity detector
TGA	thermogravimetric analysis

Appendix A
Solubility Parameters

The Hansen Solubility Parameter expresses the nature and magnitude of the interaction forces working between molecules, and can be used to predict whether one material will dissolve in another and form a solution. By applying solubility parameters to membranes, it will help understand the interactions between the membrane materials and the penetrants [Matsuura 1994].

The solubility parameter is composed of three Hansen parameters:

$$\delta_t^2 = \delta_d^2 + \delta_p^2 + \delta_h^2 \qquad \text{(A-1)}$$

where δ_t is the total solubility parameter, δ_d, δ_p and δ_h are the dispersion force component, dipole component and hydrogen bonding component of the solubility parameter, respectively.

The three parameters can be treated as the coordinates for a point in three dimensions. If the two species are closer in this three dimensional space, they are more likely to dissolve into each other. For the polymer and solvent system:

$$\Delta\delta_{S-P} = [4(\delta_{d,S} - \delta_{d,P})^2 + (\delta_{p,S} - \delta_{p,P})^2 + (\delta_{h,S} - \delta_{h,P})^2]^{1/2} \qquad \text{(A-2)}$$

where the constant 4 in the first term of the equation creates a spherical volume of solubility, $\Delta\delta_{S-P}$ is the distance between solvent and the center of polymer solubility sphere, and the notations for the polymer and the solvent are presented as *S* and *P* in the subscripts.

Therefore, in the solution-diffusion model, a higher solubility towards the penetrant molecule A will be achieved if the membrane material is closer to species A than to species B in the three dimensional space of the solubility parameters.

Table A-1 shows the solubility parameters and the components for the polymers and some commonly used solvents, and Table A-2 presents the calculated distance between the solvents and the centers of polymer solubility spheres, which indicates the affinity between the solvents and the polymers. Table A-2 tells the hydrophilicity of the polymers by comparing the calculated values (between polymers and water) horizontally.

Table A-1 Hansen solubility parameters and the components for polymers and solvents at 25 °C

Polymers and solvents [a]	δ_t ((MPa)$^{1/2}$)	δ_d ((MPa)$^{1/2}$)	δ_p ((MPa)$^{1/2}$)	δ_h ((MPa)$^{1/2}$)
Poly(vinyl alcohol) [b]	39.1	16.0	12.9	23.9
Chitosan [c]	39.0	22.81	17.13	26.60
6FDA-ODA [d]	20.6	18.7	4.7	7.1
6FDA-MDA [d]	20.5	18.9	4.6	6.5
BPADA-ODA [d]	20.4	18.8	3.8	7.1
BPADA-MDA [d]	20.4	18.9	3.7	6.6
Isopropanol	23.5	15.8	6.1	16.4
Water	47.8	15.6	16.0	42.3
Methanol	29.6	15.1	12.3	22.3
Ethanol	26.5	15.8	8.8	19.4
Cyclohexane	16.8	16.8	0.0	0.2
Toluene	18.2	18.0	1.4	2.0
Chloroform	19.0	17.8	3.1	5.3
Tetrahydrofuran	19.4	16.8	5.7	8.0
Acetone	20.0	15.5	10.4	7.0
Pyridine	21.8	19.0	8.8	5.9
Acetic acid	21.4	14.5	8.0	13.5
m-Cresol	22.7	18.0	5.1	12.9

[a] Values selected from the reference [Barton 1991],unless stated otherwise.

[b] Values selected from the reference [Matsuura 1994].

[c] Values selected from the reference [Ravindra 1998].

[d] Values estimated by using the group contribution method from the reference [Matsuura 1994]; the polymer structures as listed below:

6FDA-ODA= 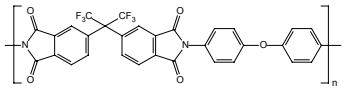

BPADA-ODA= 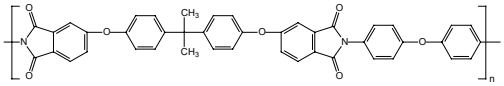

6FDA-MDA= 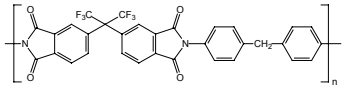

BPADA-MDA= 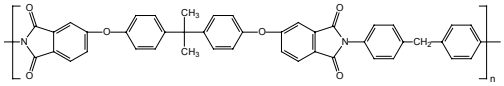

Table A-2 The affinity (in $(MPa)^{1/2}$) between polymers and solvents calculated based on solubility parameters

Solvents [a]	Poly(vinyl alcohol) [b]	Chitosan [c]	6FDA-ODA [d]	6FDA-MDA [d]	BPADA-ODA [d]	BPADA-MDA [d]
Isopropanol	10	21	11	12	11	12
Water	19	21	37	38	38	38
Methanol	2	17	18	19	19	19
Ethanol	6	18	14	15	15	15
Cyclohexane	27	34	9	9	9	9
Toluene	25	31	6	6	6	5
Chloroform	21	27	3	3	3	3
Tetrahydrofuran	18	25	4	5	5	5
Acetone	17	25	9	9	9	10
Pyridine	19	24	4	4	5	5
Acetic acid	12	23	11	12	12	12
m-Cresol	14	21	6	7	6	7

[a] Values selected from the reference [Barton 1991].

[b] Values selected from the reference [Matsuura 1994].

[c] Values selected from the reference [Ravindra 1998].

[d] Values estimated by using the group contribution method from the reference [Matsuura 1994]; the polymer structures as listed below:

6FDA-ODA= 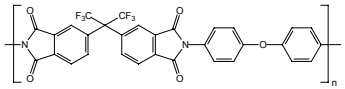

BPADA-ODA= 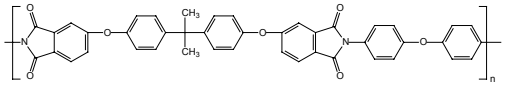

6FDA-MDA= 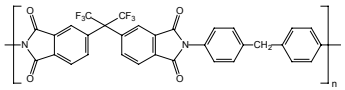

BPADA-MDA= 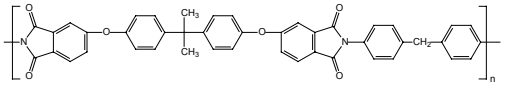

Appendix B

Calculation of the Apparent Activation Energy from the Arrhenius Equation

The Arrhenius equation can be expressed as shown in Equation 3.4, and the apparent activation energy can be obtained from ln$F$ vs. (1/T) plot based on the following form of the equation:

$$\ln F = \ln A + (-\frac{E}{R})(\frac{1}{T}) \quad \text{(B-1)}$$

$$\text{slope } k = -E/R \quad \text{(B-2)}$$

Figure B-1 shows a calculation example for water and isopropanol permeation through PVA-3TMC (feed water content 20 wt. %), and the results were also listed in Table 3.5.

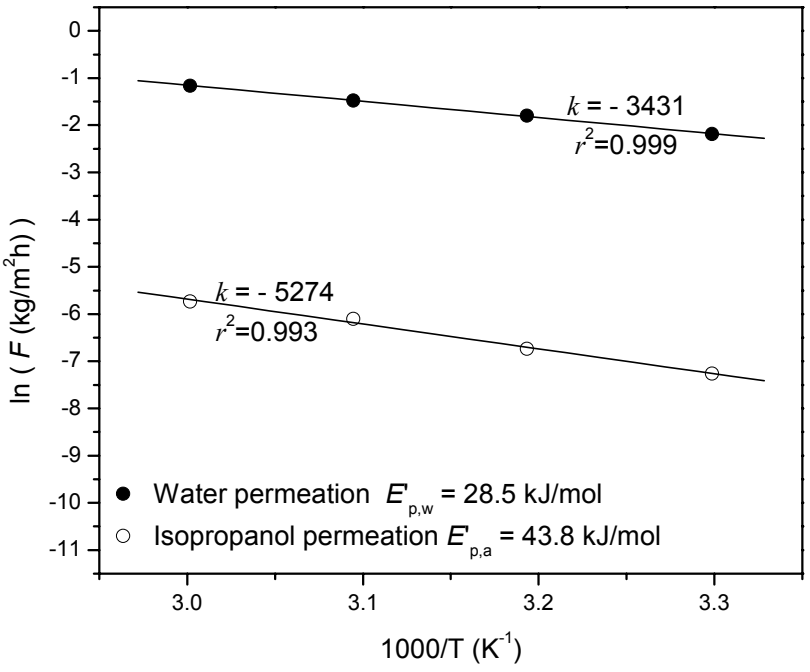

Figure B-1 Calculation of apparent activation energies from the Arrhenius equation

Appendix C
FTIR and NMR Data of Polyimides and Monomers

FTIR and NMR data for Chapter 6:

6FDA-ODA FTIR (film, cm^{-1}): 3490(vw) ν_{as} N–H, 3054(br, w) aromatic δ C–H, 1785(m) ν_{as} C=O, 1728(s) ν_s C=O, 1597(w) phenyl ring, 1502(s) phenyl ring, 1379 (m) ν C–N, 1299(m) ν_s CF_3, 1245(m) ν_{as} C–O–C, 1113(br, m) imide, 1015 (w) aromatic ring, 723(m) δ imide. ^{1}H NMR (pyridine-*d5*, δ ppm): 8.17–8.14 (4H), 8.06–8.04 (2H), 7.91 (d, J=9 Hz, 4H), 7.31 (d, J=9 Hz, 4H) ^{19}F NMR (Pyridine-*d5*, δ ppm): 61.46.

6FDA-8ODA-2DBSA FTIR (film, cm^{-1}): 3490(vw) ν_{as} N–H, 3070(br, w) aromatic δ C–H, 1785(m) ν_{as} C=O, 1727(s) ν_s C=O, 1598(w) phenyl ring, 1501(s) phenyl ring, 1380 (m) ν C–N, 1299(m) ν_s CF_3, 1243(m) ν_{as} C–O–C, 1112(br, m) imide, 1015 (w) aromatic ring, 722(m) δ imide. ^{1}H NMR (Pyridine-*d5*, δ ppm): 8.52 (0.2H), 8.17–8.04 (6.4H), 7.92–7.90 (3.2H), 7.33–7.30 (3.2 H).

6FDA-6ODA-4DBSA FTIR (film, cm^{-1}): 3494(vw) ν_{as} N–H, 3071(br, w) aromatic δ C–H, 1785(m) ν_{as} C=O, 1728(s) ν_s C=O, 1602(w) phenyl ring, 1502(s) phenyl ring, 1381 (br, m) ν C–N, 1298(m) ν_s CF_3, 1257(br, m) ν_{as} C–O–C, 1111(br, m) imide, 1015(w) aromatic ring, 721(m) δ imide. ^{1}H NMR (pyridine-*d5*, δ ppm): 8.51 (0.3H), 8.17–8.04 (6.8H), 7.92–7.90 (2.4H), 7.33–7.30 (2.4H).

6FDA-8ODA-2DABA FTIR (film, cm^{-1}): 3496(vw) ν_{as} N–H, 3071(br, w) aromatic δ C–H, 1786(m) ν_{as} C=O, 1730(s) ν_s C=O, 1599(w) phenyl ring, 1502(s) phenyl ring, 1381 (m) ν C–N, 1298(m) ν_s CF_3, 1247(br, m) ν_{as} C–O–C, 1111(br, m) imide, 1015(w) aromatic ring, 723(s) δ imide. ^{1}H NMR (pyridine-*d5*, δ ppm): 8.98–8.97(0.3H), 8.18–8.04 (6.2H), 7.93–7.90 (3.2H), 7.33–7.30 (3.2H).

6FDA-6ODA-4DABA FTIR (film, cm^{-1}): 3494(vw) ν_{as} N–H, 3034(br, w) aromatic δ C–H, 1784(m) ν_{as} C=O, 1728(s) ν_s C=O, 1599(w) phenyl ring, 1502(s) phenyl ring, 1383 (br, m) ν C–N, 1300(m) ν_s CF_3, 1244(br, m) ν_{as} C–O–C, 1102(br, m) imide, 1015(w) aromatic ring, 721(m) δ imide. ^{1}H NMR (pyridine-*d5*, δ ppm): 8.98–8.97 (0.6H), 8.20–8.04 (6.4H), 7.92–7.89 (2.4H), 7.33–7.30 (2.4H).

6FDA-8ODA-2DAPy FTIR (film, cm^{-1}): 3494(vw) ν_{as} N–H, 3081(br, w) aromatic δ C–H, 1786(m) ν_{as} C=O, 1728(s) ν_s C=O, 1595(w) aromatic ring, 1502(s) aromatic ring, 1380(m) ν C–N, 1298(m) ν_s CF_3, 1243(br, m) ν_{as} C–O–C, 1113(br, m) imide, 1015(w) aromatic ring, 723(s) δ imide.

^{1}H NMR (pyridine-*d5*, δ ppm): 8.17–8.01 (6.3H), 7.93–7.90 (3.2H), 7.33–7.30 (3.2H), ~7.32 (theoretically 0.2H, overlapped).

6FDA-9ODA-1DAPy FTIR (film, cm^{-1}): 3493(vw) ν_{as} N–H, 3070(br, w) aromatic δ C–H, 1785(m) ν_{as} C=O, 1728(s) ν_s C=O, 1596(w) aromatic ring, 1501(s) aromatic ring, 1380(m) ν C–N, 1297(m) ν_s CF_3, 1245(br, m) ν_{as} C–O–C, 1113(br, m) imide, 1015(w) aromatic ring, 722(s) δ imide. ^{1}H NMR (pyridine-*d5*, δ ppm): 8.17–8.04 (6.2H), 7.93–7.90 (3.6H), 7.33–7.30 (3.6H), ~7.22 (theoretically 0.1H, overlapped).

6FDA-8ODA-2DANT FTIR (film, cm^{-1}): 3497(vw) ν_{as} N–H, 3075(br, w) aromatic δ C–H, 1786(m) ν_{as} C=O, 1728(s) ν_s C=O, 1599(w) aromatic ring, 1502(s) aromatic ring, 1381(m) ν C–N, 1298(m) ν_s CF_3, 1244(br, m) ν_{as} C–O–C, 1109(br, m) imide, 1015(w) aromatic ring, 723(s) δ imide. ^{1}H NMR (pyridine-*d5*, δ ppm): 8.49–8.44 (0.4H), 8.27–8.04 (6.4H), 7.93–7.90 (3.2H), 7.77–7.71 (0.3H), 7.33–7.30 (3.2H).

6FDA-9ODA-1DANT FTIR (film, cm^{-1}): 3491(w) ν_{as} N–H, 3070(br, w) aromatic δ C–H, 1785(m) ν_{as} C=O, 1729(s) ν_s C=O, 1598(w) aromatic ring, 1501(s) aromatic ring, 1378(m) ν C–N, 1297(m) ν_s CF_3, 1256(br, m) ν_{as} C–O–C, 1113(br, m) imide, 1015(w) aromatic ring, 722(s) δ imide. ^{1}H NMR (pyridine-*d5*, δ ppm): 8.49–8.44 (0.4H), 8.27–8.04 (6.4H), 7.93–7.90 (3.2H), 7.77–7.71 (0.3H), 7.33–7.30 (3.2H).

FTIR and NMR data for Chapter 7:

DABN FTIR (mull, cm^{-1}): 3466(w) ν_{as} N–H, 3378(w) ν_s N–H, 2231(w) ν C≡N, 1625(br, m) ν C≡N, 1573(m) phenyl ring (skeletal vibrations), 1293(w) ν C–N, 1027(m) ν_s C–O–C. ^{1}H NMR (DMSO-*d6*, δ ppm): 7.52 (t, J=9 Hz, 1H), 7.08 (t, 2H), 6.60 (d, J=9 Hz, 2H), 6.45 (d, J=9 Hz, 2H), 6.29 (m, 4H), 5.38 (s, 4H).

BABP FTIR (mull, cm^{-1}): 3473(w) ν_{as} N–H, 3370(w) ν_s N–H, 1634(m) ν C=O, 1592(br, m) phenyl ring (Skeletal vibrations), 1281(w) ν C–N, 1226(w) ν_{as} C–O–C.^{1}H NMR (DMSO-*d6*, δ ppm): 7.76 (d, J=9 Hz, 4H), 7.06 (m, 6H), 6.42 (d, J=6 Hz, 2H), 6.29 (s, 2H), 6.24 (d, J=9 Hz, 2H), 5.30 (s, 4H).

6FDA-8ODA-2DDS FTIR (film, cm^{-1}): 3490(vw) νas N-H, 3076(br, w) aromatic δ C–H, 1785(m) ν_{as} C=O, 1728(s) ν_s C=O, 1594(w) phenyl ring, 1502(s) phenyl ring, 1379 (m) ν C–N, 1299(m) ν_s CF_3, 1245(s) ν_{as} C–O–C, 1114(br, m) imide, 726(m) δ imide. ^{1}H NMR (pyridine-*d5*, *δ* ppm): 8.47–8.45 (0.8H), 8.17–8.04 (6.8H), 7.92–7.89 (3.2H), 7.33–7.30 (3.2H).

6FDA-6ODA-4DDS FTIR (film, cm^{-1}): 3494(vw) ν_{as} N–H, 3081(br, w) aromatic δ C–H, 1786(m) ν_{as} C=O, 1728(s) ν_s C=O, 1593(w) phenyl ring, 1502(s) phenyl ring, 1377 (s) ν C–N, 1331(vw) ν_{as} SO_2, 1298(m) ν_s CF_3, 1244(s) ν_{as} C–O–C, 1101(br, m) imide, 723(m) δ imide. ^{1}H NMR (pyridine-*d5*, *δ* ppm): 8.47–8.44 (1.6H), 8.17–8.04 (7.6H), 7.92–7.88 (2.4H), 7.33–7.30 (2.3H).

6FDA-8ODA-2BADS FTIR (film, cm^{-1}): 3493(vw) ν_{as} N–H, 3070(br, w) aromatic δ C–H, 1785(m) ν_{as} C=O, 1727(s) ν_s C=O, 1584(w) phenyl ring, 1501(s) phenyl ring, 1380(m) ν C–N, 1298(m) ν_s CF_3, 1245(m) ν_{as} C–O–C, 1106(m) imide, 722(m) δ imide. ^{1}H NMR (pyridine-*d5*, *δ* ppm): 8.20–8.04 (6.8H), 7.93–7.90 (3.2H), 7.79–7.76 (0.4H), 7.71 (0.3H), 7.64–7.61 (0.8H), 7.33–7.30 (3.2H), 7.18 (0.8H).

6FDA-6ODA-4BADS FTIR (film, cm^{-1}): 3493(vw) ν_{as} N–H, 3074(br, w) aromatic δ C–H, 1785(m) ν_{as} C=O, 1727(s) ν_s C=O, 1584(w) phenyl ring, 1501(s) phenyl ring, 1380(m) ν C–N, 1326(vw) ν_{as} SO_2, 1297(m) ν_s CF_3, 1245 (s) ν_{as} C–O–C, 1106(m) imide, 722(m) δ imide. ^{1}H NMR (pyridine-*d5*, *δ* ppm): 8.19–8.01 (7.6H), 7.92–7.88 (2.4H), 7.79–7.76 (0.7H), 7.71 (0.6H), 7.64–7.61 (0.8H), 7.33–7.30 (2.4H), 7.18 (2.4H).

6FDA-8ODA-2MDA FTIR (film, cm^{-1}): 3494(vw) ν_{as} N–H, 3075(br, w) aromatic δ C–H, 2965(vw) ν_{as} CH_2, 1784(m) ν_{as} C=O, 1726(s) ν_s C=O, 1597(w) phenyl ring, 1502(s) phenyl ring, 1379(m) ν C–N, 1298(m) ν_s CF_3, 1246(br, s) ν_{as} C–O–C, 1112(br, m) imide, 723(m) δ imide. ^{1}H NMR (pyridine-*d5*, *δ* ppm): 8.17–8.04 (6.0H), 7.92–7.90 (3.2H), 7.85–7.82 (0.8H), 7.49–7.46 (0.8H), 7.33–7.30 (3.2H), 4.09 (0.4H).

6FDA-6ODA-4MDA FTIR (film, cm^{-1}): 3492(w) ν_{as} N–H, 3071(br, w) aromatic δ C–H, 2873(vw) ν_s CH_2, 1784(m) ν_{as} C=O, 1728(s) ν_s C=O, 1598(w) phenyl ring, 1502(s) phenyl ring, 1377(s) ν C–N, 1300(m) ν_s CF_3, 1260(br, s) ν_{as} C–O–C, 1095(br, m) imide, 723(m) δ imide. ^{1}H NMR (pyridine-*d5*, *δ* ppm): 8.17–8.04 (6.1H), 7.92–7.90 (2.4H), 7.85–7.82 (1.6H), 7.49–7.46 (1.6H), 7.33–7.30 (2.4H), 4.09 (0.7H).

6FDA-8ODA-2BABP FTIR (film, cm^{-1}): 3494(vw) ν_{as} N–H, 3073(br, w) aromatic δ C–H, 1784(m) ν_{as} C=O, 1728(s) ν_s C=O, 1658(m) ν C=O ketonic, 1589(m) phenyl ring, 1502(s) phenyl ring, 1379 (m) ν C–N, 1300(m) ν_s CF_3, 1246(s) ν_{as} C–O–C, 1112(br, m) imide, 721(m) δ imide. ^{1}H

NMR (pyridine-*d5*, *δ* ppm): 8.17–8.01 (6.0H), 7.96–7.89 (4.0H), 7.79–7.77 (0.8H), 7.66–7.63 (0.4H), 7.33–7.30 (3.5H), 7.24 (0.8H).

6FDA-6ODA-4BABP FTIR (film, cm^{-1}): 3493(vw) ν_{as} N–H, 3074(br, m) aromatic δ C–H, 1785(m) ν_{as} C=O, 1727(s) ν_{s} C=O, 1655(m) ν C=O ketonic, 1583(s) phenyl ring, 1501(s) phenyl ring, 1378(s) ν C–N, 1302(m) ν_{s} CF_3, 1243(s) ν_{as} C–O–C, 1102(br, m) imide, 726(m) δ imide. ^{1}H NMR (pyridine-*d5*, *δ* ppm): 8.17–8.01 (6H), 7.96–7.88 (4H), 7.79–7.78 (1.5H), 7.68–7.63 (0.8H), 7.33–7.30 (3.2H), 7.24 (1.5H).

6FDA-8ODA-2DABN FTIR (film, cm^{-1}): 3494(vw) ν_{as} N–H, 3075(br, w) aromatic δ C–H, 2231(w) ν C≡N, 1785(m) νas C=O, 1728(s) νs C=O, 1626(w) ν C≡N, 1602(br, m) phenyl ring, 1502(s) phenyl ring, 1381(s) ν C–N, 1298(m) ν_{s} CF_3, 1249(s) ν_{as} C–O–C, 1114(br, m) imide, 723(m) δ imide. ^{1}H NMR (pyridine-*d5*, *δ* ppm): 8.17–8.04 (6.0H), 7.92–7.82 (4.0H), 7.67–7.65 (0.4H), 7.38–7.30 (3.8H), 6.73–6.70 (0.4H).

6FDA-6ODA-4DABN FTIR (film, cm^{-1}): 3494(vw) ν_{as} N–H, 3071(br, w) aromatic δ C–H, 2232(w) ν C≡N, 1786(m) ν_{as} C=O, 1728(s) ν_{s} C=O, 1626(w) ν C≡N, 1604(br, m) phenyl ring, 1502(s) phenyl ring, 1378(m) ν C–N, 1298(m) ν_{s} CF_3, 1246(s) ν_{as} C–O–C, 1103(br, m) imide, 721(m) δ imide. ^{1}H NMR (pyridine-*d5*, *δ* ppm): 8.17-8.01 (6.0H), 7.92–7.82 (4.0H), 7.67–7.62 (0.8H), 7.38–7.30 (3.6H), 6.73–6.70 (0.8H).

FTIR and NMR data for Chapter 8:

6FDA-MDA FTIR (film, cm^{-1}): 3488(vw) ν_{as} N–H, 3054(br, w) aromatic δ C–H, 2980(w) ν_{as} CH_2, 2865(vw) ν_{s} CH_2, 1784(m) ν_{as} C=O, 1726(s) ν_{s} C=O, 1624(br, w) phenyl ring, 1514(s) phenyl ring, 1435(m) δ CH_2, 1377(m) ν C–N, 1298(m) ν_{s} CF_3, 1257(m) ν C–N amide, 1103(br, m) imide, 723(m) δ imide. ^{1}H NMR (pyridine-*d5*, *δ* ppm): 8.13–8.01 (6.0H), 7.85–7.82 (4.0H), 7.49–7.46 (4.0H), 4.09 (1.9H). ^{19}F NMR (pyridine-*d5*, *δ* ppm): 61.48.

6FDA-8MDA-2DBSA FTIR (film, cm^{-1}): 3493(vw) ν_{as} N–H, 3039(br, w) aromatic δ C–H, 2980(w) ν_{as} CH_2, 2868(vw) ν_{s} CH_2, 1784(m) ν_{as} C=O, 1726(s) ν_{s} C=O, 1604(w) phenyl ring, 1514(s) phenyl ring, 1435(m) δ CH_2, 1375(m) ν C–N, 1298(m) ν_{s} CF_3, 1255(m) ν C–N amide, 1103(m) imide, 722(m) δ imide. ^{1}H NMR (pyridine-*d5*, *δ* ppm): 8.51 (0.1H), 8.13–8.01 (6.4H), 7.85–7.82 (3.2H), 7.49–7.46 (3.2H), 4.09 (1.5H).

6FDA-8MDA-2DAPy FTIR (film, cm^{-1}): 3493(vw) ν_{as} N–H, 3039(br, w) aromatic δ C–H, 2978(w) ν_{as} CH_2, 2860(vw) ν_s CH_2, 1784(m) ν_{as} C=O, 1728(s) ν_s C=O, 1593(w) phenyl ring, 1514(s) phenyl ring, 1433(m) δ CH_2, 1375(m) ν C–N, 1298(m) ν_s CF_3, 1255(m) ν C–N amide, 1101(m) imide, 721(m) δ imide. ^{1}H NMR (pyridine-*d5*, *δ* ppm): 8.21–8.01 (6.4H), 7.84–7.82 (3.2H), 7.48–7.46 (3.2H), ~7.32 (theoretically 0.2H, overlapped), 4.09 (1.5H).

6FDA-9MDA-1BTDA FTIR (film, cm^{-1}): 3491(vw) ν_{as} N–H, 3039(br, w) aromatic δ C–H, 2980(w) ν_{as} CH_2, 2854(w) ν_s CH_2, 1784(m) ν_{as} C=O, 1728(s) ν_s C=O, 1514(s) phenyl ring, 1435(m) δ CH_2, 1374(m) ν C–N, 1297(m) ν_s CF_3, 1257(m) ν C–N amide, 1097(m) imide, 723(m) δ imide. ^{1}H NMR (pyridine-*d5*, *δ* ppm): 8.48 (0.2H), 8.40–8.37 (0.2H), 8.13–8.01 (5.6H), 7.85–7.77 (4.0H), 7.49–7.46 (4.0H), 4.09 (1.9H).

6FDA-9MDA-1NTDA FTIR (film, cm^{-1}): 3494(vw) ν_{as} N–H, 3038(br, w) aromatic δ C–H, 2979(w) ν_{as} CH_2, 2853(br, w) ν_s CH_2, 1785(m) ν_{as} C=O, 1725(s) ν_s C=O, 1680(m) ν amide, 1580(w) aromatic ring, 1515(s) aromatic ring, 1437(m) δ CH_2, 1376(m) ν C–N, 1301(m) ν_s CF_3, 1256(m) ν C–N amide, 1102(br, m) imide, 722(m) δ imide. ^{1}H NMR (pyridine-*d5*, *δ* ppm): 8.93 (0.4H), 8.13–8.01 (5.4H), 7.84–7.82 (3.6H), 7.49–7.46 (4.0H), 4.09 (1.9H).

6FDA-9MDA-1BPADA FTIR (film, cm^{-1}): 3491(vw) ν_{as} N–H, 3036(br, w) aromatic δ C–H, 2981(w) ν_{as} CH_2, 2858(w) ν_s CH_2, 1782(m) ν_{as} C=O, 1726(s) ν_s C=O, 1626(br, w) phenyl ring, 1514(s) phenyl ring, 1435(m) δ CH_2, 1377(m) ν C–N, 1298(m) ν_s CF_3, 1256(m) ν C–N amide, 1096(br, m) imide, 723(m) δ imide. ^{1}H NMR (pyridine-*d5*, *δ* ppm): 8.13–8.11 (5.4H), 7.95–7.93 (0.2H), 7.85–7.82 (3.6H), 7.65–7.64 (0.2H), 7.49–7.40 (4.6H), 7.28–7.25 (0.4H), 4.09–4.06 (1.9H), 1.74 (0.6H).

FTIR and NMR data for Chapter 9:

BPADA-ODA FTIR (film, cm^{-1}): 3481(vw) ν_{as} N–H, 3061(br, w) aromatic δ C-H, 2976(m) ν_{as} CH_3, 2870(br, w) ν_s CH_3, 1776(m) ν_{as} C=O, 1716(s) ν_s C=O, 1599(br, m) phenyl ring, 1502(s) phenyl ring, 1444(m) ν_{as} CH_3, 1381(m) ν C–N, 1276(m) ν C–N amide, 1238(br, m) ν_{as} C–O–C, 1078(br, m) imide, 1014(m) aromatic δ C–H, 744(m) δ imide. ^{1}H NMR (pyridine-*d5*, *δ* ppm): 7.97–7.94 (1.9H), 7.77–7.74 (3.7H), 7.66–7.65 (2.0H), 7.48–7.41 (6.2H), 7.29–7.24 (4.0H), ~7.22 (theoretically 4H, overlapped), 1.75 (6.0H).

BPADA-8ODA-2DAPy FTIR (film, cm^{-1}): 3483(w) ν_{as} N–H, 3053(br, m) aromatic δ C–H, 2978(m) ν_{as} CH_3, 2854(br, w) ν_s CH_3, 1776(m) ν_{as} C=O, 1720(s) ν_s C=O, 1599(br, m) aromatic ring, 1502(br, s) aromatic ring, 1445(m) ν_{as} CH_3, 1381(m) ν C–N, 1278(m) ν C–N amide, 1242(br, m) ν_{as} C–O–C, 1068(br, m) imide, 1014(m) aromatic δ C–H, 744(m) δ imide. ^{1}H NMR (pyridine-*d5*, *δ* ppm): 7.97–7.87 (2.0H), 7.81–7.74 (3.6H), 7.66–7.65 (1.6H), 7.48–7.41 (6.2H), 7.29–7.24 (theoretically 7.2H, overlapped), 1.75 (6.4H).

BPADA-8ODA-2DABA FTIR (film, cm^{-1}): 3481(vw) ν_{as} N-–H, 3057(br, w) aromatic δ C–H, 2974(m) ν_{as} CH_3, 2868(br, w) ν_s CH_3, 1776(m) ν_{as} C=O, 1722(s) ν_s C=O, 1598(br, m) phenyl ring, 1504(br, s) phenyl ring, 1446(m) ν_{as} CH_3, 1381(m) ν C–N, 1276(m) ν C–N amide, 1242(br, m) ν_{as} C–O–C, 1078(br, m) imide, 1015(m) aromatic δ C–H, 744(m) δ imide. ^{1}H NMR (pyridine-*d5*, *δ* ppm): 8.83 (0.2H), 8.14–8.19 (0.1H), 7.97–7.94 (2.0H), 7.77–7.74 (3.2H), 7.66–7.65 (2.0H), 7.48–7.41 (6.6H), 7.29–7.24 (theoretically 7.2H, overlapped), 1.75 (6.4H).

BPADA-8ODA-2DBSA FTIR (film, cm^{-1}): 3481(vw) ν_{as} N–H, 3053(br, w) aromatic δ C–H, 2974(m) ν_{as} CH_3, 2872(br, w) ν_s CH_3, 1778(m) ν_{as} C=O, 1722(s) ν_s C=O, 1600(br, m) phenyl ring, 1502(br, s) phenyl ring, 1446(m) ν_{as} CH_3, 1379(m) ν C–N, 1276(m) ν C–N amide, 1240(br, m) ν_{as} C–O–C, 1078(br, m) imide, 1015(m) aromatic δ C–H, 744(m) δ imide. ^{1}H NMR (pyridine-*d5*, *δ* ppm): 8.28 (0.1H), 7.97–7.91 (1.9H), 7.84–7.81 (0.4H), 7.77–7.74 (3.1H), 7.66–7.63 (2.1H), 7.48–7.41 (6.1H), 7.29-7.24 (theoretically 7.1H, overlapped), 1.75 (6.0H).

BPADA-MDA FTIR (film, cm^{-1}): 3481(vw) ν_{as} N-H, 3039(br, w) aromatic δ C–H, 2976(m) ν_{as} CH_3, 2868(br, w) ν_s CH_3, 1776(m) ν_{as} C=O, 1716(s) ν_s C=O, 1601(br, m) phenyl ring, 1514(br, m) phenyl ring, 1446(m) ν_{as} CH_3, 1373(m) ν C–N, 1276(m) ν C–N amide, 1240(br, m) ν_{as} C–O–C, 1068(br, m) imide, 1015(m) aromatic δ C–H, 744(m) δ imide. ^{1}H NMR (pyridine-*d5*, *δ* ppm): 7.95–7.92 (2.0H), 7.71–7.68 (4.0H), 7.65–7.64 (1.9H), 7.46–7.37 (10.2H), 7.28–7.26 (theoretically 4H, overlapped), 4.02 (1.8H), 1.74 (6.1H).

BPADA-8MDA-2DAPy FTIR (film, cm^{-1}): 3481(vw) ν_{as} N–H, 3039(br, w) aromatic δ C–H, 2976(m) ν_{as} CH_3, 2860(br, w) ν_s CH_3, 1776(m) ν_{as} C=O, 1722(s) ν_s C=O, 1599(br, m) aromatic ring, 1512(br, m) aromatic ring, 1445(m) ν_{as} CH_3, 1375(m) ν C–N, 1275(m) ν C–N amide, 1238(br, m) ν_{as} C–O–C, 1067(br, m) imide, 1015(m) aromatic δ C–H, 744(m) δ imide. ^{1}H NMR (pyridine-*d5*, *δ* ppm): 7.95–7.87 (2.0H), 7.81–7.78 (0.4H), 7.71–7.68 (3.2H), 7.64–7.63 (1.6H), 7.46–7.37 (9.6H), 7.28–7.24 (theoretically 4H, overlapped), 4.02 (1.5H), 1.74 (6.2H).

Appendix D

Linear Moiety Contribution Method for Gas Selectivity

The empirical linear moiety contribution method was proposed to calculate the contribution of moieties to the selectivities towards O_2/N_2, H_2/N_2, He/N_2 and CO_2/N_2. The least squares regression was applied to obtain the moiety contribution factors.

The regression model is described with matrix notation as follows

$$Y = X\delta + \varepsilon \tag{D-1}$$

The least-square estimator for δ is shown as follows:

$$\hat{\delta} = (X^T X)^{-1} X^T Y \tag{D-2}$$

Matrix D-1 Y_1 is the matrix of permeance ratios (group 1), and Matrix D-2 X_1 is the molar ratios of monomer moieties (group 1). The moiety contribution factors for permeance ratios (group 1) can be calculated as Matrix D-3 $\hat{\delta}_1$.

Matrix D-1 Permeance ratios (group 1)

Experimental data $Y_1 =$	α_{O_2/N_2}	α_{He/N_2}	α_{H_2/N_2}	α_{CO_2/N_2}
6FDA-ODA	5.1	44.9	35.5	52.0
6FDA-8ODA-2DBSA	5.5	43.3	38.8	54.3
6FDA-6ODA-4DBSA	6.0	85.0	63.9	40.2
6FDA-9ODA-1DAPy	3.6	21.8	18.8	42.5
6FDA-8ODA-2DAPy	4.5	67.6	50.2	38.1
6FDA-8ODA-2MDA	4.1	24.1	22.7	44.1
6FDA-6ODA-4MDA	4.8	55.0	48.6	35.3
6FDA-MDA	5.1	49.4	40.1	48.0
6FDA-8MDA-2DBSA	5.2	37.5	41.2	33.3
6FDA-8MDA-2DAPy	4.4	48.9	37.7	43.2

Matrix D-2 Molar ratios of monomer moieties (group 1)

$X_1 =$	6FDA	ODA	DBSA	DAPy	MDA
6FDA-ODA	1	1	0	0	0
6FDA-8ODA-2DBSA	1	0.8	0.2	0	0
6FDA-6ODA-4DBSA	1	0.6	0.4	0	0
6FDA-9ODA-1DAPy	1	0.9	0	0.1	0
6FDA-8ODA-2DAPy	1	0.8	0	0.2	0
6FDA-8ODA-2MDA	1	0.8	0	0	0.2
6FDA-6ODA-4MDA	1	0.6	0	0	0.4
6FDA-MDA	1	0	0	0	1
6FDA-8MDA-2DBSA	1	0	0.2	0	0.8
6FDA-8MDA-2DAPy	1	0	0	0.2	0.8

Matrix D-3 Moiety contribution factors for permeance ratios (group 1)

$\hat{\delta}_1 = (X_1{}^T X_1)^{-1} X_1{}^T Y_1 =$	α_{O_2/N_2}	α_{He/N_2}	α_{H_2/N_2}	α_{CO_2/N_2}
6FDA	3.6	36.4	29.4	33.8
ODA	0.6	–2.7	–0.4	9.6
DBSA	5.9	101.2	79.5	13.2
DAPy	–2.9	58.8	20.7	–28.4
MDA	1.7	5.1	9.7	12.1

The permeance ratios (group 2) are presented as Matrix D-4. From least squares regression, the moiety contribution factors (group 2) for permeance ratios can be calculated as Matrix D-5.

Matrix D-4 Permeance ratios (group 2)

Experimental data	α_{O_2/N_2}	α_{He/N_2}	α_{H_2/N_2}	α_{CO_2/N_2}
6FDA-9ODA-1DANT	4.8	37.1	32.2	55.6
6FDA-8ODA-2DANT	4.7	27.6	24.8	61.9
6FDA-8ODA-2DABA	5.7	68.9	75.4	51.7
6FDA-6ODA-4DABA	7.3	74.3	21.5	35.2
6FDA-8ODA-2DDS	3.6	19.0	17.4	50.1
6FDA-6ODA-4DDS	3.4	18.3	16.3	47.4
6FDA-8ODA-2BADS	4.0	25.5	25.1	40.0
6FDA-6ODA-4BADS	4.2	26.0	21.8	40.2
6FDA-8ODA-2BABP	3.6	19.7	18.7	46.7
6FDA-6ODA-4BABP	5.7	71.5	54.9	40.2
6FDA-8ODA-2DABN	5.3	32.4	33.3	60.7
6FDA-6ODA-4DABN	5.7	60.1	44.8	55.3
6FDA-10MDA-1BTDA	4.2	17.1	17.7	49.3
6FDA-10MDA-1NTDA	3.9	36.7	26.6	54.9
6FDA-10MDA-1BPADA	4.8	46.3	35.5	72.5

Matrix D-5 Moiety contribution factors for permeance ratios (group 2)

Moiety	α_{O_2/N_2}	α_{He/N_2}	α_{H_2/N_2}	α_{CO_2/N_2}
DANT	3.6	–20.5	–10.6	108.0
DABA	8.2	113.6	31.1	1.5
DDS	–1.7	–48.3	–37.3	24.3
BADS	0.3	–26.4	–18.6	–0.2
BABP	2.9	58.8	41.2	6.5
DABN	4.6	48.7	35.6	50.7
BTDA	–6.9	–207.4	–184.1	67.4
NTDA	–9.9	–11.4	–95.1	123.4
BPADA	–0.9	84.6	–6.1	299.4

Appendix E

Linear Moiety Contribution Method for Total Flux in Pervaporation

Y_2 is the matrix of *concentration coefficients* (group 1) and activation energies (group 1). Calculated from Matrix E-1 Y_2 and Matrix D-2 X_1, the moiety contribution factors for *concentration coefficients* (group 1) and activation energies (group 1) can be calculated as Matrix E-2 $\hat{\delta}_2$.

Matrix E-1 Concentration coefficients (group 1) and activation energies for water permeation and total flux (group 1)

Experimental data $Y_2 =$	E_p (pure water) (kJ/mol)	E_p (total flux) (kJ/mol)	n
6FDA-ODA	15.7	46.1	0.22
6FDA-8ODA-2DBSA	17.7	40.9	0.37
6FDA-6ODA-4DBSA	36.1	37.4	0.39
6FDA-9ODA-1DAPy	31.9	49.4	0.33
6FDA-8ODA-2DAPy	34.0	55.6	0.37
6FDA-8ODA-2MDA	26.6	38.5	0.31
6FDA-6ODA-4MDA	30.0	48.7	0.41
6FDA-MDA	36.0	39.8	0.27
6FDA-8MDA-2DBSA	35.6	33.7	0.33
6FDA-8MDA-2DAPy	62.7	44.1	0.34

Matrix E-2 Moiety contribution factors for concentration coefficients and activation energies for water permeation and total flux (group 1)

$\hat{\delta}_2 = (X_1^T X_1)^{-1} X_1^T Y_2 =$	E_p (pure water) (kJ/mol)	E_p (total flux) (kJ/mol)	n
6FDA	24.1	35.6	0.25
ODA	–6.7	7.1	0.03
DBSA	33.0	0.7	0.37
DAPy	98.0	27.0	0.18
MDA	16.9	6.3	0.07

Matrix E-3 Concentration coefficients and activation energies (group 2)

Experimental data	E_p (pure water) (kJ/mol)	E_p (total flux) (kJ/mol)	n
6FDA-9ODA-1DANT	15.2	34.4	0.32
6FDA-8ODA-2DANT	12.7	30.1	0.36
6FDA-8ODA-2DABA	28.6	53.6	0.35
6FDA-6ODA-4DABA	32.1	59.6	0.44
6FDA-8ODA-2DDS	21.6	36.2	0.50
6FDA-6ODA-4DDS	21.6	34.0	0.60
6FDA-8ODA-2BADS	16.8	30.8	0.37
6FDA-6ODA-4BADS	19.5	38.7	0.44
6FDA-8ODA-2BABP	22.1	39.1	0.27
6FDA-6ODA-4BABP	30.0	49.1	0.41
6FDA-8ODA-2DABN	27.8	41.9	0.28
6FDA-6ODA-4DABN	30.3	43.5	0.30
6FDA-10MDA-1BTDA	29.2	32.8	0.28
6FDA-10MDA-1NTDA	34.9	34.2	0.22
6FDA-10MDA-1BPADA	32.3	34.5	0.25

Matrix E-4 Moiety contribution factors for concentration coefficients and activation energies of water permeation and total flux (group 2)

Moiety	E_p (pure water) (kJ/mol)	E_p (total flux) (kJ/mol)	n
DANT	–30.2	–60.3	0.41
DABA	33.7	51.6	0.41
DDS	5.7	–17.0	0.88
BADS	–3.3	–13.0	0.43
BABP	23.0	16.1	0.27
DABN	29.3	7.7	0.06
BTDA	–94.6	–55.8	–0.18
NTDA	–37.6	–41.8	–0.78
BPADA	–63.6	–38.8	–0.48

From Matrix E-3, moiety contribution factors (group 2) for *concentration coefficients* and activation energies can be obtained from least squares regression as Matrix E-4.

From the *concentration coefficients* and activation energies of BPADA-based membranes shown as Matrix E-5, The average moiety contribution factors for BPADA were obtained as Matrix E-6.

Matrix E-5 Concentration coefficients and activation energies for total flux of BPADA-based membranes

Experimental data	E_p (total flux) (kJ/mol)	n
BPADA-ODA	37.9	0.43
BPADA-8ODA-2DAPy	38.6	0.18
BPADA-8ODA-2DABA	52.1	0.41
BPADA-8ODA-2DBSA	45.7	0.34
BPADA-MDA	55.6	0.43
BPADA-8MDA-2DAPy	36.9	0.44

Matrix E-6 The average contribution factors of BPADA for concentration coefficients and activation energies of total flux

Moiety	E_p (total flux) (kJ/mol)	n
BPADA	35.0	0.30

Appendix F

Linear Moiety Contribution Method for Water Flux in Pervaporation

From the same method as shown in Appendix E, moiety contribution factors for *concentration coefficients* and activation energies of water flux can be calculated for group 1 as Matrix F-2 and for group 2 as Matrix F-4.

The average contribution factors of BPADA for *concentration coefficients* and activation energies of water flux can be obtained as Matrix F-6.

Matrix F-1 Concentration coefficients and activation energies of water flux (group 1)

Experimental data	E_p (water flux) (kJ/mol)	n
6FDA-ODA	45.6	0.23
6FDA-8ODA-2DBSA	39.9	0.42
6FDA-6ODA-4DBSA	37.5	0.39
6FDA-9ODA-1DAPy	48.6	0.36
6FDA-8ODA-2DAPy	55.4	0.38
6FDA-8ODA-2MDA	38.2	0.33
6FDA-6ODA-4MDA	49.3	0.44
6FDA-MDA	40.7	0.30
6FDA-8MDA-2DBSA	33.1	0.36
6FDA-8MDA-2DAPy	45.3	0.38

Matrix F-2 Moiety contribution factors for concentration coefficients and activation energies of water flux (group 1)

Moiety	E_p (water flux) (kJ/mol)	n
6FDA	35.6	0.27
ODA	6.8	0.03
DBSA	–0.1	0.37
DAPy	28.9	0.17
MDA	7.0	0.09

Matrix F-3 Concentration coefficients and activation energies of water flux (group 2)

Experimental data	E_p (water flux) (kJ/mol)	n
6FDA-9ODA-1DANT	33.8	0.35
6FDA-8ODA-2DANT	29.5	0.41
6FDA-8ODA-2DABA	53.2	0.4
6FDA-6ODA-4DABA	58.9	0.4
6FDA-8ODA-2DDS	35.3	0.53
6FDA-6ODA-4DDS	33.6	0.63
6FDA-8ODA-2BADS	30.5	0.38
6FDA-6ODA-4BADS	38.3	0.44
6FDA-8ODA-2BABP	39.3	0.27
6FDA-6ODA-4BABP	49.1	0.41
6FDA-8ODA-2DABN	41.5	0.28
6FDA-6ODA-4DABN	43.1	0.31
6FDA-10MDA-1BTDA	32.7	0.31
6FDA-10MDA-1NTDA	33.3	0.26
6FDA-10MDA-1BPADA	34.4	0.28

Matrix F-4 Moiety contribution factors for concentration coefficients and activation energies of water flux (group 2)

Moiety	E_p (water flux) (kJ/mol)	n
DANT	–61.7	0.55
DABA	50.7	0.32
DDS	–17.8	0.91
BADS	–13.2	0.38
BABP	17.2	0.21
DABN	7.4	0.02
BTDA	–63.1	–0.24
NTDA	–57.1	–0.74
BPADA	–46.1	–0.54

Matrix F-5 Concentration coefficients and activation energies of water flux

Experimental data	E_p (water flux) (kJ/mol)	n
BPADA-ODA	37.6	0.42
BPADA-8ODA-2DAPy	38.6	0.18
BPADA-8ODA-2DABA	52.2	0.41
BPADA-8ODA-2DBSA	45.9	0.34
BPADA-MDA	55.7	0.43
BPADA-8MDA-2DAPy	36.8	0.45

Matrix F-6 Contribution factors of BPADA for concentration coefficients and activation energies of water flux

Moiety	E_p (water flux) (kJ/mol)	n
BPA	34.9	0.29

Bibliography

Acros Organics (Thermo Fisher Scientific). FTIR data accessible in http://www.acros.com (2006).

Adrova, N.A., M.I. Bessonov, L.A. Laius, and A.P. Rudakov, eds., Polyimides, A New Class of Thermally Stable Polymers, translated by K. Gingold, ed. by A.M. Schiller, Thechnomic Publishing, Stamford, CT (1970).

Agherghinei, I., Thermogravimetry – analysis of the parameters of the DTG maximum, Thermochimica Acta, 285, 57–65 (1996).

Ahn, S.-M., J.-W. Ha, J.-H. Kim, Y.-T. Lee, and S.-B. Lee, Pervaporation of fluoroethanol/water and methacrylic acid/water mixtures through PVA composite membranes, Journal of Membrane Science, 247, 51–57 (2005).

Aitken, C.L., W.J. Koros, and D.R. Paul, Effect of structural symmetry on gas transport properties of polysulfones, Macromolecules, 25, 3424–3434 (1992).

Al-Masri, M., H.R. Kricheldorf, and D. Fritsch, New polyimides for gas separation. 1. Polyimides derived from substituted terphenylenes and 4,4'-(hexafluoroisopropylidene)diphthalic anhydride, Macromolecules, 32, 7853–7858 (1999).

Al-Masri, M., D. Fritsch, and H.R. Kricheldorf, New polyimides for gas separation. 2. Polyimides derived from substituted catechol bis(etherphthalic anhydride)s, Macromolecules, 33, 7127–7135 (2000).

Alentiev, A.Y., K.A. Loza, Y.P. Yampolskii, Development of the methods for prediction of gas permeation parameters of glassy polymers: Polyimides as alternating co-polymers, Journal of Membrane Science, 167, 91–106 (2000).

Alexy, P., D. Kachova, M. Krsiak, and D. Bakos, Poly(vinyl alcohol) stabilisation in thermoplastic processing, Polymer Degradation and Stability, 78, 413–421 (2002).

Allen, S.M., M. Fujii, V. Stannett, H.B. Hopfenberg, and J.L. Williams, The barrier properties of polyacrylonitrile, Journal of Membrane Science, 2, 153–163 (1977).

Almeida, E., M. Balmayore, and T. Santos, Some relevant aspects of the use of FTIR associated techniques in the study of surfaces and coatings, Progress in Organic Coatings, 44, 233–242 (2002).

Aminabhavi, T.M., B.V.K. Naidu, S. Sridhar, and R. Rangarajan, Pervaporation separation of water-isopropanol mixtures using polymeric membranes: modeling and simulation aspects, Journal of Applied Polymer Science, 95, 1143–1153 (2005).

Arndt, K.-F., A. Richter, S. Ludwig, J. Zimmermann, J. Kressler, D. Kuckling, and H.-J. Adler, Poly(vinyl alcohol)/poly(acrylic acid) hydrogels: FT-IR spectroscopic characterization of crosslinking reaction and work at transition point, Acta Polymerica, 50, 383–390 (1999).

Ayala, D., A.E. Lozano, J. de Abajo, C. Garcia-Perez, J.G. de la Campa, K.-V. Peinemann, B.D. Freeman, and R. Prabhakar, Gas separation properties of aromatic polyimides, Journal of Membrane Science, 215, 61–73 (2003).

Baker, R.W., Future directions of membrane gas separation technology, Industrial & Engineering Chemistry Research, 41, 1393–1411 (2002).

Baker, R.W., Membrane Technology and Applications (2nd ed.), John Wiley & Sons, Chichester, West Susses, England (2004).

Barton, A.F.M., CRC Handbook of Solubility Parameters and Other Cohesion Parameters (2nd ed.),CRC Press, Boca Raton, FL (1991).

Bessonov, M.I., M.M. Konton, V.V. Kudryavtsev, and L.A. Laius, Polyimides – Thermally Stable Polymers, Consultants Bureau, New York (1987).

Biduru, S., S. Sridhar, G.S. Murthy, and S. Mayor, Pervaporation of tertiary butanol/water mixtures through chitosan membranes cross-linked with toluylene diisocyanate, Journal of Chemical Technology and Biotechnology, 80, 1416–1424 (2005).

Binning, R.C., R.J. Lee, J.F. Jennings, and E.C. Martin, Separation of liquid mixtures by permeation, Industrial & Engineering Chemistry, 53, 45–50 (1961).

Blume, I., J.G. Wijmans, and R.W. Baker, The separation of dissolved organics from water by pervaporation, Journal of Membrane Science, 49, 253–286 (1990).

Broido, A., A simple, sensitive graphical method of treating thermogravimetric analysis data, Journal of Polymer Science Part A-2: Polymer Physics, 7, 1761–1773 (1969).

Cai, B.X., Polymer membranes for separating organic mixtures, Journal of Applied Polymer Science, 101, 1160–1164 (2006).

Cai, B., Y. Li, H. Ye, and C. Gao, Effect of separating layer in pervaporation composite membrane for MTBE/MeOH separation, Journal of Membrane Science, 194, 151–156 (2001).

Carraher, C.E., and G.G. Swift, eds., Functional Condensation Polymers, Kluwer Academic, New York (2002).

Chang, Y.-H., J.-H. Kim, S.-B. Lee, and H.W. Rhee, Polysiloxaneimide membranes for removal of VOCs from water by pervaporation, Journal of Applied Polymer Science, 77, 2691–2702 (2000).

Chang, B.-J., Y.-H. Chang, D.-K. Kim, J.-H. Kim, and S.-B. Lee, New copolyimide membranes for the pervaporation of trichloroethylene from water, Journal of Membrane Science, 248, 99–107 (2005).

Chen, J.H., Q.L. Liu, X.H. Zhang, and Q.G. Zhang, Pervaporation and characterization of chitosan membranes cross-linked by 3-aminopropyltriethoxysilane, Journal of Membrane Science, 292, 125–132 (2007).

Chiang, W.-Y., and C.-L. Chen, Separation of water–alcohol mixture by using polymer membranes 6. Water-alcohol pervaporation through terpolymer of PVA grafted with hydrazine reacted SMA, Polymer, 39, 2227–2233 (1998).

Chiang, W.-Y., and Y.-H. Lin, Properties of modified poly(vinyl alcohol) membranes prepared by the grafting of new polyelectrolyte copolymers for water–ethanol mixture separation, Journal of Applied Polymer Science, 86, 2854–2859 (2002).

Chiellini, E., A. Corti, S. D'Antone, and R. Solaro, Biodegradation of poly (vinyl alcohol) based materials, Progress in Polymer Science, 28, 963–1014 (2003).

Clement, R., A. Jonquieres, I. Sarti, M.F. Sposata, M.A.C. Teixidor, and P. Locho, Original structure–property relationships derived from a new modeling of diffusion of pure solvents through polymer membranes, Journal of Membrane Science, 232, 141–152 (2004).

Coleman, M.R., and W.J. Koros, Isomeric polyimides based on fluorinated dianhydrides and diamines for gas separation applications, Journal of Membrane Science, 50, 285–297 (1990).

Devi, D.A., B. Smitha, S. Sridhar, and T.M. Aminabhavi, Pervaporation separation of isopropanol/water mixtures through crosslinked chitosan membranes, Journal of Membrane Science, 262, 91–99 (2005).

De Bartolo, L., A. Gugliuzza, S. Morrelli, B. Cirillo, A. Gordano, and E. Drioli, Novel PEEK-WC membrane with low plasma protein affinity related to surface free energy parameters, Journal of Materials Science: Materials in Medicine, 15, 877–883 (2004).

Dong, Y., Y. Ruan, H. Wang, Y. Zhao, and D. Bi, Studies on glass transition temperature of chitosan with four techniques, Journal of Applied Polymer Science, 93, 1553–1558 (2004).

Du, R., A. Chakma, and X. Feng, Interfacially formed poly(N,N-dimethylaminoethyl methacrylate)/ polysulfone composite membranes for CO_2/N_2 separation, Journal of Membrane Science, 290, 19–28 (2007).

Duan, S., T. Kouketsu, S. Kazama, and K. Yamada, Development of PAMAM dendrimer composite membranes for CO_2 separation, Journal of Membrane Science, 283, 2–6 (2006).

Dunson, D.L., Synthesis and characterization of thermosetting polyimide oligomers for microelectronics packing, Ph.D. Dissertation, Virginia Polytechnic Institute and State University, Blacksburg, VT (2000).

Durmaz-Hilmioglu, N., A.E. Yildirim, A.S. Sakaoglu, and S. Tulbentci, Acetic acid dehydration by pervaporation, Chemical Engineering and Processing, 40, 263–267 (2001).

Fang, J., K. Tanaka, H. Kita, and K. Okamoto, Pervaporation properties of ethynyl-containing copolyimide membranes to aromatic/non-aromatic hydrocarbon mixtures, Polymer, 40, 3051–3059 (1999).

Fang, J., K. Tanaka, H. Kita, and K. Okamoto, Synthesis of thianthrene-5,5,10,10-tetraoxide-containing polyimides via Yamazaki–Higashi phosphorylation method and their pervaporation properties to aromatic/nonaromatic hydrocarbon mixtures, Journal of Polymer Science Part A: Polymer Chemistry, 38, 895–906 (2000).

Feger, C., M.M. Khojasteh, and J.E. McGrath, eds., Polyimides: Materials, Chemistry and Characterization, Elsevier, New York (1989).

Feng, X., and R.Y.M. Huang, Preparation and performance of asymmetric polyetherimide membranes for isopropanol dehydration by pervaporation, Journal of Membrane Science, 109, 165–172 (1996a).

Feng, X., and R.Y.M. Huang, Pervaporation with chitosan membranes. I. Separation of water from ethylene glycol by a chitosan/polysulfone composite membrane, Journal of Membrane Science, 116, 67–76 (1996b).

Feng, X., and R.Y.M. Huang, Liquid separation by membrane pervaporation: a review, Industrial & Engineering Chemistry Research, 36, 1048–1066 (1997).

Finch, C.A., Polyvinyl Alcohol, Properties and Applications, Wiley-Interscience, New York (1973).

Fox, T.G., Influence of diluent and of copolymer composition on the glass temperature of a polymer system, Bulletin of the American Physical Society, Series 2, 1–2, 123 (1956).

Freeman, B., and I. Pinnau, Separation of gases using solubility-selective polymers, Trends in Polymer Science, 5, 167–173 (1997).

Freger, V., E. Korin, J. Wisniak, and E. Korngold, Measurement of sorption in hydrophilic pervaporation: sorption modes and consistency of the data, Journal of Membrane Science, 164, 251–256 (2000).

Ge, J., Y. Cui, Y. Yan, and W. Jiang, The effect of structure on pervaporation of chitosan membrane, Journal of Membrane Science, 165, 75–81 (2000).

Gholap, S.G., J.P. Jog, and M.V. Badiger, Synthesis and characterization of hydrophobically modified poly(vinyl alcohol) hydrogel membrane, Polymer, 45, 5863–5873 (2004).

Gibbs, J.H., and E.A. DiMarzio, Nature of the glass transition and the glassy state, Journal of Chemical Physics, 28, 373–383 (1958).

Gilman, J.W., D.L. VanderHart, and T. Kashiwagi, Thermal decomposition chemistry of poly(vinyl alcohol), Fire and Polymers. II. Materials and Test for Hazard Prevention, ACS Symposium Series 599 (Chapter 11), 161–185 (1994).

Gimenez, V., A. Mantecon, and V. Cadiz, Modification of poly(vinyl alcohol) with acid chlorides and crosslinking with difunctional hardeners, Journal of Polymer Science Part A: Polymer Chemistry, 34, 925–934 (1996).

Gimenez, V., A. Mantecon, J.C. Ronda, and V. Cadiz, Poly(vinyl alcohol) modified with carboxylic acid anhydrides: crosslinking through carboxylic groups, Journal of Applied Polymer Science, 65, 1643–1651 (1997).

Gimenez, V., J.A. Reina, A. Mantecon, and V. Cadiz, Unsaturated modified poly(vinyl alcohol). Crosslinking through double bonds, Polymer, 40, 2759–2767 (1999).

Gohil, J.M., A. Bhattacharya, and P. Ray, Studies on the cross-linking of poly(vinyl alcohol), Journal of Polymer Research, 13, 161–169 (2006).

Good, R.J., and C.J. van Oss, The modern theory of contact angles and the hydrogen bond components of surface energies, in Modern Approach to Wettability: Theory and Applications, ed. by M.E. Schrader and G. Loeb, Plenum Press, New York (1991).

Gref, R., Q.T. Nguyen, P. Schaetzel, and J. Neel, Transport properties of poly(vinyl alcohol) membranes of different degrees of crystallinity. I. Pervaporation results, Journal of Applied Polymer Science, 49, 209–218 (1993).

Gu, Z.Y., P.H. Xue, and W.J. Li, Preparation of the porous chitosan membrane by cryogenic induced phase separation, Polymers for Advanced Technologies, 12, 665–669 (2001).

Guinesi, L.S., and E.T.G. Cavalheiro, The use of DSC curves to determine the acetylation degree of chitin/chitosan samples, Thermochimica Acta, 444, 128–133 (2006).

Guo, Q., H. Ohya, and Y. Negishi, Investigation of the permselectivity of chitosan membrane used in pervaporation separation II. Influences of temperature and membrane thickness, Journal of Membrane Science, 98, 223–232 (1995).

Guo, W.F., and T.-S. Chung, Study and characterization of the hysteresis behavior of polyimide membranes in the thermal cycle process of pervaporation separation Journal of Membrane Science, 253, 13–22 (2005).

Hao, J., K. Tanaka, H. Kita, and K. Okamoto, The pervaporation properties of sulfonyl-containing polyimide membranes to aromatic/aliphatic hydrocarbon mixtures, Journal of Membrane Science, 132, 97–108 (1997).

Heath, D.R., and J.G. Wirth, Aminophenoxy benzonitriles and their reaction products, Ger. Offen. (Patent) DE2202167 (1972).

Hegazy, E.-S.A., K.M. El-Salmawy, and A.A. El-Naggar, Recovery of heavy metals from aqueous solution by using radiation crosslinked poly(vinyl alcohol), Journal of Applied Polymer Science, 94, 1649–1656 (2004).

Heuchel, M., and D. Hofmann, Molecular modelling of polyimide membranes for gas separation, Desalination, 144, 67–72 (2002).

Hind, A.R., S.K. Bhargava, and A. McKinnon, At the solid/liquid interface: FTIR/ATR – the tool of choice, Advances in Colloid and Interface Science, 93, 91–114 (2001).

Hirai, T., T. Okinaka, S. Hayashi, Y. Amemiya, and K. Kobayashi, PH-induced structure change of poly(vinyl alcohol) hydrogel crosslinked with poly(acrylic acid), Angewandte Makromolekulare Chemie, 240, 213–219 (1996).

Hirayama, Y., T. Yoshinaga, Y. Kusuki, K. Ninomiya, T. Sakakibara, and T. Tamari, Relationship of gas permeability with structure of aromatic polyimides I, Journal of membrane Science, 111, 169–182 (1996a).

Hirayama, Y., T. Yoshinaga, Y. Kusuki, K. Ninomiya, T. Sakakibara, and T. Tamari, Relationship of gas permeability with structure of aromatic polyimides II, Journal of membrane Science, 111, 183–192 (1996b).

Ho, W.S.W., and K.K. Sirkar, eds., Membrane Handbook, Van Nostrand Reinhold, New York (1992).

Hodge, R.M., G.H. Edward, and G.P. Simon, Water absorption and states of water in semicrystalline poly(vinyl alcohol) films, Polymer, 37, 1371–1376 (1996a).

Hodge,R.M., T.J. Bastow, G.H. Edward, G.P. Simon, and A.J. Hill, Free volume and the mechanism of plasticization in water-swollen poly(vinyl alcohol), Macromolecules, 29, 8137–8143 (1996b).

Hoehn, H.H., Heat treatment of membranes of selected polyimides, polyesters and polyamides, US Patent 3,822,202 (1974).

Huang R.Y.M., ed., Pervaporation Membrane Separation Processes, Elsevier, Amsterdam, the Netherlands (1990).

Huang, R.Y.M., and J.-J. Shieh, Crosslinked blended poly(vinyl alcohol)/N-methylol nylon-6 membranes for the pervaporation separation of ethanol-water mixtures, Journal of Applied Polymer Science, 70, 317–327 (1998).

Huang, R.Y.M., and X. Feng, Pervaporation of water/ethanol mixtures by an aromatic polyetherimide membrane, Separation and Purification Technology, 27, 1583–1579 (1992).

Huang, R.Y.M., and X. Feng, Dehydration of isopropanol by pervaporation using aromatic polyetherimide membranes, Separation and Purification Technology, 28, 2035–2048 (1993a).

Huang, R.Y.M., and X. Feng, Resistance model approach to asymmetric polyetherimide membranes for pervaporation of isopropanol/water mixtures, Journal of Membrane Science, 84, 15–27 (1993b).

Huang, R.Y.M., R. Pal, and G.Y. Moon, Crosslinked chitosan composite membrane for the pervaporation dehydration of alcohol mixtures and enhancement of structural stability of chitosan/polysulfone composite membranes, Journal of Membrane Science, 160, 17–30 (1999).

Huang, R.Y.M., G.Y. Moon, and R. Pal, *N*-acetylated chitosan membranes for the pervaporation separation of alcohol/toluene mixtures, Journal of Membrane Science, 176, 223–231 (2000).

Huang, R.Y.M., G.Y. Moon, and R. Pal, Chitosan/anionic surfactant complex membranes for the pervaporation separation of methanol/MTBE and characterization of the polymer/surfactant system, Journal of Membrane Science, 184, 1–15 (2001a).

Huang, R.Y.M., P. Shao, X. Feng, and C.M. Burns, Pervaporation separation of water/isopropanol mixture using sulfonated poly(ether ether ketone) (SPEEK) membranes: transport mechanism and separation performance, Journal of Membrane Science, 192, 115–127 (2001b).

Hwang, S.T., and K. Kammermeyer, Membranes in Separation, Vol. III of Techniques of Chemistry, ed. by A. Weissberger, R.E. Krieger Publishing, Malabar, FL (1984).

Hyun, S.H., J.K. Song, B.I. Kwak, J.H. Kim, and S.A. Hong, Synthesis of ZSM-5 zeolite composite membranes for CO_2 separation, Journal of Membrane Science, 34, 3095–3105 (1999).

Isiklan, N., and O. Sanli, Separation characteristics of acetic acid–water mixtures by pervaporation using poly(vinyl alcohol) membranes modified with malic acid, Chemical Engineering and Processing, 44, 1019–1027 (2005).

Islam, M.N., W. Zhou, T. Honda, K. Tanaka, H. Kita, and K. Okamoto, Preparation and gas separation performance of flexible pyrolytic membranes by low-temperature pyrolysis of sulfonated polyimides, Journal of Membrane Science, 261, 17–26 (2005).

Ito, A., M. Sato, and T. Anma, Permeability of CO_2 through chitosan membrane swollen by water vapor in feed gas, Die Angewandte Makromolekulare Chemie, 248, 85–94 (1997).

Jang, J., and D.K. Lee, Plasticizer effect on the melting and crystallization behavior of polyvinyl alcohol, Polymer, 44, 8139-8143 (2003).

Javaid, A., Membranes for solubility-based gas separation applications, Chemical Engineering Journal, 112, 219–226 (2005).

Jegal, J., and K.-H. Lee, Chitosan membranes crosslinked with sulfosuccinic acid for the pervaporation separation of water/alcohol mixtures, Journal of Applied Polymer Science, 71, 671–675 (1999).

Jia, L., and J. Xu, A simple method for prediction of gas permeability of polymers from their molecular structure, Polymer Journal, 23, 1–6 (1991).

Jiraratananon, R., A. Chanachai, R.Y.M. Huang, and D. Uttapap, Pervaporation dehydration of ethanol–water mixtures with chitosan/hydroxyethylcellulose (CS/HEC) composite membranes: I. Effect of operating conditions, Journal of Membrane Science, 195, 143–151 (2002a).

Jiraratananon, R., A. Chanachai, and R.Y.M. Huang, Pervaporation dehydration of ethanol-water mixtures with chitosan/hydroxyethylcellulose (CS/HEC) composite membranes: II. Analysis of mass transport, Journal of Membrane Science, 199, 211–222 (2002b).

Jonquieres, A., D. Roizard, J. Cuny, A. Vicherat, and P. Lochon, Polarity measurements in block copolymers (polyurethaneimides) and correlation with their pervaporation features, Journal of Applied Polymer Science, 56, 1567–1579 (1995).

Jonquieres, A., R. C1ement, D. Roizard, and P. Lochon, Pervaporative transport modelling in a ternary system: ethyltertiarybutylether/ethanol/polyurethaneimide, Journal of Membrane Science, 109, 65–76 (1996a).

Jonquieres, A., D. Roizard, J. Cuny, and P. Lochon, Solubility and polarity parameters for assessing pervaporation and sorption properties. A critical comparison for tertiary systems alcohol/ether/ polyurethaneimide, Journal of Membrane Science, 121, 117–133 (1996b).

Jonquieres, A., D. Roizard, and P. Lochon, Polymer design for pervaporation membranes: Influence of the soft segment size of block copolymers (polyurethaneimides or polyureaimides) on their pervaporation features, Journal of Membrane Science, 118, 73–94 (1996c).

Jonquieres, A., C. Dole, R. Clement, and P. Lochon, Synthesis and characterization of new highly permeable polyamideimides from dianhydride monomers containing amide functions: An application to the purification of a fuel octane enhancer (ETBE) by pervaporation, Journal of Polymer Science Part A: Polymer Chemistry, 38, 614–630 (2000).

Jonquieres, A., R. Clement, and P. Lochon, New film-forming poly(urethane-amide-imide) block copolymers: Influence of soft block on membrane properties for the purification of a fuel octane enhancer by pervaporation, European Polymer Journal, 41, 783–795 (2005).

Kaba, M., N. Raklaoui, M.-F. Guimon, and A. Mas, Improvement of the water selectivity of ULTEM poly(ether imide) pervaporation films by an allylamine-plasma-polymerized layer, Journal of Applied Polymer Science, 97, 2088–2096 (2005).

Kang, Y.S., B. Jung, and U.Y. Kim, Pervaporation of water/ethanol mixture through hydrophilically modified polyimide membrane, Molecular Crystals and Liquid Crystals, 224, 137–146 (1993).

Kariduraganavar, M.Y., S.S. Kulkarni, and A.A. Kittur, Pervaporation separation of water-acetic acid mixtures through poly(vinyl alcohol)-silicone based hybrid membranes, Journal of Membrane Science, 246, 83–93 (2005).

Katarzynski, D., and C. Staudt-Bickel, Separation of multi component aromatic/aliphatic mixtures by pervaporation with copolyimide membranes, Desalination, 189, 81–86 (2006).

Kazama, S., T. Teramoto, and K. Haraya, Carbon dioxide and nitrogen transport properties of bis(phenyl)fluorene-based cardo polymer membranes, Journal of Membrane Science, 207, 91–104 (2002).

Kim, S., and J.K. Park, Characterization of thermal reaction by peak temperature and height of DTG curves, Thermochimica Acta. 264, 137–156 (1995).

Kim, T.H., W.J. Koros, G.R. Husk, and K.C. O'Brien, Relationship between gas separation properties and chemical structure in a series of aromatic polyimides, Journal of Membrane Science, 37, 45–62 (1988).

Kim, K.W., S.C. Choi, S.S. Kim, S.J. Cho, and C.N. Whang, Synthesis of crystalline polyimide film by ionized cluster-beam deposition, Journal of Materials Science, 28, 1537–1541 (1993a).

Kim, Y.J., T.E. Glass, G.D. Lyle, and J.E. McGrath, Kinetic and mechanistic investigations of the formation of polyimides under homogeneous conditions, Macromolecules, 26, 1344–1358 (1993b).

Kim, J.-H., B.-J. Chang, S.-B. Lee, and S.Y. Kim, Incorporation effect of fluorinated side groups into polyimide membranes on their pervaporation properties, Journal of Membrane Science, 16, 185–196 (2000a).

Kim, J.H., K.-H. Lee, and S.Y. Kim, Pervaporation separation of water from ethanol through polyimide composite membranes, Journal of Membrane Science, 169, 81– 93 (2000b).

Kim, Y.K., H.B. Park, and Y.M. Lee, Synthesis and characterization of metal-containing sulfonated polyimide membranes and their gas separation properties, Desalination, 145, 389–392 (2002).

Kim, J.H., E.J. Moon, and C.K. Kim, Composite membranes prepared from poly(m-aminostyrene-co-vinyl alcohol) copolymers for the reverse osmosis process, Journal of Membrane Science, 216, 107–120 (2003).

Kim, Y.-H., H.-S. Kim, and S.-K. Kwon, Synthesis and characterization of highly soluble and oxygen permeable new polyimides based on twisted biphenyl dianhydride and spirobifluorene diamine, Macromolecules, 38, 7950–7956 (2005).

Kober, P.A., Pervaporation, perstillation and percrystallization, Journal of Membrane Science, 100, 61–64 (1995).

Koros, W.J., Gas separation membranes: Needs for combined materials science and processing approaches, Macromolecular Symposia, 188, 13–22 (2002).

Koros, W.J., and G.K. Fleming, Membrane-based gas separation, Journal of Membrane Science, 83, 1–80 (1993).

Kouketsu, T., S. Duan, T. Kai, Shingo Kazama, and K. Yamada, PAMAM dendrimer composite membrane for CO_2 separation: Formation of a chitosan gutter layer, Journal of Membrane Science, 287, 51–59 (2007).

Krajewska, B., Membrane-based processes performed with use of chitin/chitosan materials, Separation and Purification Technology, 41, 305–312 (2005).

Krasemann, L., and B. Tieke, Composite membranes with ultrathin separation layer prepared by self-assembly of polyelectrolytes, Materials Science and Engineering C: Biomimetic and Supramolecular Systems, 8-9, 513–518 (1999).

Krea, M., D. Roizard, N. Moulai-Mostefa, and D. Sacco, New copolyimide membranes with high siloxane content designed to remove polar organics from water by pervaporation, Journal of Membrane Science, 241, 55–64 (2004).

Krumova, M., D. Lopez, R. Benavente, C. Mijangos, and J.M. Perena, Effect of crosslinking on the mechanical and thermal properties of poly(vinyl alcohol), Polymer, 41, 9265–9272 (2000).

Kumeta, K., and I. Nagashima, Crosslinking reaction of poly(vinyl alcohol) with poly(acrylic acid) (PAA) by heat treatment: effect of neutralization of PAA, Journal of Applied Polymer Science, 90, 2420–2427 (2003).

Kuznicki, S.M., T.W. Langner, J.S. Curran, and V.A. Bell, Macroporaus aluminosilicate desiccant, preparation from sodalite and use in enthalpy energy wheels, US Patent 6,379,436, (2002).

Lai, J.Y., S.-H. Li, and K.-R. Lee, Permselectivities of polysiloxaneimide membrane for aqueous ethanol mixture in pervaporation, Journal of Membrane Science 93, 273–282 (1994).

Lee, C.H., Theory of reverse osmosis and some other membrane permeation operations, Journal of Applied Polymer Science, 19, 83–95 (1975).

Lee C.H., and W.H. Hong, Influence of different degrees of hydrolysis of poly(vinyl alcohol) membrane on transport properties in pervaporation of IPA/water mixture, Journal of Membrane Science, 135, 187–193 (1997).

Lee, Y.M., D. Bourgeois, and G. Belfort, Sorption, diffusion, and pervaporation of organics in polymer membranes, Journal of Membrane Science, 44, 161–181 (1989).

Lee, Y.M., S.Y. Nam, and D.J. Woo, Pervaporation of ionically surface crosslinked chitosan composite membranes for water-alcohol mixtures, Journal of Membrane Science, 133, 103–110 (1997).

Lehermeier, H.J., J.R. Dorgan, and J.D. Way, Gas permeation properties of poly(lactic acid), Journal of Membrane Science, 190, 243–251 (2001).

Li, C.-L., and K.-R. Lee, Dehydration of ethanol/water mixtures by pervaporation using soluble polyimide membranes, Polymer International, 55, 505–512 (2006).

Li, Y., X. Wang, M. Ding, and J. Xu, Effects of molecular structure on the permeability and permselectivity of aromatic polyimides, Journal of Applied Polymer Science, 61, 741–748 (1996).

Li, B., G. Fan, T. He, and M. Ding, Gas separation with organo-soluble high performance aromatic polyimide films, Die Angewandte Makromolekulare Chemie, 253, 65–70 (1997).

Li, J., C. Chen, B. Han, Y. Peng, J. Zou, and W. Jiang, Laboratory and pilot-scale study on dehydration of benzene by pervaporation, Journal of Membrane Science, 203, 127–136 (2002).

Lin, H., and B.D. Freeman, Materials selection guidelines for membranes that remove CO_2 from gas mixtures, Journal of Molecular Structure, 739, 57–74 (2005).

Liu, Q.-L., and J. Xiao, Silicalite-filled poly(siloxane imide) membranes for removal of VOCs from water by pervaporation, Journal of Membrane Science, 230, 121–129 (2004).

Liu, Q., Z. Zhang, and H. Chen, Study on the coupling of esterification with pervaporation, Journal of Membrane Science, 182, 173–181 (2001).

Liu, L., A. Chakma, and X. Feng, A novel method of preparing ultrathin poly(ether block amide) membranes, Journal of Membrane Science, 235, 43–52 (2004).

Liu, R., X. Qiao, and T.-S. Chung, The development of high performance P84 co-polyimide hollowfibers for pervaporation dehydration of isopropanol, Chemical Engineering Science, 60, 6674–6686 (2005).

Liu, Y.-L., C.-H. Yu, K.-R. Lee, and J.Y. Lai, Chitosan/poly(tetrafluoroethylene) composite membranes using in pervaporation dehydration processes, Journal of Membrane Science, 287, 230–236 (2007).

Lukas, J., K. Richau, H.-H. Schwart, and D. Paul, Surface characterization of polyelectrolyte complex membranes based on sodium cellulose sulfate and various cationic components, Journal of Membrane Science, 131, 39–47 (1997).

Maier, G., Gas separation with polymer membranes, Angewandte Chemie International Edition, 37, 2960–2974 (1998).

Mallapragada, S.K., and N.A. Peppas, Dissolution mechanism of semicrystalline poly(vinyl alcohol) in water, Journal of Polymer Science Part B: Polymer Physics, 34, 1339–1346 (1996).

Mandal S., and V.G. Pangarkar, Effect of membrane morphology in pervaporative separation of isopropyl alcohol-aromatic mixtures – a thermodynamic approach to membrane selection, Journal of Applied Polymer Science, 90, 3912–3921 (2003).

Matsuura, T., Synthetic Membranes and Membrane Separation Processes, CRC Press, Boca Raton, FL (1994).

McDowell, W.H., and W.O. Kenyon, Some relationships between polyvinyl acetates and polyvinyl alcohols, Journal of the American Chemical Society, 62, 415–417 (1940).

McHattie, J.S., W.J. Koros, and D.R. Paul, Gas transport properties of polysulphones: 1. Role of symmetry of methyl group placement on bisphenol rings, Polymer, 32, 840–850 (1991).

McNeill, I.C., Thermal degradation mechanisms of some addition polymers and copolymers, Journal of Analytical and Applied Pyrolysis, 40-41, 21–41 (1997).

Metayer, M., and C.O. M'Bareck, Semi-interpenetrating networks (sIPN). Preparation of ion-exchange membranes, using a gaseous crosslinking reagent, Reactive and Functional Polymers, 33, 311–321 (1997).

Miranda, T.M., A.R. Goncalves, and M.P. Amorim, Ultraviolet-induced crosslinking of poly(vinyl alcohol) evaluated by principal component analysis of FTIR spectra, Polymer International, 50, 1068–1072 (2001).

Mittal, K.L., ed., Polyimides, Synthesis, Characterization, and Applications, Vol. 1, Plenum Press, New York (1984).

Moon, G.Y., Synthesis and preparation of polysaccharide based membranes for the pervaporation separation of liquid mixture systems of industrial interest, Ph.D. Dissertation, University of Waterloo, Waterloo, ON (2000).

Morisato, A., N.R. Miranda, B.D. Freeman, H.B. Hopfenberg, G. Costa, A. Grosso, and S. Russo, The influence of chain configuration and, in turn, chain packing on the sorption and transport properties of poly(tert-butyl acetylene), Journal of Applied Polymer Science, 49, 2065–2074 (1993).

Mulder, M, Basic Principles of Membrane Technology, Kluwer Academic Publishers, Dordrecht, Boston and London, (1991).

Muruganandam, N., W.J. Koros, and D.R. Paul, Gas sorption and transport in substituted polycarbonates, Journal of Polymer Science Part B: Polymer Physics, 25, 1999–2026 (1987).

Musale, D.A., A. Kumar, and G. Pleizier, Formation and characterization of poly(acrylonitrile)/ chitosan composite ultrafiltration membranes, Journal of Membrane Science, 154, 163–173 (1999).

Nabe, A., E. Staube, and G. Belfor, Surface modification of polysulfone ultrafiltration membranes and fouling by BSA solutions, Journal of Membrane Science, 133, 57–72 (1997).

Nakanishi, K., and P.H. Solomon, Infrared Absorption Spectroscopy, 2nd ed., Holden-Day Inc., San Francisco, CA (1977).

Nam, S.Y., and Y.M. Lee, Pervaporation of ethylene glycol–water mixtures: I. Pervaporation performance of surface crosslinked chitosan membranes, Journal of Membrane Science, 153, 155–162 (1999a).

Nam, S.Y., and Y.M. Lee, Pervaporation separation of methanol/methyl t-butyl ether through chitosan composite membrane modified with surfactants, Journal of Membrane Science, 157, 63–71 (1999b).

Nam, S.Y., H.J. Chun, and Y.M. Lee, Pervaporation separation of water-isopropanol mixture using carboxymethylated poly(vinyl alcohol) composite membranes, Journal of Applied Polymer Science, 72, 241–249 (1999).

Nawawi, M. G.M., and R.Y.M. Huang, Pervaporation dehydration of isopropanol with chitosan membranes, Journal of Membrane Science, 24, 53–62 (1997).

Niwa, M., S. Nagaoka, H. Kawakami, Preparation of novel fluorinated block copolyimide membranes for gas separation, Journal of Applied Polymer Science, 100, 2436–2442 (2006).

Oh, H.-K., K.-H. Song, K.-R. Lee, and J.-M. Rim, Prediction of sorption and flux of solvents through PDMS membrane, Polymer, 42, 6305–6312 (2001).

Ohya, H., V.V. Kudryavtsev, and S.I. Semenova, eds., Polyimide Membranes, Applications, Fabrications, and Properties, Gordon and Breach Publishers, Amsterdam, the Netherlands (1996).

Oikawa, E., K. Nozawa, T. Kaneko, and T. Aoki, Pervaporation of nonaqueous ethanol azeotropes through interpenetrating polymer network membranes prepared from poly(4-vinylpyridine) and poly(vinyl alcohol), Journal of Applied Polymer Science, 82, 2729–2738 (2001).

Okada, T., M. Yoshikawa, and T. Matsuura, A study on pervaporation of ethanol/water mixtures on the basis of pore flow model, Journal of Membrane Science, 59, 151–168 (1991).

Okamoto, K., N. Tanihara, H. Watanabe, K. Tanaka, H. Kita, A. Nakamura, Y. Kusuki, and K. Nakagawa, Vapor permeation and pervaporation separation of water-ethanol mixtures through polyimide membranes, Journal of Membrane Science, 68, 53–63 (1992).

Okamoto, K., H. Wang, T. Ijyuin, S. Fujiwara, K. Tanaka, and H. Kita, Pervaporation of aromatic/non-aromatic hydrocarbon mixtures through crosslinked membranes of polyimide with pendant phosphonate ester groups, Journal of Membrane Science, 157, 97–105 (1999).

Pandey, P., and R.S. Chauhan, Membranes for gas separation, Progress in Polymer Science, 26, 853–893 (2001).

Park, J.Y., and D.R. Paul, Correlation and prediction of gas permeability in glassy polymer membrane materials via a modified free volume based group contribution method, Journal of Membrane Science, 125, 23–39 (1997).

Park, H., R.M. Meertens, and M.H.V. Mulder, Sorption of alcohol-toluene mixtures in poly(acrylic acid)-poly(vinyl alcohol) blend membranes and its role on pervaporation, Industrial & Engineering Chemistry Research, 37, 4408–4417 (1998).

Park, J.-S., J.-W. Park, and E. Ruckenstein, On the viscoelastic properties of poly(vinyl alcohol) and chemically crosslinked poly(vinyl alcohol), Journal of Applied Polymer Science, 82, 1816–1823 (2001).

Paul, D.R., and Y.P. Yampol'skii, eds., Polymeric Gas Separation Membranes, CRC Press, Boca Raton, FL (2000).

Pawlish, C.A., A. Macris, and R.L. Laurence, Solute diffusion in polymers. 1. The use of capillary column inverse gas chromatography, Macromolecules, 20, 1564–1578 (1987).

Pawlish, C.A., J.R. Bric, and R.L. Laurence, Solute diffusion in polymers. 2. Fourier estimation of capillary column inverse gas chromatography data, Macromolecules, 21, 1685–1698 (1988).

Perry, J.D., K. Nagai, and W.J. Koros, Polymer Membranes for Hydrogen Separations, MRS Bulletin, 31, 745–749 (2006).

Peters, T.A., C.H.S. Poeth, N.E. Benes, H.C.W.M. Buijs, F.F. Vercauteren, and J.T.F Keurentjes, Ceramic-supported thin PVA pervaporation membranes combining high flux and high selectivity; contradicting the flux-selectivity paradigm, Journal of Membrane Science, 276, 42–50 (2006).

Pinel, E., D. Brown, C. Bas, R. Mercier, N.D. Alberola, and S. Neyertz, Chemical Influence of the Dianhydride and the Diamine structure on a series of copolyimides studied by molecular dynamics simulations, Macromolecules, 35, 10198–10209 (2002).

Piroux, F., E. Espuche, R. Mercier, and M. Pineri, Sulfonated copolyimides: Influence of structural parameters on gas separation properties, Desalination, 145, 371–374 (2002a).

Piroux, F., E. Espuche, R. Mercier, M. Pineri, and G. Gebel, Gas transport mechanism in sulfonated polyimides Consequences on gas selectivity, Journal of Membrane Science, 209, 241–253 (2002b).

Piroux, F., E. Espuche, R. Mercier, The effects of humidity on gas transport properties of sulfonated copolyimides, Journal of Membrane Science, 232, 115–122 (2004).

Pithan, F., and C. Staudt-Bickel, Crosslinked copolyimide membranes for phenol recovery from process water by pervaporation, ChemPhysChem, 4, 967–973 (2003).

Pithan, F., C. Staudt-Bickel, and R.N. Lichtenthaler, Synthesis of highly fluorinated copolyimide membranes for the removal of high boiling organics from process water and wastewater by pervaporation, Desalination, 148, 1–4 (2002a).

Pithan, F., C. Staudt-Bickel, S. Hess, and R.N. Lichtenthaler, Polymeric membranes for aromatic / aliphatic separation processes, ChemPhysChem, 3, 856 –862 (2002b).

Powell, C.E., and G.G. Qiao, Polymeric CO_2/N_2 gas separation membranes for the capture of carbon dioxide from power plant flue gases, Journal of Membrane Science, 279, 1–49 (2006).

Pradhan, N.C., C.S. Sarkar, S. Niyogi, and B. Adhikari, Separation of phenol-water mixture by membrane pervaporation using polyimide membranes, Journal of Applied Polymer Science, 83, 822–829 (2002).

Pramoda, K., S. Liu, and T.-S. Chung, Thermal imidization of the precursor of a liquid crystalline polyimide, Macromolecular Materials and Engineering, 287, 931–937 (2002).

Qariouh, H., R. Schue, F. Schue, and C. Bailly, Sorption, diffusion and pervaporation of water/ethanol mixtures in polyetherimide membranes, Polymer International, 48, 171–180 (1999).

Qiao, X., and T.-S. Chung, Fundamental characteristics of sorption, swelling, and permeation of P84 co-polyimide membranes for pervaporation dehydration of alcohols, Industrial & Engineering Chemistry Research , 44, 8938–8943 (2005).

Qiao, X., and T.-S. Chung, Diamine modification of P84 polyimide membranes for pervaporation dehydration of isopropanol, AIChE Journal, 52, 3462–3472 (2006).

Qiao, X., T.-S. Chung, and K.P. Pramoda, Fabrication and characterization of BTDA-TDI/MDI (P84) co-polyimide membranes for the pervaporation dehydration of isopropanol, Journal of Membrane Science, 264, 176–189 (2005).

Qiao, X., T.-S. Chung, and R. Rajagopalan, Zeolite filled P84 co-polyimide membranes for dehydration of isopropanol through pervaporation process, Chemical Engineering Science, 61, 6816–6825 (2006).

Rautenbach, R., and U. Hommerich, Experimental study of dynamic mass-transfer effects in pervaporation, AIChE Journal, 44, 1210–1215 (1998).

Ravindra, R., K.R. Krovvidi, and A.A. Khan, Solubility parameter of chitin and chitosanl, Carbohydrate Polymers, 36, 121–127 (1998).

Ren, J., C. Staudt-Bickel, and R.N. Lichtenthaler, Separation of aromatics/aliphatics with crosslinked 6FDA-based copolyimides, Separation and Purification Technology, 22-23, 31–43 (2001).

Rhim, J.-W., C.-K. Yoem, and S.-W. Kim, Modification of poly(vinyl alcohol) membranes using sulfosuccinic acid and its application to pervaporation separation of water-alcohol mixtures, Journal of Applied Polymer Science, 68, 1717–1723 (1998).

Rhim, J.-W., S.-W. Lee, and Y.-K. Kim, Pervaporation separation of water–ethanol mixtures using metal-ion-exchanged poly(vinyl alcohol) (PVA)/sulfosuccinic acid (SSA) membranes, Journal of Applied Polymer Science, 85, 1867–1873 (2002).

Robeson, L.M., Correlation of separation factor versus permeability for polymeric membranes, Journal of Membrane Science, 62, 165–185 (1991).

Robeson, L.M., W.F. Burgoyne, M. Langsam, A.C. Savoca, and C.F. Tien, High performance polymers for membrane separation, Polymer, 35, 4970–4978 (1994).

Robeson, L.M., C.D. Smith, and M. Langsam, A group contribution approach to predict permeability and permselectivity of aromatic polymers, Journal of Membrane Science, 132, 33–54 (1997).

Ruiz, J., A. Mantecon, and V. Cadiz, Synthesis and swelling characteristics of acid-containing poly(vinyl alcohol) hydrogels, Journal of Applied Polymer Science, 81, 1444–1450 (2001).

Sada, E., and T. Morisue, Isothermal vapor–liquid equilibrium data of isopropanol - water system, Journal of Chemical Engineering of Japan, 8, 191–195 (1975).

Salame, M., Prediction of gas barrier properties of high polymers, Polymer Engineering and Science, 26, 1543–1546 (1986).

Sarkhel, D., D. Roy, M. Bandyopadhyay, and P. Bhattacharya, Studies on separation characteristics and pseudo-equilibrium relationship in pervaporation of benzene–cyclohexane mixtures through composite PVA membranes on PAN supports, Separation and Purification Technology, 30, 89–96 (2003).

Schauer, J., P. Sysel, V. Marousek, Z. Pientka, J. Pokorny, and M. Bleha, Pervaporation and gas separation membranes made from polyimide/polydimethylsiloxane block copolymer, Journal of Applied Polymer Science, 61, 1333–1337 (1996).

Schleiffelder, M., and C. Staudt-Bickel, Crosslinkable copolyimides for the membrane-based separation of p-/o-xylene mixtures, Reactive & Functional Polymers, 49, 205–213 (2001).

Shaban, H.I., Using pervaporation technique to separate water from organics, Chemical Engineering and Processing, 35, 429–434 (1996).

Shafee, E.E., and H.F. Naguib, Water sorption in cross-linked poly(vinyl alcohol) networks, Polymer, 44, 1647–1653 (2003).

Shah, M.R., R.D. Noble, and D.E. Clough, Analysis of transient permeation as a technique for determination of sorption and diffusion in supported membranes, Journal of Membrane Science, 280, 452–460 (2006).

Shao, P., Pervaporation dehydration membranes based on chemically modified poly(ether ether ketone), Ph.D. Dissertation, University of Waterloo, Waterloo, ON (2003).

Shao, P., and R.Y.M. Huang, Polymeric membrane pervaporation, Journal of Membrane Science, 287, 162–179 (2007).

Shen, J.-N., L.-N. Wu, J.-H. Qiu, and C.-J. Gao, Pervaporation separation of water/isopropanol mixtures through crosslinked carboxymethyl chitosan/polysulfone hollow-fiber composite membranes, Journal of Applied Polymer Science, 103, 1959–1965 (2007).

Shimazu, A., T. Miyazaki, T. Matsushita, M. Maeda, K. Ikeda, Relationships between chemical structures and solubility, diffusivity, and permselectivity of 1,3-butadiene and n-butane in 6FDA-based polyimides, Journal of Polymer Science Part B: Polymer Physics, 37, 2941–2949 (1999).

Shimazu, A., T. Miyazaki, M. Maeda, and K. Ikeda, Relationships between the chemical structures and the solubility, diffusivity, and permselectivity of propylene and propane in 6FDA-based polyimides, Journal of Polymer Science Part B: Polymer Physics, 38, 2525–2536 (2000).

Shimidzu, T., and M. Yoshikawa, Chapter 7. Synthesis of novel copolymer membranes for pervaporation, in Pervaporation Membrane Separation Processes, ed. by R.Y.M. Huang, Elsevier, Amsterdam, the Netherlands, 321–361 (1991).

Sillion, B., R. Mercier, and D. Picq, Polyimides and other high- temperature polymers, in Synthetic Methods in Step-Growth Polymers, ed. by M.E. Rogers and T.E. Long, Wiley, New York (2003).

Silva, E.D., L. Lebrun, and M. Metayer, Elaboration of a membrane with bipolar behaviour using the semi-interpenetrating polymer networks technique, Polymer, 43, 5311–5320 (2002).

Silverstein, R.M., G.C. Bassler, and T.C. Morrill, Spectrometric Identification of Organic Compounds, Wiley, New York (1997).

Singh-Ghosal, A., and W.J. Koros, Energetic and entropic contributions to mobility selectivity in glassy polymers for gas separation membranes, Industrial & Engineering Chemistry Research, 38, 3647–3654 (1999).

Smirnov, L.V., N.P. Kulikova, and N.V. Platonova, Infrared spectra of polyvinylalcohol, Polymer Science U.S.S.R., 9, 2849–2856 (1967).

Sokolov, L.B., Synthesis of Polymers by Polycondensation, Israel Program for Scientific Translations, Jerusalem, Israel (1968).

Sommer, S., and T. Melin, Design and optimization of hybrid separation processes for the dehydration of 2-propanol and other organics, Industrial & Engineering Chemistry Research, 43, 5248–5259 (2004).

Sperling, L.H., Introduction to Physical Polymer Science, 3rd ed., Wiley, New York (2001).

Sridhar, S., G. Susheela, G.J. Reddy, and A.A. Khan, Crosslinked chitosan membranes: Characterization and study of dimethylhydrazine dehydration by pervaporation, Polymer International, 50, 1156–1161 (2001).

Sroog, C.E., Polyimides, Progress in Polymer Science, 16, 561–694 (1991).

Sroog, C.E., A.L. Endrey, S.V. Abramo, C.E. Berr, W.M. Edwards, and K.L. Olivier, Aromatic polypyromellitimides from aromatic polyamic acids, Journal of Polymer Science Part A 3, 1373–1390 (1965).

Staudt-Bickel, C., and W.J. Koros, Improvement of CO_2/CH_4 separation characteristics of polyimides by chemical crosslinking, Journal of Membrane Science, 155, 145–154 (1999).

Stern, S.A. The "barrer" permeability unit, Journal of Polymer Science Part A-2: Polymer Physics, 6, 1933–1934 (1968).

Stern, S.A., Polymers for gas separations: the next decade, Journal of Membrane Science, 94, 1–65 (1994).

Stern, S.A., Y. Mi, and H. Yamamoto, Structure/permeability relationships of polyimide membranes. Applications to the separation of gas mixtures, Journal of Polymer Science Part B: Polymer Physics, 27, 1887–1909 (1989).

Sun, H., L. Lu, F. Peng, H. Wu, and Z. Jiang, Pervaporation of benzene/cyclohexane mixtures through CMS-filled poly(vinyl alcohol) membranes, Separation and Purification Technology, 52, 203–208 (2006).

Svang-Ariyaskul, A., R.Y.M. Huang, P.L. Douglas, R. Pal, X. Feng, P. Chen, and L. Liu, Blended chitosan and polyvinyl alcohol membranes for the pervaporation dehydration of isopropanol, Journal of Membrane Science, 280, 815–823 (2006).

Tanabe, Y., K. Yamaguchi, Y. Yoshikawa, K. Sugimoto, and T. Yamaguchi, 4,4'-Bis(aminophenoxy) benzophenones, Jpn. Kokai Tokkyo Koho (Patent) JP61221158 (1986).

Tanaka, K., M.N. Islam, M. Kido, H. Kita and K. Okamoto, Gas permeation and separation properties of sulfonated polyimide membranes, Polymer, 47, 4370–4377 (2006).

Tanihara, N., K. Tanaka, H. Kita, and K. Okamoto, Pervaporation of organic liquid mixtures through membranes of polyimides containing methyl-substituted phenylenediamine moieties, Journal of Membrane Science, 95, 161–169 (1994).

Tanihara, N., N. Umeo, T. Kawabata, K. Tanaka, H. Kita, and K. Okamoto, Pervaporation of organic liquid mixtures through poly(ether imide) segmented copolymer membranes, Journal of Membrane Science, 104, 181–192 (1995).

Teng, M.-Y., C.-L. Li, K.-R. Lee, and J.-Y. Lai, Permselectivities of 3,3',4,4'-benzhydrol tetracarboxylic dianhydride based polyimide membrane for pervaporation, Desalination, 193, 144–151 (2006).

Timashev, S.F., and T.J. Kemp, Physical Chemistry of Membrane Processes, Ellis Horwood, New York (1991).

Toshima, N., ed., Polymers for Gas Separation, VCH Publishers, New York (1992).

Toti, U.S., and T.M. Aminabhavi, Synthesis and characterization of polyacrylamide grafted sodium alginate membranes for pervaporation separation of Water + isopropanol mixtures, Journal of Applied Polymer Science, 92, 2030–2037 (2004).

Touil, S., S. Tingry, J. Palmeri, S. Bouchtalla and A. Deratani, Preparation and characterization of α-cyclodextrin-containing membranes-application to the selective extraction of xylene isomers, Polymer, 46, 9615–9625 (2005).

Tsai, H.A., H.C. Chen, W. L. Chou, K.R. Lee, M.C. Yang, and J.Y. Lai, Pervaporation of water/alcohol mixtures through chitosan/cellulose acetate composite hollow-fiber membranes, Journal of Applied Polymer Science, 94, 1562–1568 (2004).

Tsuda, M., Schotten-Baumann esterification of poly(vinyl alcohol). I., Die Makromolekulare Chemie, 72, 174–182 (1964).

Tual, C., E. Espuche, M. Escoubes, and A. Domard, Transport properties of chitosan membranes: influence of crosslinking, Journal of Polymer Science Part B: Polymer Physics, 38, 1521–1529 (2000).

Turnbull, D., and M.H. Cohen, Free-volume model of the amorphous phase: Glass transition, Journal of Chemical Physics, 34, 120–125 (1961).

Upadhyay, D.J., and N.V. Bhat, Separation of azeotropic mixture using modified PVA membrane, Journal of Membrane Science, 255, 181–186 (2005).

Van Baelen, D., B. Van der Bruggen, K. Van den Dungen, J. Degreve, and C. Vandecasteele, Pervaporation of water-alcohol mixtures and acetic acid-water mixtures, Chemical Engineering Science, 60, 1583–1590 (2005).

Van den Beukel, A., and J. Sietsma, The glass transition as a free volume related kinetic phenomenon, Acta Metallurgica et Materialia, 38, 383–389 (1990).

Van Oss, C.J. and R.F. Giese, The hydrophilicity and hydrophobicity of clay minerals, Clays and Clay Minerals, 43, 474–477 (1995).

Van Oss, C.J., J. Visser, D.R. Absolom, S.N. Omenyi, and A.W. Neuman, The concept of negative hamaker coefficients. II. Thermodynamics, experimental evidence and applications, Advances in Colloid and Interface Science, 18, 133–148 (1983).

Van Oss, C.J., R.F. Giese, and W. Wu, On the predominant electron-donicity of polar solid surfaces, Journal of Adhesion, 63, 71–88 (1997).

Volkov, V.V., Separation of liquids by pervaporation through polymeric membranes, Russian Chemical Bulletin, 43, 187–198 (1994).

Wang, X.-P., and Z.Q. Shen, Studies on the effects of copper salts on the separation performance of chitosan membranes, Polymer International, 49, 1426–1433 (2000).

Wang, X.-P., Z.-Q. Shen, F.-Y. Zhang, and Y.-F. Zhang, A novel composite chitosan membrane for the separation of alcohol-water mixtures, Journal of Membrane Science, 119, 191–198 (1996).

Wang, X.-P., Z.-Q. Shen, and F.-Y. Zhang, Pervaporation separation of water/alcohol mixtures through hydroxypropylated chitosan membranes, Journal of Applied Polymer Science, 69, 2035–2041 (1998).

Wang, H.-H., T.-W. Shyr, and M.-S. Hu, The elastic property of polyvinyl alcohol gel with boric acid as a crosslinking agent, Journal of Applied Polymer Science, 74, 3046–3052 (1999).

Wang, H., T. Ugomori, K. Tanaka, H. Kita, K. Okamoto, and Y. Suma, Sorption and pervaporation properties of sulfonyl-containing polyimide membrane to aromatic/non-aromatic hydrocarbon mixtures, Journal of Polymer Science Part B: Polymer Physics, 38, 2954–2964 (2000a).

Wang, H., T. Ugomori, Y. Wang, K. Tanaka, H. Kita,K. Okamoto, and Y. Suma, Sorption and pervaporation properties of crosslinked membranes of poly(ethylene oxide imide) segmented copolymer to aromatic/nonaromatic hydrocarbon mixtures, Journal of Polymer Science Part B: Polymer Physics, 38, 1800–1811 (2000b).

Wang, Y.C., Y.S. Tsai, K.R. Lee, and J.Y. Lai, Preparation and pervaporation performance of 3,3-bis[4-(4-aminophenoxy)phenyl] phthalide based polyimide membranes, Journal of Applied Polymer Science, 96, 2046–2052 (2005).

Wang, L., J. Li, Z. Zhao, and C. Chen, Synthesis and characterization of soluble polyimides Derived from 4,4'-diamino-3,3'-dimethyldiphenylmethane and their pervaporation performances, Journal of Macromolecular Science, Part A: Pure and Applied Chemistry, 43, 305–314 (2006a).

Wang, L., Z. Zhao, J. Li, and C. Chen, Synthesis and characterization of fluorinated polyimides for pervaporation of n-heptane/thiophene mixtures, European Polymer Journal, 42, 1266–1272 (2006b).

Wei, Y.C., S.M. Hudson, J.M. Mayer, and D.L. Kaplan, The crosslinking of chitosan fibers, Journal of Polymer Science Part A: Polymer Chemistry, 30, 2187-2193 (1992).

Wijmans, J.G., and R.W. Baker, The solution-diffusion model: a review, Journal of Membrane Science, 107, 1–21 (1995).

Wikipedia (the free encyclopedia). Isopropanol-water VLE data accessible in the supplementary data page of Isopropyl alcohol. http://en.wikipedia.org/wiki/Isopropyl_alcohol_(data_page) (2007).

Wilburn, F.W., The determination of kinetic parameters from DTG curves – fact or fiction?, Thermochimica Acta, 340-341, 77–87 (1999).

Wilson, D., H.D. Stenzenberger, and P.M. Hergenrother, eds., Polyimides, Chapman and Hall, New York (1990).

Wind, J.D., D.R. Paul, and W.J. Koros, Natural gas permeation in polyimide membranes, Journal of Membrane Science, 228, 227–236 (2004).

Won, W., X. Feng, and D. Lawless, Pervaporation with chitosan membranes: Separation of dimethyl carbonate/methanol/water mixtures, Journal of Membrane Science, 209, 493–508 (2002).

Won, W., X. Feng, and D. Lawless, Separation of dimethyl carbonate/methanol/water mixtures by pervaporation using crosslinked chitosan membranes, Separation and Purification Technology, 31, 129–140 (2003).

Wu, R.J., and Q. Yuan, Gas permeability of a novel cellulose membrane, Journal of Membrane Science, 204, 185–194 (2002).

Xiao, S., R.Y.M. Huang, and X. Feng, Preparation and properties of trimesoyl chloride crosslinked poly(vinyl alcohol) membranes for pervaporation dehydration of isopropanol, Journal of Membrane Science, 286, 245–254 (2006).

Xu, W., D.R. Paul, and W.J. Koros, Carboxylic acid containing polyimides for pervaporation separations of toluene/iso-octane mixtures, Journal of Membrane Science, 219, 89–102 (2003).

Xu, Y., C. Chen, P. Zhang, B. Sun, and J. Li, Pervaporation properties of polyimide membranes for separation of ethanol + water mixtures, Journal of Chemical & Engineering Data, 51, 1841–1845 (2006).

Xu, Y., C. Chen, and J. Li, Experimental study on physical properties and pervaporation performances of polyimide membranes, Chemical Engineering Science, 62, 2466–2473 (2007).

Yamasaki, A., T. Shinbo, and K. Mizoguchi, Pervaporation of benzene/cyclohexane and benzene/n-hexane mixtures through PVA membranes, Journal of Applied Polymer Science, 64, 1061–1065 (1997).

Yampolskii, Y., I. Pinnau and B. Freeman, eds., Materials Science of Membranes for Gas and Vapor Separation, John Wiley & Sons, Chichester, West Susses, England (2006).

Yanagishita, H., C. Maejima, D. Kitamoto, and T. Nakane, Preparation of asymmetric polyimide membrane for water/ethanol separation in pervaporation by the phase inversion process, Journal of Membrane Science, 86, 231–240 (1994).

Yanagishita, H., D. Kitamoto, K. Haraya, T. Nakane, T. Okada, H. Matsuda, Y. Idemoto, and N. Koura, Separation performance of polyimide composite membrane prepared by dip coating process, Journal of Membrane Science, 188, 165–172 (2001).

Yang, L., Y. Kang, Y. Wang, L. Xu, H. Kita, and K. Okamoto, Synthesis of crown ether-containing copolyimides and their pervaporation properties to benzene/cyclohexane mixtures, Journal of Membrane Science, 249, 33–39 (2005).

Yeom, C.-K., and K.-H. Lee, Pervaporation separation of water-acetic acid mixtures through poly(vinyl alcohol) membranes crosslinked with glutaraldehyde, Journal of Membrane Science, 109, 257–265 (1996).

Yeom, C.K., J.G. Jegal, and K.H. Lee, Characterization of relaxation phenomena and permeation behaviors in sodium alginate membrane during pervaporation separation of ethanol-water mixture, Journal of Applied Polymer Science, 62, 1561–1576 (1996).

Yoon, K., K. Kim, X. Wang, D. Fang, B.S. Hsiao, and B. Chu, High flux ultrafiltration membranes based on electrospun nanofibrous PAN scaffolds and chitosan coating, Polymer, 47, 2434–2441 (2006).

Yu, J., C.H. Lee, and W.H. Hong, Performances of crosslinked asymmetric poly(vinyl alcohol) membranes for isopropanol dehydration by pervaporation, Chemical Engineering and Processing, 41, 693–698 (2002).

Zeng, X., and E. Ruckenstein, Control of pore sizes in macroporous chitosan and chitin membranes, Industrial & Engineering Chemistry Research, 35, 4169–4175 (1996a).

Zeng, X., and E. Ruckenstein, Supported chitosan-dye affinity membranes and their protein adsorption, Journal of Membrane Science, 117, 271–278 (1996b).

Zhai, M., F. Yoshii, T. Kume, and K. Hashim, Syntheses of PVA/starch grafted hydrogels by irradiation, Carbohydrate Polymers, 50, 295–303 (2002).

Zhang, L., P. Yu, and Y. Luo, Separation of caprolactam–water system by pervaporation through crosslinked PVA membranes, Separation and Purification Technology, 52, 77–83 (2006).

Zhang, L., P. Yu, and Y. Luo, Comparative behavior of PVA/PAN and PVA/PES composite pervaporation membranes in the pervaporative dehydration of caprolactam, Journal of Applied Polymer Science, 103, 4005–4011 (2007a).

Zhang, W., G. Li, Y. Fang, and X. Wang, Maleic anhydride surface-modification of crosslinked chitosan membrane and its pervaporation performance, Journal of Membrane Science, 295, 130–138 (2007b).

Zhou, F., and W.J. Koros, Study of thermal annealing on Matrimid® fiber performance in pervaporation of acetic acid and water mixtures, Polymer, 47, 280–288 (2006).

Publications and Presentations

Publications in Journals

[1] S. Xiao, R.Y.M. Huang, and X. Feng, Preparation and properties of trimesoyl chloride crosslinked poly(vinyl alcohol) membranes for pervaporation dehydration of isopropanol, Journal of Membrane Science, 286(1–2), 245–254 (2006).

[2] S. Xiao, R.Y.M. Huang and X. Feng, Synthetic 6FDA-ODA copolyimide membranes for gas separation and pervaporation: Functional groups and separation properties, Polymer, 48(18), 5355–5368 (2007).

[3] S. Xiao, X. Feng and R.Y.M. Huang, Investigation of sorption properties and pervaporation behaviors under different operating conditions for trimesoyl chloride-crosslinked PVA membranes, Journal of Membrane Science, 302(1–2), 36–44 (2007).

[4] S. Xiao, X. Feng and R.Y.M. Huang, Trimesoyl chloride crosslinked chitosan membranes for CO_2/N_2 separation and pervaporation dehydration of isopropanol, Journal of Membrane Science, in press.

[5] S. Xiao, X. Feng and R.Y.M. Huang, Synthesis and properties of 6FDA-MDA copolyimide membranes: Effects of diamines and dianhydrides on gas separation and pervaporation properties, Macromolecular Chemistry and Physics, in press.

Presentations at Conferences

[1] S. Xiao, X. Feng, and R.Y.M. Huang, Hydrophilic polyimide membranes containing carboxylic acid groups: synthesis and pervaporation properties, International Congress on Membranes and Membrane Processes (ICOM), Seoul, Korea, 21–26 August, 2005.

[2] S. Xiao, X. Feng, and R.Y.M. Huang, Modification of PVA membranes for pervaporation dehydraton of isopropanol, 56th Canadian Chemical Engineering Conference, Sherbrooke, QC, 15–18 October, 2006.